The University of Nottingham

EX VIVO MODELLING OF OESOPHAGO-GASTRIC CANCER

MR JOHN H SAUNDERS, BMBS, BMedSci, MRCS.

Thesis submitted to the University of Nottingham

for the degree of Doctor of Philosophy

October 2017

Abstract

Introduction

The response to neoadjuvant chemotherapy in oesophago-gastric (OG) cancer is only 40%, so over half of the patient's disease will progress, whilst they also suffer the toxic chemotherapy side-effects. A model to predict chemotherapy response would provide a marked clinical benefit, by enabling personalised treatment of OG cancer.

Methods

Live chemo-naïve tumour biopsies were obtained following informed consent at staging endoscopy, before patients underwent their routine neoadjuvant chemotherapy. Tumour cells from the endoscopic biopsies were expanded, using an *in vitro* feeder layer system and supplemented medium. With ethics committee approval and under Home Office guidance, these individual patient cancer cells were engrafted into immuno-compromised mice, where they formed representative tumour xenografts. Primary patient tissue, the corresponding individual patient cancer cells and their matching xenografts were analysed using immunohistochemistry, demonstrating that the *in vitro* and *in vivo* cells had retained the characteristics of the original patient's oesophageal adenocarcinoma.

To model the human tumour micro-environment (TME), a three dimensional tumour growth assay (3D-TGA) was developed, whereby the individual patient's primary tumour cells were grown as 3D cancer cell clusters. This was performed by seeding individual patient's primary tumour cells within a biological basement membrane extract, rich in extracellular matrix (ECM)

components, with and without human mesenchymal stem cells to provide stromal support.

The individual patient cancer clusters in the 3D-TGA were subjected to detailed chemotherapeutic assessment, to quantify their chemo-sensitivity to the standard chemotherapy which was administered to the patient in the clinic. This 3D-TGA predicted chemo-sensitivity was then compared with the patient's actual clinical chemotherapy response, as measured by the histological tumour regression grade, which directly relates to prognosis. In combination with standard platinum-based chemotherapy, the 3D-TGA was assessed as a platform for evaluating new chemotherapeutics: the novel emerging HDAC inhibitor Panobinostat, and the phosphodiesterase type 5 inhibitor Vardenafil, which has recently been shown to be active against cancer stroma, were evaluated.

Results

Individual patient tumours were grown from primary endoscopic biopsy tissue in over half of samples obtained within a clinically applicable timescale of 2-4 weeks. Incorporating human mesenchymal cells into the 3D-TGA significantly changed the growth and drug resistance profiles ($p < 0.005$). This 3D-TGA chemo-response in the presence of stroma reflected the clinical chemo-sensitivity, with an accurate correlation between the 3D-TGA predicted chemo-resistance and actual clinical response for the patients evaluated.

As well as predicting potential chemo-sensitivity for individual patients, the method allows individual drugs and combinations to be evaluated, trends in chemo-sensitivity between patients to be appraised, and analysis of the effect of the TME on tumour growth and chemotherapy resistance.

Combination with Panobinostat enhanced response and proved efficacious in otherwise chemo-resistant tumours. Addition of PDE5i demonstrated an overall significantly enhanced chemotherapeutic response ($p=0.003$), and consequently provided efficacy in 60% of the otherwise chemo-resistant tumours.

Discussion

The novel method of growing individual patient OG cancers, using a 3D model with specific components of the tumour micro-environment in particular ECM and mesenchymal cells, provides a clinically-relevant oesophageal cancer model with application for chemo-sensitivity testing. Mesenchymal cells have a significant effect enhancing chemotherapy drug resistance in OG cancer, and this 3D model allowed identification of patients in which stromal targeting using PDE5i provided a significant reduction in chemotherapy drug resistance. In these patients, addition of PDE5i to routine chemotherapy could result in a marked change in the clinical efficacy of their chemotherapy regimen.

The 3D model's chemo-response accurately reflects individual patients' clinical chemo-sensitivity and so this research has direct clinical application: if this assay proves to be predictive across a wider patient population, then following clinical trials, it could potentially be used to routinely guide individual patient therapy in the clinic, with administration of tailored chemotherapy for individual patient benefit.

Acknowledgements

Affiliation:

Cancer Biology Unit, Division of Cancer and Stem Cells, School of Medicine, University of Nottingham, NG7 2QL, UK

Supervisors:

Dr Anna M Grabowska

Dr David Onion

Mr Simon L Parsons

Personal Funding:

Royal College of Surgeons Research Fellowship Fund

Rotary International

Technical and Clinical Support:

Members of the *Ex Vivo* Cancer Pharmacology Centre of Excellence (EVPC), Cancer Biology Unit, University of Nottingham:

Mrs P Collier, Dr V Pang, Mr MS Dorrington, Dr R Argent, Dr PA Clarke, Mr AM Reece-Smith, Ms A Ritchie, Mrs M Meakin.

Members of the Department of Upper GI Surgery, Nottingham University Hospitals NHS Trust:

Dr I Soomro, Dr P Kaye, Mr NT Welch, Mr JP Duffy, Mr JA Catton.

Recognition:

The patients who kindly donated their tumour material to this project and the subsequent follow up throughout their journey with cancer.

Publications:

Individual patient oesophageal cancer 3D models for tailored treatment

John H. Saunders, David Onion, Pamela Collier, Matthew S. Dorrington, Richard H. Argent, Philip A. Clarke, Alex M. Reece-Smith, Simon L. Parsons, Anna M. Grabowska.

Oncotarget. 2017 Apr 11; 8(15): 24224–24236.

Mutational signatures in esophageal adenocarcinoma define etiologically distinct subgroups with therapeutic relevance.

Secrier M, Li X, de Silva N, Eldridge MD, Contino G, Bornschein J, MacRae S, Grehan N, O'Donovan M, Miremadi A, Yang TP, Bower L, Chettouh H, Crawte J, Galeano-Dalmau N, Grabowska A, **Saunders J**, Underwood T, Waddell N, Barbour AP, Nutzinger B, Achilleos A, Edwards PA, Lynch AG, Tavaré S, Fitzgerald RC.

Nature Genetics. 2016 Oct;48(10):1131-41.

Table of Contents

1 Introduction 1

1.1 Clinical Management of OG Cancer 2

1.1.1 Epidemiology 2

1.1.2 Diagnosis and Staging 3

1.1.3 Chemotherapeutic Treatment 3

1.1.4 Adjunctive Monoclonal Antibody Therapies 5

1.1.5 Standard Therapy in the UK for adenocarcinoma 8

1.2 Strategies to Guide Therapy 1

1.2.1 TRG and nodal down-staging 1

1.2.2 PET-CT to guide Therapy 4

1.2.3 Biomarkers in OG Cancer 6

1.2.4 DNA Damage Repair 7

1.2.5 Molecular Characterisation 10

1.3 Tumour Microenvironment 12

1.3.1 Tumour stroma interactions in OG cancer 12

1.3.2 Mesenchymal cells and CAFs within tumours 12

1.3.3 The role of the TME context 13

1.3.4 Stromal cell-induced drug resistance 13

1.3.5 Stromal fibroblast genetic signature can predict outcome 14

1.3.6 Mechanisms of stromal cell drug resistance 14

1.3.7 Potential tumour stroma active chemotherapeutics 16

1.3.7.1 Therapeutics targeting stromal signalling pathways 16

1.3.7.2 Therapeutics targeting stromal cells and inflammatory cytokines 16

1.3.7.3 Therapeutic DNA vaccines to target stromal cells 17

1.4 Preclinical Cancer Models 18

1.4.1 Current Pre-Clinical Models.....18

1.4.2 Establishment of Primary Patient Tumour Tissue 19

1.4.2.1 Culture methods 20

1.4.2.1.1 2D subculture.....20

1.4.2.1.2 Explant cell culture.....20

1.4.2.1.3 Precision–cut slice.....21

1.4.2.1.4 Sandwich culture 21

1.4.2.1.5 Cancer stem cell isolation 21

1.4.2.1.6 Organoid cell culture 22

1.4.2.1.7 Chemical reprogramming.....22

1.4.2.2 Refining methods to establish Primary Cell Cultures 22

1.4.2.2.1 (1) Feeder layer co-culture.....23

1.4.2.2.2 (2) Spheroid formation from cell aggregates on ultra-low attachment plates 26

1.4.2.2.3 (3) Epithelial organoids.....26

1.4.2.2.4 (4) Suspension of crypt clusters on ultra-low attachment plates 28

1.4.2.2.5 Conclusions.....32

1.4.3 Cell Culture in Two and Three Dimensions.....34

1.4.3.1 Xenograft Models 35

1.4.3.2 In Vitro 3D Models 36

1.4.3.2.1 Spheroids 37

1.4.3.2.2 Scaffolds.....38

1.4.3.2.3 Biological Hydrogels 39
1.4.3.2.4 Extra Cellular Matrix.....40
1.4.3.3 Specialised vs generalised applications of 3D models 41
1.4.3.4 Using 3D models for chemotherapeutic assays...42
1.5 OG Cancer Models for Chemotherapeutic Evaluation 45
1.5.1 OG cancer spheroid models 46
1.5.2 OG cancer organotypic models.....46
1.5.3 OG cancer tumour xenograft models 47
1.5.4 OG cancer clonogenic models 47
1.5.5 The Nottingham 3D-Tissue Growth Assay 47
1.5.6 Summary of OG cancer models.....49
1.6 *Ex vivo* chemotherapy drug evaluation.....51
1.6.1 Clinical chemotherapy regimen 51
1.6.2 The challenge of measuring delivered drug concentrations in the dynamic patient *in vivo* state 51
1.6.3 The challenges of comparing population drug pharmacokinetics with static *ex vivo* cultures 53
1.6.4 Epirubicin.....55
1.6.5 Cisplatin.....56
1.6.6 5-Fluorouracil 58
1.6.7 Capecitabine.....59
1.6.8 Novel emerging chemotherapeutics 60
1.6.8.1 Panobinostat 61
1.6.8.2 Vardenafil 63
1.6.9 Peak serum concentration of chemotherapy agents .65
1.7 OG Cancer Characterisation 66

1.7.1 Overview 66
1.7.2 Candidate markers for malignant epithelial characterisation 67
1.7.2.1 E-cadherin 67
1.7.2.2 Cytokeratin 68
1.7.2.3 Aneuploidy 68
1.7.2.4 Epithelial cell adhesion molecule 68
1.7.2.5 p53 71
1.7.2.6 Trefoil Factor 3 74
1.7.3 Cancer Stem Cells in OG cancer 74
1.7.3.1 Characteristics 74
1.7.3.2 Identification 75
1.7.3.3 ALDH in OG cancer 77
1.7.3.4 CD44 in OG Cancer 78
1.8 Study Outline 81
1.8.1 Study Rationale 81
1.8.2 Study Hypothesis 82
1.8.3 Study Aims 82
1.8.4 Study Design 82
2 Materials and Methods 84
2.1 Tissue Collection 84
2.1.1 Patient identification 84
2.1.2 Tissue collection 86
2.2 Tissue Culture 90
2.2.1 Tissue disaggregation 90
2.2.2 Preparation of feeder layer 92
2.2.3 Establishment and expansion of primary cells 93

2.3 Patient-Derived Xenografts 98
2.4 Characterisation 99
2.4.1 Immunohistochemistry 99
2.4.2 Flow cytometry 104
2.4.2.1 Intracellular staining with directly conjugated antibodies (Cytokeratin) 104
2.4.2.2 Surface staining with directly conjugated antibodies (HLA, EpCam, CD44) 107
2.4.2.3 Intra-cellular enzyme induced fluorescence with ALDH substrate conversion 109
2.4.3 Immunofluorescence 113
2.5 Three-Dimensional Tumour Growth Assay 116
2.5.1 OG cancer 3D-TGA method 116
2.5.2 Measurement of growth and cytotoxicity with alamarBlue 119
2.5.3 Formulation of TME RPMI 120
2.5.4 Formulation of Base Media and additional Growth Factors 120
2.5.5 Generation of mCherry hMSCs 123
2.5.6 Bright field imaging 123
2.5.7 Chemotherapeutic pharmacology 123
2.5.8 Calculation of chemo-toxicity 127
2.5.9 Statistical analysis 127
3 Results 1: Establishment and Characterisation of primary OG cancer cells 128
3.1 Overview & Aim 128
3.2 Results 129
3.2.1 Establishment of *ex vivo* OG cancers 129

3.2.1.1 Tissue transfer media 129
3.2.1.2 Disaggregation 132
3.2.1.3 Microbial and fungal contamination 132
3.2.1.4 Cell senescence following cryopreservation..... 134
3.2.1.5 Success at establishing primary OG cancer close-to-patient cells 134
3.2.2 Immunohistochemistry Characterisation 144
3.2.3 Patient-Derived Xenografts..... 153
3.2.4 Flow cytometric identification of potential cancer stem cells 157
3.2.4.1 Cytokeratin 157
3.2.4.2 HLA..... 159
3.2.4.3 EpCam..... 161
3.2.4.4 CD44..... 162
3.2.4.5 EpCam and CD44+ cell sub population 163
3.2.4.6 ALDH..... 164
3.2.4.7 Overall evaluation of CSC marker presence within the close-to-patient cells 166
3.3 Conclusions 169
4 Results 2: OG Cancer 3D-TGA Optimisation 170
4.1 Overview & Aim 170
4.2 Results..... 171
4.2.1 Growth using the standard baseline 3D-TGA..... 171
4.2.2 Alteration of BME concentration and ROCKi supplementation..... 172
4.2.3 Adjustment of media, timescale and re-feeding..... 182

4.2.4 Evaluation of supplementary serum, growth factors and stromal co-culture 192
4.2.5 Cell functionality within the 3D-TGA 202
4.2.6 Finalised assay conditions and use for chemotherapeutic drug evaluation 204
4.3 Conclusions 211
5 Results 3: Chemotherapeutic Evaluation using the OG Cancer 3D-TGA 212
5.1 Overview & Aim 212
5.2 Results 213
5.2.1 Study group and Demographics 213
5.2.2 Pathological features and clinical correlation 215
5.2.3 Growth, cluster formation and hMSC co-culture 215
5.2.4 Application of chemotherapeutic drugs to the 3D-TGA and evaluation of sensitivity and resistance 220
5.2.5 Single drug and combination chemo-toxicity profiles for the patient cohort 223
5.2.6 Drug efficacy increases in combination 225
5.2.7 Effect of hMSCs on drug sensitivity 226
5.2.8 The 3D-TGA using close-to-patient cells with mesenchymal cell co-culture accurately models clinical chemo-sensitivity 229
5.2.9 Chemo-sensitivity was unchanged pre and post neoadjuvant chemotherapy 231
5.2.10 The novel HDACi Panobinostat provides enhanced chemo-sensitivity 232
5.2.11 Administration of PDE5i drugs alone exhibit no chemotoxic effect 238

5.2.12 Mesenchymal co-culture induced ECF chemotherapy resistance affected by the administration of the PDE5i Vardenafil 240

5.2.13 The addition of PDE5i to ECF chemotherapy overall increases chemo-sensitivity in the presence of stromal co-culture 246

5.2.14 Adjunctive PDE5i therapy only demonstrates efficacy for individual patients 253

5.3 Conclusion 257

6 Discussion 258

6.1 Summary of research 258

6.2 Establishment and Characterisation 259

6.2.1 Establishment of *ex vivo* OG cancer cells 259

6.2.2 Expression of the potential OAC CSC in the different tissue and culture settings 262

6.2.3 Establishment of patient-derived xenografts 265

6.3 3D-TGA Optimisation 268

6.3.1 Growth and cytotoxicity 268

6.3.2 Matrix Stiffness 269

6.3.3 ROCKi supplementation 270

6.3.4 Microenvironment dependant TFF3 expression 272

6.4 Chemotherapeutic Evaluation 274

6.4.1 Mesenchymal cell co-culture increases chemo-resistance 274

6.4.2 The 3D-TGA accurately models clinical chemo-sensitivity 274

6.4.3 Efficacy of combination chemotherapy 275

6.4.4 Chemo-sensitivity was unchanged pre and post neoadjuvant chemotherapy 275
6.4.5 Novel Drug Assessment: Panobinostat 276
6.4.6 Evaluation of cancer stroma targeting PDE5i drugs 277
6.4.7 Tumour Stroma 279
6.5 Limitations and Opportunities 284
6.5.1 Evaluation of close-to-patient OG cancer cell lines. 284
6.5.2 Tumour heterogeneity 286
6.5.3 Assessment of clinical response to chemotherapy.. 288
6.5.4 Evaluation of *ex vivo* chemo-sensitivity 289
6.5.5 Opportunities for future work 291
6.6 Research Conclusions 293
7 References 295
8 Appendices 335
8.1 Epcam optimisation 335
8.2 CD44 optimisation 338
8.3 p53 optimisation 341
8.4 ALDH optimisation 344
8.5 TFF3 optimisation 348
8.6 TFF3 Heterogeneity within Oesophageal Adenocarcinoma tissue 350
8.7 TFF3 Immunofluorescence 353

List of Figures

Figure 1. Mandard Tumour Regression Grading 2
Figure 2. Appearance of primary close-to-patient cell cultures using Feeder Layer system 135
Figure 3. Flow chart demonstrating application of Inclusion Criteria to recruited Study Patients 143
Figure 4. Histological characterisation of the patient's cancer, corresponding close-to-patient cell line and xenograft tissue..152
Figure 5. Cytokeratin (AF 488) 158
Figure 6. HLA class I (PE-A) 160
Figure 7. EpCam (AF 647) 161
Figure 8. CD44 (PE-Cy7) 162
Figure 9. EpCam (AF 647) vs CD44 (PE-Cy7) 163
Figure 10. ALDH (AF 488).....166
Figure 11. Summary of flow cytometry characterisation of the close-to-patient cancer cell cultures 167
Figure 12. OG cancer primary cells do not grow in the standard baseline 3D-TGA conditions 172
Figure 13. OG cancer growth in the TGA with BME concentration of 0, 3 and 6mg/ml.....174
Figure 14. Primary patient OG cancer cells are not suspended in the 3D matrix at a 3mg/ml BME concentration 176
Figure 15. OG cancer exhibits different growth in the 3D-TGA with BME concentration of 3mg/ml and 6mg/ml 177
Figure 16. Presence of ROCKi in the 3D-TGA can affect OG cancer growth at different BME concentrations 180
Figure 17. Presence of ROCKi slightly increases OG cancer growth in the 3D-TGA with BME concentration of 6mg/ml.....181
Figure 18. Primary patient OG cancer cells form infrequent clusters in the 3D matrix at a 6mg/ml BME matrix concentration in the 3D-TGA.....182

Figure 19. F.Media and Base Media, but not TME RPMI media, support OG cancer growth in the 3D-TGA 185
Figure 20. Primary patient OG cancer cells grow in cancer cell clusters in the 3D matrix, with Base Media and F.Media but not TME RPMI 186
Figure 21. Primary patient OG cancer cells exhibit progressive clusters formation and growth over a 10 day time period 188
Figure 22. Primary patient OG cancer cells exhibit multicellular cluster formation 190
Figure 23. Growth pattern in the 3D-TGA over an extended time period with different media and re-feeding 191
Figure 24. F.Media without foetal calf serum adequately supports OG cancer growth in the 3D-TGA 194
Figure 25. Co-cultured hMSCs do not require MMC growth arrest to prevent excessive hMSC growth in the 3D-TGA 195
Figure 26. There was no difference in the growth of hMSCs in the 3D-TGA, as measured by alamarBlue 196
Figure 27. 3D-TGA co-cultured hMSCs in all media conditions demonstrate the same minimal growth as when growth arrested or when grown alone, as measured by mCherry fluorescence. 197
Figure 28. Primary patient OG cancer cells grow in cancer cell clusters in the 3D matrix, in conjunction with the co-cultured mCherry hMSCs 200
Figure 29. OG cancer cells co-cultured in the 3D-TGA with hMSCs form composite clusters of multi-cell types 201
Figure 30. OG Cancer Cells express TFF3 when cultured in the 3D-TGA in the presence of hMSCs 203
Figure 31. Endorsement of the modified conditions that support OG cancer growth in the 3D-TGA 205
Figure 32. mCherry hMSCs in 3D-TGA co-culture have consistently plateaued growth pattern 205

Figure 33. Primary patient OG cancer cells in the 3D-TGA exhibit reproducible cancer cell growth and cluster formation 207
Figures 34. Primary patient OG cancer cells in the 3D-TGA exhibit a dose response effect when exposed to increasing concentrations of chemotherapeutics 210
Figure 35. Growth in the 3D-TGA.....217
Figure 36. Evaluation of individual patient OG cancer 3D-TGA chemotherapeutic sensitivity.....223
Figure 37. Panel of Response to Chemotherapy Agents 224
Figure 38. Sensitivity to Cisplatin/5-FU doublet compared to ECF triplet chemotherapy. 225
Figure 39. Sensitivity to ECF chemotherapy in the presence and absence of hMSCs 227
Figure 40. Influence of mesenchymal co-culture upon chemo-toxicity for individual and drug combinations 228
Figure 41. The *ex vivo* 3D-TGA co-culture chemotherapy response correlates accurately with the histopathological chemotherapy response for individual patients.....230
Figure 42. OG cancer chemosensitivity pre and post neoadjuvant chemotherapy is unchanged, whether modelled with or without hMSCs. 231
Figure 43. Combining ECF chemotherapy with Panobinostat provides enhanced chemo-sensitivity: Examination of the effect of stromal cell co-culture.....234
Figure 44. Combining ECF chemotherapy with Panobinostat provides enhanced chemo-sensitivity: Examination of the effect of ECF combination with Panobinostat.....236
Figure 45. Cells grown in the 3D-TGA do not demonstrate chemo-toxicity upon exposure to increasing concentrations of the PDE5i Vardenafil.....239
Figure 46. The alternate effects of PDE5i on close-to-patient cells demonstrating hMSC co-culture induced chemo-resistance

to ECX chemotherapy: Addition of the PDE5i agent Vardenafil can increase chemo-sensitivity. 242
Figure 47. The alternate effects of PDE5i on close-to-patient cells demonstrating hMSC co-culture induced chemo-resistance to ECX chemotherapy: Addition of the PDE5i agent Vardenafil can have no effect upon chemo-sensitivity. 244
Figure 48. Combination therapy of ECF chemotherapy with a PDE5i provides enhanced chemo-sensitivity in the presence of hMSC co-culture: Examination of the effect of ECF combination with PDE5i 248
Figure 49. Combination therapy of ECF chemotherapy with a PDE5i provides enhanced chemo-sensitivity in the presence of hMSC co-culture: Examination of the effect of stromal cell co-culture. 249
Figure 50. The comparative efficacy of combination therapy of ECF chemotherapy and PDE5i across the cohort of patient OG cancers 252
Figure 51. The efficacy of the co-culture dependant ECF and PDE5i combination chemotherapy should be considered with respect to the IC_{50} confidence intervals 256

List of Tables

Table 1. Mandard Tumour Regression Grading 2
Table 2. Summary of methods for establishing primary patient tissue.....29
Table 3. Particulars of each immunohistochemistry technique101
Table 4. Particulars of Flow Cytometry Intra-cellular Antibodies 106
Table 5. Details of antibodies and controls used for flow cytometry and IHC 111
Table 6. Base Media Formulation 121
Table 7. Additional Growth Factors 122
Table 8. Calculations of the final concentrations of drug to be delivered in the 3D-TGA as a media overlay (as 1/3 of the total well volume) from stock concentrations.....125
Table 9. Calculations of the drug the combinations in serum free medium, for serial 10 fold dilutions which encompass the endpoint tissue concentrations 126
Table 10. Comparison candidate tissue transfer media 131
Table 11. Success of establishing *in vitro* close-to-patient cells from biopsies and the paired resected tumours 136
Table 12. Oncological and Demographic Characteristics.....137
Table 13. Clinical Characteristics of the 28 patients from which cell cultures were established.....138
Table 14. Histological characteristics of each patient, and corresponding close-to-patient cells, pre & post chemotherapy 148
Table 15. Primary patient cell cultures & PDX establishment .155
Table 16. PDX Histology: characteristics of each patient where a PDX was generated, and corresponding close-to-patient cells and patient-derived xenograft 156
Table 17. Patient demographics, tumour staging & treatment 214

Abbreviations

3D-TGA – Three Dimensional Tumour Growth Assay

TME - Tumour Micro Environnent

TRG – Tumour Regression Grade

GOJ – Gastro Oesophageal Junction

hMSC – Human Mesenchymal Stem Cells

BME – Basement Membrane Extract

OAC - Oesophageal Adenocarcinoma

ECF – Epirubicin / Cisplatin / Fluorouracil

HDACi – Histone Deacetylase inhibitor

SOC – Standard of Care

TFF3 - Trefoil Factor 3

FFPE – Formalin Fixed Paraffin Embedded

IHC – Immunohistochemistry

CSC – Cancer Stem Cell

1 Introduction

Worldwide, OG malignancy is still the second highest cause of death from cancer, despite a steady decrease in mortality over the last 30 years (1). There are over 8,000 new diagnoses of oesophageal cancer per year in the UK, and the incidence is increasing (2). As the malignancy frequently presents at an advanced stage, overall mortality rate remains alarmingly high, with a 5 year survival of only 12% in the UK.(3)

In the UK oesophageal cancer is routinely treated with neoadjuvant chemotherapy and resectional surgery, followed by adjuvant chemotherapy.(4) However, the response rate to neoadjuvant chemotherapy is only 40%, so over half of these patients will not benefit, whilst suffering toxic chemotherapy side effects and carcinoma progression.(5, 6)

A model to understand the mechanisms of chemo-resistance in tumours and potentially develop a test to predict which patients are most likely to benefit from chemotherapy would provide a marked clinical advantage and provide patients with personalised treatment of their oesophageal cancer.

1.1 Clinical Management of OG Cancer

1.1.1 Epidemiology

The incidence of OG cancer is strongly related to age, with 70% of cases diagnosed in patients above the age of 70 (3) and a broad male predominance of 2.5:1 (7). The majority of oesophageal cancers are epithelial in origin and histologically are either squamous cell carcinoma (SCC) or adenocarcinoma (AC), presenting in the UK in an approximate 35:65 ratio (8-10).

Worldwide the majority of oesophageal cancers are SCC (80-85%), however in the UK over the past 20 years the incidence of SCC has declined, and there has been a year on year increase in the incidence of oesophageal AC, particularly in Caucasian males(11-13).

In western countries risk factors have altered: the synergistic action of smoking and alcohol consumption for SCC development are in decline (14, 15), and although cigarette smoking is also a risk factor for AC, the recent increase in AC is thought to be driven by the rise in chronic gastro-oesophageal reflux disease (GORD), Barrett's metaplasia (16) and the obesity epidemic (17-19).

UK incidence rates are considerably higher than the EU average, with AC in particular predominance (8). The age-standardised measure of years of life lost (YLL) for oesophageal cancer in the UK in 2010 was not only significantly higher than the mean YLL rate across 18 comparator countries (the EU nations and North America), but the UK was also ranked with the worst YLLs against these comparator nations (20).

1.1.2 Diagnosis and Staging

The classic but non-specific features of dyspepsia, loss of appetite, weight loss and vomiting in those over the age of 55 demand investigation for potential cancer. The UK DoH guidelines recommend urgent gastroscopy (21) with an overall detection rate of 1-3% (22, 23). PPI treatment should be with-held before the endoscopy to prevent delayed or missed diagnosis (24, 25).

OG cancer is staged using the TNM system, which (as published by the American Joint Committee on Cancer) are on their 7th edition (2010) (26, 27). The standard staging investigations used in the UK includes computed-tomography (CT) of the chest, abdomen and pelvis assesses for distant metastasis and local disease invasion. Positron Emission Tomography integrated with CT (PET-CT) has become an increasingly important adjunct to detect occult metastasis and loco-regional lymph node involvement. Endoscopic Ultrasound (EUS) provides information regarding the level of local tumour invasion, nodal metastasis and resectability. Laparoscopy is undertaken for distal oesophageal, GOJ or gastric tumours for visualization of peritoneal micro-metastasis, and obtaining peritoneal cytology. It can also be used to assess potential resectability for gastric carcinomas (7).

1.1.3 Chemotherapeutic Treatment

The mainstay of curative treatment is resection. However, even with clear (R0) resection margins are achieved, then long term survival will rarely exceed 20% without adjunctive chemotherapy (28). Despite the consensus that surgery in conjunction with chemotherapy or chemo-radiotherapy provides better postoperative outcomes for patients with locally advanced

oesophageal and GOJ cancer, debate remains over treatment regimens and modalities.

Adjuvant chemo-radiotherapy was advocated in the US following a trial in 2001, and the 10-year follow-up results continue to demonstrate a significant survival benefit after complete resection (29), despite concerns that inadequate surgical staging (particularly the extent of lymphadenectomy) may have led to an overestimation of benefit.

Neoadjuvant chemoradiotherapy (neoCRT) showed improved survival outcomes in two small early trials (30, 31) and has subsequently been followed by the more recent CROSS trial (32). The Dutch CROSS trial gave neoCRT to both oesophageal SCC and AC, and showed an 11% improvement in 3-year survival vs surgery alone.

Neoadjuvant chemotherapy alone in the MRC OE02 trial showed that treatment of SCC and AC with 2 cycles of Cisplatin and 5-Fluoruricil (CF) improved 5 year survival outcomes to 23%, compared with 17% for surgery alone (33). Patients with involved resection margins had dramatically poorer outcomes though, with 3-year survival for R0 and R1 of 42%, 18% respectively.

Neoadjuvant and adjuvant chemotherapy has been trialed peri-operatively. An initial US trial showed little survival benefit (34), however the large UK Medical Research Council MAGIC trial (ECF) showed improved survival to 36% from 23% at 5 years, for both GOJ (and gastric) adenocarcinomas (4), as did the French FNLCC 94012 trial (CF) (35), with both demonstrating up to a 14% improvement in 5 year survival.

A direct comparison between neoadjuvant chemotherapy and neoCRT was attempted in the POET trial (36). This demonstrated

(despite closing prematurely due to low accrual) significantly higher rates of pathological complete response and node negative status amongst patients receiving neoCRT. Since this time the Neo-AEGIS trial(37) (oesophageal and GOJ) and TOPGEAR trial(38) (Gastric) have been launched which directly compare the MAGIC and CROSS protocols in an attempt to answer definitively whether multimodal therapy will provide a benefit over peri-operative chemotherapy.

Due to mixed trial groups and no head to head comparison with neoCRT, there is no current international consensus for the preferred best treatment regimen for oesophageal and GOJ carcinoma; and different countries are advocates for different therapeutic approaches. It is clear however, that patient responses within each regimen vary and no one treatment modality or drug holds the key to effective therapy, so improved preclinical models to allow in depth scientific scrutiny are required.

1.1.4 Adjunctive Monoclonal Antibody Therapies

The EGF-R and HER2 epidermal growth factors are overexpressed in sub-populations of oesophagogastric cancer and are ideal targets for focussed therapy.

HER2 is a proto-oncogene on chromosome 17, and is made from membrane-bound receptor tyrosine kinases that transmit extracellular signals to initiate intracellular signalling pathways. HER2 is overexpressed at a varying rate: Barrett's 24%, SCC 32%, AC 21%, gastric 6-36%, with a predominance in GOJ tumours and a geographical variance (Asia prevalent), dependent upon the method used for detection (IHC and FISH) (39-43). HER2 status is now defined as positive (IHC 3+ or FISH positive) in gastric cancer based on these specific staining patterns. Differences in HER2 expression are mainly due to the

site of the tumour (GOJ / gastric) and histological type(44). Studies of GOJ/gastric cancer have contradictory findings regarding the prognostic relevance of HER2, unlike in breast cancer(43).

The ToGA study showed that trastuzumab in combination with chemotherapy significantly improved overall survival in patients with HER2-positive advanced GOJ / gastric, and this was best in patients with high HER2 expression(44). The regimen was therefore integrated into UK clinical practice for advanced tumours. This is therefore the only targeted therapy for OG cancer in routine clinical use in UK practice.

There have been encouraging case reports of Trastuzumab use as part of perioperative chemotherapy for locally advanced gastric cancer(45) and clinical trials are now underway in Europe (HerFLOT) (NCT01472029). The results of these studies may support an indication for trastuzumab as part of a perioperative chemotherapeutic regimen for treating HER2-positive gastric cancer.

Future HER2 directed drugs have been in development such as T-DM1. Here trastuzumab is conjugated to a cytotoxic compound, emtansine (DM1). Upon binding of the trastuzumab T-DM1 is internalized releasing the potent cytotoxic. However an initial trial by genentech did not show superiority. An encouraging pilot study of neoCRT with additional Trastuzumab (46) has led to a current randomised trial, (RTOG 1010) studying the addition of Trastuzumab to neoCRT for localised HER2-overexpressing oesophageal and GOJ cancers.

The outcomes with anti-EGF antibodies, such as Cetuximab and Panitumumab, have not been so encouraging. The addition of Cetuximab to CF chemotherapy for gastric cancer showed no

benefit in progression free survival (PFS) and increased rates of drug related adverse events (47). Cetuximab in combination with neoCRT (Cisplatin, paclitaxel) in inoperable oesophageal cancer (RTOG 0436) showed a lack of superiority in the Cetuximab arm. The UK SCOPE1 trial also examining neoCRT (Cisplatin, Capecitabine) in combination with Cetuximab is yet to report (48).

Angiogenesis is a critical step for tumour growth, and its inhibition by blocking vascular endothelial growth factor (VEGF), or its receptor (VEGFR), has been proposed as a potential molecular target for exploitation.

Bevacizumab (Avastin) is a monoclonal antibody to VEGF and is currently used successfully for the treatment of colorectal cancer. Initial phase II trials in OG cancer patients were encouraging - those treated with Irinotecan/Cisplatin chemotherapy and Bevacizumab had a response rate of 65%(49), with similar figures reported by other groups (50). However, the intercontinental phase III AVAGAST trial in inoperable gastric or GOJ cancer provided only a minor benefit from the addition of Bevacizumab (51).The following ST03 trial showed no survival benefit from the addition of Bevacizumab to ECX chemotherapy in gastric, GOJ or lower oesophageal cancers, and moreover, demonstrated a higher anastomotic leak rate (24% vs 10%) and impaired wound healing (12% vs 7%)(52). Similarly, no survival benefit was seen by the combination of neoCRT with Bevacizumab when studied in patients with GOJ ACs (50).

Ramucirumab is a monoclonal vascular endothelial growth factor receptor-2 (VEGFR-2) antagonist, blocking the binding of VEGF to VEGFR2, and thus preventing many of the downstream effects of VEGF mediated angiogenesis(53). Two randomised, placebo-

controlled, double-blind, phase 3 trials were completed to evaluate its clinical effectiveness as both monotherapy and in combination therapy. Both the RAINBOW (Ramucirumab combination therapy with paclitaxel) (54) and REGARD (Ramucirumab monotherapy) (55) trials showed an overall survival benefit for patients with advanced gastric or GOJ adenocarcinoma (who had disease progression after first-line chemotherapy), of an extra 2 months compared with placebo.

1.1.5 Standard Therapy in the UK for adenocarcinoma

Following the publication of the MAGIC trial in 2006, Nottingham University Hospitals, in line with the majority of UK centres, has adopted this peri-operative chemotherapy regimen as the standard of care for the treatment of OG adenocarcinoma. It involves 3 cycles of Epirubicin, Cisplatin and 5-Fluorouracil (ECF) pre and post operatively. In recent years, the infusional 5-Fluorouracil component has been updated to the oral pro-drug Capecitabine (Xeloda), which was shown in the REAL2 trial to be equally as efficacious, resulting in the commonly administered ECX regimen (56). Where necessary, to reduce the nephrotoxic side effects from platinum based drugs, Cisplatin is switched for Oxaliplatin, with an EOX regimen resulting.

1.2 Strategies to Guide Therapy

Given the limited response rate to peri-operative chemotherapy, neoCRT and the newer molecularly targeted drugs, approximately 60% of the patients that routinely undergo treatment will have chemo-resistant malignancies. As well as not benefiting from the adjunctive therapy, they will undergo disease progression whilst suffering significant toxicity from these regimens (57). Therefore, a predictive marker that forecasts pathological response to therapy and could be used to guide treatment is in great demand, discriminating between those likely to respond to neoadjuvant therapy and those who instead would benefit from early surgery (6).

1.2.1 TRG and nodal down-staging

Surrogate markers of tumour response to therapy frequently employed are decrease in tumour size, stage, nodal status and Mandard Tumour Regression Grade (TRG).

The Mandard TRG is a histopathological measure of tumour response to chemotherapy, graded 1-5 (Table 1 and Figure 1), where cancers with a TRG of 1-3 are considered chemo-sensitive and TRG 4-5 chemo-resistant, which directly relates to prognosis.(5, 58) This is broadly comparable to the Becker grading system, which assesses histopathological response in a similar fashion.

Table 1. Mandard Tumour Regression Grading	
Grade	**Definition**
1	No residual cancer
2	Rare residual cancer cells
3	Increase in cancer cell numbers, but fibrosis predominates
4	Residual cancer outgrowing fibrosis
5	Absence of regressive changes

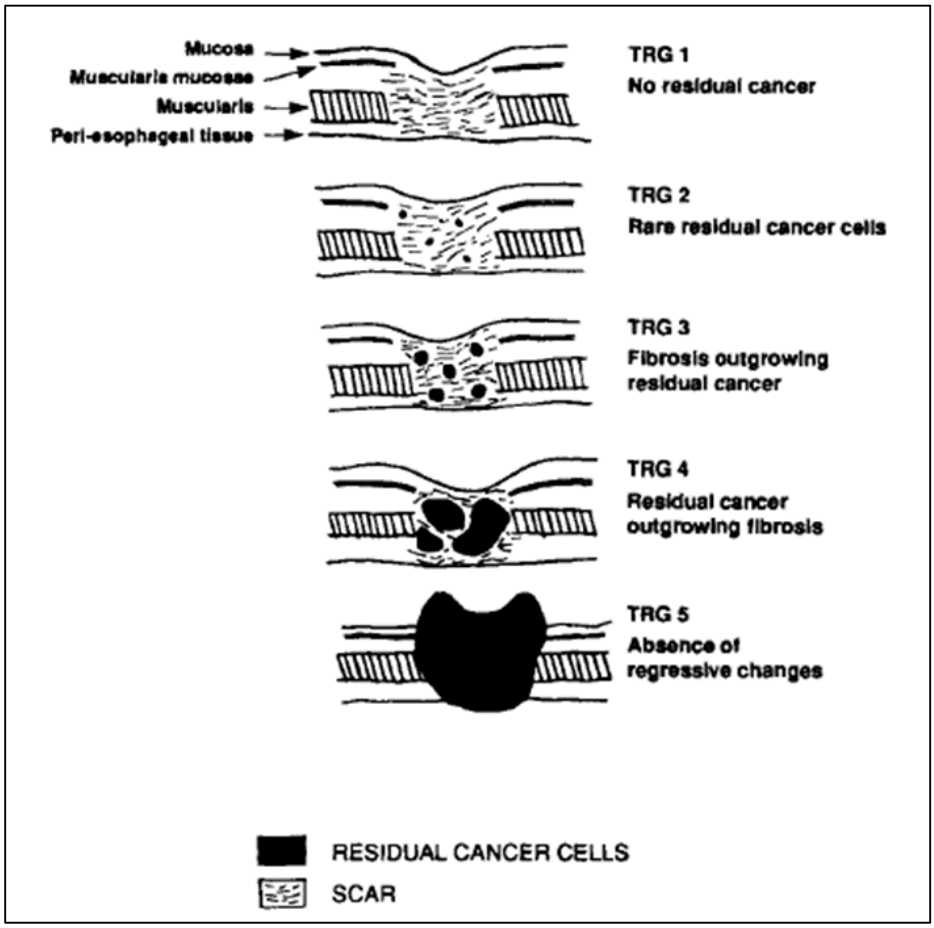


Figure 1. Mandard Tumour Regression Grading

The visual features of tumour regression grading by Mandard et al (59)

Despite all of the surrogate markers of tumour response (decrease in tumour size, stage, nodal status, TRG) correlating highly with disease-free survival, on multivariate analysis, only TRG remains a significant predictor of disease-free survival (TRG 1-3 vs TRG 4-5, $p<0.001$) (59). Similarly, Mandard histopathological analysis of response to cytotoxic therapy has also been shown to predict survival benefit in gastric cancer (60, 61). These results demonstrating the reliability of Mandard TRG as a marker of response to chemotherapy, and its usefulness as a prognostic indicator, have been validated in both the UK (5) and China (62).

However, there are some drawbacks;

1. A histopathological Mandard TRG can only be obtained following neoadjuvant therapy and resectional surgery so cannot be used in the initial stages following diagnosis to predict the response to neoadjuvant therapy.

2. Mandard TRG is subject to grading subjectivity (i.e. there is inter-user variability between different histopathologists examining the malignant tissue), however this variability is only usually seen within the grading of a resistant cancer (i.e. classing as TRG 4 or a TRG 5) or within the grading of a sensitive cancer (i.e. TRG 1 vs TRG 2) rather than a disagreement between the sensitive (TRG 1-3) or resistant (TRG4-5) nature of the cancer itself.

3. Sampling error can introduce bias. The assessment of TRG is only as accurate as with the number and position of places within the tumour bulk which have been sampled, and how reflective they are of the overall tumour itself.

4. Mandard TRG only assesses the chemotherapy response of the primary tumour. This is considered by some to be inadequate as nodal metastases are a common site of recurrence following surgery and therefore nodal down staging a key predictor of chemo-response (63). However, there is currently no method of objectively and reliably measuring the regression or progression of nodal disease, despite PET initially appeared promising (64).

Despite the outlined drawbacks, and in the absence of materially better and validated system, Mandard TRG is currently the only universal standardised and accepted method for objectively measuring chemotherapy response.

1.2.2 PET-CT to guide Therapy

Positron Emission Tomography (PET) visualises the metabolic characteristics of tumours using a radiolabelled metabolite 18F-flurodeoxyglucose (18F-FDG) whose uptake is associated with an increased rate of glycolysis and glucose transport. FDG avidity and metabolic activity is measured with standard uptake values (SUVs), which is representative of both tumour proliferation and number of viable cells.

PET is routinely used in the initial staging of all patients with OG cancer as it can detect distant metastatic disease, in patients who are otherwise thought to have curable disease. It has been shown to detect distant metastases (not seen on CT scanning alone) in 15-20% of patients. (65-68). PET is now routinely combined with CT scanning to provide a higher resolution imaging modality, 'PET-CT', with increased sensitivity (69).

The maximum SUV from the initial staging PET scan has been shown in multiple studies to correlate with overall prognosis however, this is without consistently reaching statistical

significance (70, 71) and must take into account that a raised SUVmax is associated with a significantly better response to neoCRT (72)

Unlike serial CT scans, PET can however predict a prognostic response following induction chemotherapy (73, 74). If there is a reduction of SUV max by 35% or more than the overall 2 year survival increases from 37% in non-responders to 60% in responders (75, 76). The post-induction chemotherapy PET-CT at 2 weeks can also predict response to subsequent neoCRT (77) and histological response (78). However, due to the unavoidable false-positive results from radiation inflammation, PET–CT post neoCRT has not been a sufficiently sensitive tool to predict pathological response. As a result of conflicting predictive / prognostic outcomes from PET–CT both post induction neoCRT (79, 80) and after full neoCRT (81, 82), PET-CT during and after neoCRT is not considered significantly accurate enough for patient response identification.

The identification (using PET) of early chemotherapy responders following induction chemotherapy, in the MUNICON trial (64) showed that early responders had an improved event-free survival (from 14 to 29 months) and overall survival at 2 years (from 26% to 37%). This suggests that instead of continuing ineffective chemotherapy, non–responders may benefit from either a change in chemotherapy regimen or proceeding directly to surgery. However, these exciting results have not been reproduced and there are two current trials (HICON trial & CALGB trial 80803) examining the benefits of switching to an alternate chemotherapy or neoCRT regimen if deemed a PET non-responder following induction chemotherapy (83).

Interestingly, although PET CT has not been shown to be accurate at predicting prognosis following neoCRT if surgery is

performed (84), it has been shown that if the SUV is lower than 4.6 the patient survival was comparable if they underwent surgery and received tri-modality treatment or simply received bimodality therapy without surgery (85). This suggests that surgery removes any residual disease, altering the PET prognostic prediction. However, whether a substantial reduction tumour metabolism to less than 4.6 by neoCRT is an as-clinically-effective treatment option as surgical resection, will need to be judged by a large well-structured randomised clinical trial (86).

Although trials with PET-CT have shown promising results at predicting patient response to therapy, these population studies have been used to predict response to whole chemotherapy regimens, rather than individual drugs, without measuring the actual efficacy of each drug. Also these PET-CT trials cannot direct clinicians to which other chemotherapeutic drugs the patient's tumour is sensitive to, or not. At best, it can only inform the clinician that the previous standard regimen was effective or ineffective. However, pre-clinical cancer models (where individual drugs, their potential synergy, interactions and the actual tumour biology can be examined) offer a potential step change in cancer treatment beyond what is currently possible.

1.2.3 Biomarkers in OG Cancer

The study of cancer biology has resulted in the identification of specific biomarkers (e.g. Ca125, PSA) routinely used to aid diagnosis and prognosis in common cancers such as ovarian and prostate.

Biomarkers have been examined for 3 main purposes in OG cancer:

- those diagnosing OG cancer; as early changes can be complex to monitor against a background of Barrett's metaplasia(87).
- those investigating prognosis (assessment of the likelihood of survival); as the current TNM system is limited as it only provides a snapshot in time of the stage of the malignancy, rather than a reflection of aggressiveness and ultimate survival.
- those predicting a specific response to therapy; as despite an overall patient cohort experiencing therapeutic benefit, only certain members of the cohort may actually have a meaningful response.

Despite extensive research in OG cancer there still remains no routinely applicable diagnostic or prognostic biomarker for OG cancer and there is only equivocal data for the limited number of markers that may predict treatment response to traditional chemotherapeutics (6, 88).

HER2 status for the focussed use of Trastuzumab, is the only currently used biomarker in OG cancer. However it is only applicable to patients with advanced GOJ / gastric carcinoma, but does identify the key small (<25%) target group with cancers that will potentially benefit from Trastuzumab therapy (42).

1.2.4 DNA Damage Repair

DNA is constantly being damaged by insults (e.g. ionising radiation) as well as spontaneous alterations. To prevent these from resulting in mutagenic changes, mammalian cells have developed advanced DNA damage sensor and repair mechanisms to maintain homeostasis. These are so essential that loss of the function of the DNA repair genes results in marked vulnerability to early cancer development (e.g. in hereditary non polyposis

colon cancer). Conversely, established tumours also have a functioning DNA damage repair system, which can enable repair of the DNA damage intentionally done by radiotherapy and chemotherapy. Tumours with highly functioning DNA damage repair pathways may therefore display increased chemo-resistance to chemotherapeutics such platinum or alkylating drugs which cause DNA damage (89). Expression of DNA repair factors in tumours is of interest, as this not only may guide potential patient chemo-sensitivity, but also provide a potential new target for anticancer drugs (where there is a difference between tumour and normal tissue), and also as sensitizing agents so that when used in concert with DNA damage inducing chemotherapeutics they could reduce drug resistance (90). Clinico-pathological correlation studies support these hypotheses, for example in oesophagogastric cancer, where initial observational studies showed that key DNA repair proteins e.g. XRCC1 and ATM, are related to stage of tumour and subsequent poor survival (91).

There are many different and complex DNA damage repair pathways which provide possible new targets for therapy and potential for personalisation of treatment, however I will only touch upon a few examples relevant to oesophagogastric cancer.

Human AP endonuclease (APE 1) is a endonuclease involved in the base excision repair (BER) DNA damage repair pathway. In many cancer types (including ovarian, lung and melanoma) low levels of APE1 expression are a marker of improved response to radiotherapy and chemotherapy (92). In chemo-exposed OG cancer, the prognosis of patients with APE1 positive tumours correlated with worse overall survival (93). Clinical correlation of APE1 expression has lead to development of APE1 inhibitors, which *in vitro* sensitize resistant cancer cells to conventional

chemotherapy, and as a result clinical trials are currently underway (92).

The nucleotide excision repair (NER) DNA damage repair pathway involves removal (rather than repair) of the damaged bases through endonuclease excision. The excision repair cross complementing group 1 - xeroderma pigmentosum complementation group F (ERCC1-XPF) is essential for NER endonuclease function. Initial preclinical studies suggesting high levels of ERCC1 were associated with platinum chemotherapy resistance were confirmed by patient studies in colorectal and lung cancer (94), where it was subsequently trialled to provide ERCC1 tailored chemotherapy in lung cancer (95). In gastro-oesophageal cancer, nuclear ERCC1 expression by IHC correlated with lack of response to neoadjuvant platinum-based chemotherapy and was associated with worse survival (58). This was also studied in oesophageal cancer in patients with variations or polymorphisms within genes of the NER pathway (inc. ERCC1), it showed significantly improved outcome for cisplatin treated patients (96). However, in gastric cancer the opposite was found. Patients with low expression of ERCC1 were more likely to respond to 5-FU/oxaliplatin and have longer survival than those with high ERCC1 expression(97). As a result there are now trials to investigate high ERCC1 expression in advanced OG cancer and potential prediction of response and the subsequent benefit from platinum-based chemotherapy (92).

Human DNA-unwinding helicase RECQL4 has been recently studied in gastric cancer as it is involved in various DNA repair pathways and has been reported to be significantly associated with clinical outcome in sarcoma, prostate and breast cancer (98). In gastric cancer it was found that high RECQL4 expression in cell lines displayed a greater resistance to cisplatin treatment,

an in patients this high expression correlated with poor survival (99). RECQL4 is thought to promote cisplatin resistance by regulating the transcription factor AKT–YB1, activating the multidrug resistance (MDR1) gene pathway (99). The RECQL4 helicase or the AKT–YB1–MDR1 axis now provides a potential target which can be disrupted to try and improve treatment response in OG cancer.

1.2.5 Molecular Characterisation

Whole genome sequencing has recently revolutionised our understanding of the molecular biology and subsequent characterisation of oesophageal and gastric cancer. The Cancer Genome Atlas Research Network performed a comprehensive molecular evaluation of 295 primary gastric adenocarcinomas and subsequently grouped them into four main sub-types which was distinct from age, gender, site, and lauren classification (100): tumours positive for Epstein–Barr virus, extreme DNA hypermethylation, genomically stable tumours, and tumours with chromosomal instability, which show marked aneuploidy and focal amplification of receptor tyrosine kinases. The UK OCCAMS (Oesophageal Cancer Clinical and Molecular Stratification) collaboration group, performed whole genome sequencing on 129 patients with oesophageal adenocarcinoma showing the genetic complexity and heterogeneity this cancer (101). It is dominated by copy number alterations, frequent large-scale rearrangements, co-amplification of receptor tyrosine kinases, and downstream mitogenic activation is abundant. Despite the immense heterogeneity, these mutational signatures were able to be loosely grouped into three distinct molecular subtypes: (i) enrichment for BRCA signature with prevalent defects in the homologous recombination pathway, (ii) dominant T>G mutational pattern associated with a high mutational load and neoantigen burden, (iii) C>A/T mutational pattern with evidence

of an aging imprint. Whilst the Identification of these subtypes provides a framework for potential patient stratification in future trials of targeted therapies, the vast challenge remains with how these broad molecular subtype groups will be of any use in help guide treatment approaches in robust fashion, and if they will be able to predict any therapy response a reliable manner.

1.3 Tumour Microenvironment

1.3.1 Tumour stroma interactions in OG cancer

The stromal component of the microenvironment has been shown not only to potentiate tumour desmoplasia, cancer cell proliferation (102) and differentiation (103, 104); but also drive tumour functions, such as cancer invasion (105-107). Most OACs contain a cancer associated fibroblast (CAF)-rich stroma; this may explain the highly infiltrative nature of the disease (108, 109), where stromal genes relating to pro-inflammatory pathways have been shown to relate to invasive disease and predict outcome (110). Indeed, in OAC, *in vitro* studies have shown paracrine interaction between CAF-secreted periostin and OAC-expressed integrins leading to increased tumour cell invasion (111). This is mirrored in patient samples where periostin expression by CAFs at the tumour-stromal interface correlates with poor overall and disease-free survival, underlining the key importance of the tumour stroma in OAC (111). It has therefore been postulated that a tumour can be considered as a primitive organ, consisting of a complex interplay between supporting cell types rather than just a mass of genetically abnormal epithelial cells (112, 113). This multicellular make-up of the tumour-organ is considered to be both heterogeneous and dynamic and is considered to actively influence therapeutic response and resistance(114).

1.3.2 Mesenchymal cells and CAFs within tumours

Human mesenchymal stem cells (hMSCs) have been shown to not only migrate to malignant sites within the patient, but transform into CAFs on arrival to the tumour site (115) and contribute to the formation of the tumour-associated stroma (116, 117) and promote tumour growth through the contribution of microvascularisation, fibrovascular networks, and the

production of tumour stimulating paracrine factors(115, 118). This is deleterious modification by the tumour of the intended protective function of hMSCs into a CAF-like phenotype, which encourages growth and supports tumour development (119). Thus, in the appropriate setting, hMSCs can be used to model the presence of stromal support as an accepted surrogate for the ubiquitous cancer associated fibroblast (CAF) cell (120).

1.3.3 The role of the TME context

It has been proposed that the microenvironmental context of the tumour itself (e.g. primary, LN, sites of metastases) within the body has influence on these tumour stromal-epithelial interactions, and thus conferring drug resistance to different classes of chemotherapeutics (121). The physical microenvironment itself is also thought to provide a *de novo* element of drug resistance; by both providing a physical barrier to drug ingress and by allowing dormant tumour cells to remain polar and thus blend into the organized environmental context and avoid exposure (122). The surviving foci of malignancy will then have developed an acquired resistance as a result of the therapy induced clonal selection(123). It is this adaptive, environment-mediated drug resistance, from reciprocal signalling between tumour and stroma and scaffold, that has been proposed to be a dominant force in recurrent multidrug resistant cancer (122).

1.3.4 Stromal cell-induced drug resistance

The mechanistic role of stromal cells and the micro-environmental interactions within the tumour-organ contributing to chemo-resistance is increasingly becoming a key area for research and a crucial consideration for the development of active anti-cancer therapeutics, particularly in OAC where

tumours frequently have a CAF rich stroma and there is an overwhelming problem with chemotherapeutic drug resistance.

1.3.5 Stromal fibroblast genetic signature can predict outcome

In other cancer types e.g. breast, micro-array analysis of stromal cells found a gene signature predictive of resistance to chemotherapy and that this was more strongly predictive in samples that had a larger stromal component (124). The genome of the stromal component of OG has also been examined and was able to discriminate between pre-invasive and invasive disease and predict poor prognosis(110). This evidence points to the presence of CAFs and stromal interactions between OG epithelial cells within the TME being as important in relation to tumour invasion and drug resistance, as they are to the key starting point of carcinoma establishment and growth.

1.3.6 Mechanisms of stromal cell drug resistance

Although mesenchymal cell-induced cancer progression and chemo-resistance have been previously reliably described in both different environments and tumour types, there is a lack of conclusive evidence about the chief mechanisms by which stromal cells (such as mesenchymal and cancer associated fibroblast (CAF) cells) induce these effects(125). Stroma-cancer cell interactions can be broadly considered as direct cell contact, secreted signalling factors (such as cytokines, chemokines and growth factors), or hypoxia driven. Direct cell contact interactions have been shown in different cancers; for example, MSC produced TGF-β1 promoting chemo-resistance in leukaemia(126), stromal cell oncologic trogocytosis in ovarian cancer(127, 128), and CXCR4 antagonists preventing MSC induced imatinib chemo-resistance in leukaemia cells(129). Secreted factor interactions have reported alternative

mechanisms for platinum-based chemotherapy resistance; for example MSC culture supernatant was able to confer carboplatin resistance to ovarian cancer cells by inhibiting the activation of effector caspases and apoptosis blockade through the activation of PI3K/Akt pathway signalling(130), and in cholangiocarcinoma(131), or the demonstration of MSCs stimulating resistance to carboplatin and Cisplatin via secretion of platinum-induced polyunsaturated fatty acids (PIFAs)(130), additionally another group showed that MSC induced IL-6 and IL-8 release by macrophages allowed ovarian cancer cells to display platinum chemo-resistance(132), and in prostate cancer secretion of WNT-16b from stromal fibroblasts could also promote resistance(133). The secretion of the αVβ3 & 5 ligand periostin allows CAFs to regulate ECM composition, facilitate malignant cell adhesion, migration and apoptosis resistance through PI3K-Akt/PKB activation(134).

Hypoxia-driven interactions have also been demonstrated; for example, MSCs can influence the formation of the hypoxic niche and expression of high levels of HIF1-α (135), and promotes cell survival and confer resistance in leukaemia (136). Clearly, although MSCs are potent mediators of resistance to chemotherapy, the key factors and mechanisms in the tumour microenvironment have yet to be fully identified. This may be because the cross-talk between stromal cells and cancer cells is context dependant, or because a diversity of complementary mechanisms is concurrently occurring, and also, these interactions may differ between micro-environments, cancer types and be adaptive in response to the selection pressure applied by chemotherapeutics(114). To achieve a durable response a multi-focussed approach that targets both the tumour cells and other components of the microenvironment such as the stromal support maybe required.

1.3.7 Potential tumour stroma active chemotherapeutics

Targeting tumour related stromal cells is an attractive option. In comparison to the genetically unstable cancer cells, CAFs are a more steady genetic target and therefore have less variable pathways for signalling interactions(121), are less likely to develop drug resistance (122), and also represent a feasible target for immunotherapy with anti-cancer vaccines (125)

1.3.7.1 Therapeutics targeting stromal signalling pathways

So far, drugs targeting tumour signalling pathways within the TME have been disappointing.(114) For example, the hedgehog pathway was thought to hold great promise. Pre-clinical data demonstrating increased expression of Hedgehog ligands in many tumour types, with hedgehog ligands lead to the activation of stromal fibroblasts and inducing further tumorigenesis and affecting tumour neo-angiogenesis.(137) As well as those few with Hedgehog pathway mutation, it was proposed that Hedgehog pathway inhibition would more broadly reduce the desmoplastic stroma formation.(138, 139) However, despite this promising pre-clinical data, this never translated into clinical effectiveness and no benefit was seen when combined with standard therapy in pancreatic(140), ovarian(141) or colorectal cancer(142).

1.3.7.2 Therapeutics targeting stromal cells and inflammatory cytokines

There has been some limited initial success by attempting to target CAFs instead of normal fibroblasts with anti-tenascin-C or anti-FAP molecules. Despite promising results from a phase II trial of the anti-tenascin monoclonal antibody 81C6 in glioma (143) this approach is undergoing continued clinical trials and still holds orphan status at the European Medicines Agency.

The use non-steroidal anti-inflammatory drugs (NSAIDs) to inhibit stromal cell mediated inflammation and cytokine release has been shown to globally lower the risk of colon and breast cancer, and it has been proposed that regular treatment with these and might help prevent lung, oesophageal and stomach cancers. (144)

1.3.7.3 Therapeutic DNA vaccines to target stromal cells

A DNA vaccine has been developed which uses CD8+ T cells to target fibroblast activation protein (FAP) to specifically kill CAFs, and decrease the collagen I expression and re-organisation (which is one of the major contributors to tumour desmoplasia) and therefore improve (up to 70%) drug uptake. Testing in pre-clinical mouse models showed promising initial efficacy. Combination of the vaccine with doxorubicin resulted in tumour retardation or complete tumour rejection in half of the mice, compared to no effect from doxorubicin treatment alone (145). This approach, like others(146) has not yet enjoyed the translational success required to made the jump into routine clinical practice.

1.4 Preclinical Cancer Models

Most current pre-clinical cancer models use long-established cancer cell-lines grown on a 2D plastic flasks supplemented by animal serum. These models have had their clinical relevance questioned, as they poorly reflect results generated using patient tissue (147, 148) and lack many components of the tumour micro-environment (149, 150), so often do not accurately reflect the clinical scenario(151). Many promising drugs developed using these models fail to make the leap from efficacy in the laboratory to success in phase III clinical trials and beyond(152). This lack of translation from bench to bedside would suggest a need for more accurate pre-clinical laboratory models to simulate the human clinical scenario(153). Animal models of xenografted patient tumours have been used, but these require a large expansion of tumour material for implantation, take weeks-months to develop and cannot easily test drugs in different concentrations or combinations(154). Although the xenografted tumours have a complex tumour micro-environment (TME), the human stromal cells are replaced by cells of murine origin and the models have not been shown to be reliably predictive of clinical efficacy (155).

1.4.1 Current Pre-Clinical Models

Although the current neoadjuvant & adjuvant chemotherapy drug regimens for OG cancer confer a significant survival benefit, this is limited, as only approximately 40-50% of tumours demonstrate pathological response to the treatment. So there is both a need to develop new targeted drugs for OG cancer, and also to develop robust methods for testing these drugs against patient-derived tumours within pre-clinical tumour models, so that accurate drug efficacy can be established.

Preclinical tumour models have been used in the laboratory for many years and are a mainstay of the pharmaceutical industries drug discovery and development processes. The current routine practice of 2D *in vitro* cell culture, representation of patient tumours using cell lines, followed by *in vivo* animal studies has resulted in an approximate 11% success rate in bringing a drug to market in the US and Europe (152, 156, 157). This demonstrates the fundamental disconnect between current pre-clinical tumour models and the *in vivo* disease (151, 153, 154, 158).

Two main issues are being addressed in an attempt to make these preclinical tumour models more relevant: firstly, the use of primary patient tumour material rather than cell lines;, and secondly, the application of 3D models, rather than 2D assays. These are discussed below.

1.4.2 Establishment of Primary Patient Tumour Tissue

The majority of preclinical models use cell-lines grown in 2D *in vitro* culture or as subcutaneous tumour xenografts. However, although widely used, these cell lines have been shown to be poorly predictive of clinical efficacy (155). Such lines have undergone unnatural clonal selection for cells that can survive in culture on 2D plastic surfaces (148), evidenced by only a 5% overlap between the genes up-regulated in cell lines and those up-regulated in primary tumour samples(159). Up regulated pathways not seen in primary cancer cells included ATP synthesis, cell cycle, oxidative phosphorylation, and down-regulation of pathways involved cell communication, cell adhesion molecules, and ECM-receptor interaction (160). Importantly, with reference to chemotherapy resistance, a recent study demonstrated that the drug resistance gene signatures of

established cell lines in 2D or xenograft culture bore no relation to the freshly isolated human tumour tested (147).

Given the variability of individual patient tumour responses to standard drug regimens and the complex genetic diversity seen between individual patient tumours, it is unsurprising that using the standard immortalised cell lines in 3D culture to evaluate new chemotherapy treatments has not been predictive of outcome (161-163). Therefore, the procurement and maintenance of primary tumour cell populations from patient solid tumours is of key importance to developing clinically relevant tumour chemo-sensitivity results (164, 165).

Establishing and then maintaining primary tumour cells populations in the laboratory (which are representative of the original tissue) is challenging, labour intensive and time consuming. The differing proposed methods and their varying degrees of success are outlined below.

1.4.2.1 Culture methods

1.4.2.1.1 2D subculture

2D cultures have been employed for many years as the mainstays of tissue culture, but despite serial subcultures, have failed to produce representative tumour lines with tissue-specific characteristics of the original tumour, and so are not used to establish primary tumour cell lines.

1.4.2.1.2 Explant cell culture

This involves placing pieces of the tumour that have been excised directly into serum enriched media on to a 2D plate and then this is monitored carefully, with serial subcultures undertaken to derive the primary tumour cell lines. The technique is easily performed however, the success rate is at

best only of 50%, and the problem of unrepresentative subcultures still remains (166).

1.4.2.1.3 Precision–cut slice

These are similar to the explant culture system, but with a strict tissue thickness of around 160 micrometres allowing a ready supply of nutrients and oxygen, which helps to grow the cells and preserve their morphology. This stringent slice thickness can make the technique somewhat inaccessible, but does initially maintain a primary tumour growth rate of >50% (167).

1.4.2.1.4 Sandwich culture

This provides a nutritionally depleted environment where the tumour cells (which have been conditioned to this environment) survive whilst normal cells do not (168). This method selects out for the most robust and immortal malignant cell populations before returning them to routine 2D culture conditions for expanding. This method also facilitates the cell populations to simulate and retain the morphology and tissue specific biochemical function seen *in vivo*. However, sandwich culture selects for a set of tumour cells that can tolerate hypoxia, and thus the original heterogeneous tumour cell population will be limited.

1.4.2.1.5 Cancer stem cell isolation

Cancer cell selection using different surface markers has been encouraging in the laboratory setting, and holds great promise for their subsequent expansion and study within a cancer. However, many malignancies (including OG cancer) do not have definitively characterised cancer stem cell markers. Also these stem cell markers will simply identify a sub-population of cells within the tumour and may reduce the natural heterogeneity of the tumour or risk missing other cancer stem cells that we do not have markers for at this time (169).

1.4.2.1.6 Organoid cell culture

This novel method has been used with much excitement in developing primary tumour cell lines from colorectal cancers using biological scaffolds such as Matrigel or collagen.(170) The complexity of the 3D assays, different seeding densities, the proportions of dead cells following tumour disaggregation, the difficulty re-feeding the assay and ability to passage the resultant tumour tissue makes its routine use for modelling individual patient cancers within a clinically applicable timescale a significant challenge. However, many of the principles of primary tissue establishment and 3D organoid growth have provided significant insights into the methods and tools required to establish and grow primary patient cancers.(171)

1.4.2.1.7 Chemical reprogramming

RhoKinase inhibitor (ROCKi) can be used in the presence of feeder fibroblast cells to conditionally reprogram epithelial cells and induce a stem-like state without the modification of phenotype, and without genetic drift (172, 173). This method allows routinely obtained primary cells from a variety of tissue to proliferate rapidly. However, it is as yet unclear whether this represents a heterogeneous population or simply a super-selected homogeneous subset of cells, which do not reflect the original tissue.

1.4.2.2 Refining methods to establish Primary Cell Cultures

The growth of malignant cells has been achieved from individual patient tissue in the usual form of cell lines (which grow in an unlimited fashion but are very difficult to establish), or in organotypic cultures which can be established (with much care in a relatively time consuming manner from pieces of patient tissue), but only last for a short period (174, 175). It has not

been possible to continuously propagate adult epithelial cells in culture without permanently compromising their normal phenotype for example using exogenous viral oncogenes or cellular gene transduction e.g. using the hTERT method (172, 176).

The *in vivo* xenograft pathway for establishing individual patient OG cancers is well-described and are of much value as they accurately phenotypically and genetically recapitulate the primary patient tumours(177-179). But success rates are low (approx. 10 - 30%) despite extensive trials using different strains of immunocompromised mice (154, 180-182). To markedly expand the tumour bulk and use many different mice for different experimental conditions is not only costly and time consuming (and therefore not available to all researchers), but also comes with ethical considerations concerning the use of excessive animals. Unfortunately, there is limited ability to perform multiple and complex investigations of these xenografted tumours as once ex-planted *in vitro* for experimentation, they only survive for a short period in the tissue culture environment (183, 184).

In the last few years, four groups have published work demonstrating enduring *in vitro* primary growth of individual patient's intestinal cancers, each with varying degrees of success and all using slightly dissimilar methods and different supplemental growth factors to stimulate growth.

1.4.2.2.1 (1) Feeder layer co-culture

Conditional re-programming of normal and malignant epithelial cells was induced by using a 3T3-J2 feeder cell layer and media supplemented with Rho Kinase Inhibitor Y-27632 (ROCKi). This resulted in indefinite *in vitro* cellular proliferation, in a stem like phenotype. (172) The established 2D primary patient tissue

could then be grown as 3D Sphere or Xenografts. (Table 2, column 1) For 3D, the 'on-the-top method' was used (185), where the cells were plated in media containing 2% matrigel, on-top of matrigel bed. However, these only continued to proliferate for a limited period when transferred to Matrigel in the absence of ROCKi and the feeder layer.

The induction of conditionally-reprogrammed cells (CRCs) is rapid (days) and results from reprogramming of the entire cell population rather than the selection of a minor sub-population. The CRCs share the characteristics of adult stem cells, and do not over express the characteristic transcription factor sets of embryonic (ESC) or induced pluripotent stem cells (iPSC). These cells have an unchanging karyotype and are not genetically unstable, unlike those established from induced pluripotent stem cells, and can differentiate into tissues of all lineages in culture and form teratomas in mice. (173)

These conditionally reprogrammed cells (CRCs) stopped proliferating and underwent terminal differentiation if either the ROCKi or the feeder cells were withdrawn, forming epithelial structures consistent with their heritage. This reprogramming is reversible, with normal keratinocyte cells developing a well-differentiated stratified squamous epithelium or normal tracheal cells placed in a fluid-air interface developing into a ciliated airway epithelium. Furthermore, these epithelia exhibited the correct pattern of differentiation specific protein expression throughout the cell layers. (173)

The mechanism appears to be a combination of feeder cells and Y-27632 provide two distinct activities that promote unrestricted cell proliferation: induction of telomerase and cytoskeletal remodelling and/or interference with the p16/Rb pathway.(172, 186, 187) In a recent study it was shown that the ROCKi (Y-

27632) specifically promotes proliferation via suppression of cell differentiation induced by the presence of calcium and serum (which usually rapidly induces terminal differentiation). But without J2 Feeder cells, Y-27632 alone did not induce conditional immortalisation, therefore Y-27632 inhibits terminal differentiation and promotes transient cell proliferation, but cannot bypass signals of senescence or crisis. (187)

Transwell culture and conditioned medium was used to demonstrate that direct physical contact between the irradiated feeder cells and primary cells is not required for the induction of conditional reprogramming and immortalization. This implies that the feeder cells release one or more diffusible factors that cooperate with Y-27632 to promote keratinocyte proliferation and survival. (187)

The irradiation of the feeder cells maintains metabolically activity, but induces growth arrest and eventual apoptosis. This irradiation induced growth arrest has been shown to be essential for the production and/or release of the factors that impart activity to conditioned medium. These factors are released only after a 24-hour delay after irradiation and continue to be released for the next 72 hours. The timing of this release correlates with the onset of radiation-induced apoptosis of the feeder cells, as evidenced by a dramatic increase in activity of caspases 3 and 7 activity after 24 hours. It is not strange that apoptotic factors should drive growth as it is well established that apoptotic cells release factors that promote proliferation in surrounding cells during wound healing and tissue regeneration in mice and other species(187).

1.4.2.2.2 (2) Spheroid formation from cell aggregates on ultra-low attachment plates

Following the suspension of disaggregated cells on ultra-low attachment plates, ROCKi was used to facilitate the establishment of spheroids from primary colon cancer, which expressed stem-cell markers and induced tumours in mice. (Table 2, column 2) There was tumorigenic diversity with different levels expression of the stem-cell marker CD44, and variants of the marker itself. Tumours with cells expressing high levels of CD44, were associated with increased sphere forming ability, expression of the activating form of B-catenin and elevated levels of glycolytic genes. On removal of ROCKi cellular differentiation occurred and, CD44-high cells differentiated into CD44-low cells. (188)

1.4.2.2.3 (3) Epithelial organoids

Toshiro Sato and Hans Clevers have published extensively on growing *in vitro* self-organizing miniature gut tissue which is architecturally and physiologically representative of normal intestinal stem cells(189). They regard the Wnt signalling as a pivotal requirement for intestinal crypt proliferation, and the Wnt activator R-spondin1 (which is a ligand for Lgr5 – which is a marker of intestinal stem cells) induces dramatic crypt hyperplasia *in vivo*. By growing normal primary intestinal epithelium in Wnt-agonistic R-spondin supplemented 3D culture they have shown that this tissue can grow into ever-expanding epithelial organoids that retain their original organ identity(189).

Their focus has mainly been on the replication of normal functional gut, however they have demonstrated that a modified version of their culture system can be used to culture malignant colonic and metaplastic Barrett's Epithelium.(171) (Table 3, column 3) However, normal oesophageal squamous epithelium

or oesophageal carcinoma growth wasn't reported despite this highly supplemented state, and the previously described 3D cell culture establishment of Barrett's observed by Sato et al (171) was limited proliferation, before growth arrest, despite the initial use of ROCKi to avoid anoikis. Organoids were passaged 1:5 every week, and the culture medium changed every 2 days. For passage, Organoids and Matrigel were mechanically disrupted before washing and resuspension in Matrigel with fresh culture medium.

Supplementary growth factors required for organoid culture: The key factors they describe are as follows: Wnt and R-spondin-1 was essential to activate Wnt signal in intestinal crypts. Epidermal growth factor (EGF) was required for signalling associated with intestinal proliferation. Addition of Noggin induced expansion of crypt numbers. Isolated intestinal cells undergo anoikis outside the normal tissue context so they proposed that Matrigel was used to support intestinal epithelial growth because laminin is enriched at the crypt bases. Using a combination of these four key growth factors allowed indefinite expansion of murine colonic crypts *in vitro*, and the addition of further (tissue specific) growth factors allowed normal human gut to proliferate also - in particular, Nicotinamide, A83-01 (an Alk 4/5/7 inhibitor) and SB202190 (a p38 inhibitor)). This cocktail of growth factors constituted the full 'Human Intestinal Stem Cell Culture' (HISC) Condition required for growth of normal human colonic epithelium.

Under the normal HISC culture conditions, normal oesophageal epithelium transiently proliferated for 1 week, but the organoids could not be passaged. Interestingly although they were unable to create cultures of the squamous oesophageal epithelium, they did have some limited success (20-30% of cases) establishing of

Barrett's Oesophagus, which required additional stimulation with Fibroblast Growth Factor (FGF). Addition of fibroblast growth factor 10 (100 ng/mL) to the HISC condition enabled the Barrett's epithelium organoids to form budding structures and significantly prolonged the culture duration (>3 months). For differentiation to form the representative Barrett's epithelium, the Nicotinamide and SB202190 are withdrawn and following the addition of the Notch inhibitor (DBZ) to the medium. This blocked proliferation and induced goblet cell differentiation.

1.4.2.2.4 (4) Suspension of crypt clusters on ultra-low attachment plates

Fresh colonic cancer tissue (briefly refrigerated overnight enabling tissue transfer following surgery) was used to produce spheroid cultures from crypts and cell clusters, suspended in media using specifically ultra-low attachment plates, with 80% success rate in the presence of 10umol/L ROCKi. (Table 2, column 4) The spheres were characterised to be of epithelial origin (IHC for EpCam and Cytokeratin) with differentiation characteristics (structure and goblet cells) similar to the patient's cancer. When the spheres were immobilised in matrigel, they grew into large complex colonies, forming a lumen – 'a property that can be used to identify cancer stem cells'. Time lapse photography and video showed a characteristic dynamic movement of cells within colonies, and that debris and dead cells continued to be extruded from the colonies as they grew (confirmed by fluorescence dye). They also performed some very limited drug testing without clinical correlation using routine colorectal chemotherapeutics such as 5-FU, showing that they could induce cell death using Presto Blue dye. They also used time lapse videos- colony size decreased and cell movement reduced by drugs - so necrotic material essentially static. (190)

Table 2. Summary of methods for establishing primary patient tissue				
	(1) Feeder layer co-culture	**(2) Spheroid formation from cell aggregates on ultra-low attachment plates**	**(3) Epithelial organoids**	**(4) Suspension of crypt clusters on ultra-low attachment plates**
What tissue	Fresh & cryopreserved tissue	Fresh tissue	Fresh surgical resection tissue and biopsies	Resectional tissue & biopsies, refrigerated overnight.
How disaggregated	Minced and digested (dispase, collagenase) and strained (70 uM)	Minced and digested (DNase I, collagenase) and strained (70 uM)	Minced and digested (dispase, collagenase). "After the digestion, tissue fragments were manually picked under the microscope"	Minced and then mechanically broken up by shaking in a bijou with glass beads & DMEM until media cloudy, and supernatant removed (to discard single cells). Then strained (250 uM), so that only loose cell clusters & intact crypts were used.

How established	Primary cells co-cultured with irradiated 3T3 J2 feeder layer in F-Media with supplementation. Growing cells separated with differential trypsinization and then dispersed in supplemented serum free media containing 2% matrigel, on-top of matrigel bed.	Primary cells seeded in supplemented Stempro Media on ultra-low attachment culture plates (corning) where they formed into colonic cancer spheroids made by aggregates of the exponentially growing cells. To passage, the spheroids were dissociated weekly with acutase into single cells, and re-plated where the growing cells again formed spheroids	Cells/tissue fragments counted and embedded in Matrigel and seeded into 48 well plates (1000 cells per 25uL Matrigel per well). Matrigel Polymerised and then overlaid with 250uL/well 'Human Intestinal Stem Cell Culture' (HISC) which is Base Media supplemented with growth factors particular to that tissue.	Pellet re-suspended in 'Primary Medium' with supplementation and plated on a suspension culture plate. After 7 days the uncontaminated wells were pooled into ultra-low attachment flask. Media changed every 4 days from this point onwards. 'The primary cells formed into colonic cancer spheroids'
Media	F.Media (F-12 /DMEM, FBS, hydrocortisone, insulin, cholera toxin, adenine)	StemPro hESC SFM (human embryonic stem cell, and serum & feeder-free medium). An artificial serum replacement media for nutrition and stimulation	Base Media (DMEM/F12, HEPES, GlutaMAX-I, B27, NAC) optimised to HISC media with universal and tissue specific additions.	Excel 620 low protein medium with 2% StemPro hESC supplement & 2-mercaptoethanol (1 mM)

Supplemental Growth Factors	ROCKi (10 umol/L), EGF (10 ng/ml)	ROCKi (20-50 μmol/L), bFGF (8 ng/ml)	ROCKi (10 umol/L), EGF, Nicotinamide (facultative), SB202190 (p38 inhibitor), noggin, R-spondin1, Wnt-3A, Gastrin, TGFβi A-83-01 Barrett's also needed FGF-10 (100ng/ml).	ROCKi (10 μM), EGF (10 ng/ml), Fibroblast growth factor (FGF-10) (100 ng/mL), Endothelin 3 (30 μM)
Success of establishment	50% from gut (with serum) 100% from breast, lung, prostate	66% (10 of 15) established, and maintained for 1 month 33% (5) could be maintained for >6 months.	Colon Cancer: 50–90% Barrett's : 20-30% Normal oesophageal squamous epithelium unsuccessful	80% growing in culture for >1 month. Colony doubling time = 2–12 weeks.
How measured in 3D	Colony counts	Sphere & colony counts	Colony counts & passages	Colony counts & viability assays

1.4.2.2.5 Conclusions

All four groups use a different methodology (Table 2) but achieve the same purpose, successfully expanding primary cells from patient tissue. They all show CSC markers are present following the *ex vivo* establishment, and (where examined) demonstrate the same karyotype throughout passages and environments, with similar gene expression, suggesting that these cells are not transformed (as seen in hTERT immortalisation) but are resisting environmental and cellular cues inducing anoikis and apoptosis. However, despite the success reported, none of the groups have managed to culture malignant OG tissue.

Although different methodology and model systems are reported, there are similarities between the approaches, for example all methods use induction by ROCKi. Also, two of the methods use a similar model: (2) 'Spheroid formation from cell aggregates' and (4) 'Suspension of crypt clusters' use the ultra-low attachment plates to prevent cell attachment and suspend the cells in growth media. Whilst it is correct to say that these primary cells are subsequently growing in 3D as aggregates, they are not growing in a 3D tissue microenvironment where the cells are growing in contact in 3D with biologically active structures around them as occurs with matrigel/BME.

It would be ideal to replicate the tumour 3D tissue microenvironment, so the organoid and feeder cell (with its later transfer to matrigel following culture establishment) methods are of most interest. However, there are marked differences between these two methods and models systems, with both intrinsic advantages and disadvantages. These are best summarised in a column format for direct comparison.

Organoids	**Feeder layer**
Direct to 3D in matrigel	2D on feeder layer initially for establishment
Initial growth and establishment difficult	High initial establishment rates reported
Extensive supplementation (Wnt /R-spondin) ?relevant to oesophagus	Chemical re-programming with ROCKi throughout
Slow to grow and passage	Rapid expansion in potentially clinically applicable timescale
Passaging and subsequent re-feeding challenging with particular kit needed	Ease of setting up assay on feeder layer of cells with readily available kit.
Phenotypic and genetic stability	Phenotypic and genetic stability
Clonal representation	Unclear if clonal selection with loss of original heterogeneous
Variable seeding density and organoid size difficult for accurate drug assays	Reliable seeding of cells ion 3D for reproducible drug assays

The obvious attractions of the organoid system going is going straight to 3D, however despite the relative complexity of the method, extensive supplementation and their previous exhaustive but ultimately unsuccessful efforts, they were unable establish oesophageal cancer tissue in culture. The key advantage from using the feeder layer system is being able to provide mesenchymal support, re-establishing the important cell-

cell interactions which as previously detailed (Introduction 1.3) have such an effect on cell behaviour.

I have therefore taken the pragmatic decision to explore the Feeder layer system, as this is simpler, has a reported higher establishment rate, and the initial goal (as yet unachieved by any other group) is to establish cultures of oesophageal cancer *in vitro*. It will also allow restoring the stromal cell component of the TME. However, I will be flexible to modify the method to incorporate aspects for the organoid method as possible to try and achieve a close-to-patient environment as possible to replicate growth in a 3D-tumour microenvironment.

1.4.3 Cell Culture in Two and Three Dimensions

The applicability of the traditional two dimensional (2D) cell culture methods used to grow tumour cells in flat plastic flasks have been widely questioned, and much of the preclinical modelling focus has changed to three dimensional (3D) culture technologies as they have become more available with improved physiological relevance. Whilst 3D cell culture is now used widely in academia, industry still continues to rely on 2D culture methods until 3D methods can provide a reproducible, biological relevant, high throughput 3D assay at an acceptable cost. This has resulted in an astonishing number of different 3D culture methods, each with their own experimental use, advantages and restrictions.

To appreciate the purpose and design of the 3D cell culture methods, one must first understand the limitations posed by traditional 2D preclinical tumour models. Growing cells on flat plastic 2D plates in monocultures allows relatively easy cell maintenance and growth. It keeps the tumour cells being studied free from contamination and competing growth by other cell types allowing expansion and focused study and directed DNA

and protein analysis. However, this is quite different from the *in vivo* tumour cells which are part of a complex, malleable, 3D tumour microenvironment (TME). This TME consists of an extra-cellular matrix (ECM) and other cell types, resulting in continuous dynamic interactions between the tumour, ECM and its own stromal component, and interactions with host tissues, angiogenesis and the host immune system. These complex interactions (which are not present in simple 2D tissue culture) have been shown to have an impact on invasive cancer growth(118), metastasis(117) and drug resistance(123). Importantly, it is this dynamic interplay between the malignant epithelial cells and the TME which implicates the TME as one of the dominant forces in cancers exhibiting multi-drug resistance (122).

1.4.3.1 Xenograft Models

Tumour xenografts in immunocompromised animals have been refined over many years, and now preferentially use primary patient tumour material rather than cell lines. These are ideally grown at the anatomical site of disease resulting in orthotopic patient-derived xenograft (PDX) models. Whilst PDXs provide an excellent model of close-to-patient tumour epithelial cells and a 3D TME, it is not a humanised environment and cells of murine origin swiftly replace the human stromal component of the tumour. For example, when the PDX stroma was examined mechanistically rather than genomically, it can be shown that key receptor tyrosine kinase receptors in the PDX TME such as the cMET receptor is not cross species compatible and the pathway is inactive i.e. Murine stromal HGF does not activate human C-Met in xenografted tumours (191). Therefore, despite the apparent genetic similarity of the PDX, the TME interactions are not always replicated and performing detailed drug efficacy studies in mice may be misleading.

As well as the issue with inter-species compatibility, and aside from the animal husbandry, working with animal models is practically complex due to the tissue being embedded within the flank of a mouse, the relevant cellular interactions are difficult to study in a controlled fashion. Xenograft tumour models also require relatively large amounts of tumour material to be implanted to increase the likelihood of tumour to establish. There is an extended growth phase of weeks to months and the resultant xenografted tumour cannot be tested simultaneously with different chemotherapeutic agents in different combinations, at different concentrations. This costly and time consuming approach can be considered a clumsy screening method, and makes it demanding to follow the ethical principles for animal experimentation (reduce, replace, refine) (192).

1.4.3.2 In Vitro 3D Models

Many 3D cell culture methods have aimed to replicate the *in vivo* tumour microenvironment (TME) by humanising the 3D models, thus avoiding some the problems associated with the 3D xenografted model. These ever evolving 3D pre-clinical tumour models have already shown that tumour cell behaviour is intimately influenced by its surrounding micro-environment (193), giving rise to altered growth patterns (102), metabolic activity and drug efficacy (194), both in the tumour cells and in a reciprocal fashion in the surrounding co-cultured stromal cells (195), and are therefore thought to represent the current best method we have at our disposal to replicate and study cancer *ex vivo*, and guide subsequent drug development.

3D cell culture models have developed significantly since the early demonstrations of 3D cellular structure formations and interactions pioneered by Mina Bissell (196-198). Methods have now been adapted to a wide range of cell types, organ systems,

and experimental models to study different aspect of cancer biology, from invasion assays and angiogenesis models, to collagen-implanted spheroids for drug discovery and organotypic human skin reconstructs for testing cosmetics (199).

There are currently a large and diverse number of 3D *in vitro* cell culture methods, models and products on the market, but they can be broadly classified as either scaffold free or using 3D scaffold (natural or synthetic). Scaffold-free techniques are mainly based around generating spheroids using multiple techniques including the hanging drop method which can be scaled to 384 well plates (200), micro-beads in bio-reactors, honeycombed plates (201) and nano-imprinted well plates (202).

1.4.3.2.1 Spheroids

Spheroids have been in existence since the 1970s as 'tumour cell aggregates' when used to assess the mechanism and action of chemotherapy and radiotherapy. However, with the advent of 3D culture techniques their use has become more prominent again in recent years (203), especially as they can mimic *in vivo* solid tumour structures with hypoxic areas and altered growth patterns, and provide a similar TME, increased intracellular signalling and phenotypic activity (176).

There have been many varied methods used to make representative tumour spheroids including:

- gel/matrix-based culture (102, 185),
- liquid on agar (204, 205),
- polyHEMA coated plates (206, 207),
- low binding plates (208, 209),
- spontaneous aggregation (210),
- hanging drops (200, 211),

- polymeric scaffolds (212, 213),
- rotary cell culture systems(214, 215),
- bioreactors (216, 217).

Each of these methods has its pros and cons (218, 219), and there is no single reproducible method that is accepted for standardised use in the study of tumours in a representative 3D tumour microenvironment.

Despite tumour spheroids modelling a pseudo-3D microenvironment, the spheroids have uneven sizes, and constructs frequently have areas where some tumour cells grow and others undergo apoptosis in an unpredictable fashion. Spheroids thus remain an attractive research tool for studying basic cancer biology, but producing identical standardised spheroids remains the challenge that precludes their use in directly comparative drug studies. However, as technology has developed, many of the spheroid forming and culturing techniques have become automated to develop 'high-through-put' techniques that are more reliable and reproducible and therefore of more practical use to the pharmaceutical industry in cancer research and the screening of new chemotherapy agents (203).

1.4.3.2.2 Scaffolds

Scaffold-based 3D cultures are formed by either seeding the cells onto a preformed 3D acellular matrix like AlgiMatrix or polyethylene glycol (PEG), or dispersing the cells in a liquid which then polymerises to form a scaffold such as Matrigel or QGel.

The inert mechanical structure of natural (e.g. cellulose) or synthetic scaffolds (e.g. PEG) can be manipulated to mimic the tumour architecture and then functionalised with binding sites,

which can be altered to suit the tumour indication and also allow assessment of potential targets for stimulation and binding (220). However, assay analysis can be fraught with problems like potential interactions with screening compounds and dyes, or great difficulty in swift cell recovery for RNA and protein analysis (221). Other synthetic scaffolds such as agarose have been miniaturized within a micro-fluidic cell culture chips which can then be perfused by integrated pneumatic micro-pumps, to reproduce the dynamic environment seen *in vivo* and provide the key stimulus this provides driving cell functionality (222). Other sub-centimetre models have used microsphere or bead encapsulates with microliter sizes on cell-based gel microarrays or 3-D pendant style gel cultures with some success (223). However, despite the impressive manufacturing micro-precision providing reproducibility and versatile properties, these artificial scaffolds still require addition of some extra-cellular matrix (ECM) like material to allow binding and microenvironment interactions. The natural proteins scaffolds such as collagen I or fibrin already have some endogenous cell adhesion sites, but before use in 3D, the models require extensive processing (158).

1.4.3.2.3 Biological Hydrogels

Biological liquid hydrogels have been extensively used, such as Collagen I mimicking the ECM and Matrigel as a recombinant Basement Membrane Gel. These methods are some of the most popular and generally accepted 3D models, as many cell types have been shown to exhibit tissue specific architecture when grown in these gels. However, caution must be exercised when working with these gels for a number of reasons.

Firstly, regarding basement membrane-type products, there is a presumption that they are comparable to native ECM, but as they are Murine in origin (from the Englebreth-Holm-Swarm

mouse sarcoma) their contents can be poorly defined, varying from batch to batch, and containing different extracellular matrix components and growth factors (224). Any inter-batch variation could lead to different experimental outcomes.

Secondly, the use of single matrix components (e.g. collagen) or a single adhesion ligand (e.g. arginine–glutamate–aspartic acid peptide) may not act as a functional equivalent to the *in vivo* ECM which will consist of many proteins.

Thirdly, the manipulation of the natural proteins through the manufacturing process that will alter their conformation, structure, ligand binding sites etc. and reduce their functional similarity to the native *in vivo* ECM.

Fourthly, biological matrixes can suffer from the difficulty in subsequent cell extraction for passage and RNA analysis, and can also face other matrix specific problems such auto-fluorescence of collagenous scaffolds (158).

1.4.3.2.4 Extra Cellular Matrix

Studies in 3D models have found ECM stiffness as a regulator of various tissue parameters in cancer progression, and so the tensile strength of the TME is thought to have key (and frequently underappreciated) influence. The changes in cellular phenotypes and signalling pathways activated by biomechanical cues may also be distinct from those activated by soluble factors and stromal cells (219).

Under normal physiological conditions, ECM derived from different tissues exhibits its own unique tissue architectures, mechanical properties (e.g. elastic energies, moduli), protein compositions, and molecular complexities (225). These properties can be modulated as a function of normal processes such as wound healing, or via pathological manifestations such

as cancer induction (226). Hence, it seems that creative focus in this area should be more on producing easily-modified matrix components that can be mixed and matched to closely re-create native biochemistry and matrix rigidity, rather than pursuing a universal master ECM mix. In any case, care should be taken in understanding the culture model, the validation processes, and the advantages and limitations prior to a model's use in drug development, toxicology, and other related applied research (158).

1.4.3.3 Specialised vs generalised applications of 3D models

Many of the 3D culture systems developed by research groups are for highly specialised applications that focus on investigating and answering specific scientific questions. They are therefore frequently complex to create, and variable to maintain, in order to achieve their exact biological relevance(227). However, the pharmaceutical industry ideally requires a simple, reproducible and standardised HTS assay that could be universally applied for drug screening and development, providing reliable results and automation, all at a reasonable expense. Combining all the goals of academia and industry is unlikely to be universally achieved. Also, this may not be a commendable goal: the significant commercial and academic efforts seek to create a "one-size-fits-all" matrix accommodating any cell type or cell line applicable to many culture surfaces and cell types, may be at risk of ignoring the development of organ-specific or pathology-specific models that precisely recapitulate and promote clinically cell pathways. However, with technology advancing, a suitable model may be found that can be adapted to fulfil different research and development goals (218).

One potential future method that may bridge these barriers and provide a universal platform for study, attempting to reproduce *in vitro* the structures and functions of the whole organ, and faithfully replicate the *in vivo* situation, is the ambitious 'organs-on-chips' project undertaken at the Wyss Institute. They use micro engineered biomimetic systems containing microfluidic channels lined by living human cells, which replicate key functional units of living organs to reconstitute integrated human organ-level pathophysiology *in vitro*. These cell-culture microenvironments support both tissue differentiation and recapitulate the tissue–tissue interfaces, spatiotemporal chemical gradients, and mechanical microenvironments of living organs. These micro devices can be used to study normal human physiology in an organ-specific context, create *in vitro* models of human disease, and potentially test the efficacy and toxicity of drugs and chemicals.(228, 229).

1.4.3.4 Using 3D models for chemotherapeutic assays

Spheroid formation with the epithelial cells (for example using a hanging drop technique) prior to 3D implantation within a matrix is an attractive technique and is the frequent method used by other groups studying multi-cell aggregate responses to chemotherapeutics (230). However, within the bounds of our study goals, this spheroid method of cluster formation wouldn't be helpful for a number of reasons. Firstly, it is unclear whether the particular cells within the spheroid would have come together naturally *in vivo*. Secondly, with the different sized clusters, the larger cell spheroids will have an altered exposure to any chemotherapy due to altered drug penetrance and this will affect drug response. Thirdly, if the cells are clumped together unnaturally in a spheroid, then a proportion of the cells making up the spheroid maybe dead and therefore a measure of change

in the spheroid size will be an unrealistic measure of growth of the assay. Fourthly, the spheroids by their very nature will be of individual and non-reproducible sizes. Thus it will be impossible to objectively quantify and compare different conditions in the assay, if the size and subsequent growth of the spheroid cells in the assay are all different.

Other groups attempting to establish primary cells in 3D culture have tried to avoid these problems by using cell aggregates (very small incompletely dissociated multi-cellular tissue pieces). However, these can face similar problems with both different sizes of the aggregates in each well and different numbers of aggregates per well. This can similarly occur when passaging spheroids and organoids, where following attempted initial dissociation with accutase, the Matrigel is manually broken up with pipette tip, fragmenting the existing organoids, rather than splitting into single cells. This results in non-reproducible fragments resulting in uneven seeding and growth, where it is unclear which are dead or alive. Therefore, although these methods have resulted in successfully reported growth of these primary cells in 3D, these methods are not easily transferrable for drug testing which needs similar size cell clusters and the same number per well for accurate and reproducible responses on being challenged with chemotherapeutics in drug testing assays.

Ideally by seeding a known and duplicated number of individual cells in multiple wells these can then grow into multi-cell clusters, formed with the different cells in the position and interactions which they choose and growing in the proportions they require. Assuming a similar growth rate, these clusters should be of an equivalent size as they have developed from

single cells over the same time period, enabling a repeated and uniform assay for reliable chemotherapeutic response evaluation.

1.5 OG Cancer Models for Chemotherapeutic Evaluation

There is a persistently high (and up to 95%) failure rate to bring promising drugs from the laboratory into successful clinical practice (199). Although cancer cell lines have been used to study many aspects of cancer biology, and historically provided much of the basic cell biology data for drug discovery and development studies, their use in studies with direct application to clinical cancer research outcomes is questionable.

Recent genetic analysis showed that the classically used oesophageal adenocarcinoma cell line, OE33, does not bear close resemblance to a spectrum of freshly obtained tumour samples from patients(231). Indeed, studies have shown that the multi-drug resistance genetic transcriptome of cancer cell lines, grown either *in vitro* or *in vivo*, bear more resemblance to each other, regardless of the tissue of origin, than to the fresh comparative clinical tumour samples that they meant to represent. This emphasizes the importance of using of primary close-to-patient tissue in tumour models that can more closely represent the *in vivo* tumour. (147)

Despite the overwhelming evidence that *in vitro* three-dimensional tumour cell cultures more accurately reflect the complex *in vivo* microenvironment than simple two-dimensional cell monolayers, with respect to gene expression profiles, signalling pathway activity and drug sensitivity (232), there is still a need for further development and refinement for more accurate 3D cell models of disease (233), with particular reference to using close-to-patient tumour cells.

To accurately perform mechanistic studies, to assess the causes of chemotherapy drug resistance and potential targets to exploit, and run high throughput drug screening assays, the 3D model should be as patient relevant as possible and use close-to-

patient epithelial tissue, as well as the well key micro-environmental components of using a humanised 3D structure and stromal support cells.

A number of different OG cancer 3D models have been proposed in the attempt to model the tumour microenvironment, in a more reproducible and patient relevant fashion.

1.5.1 OG cancer spheroid models

Although there have been significant advances in establishment and analysis of 3D tumour spheroid-based functional assays (232) technical difficulties still remain with truly representative multicellular tumour spheroid formation, and the resultant automated imaging and screening, data collection and analysis have prevented a robust miniaturised spheroid model becoming standardised for target validation and high throughput screening. (230)

1.5.2 OG cancer organotypic models

Three-dimensional organotypic models of the normal oesophagus using cell lines (HET-1A; the most commonly used normal oesophageal squamous cell line) have been shown to be un-representative (234), as the cells do not have the characteristics of normal oesophageal squamous cells. However, models using normal primary oesophageal squamous cells and fibroblasts have been successful (234, 235). Organotypic models for studying oesophageal cancer using both cell lines (OE21 & 19) (234)and hTert immortalised primary tumour tissue(175) have been more successful. These 3D organotypic models have provided valuable insights into the tumour stroma interactions in particular, with activation of fibroblast dependant tumour development, invasion and differentiation (106, 236, 237). However, these models are complex, time consuming, non-passageable and low throughput, and utilise genetically altered primary patient material.

1.5.3 OG cancer tumour xenograft models

There is a paucity of PDX model use in OAC, possibly due to the difficulty engrafting patient samples with best reports of 32%. However, once established, they have been shown to maintain similar histology and morphological characteristics even after multiple passaging (181). This time-consuming, lengthy and high intensity methodology doesn't lend itself well to complex multi-variable studies or high throughput drug screening; however, it can be used for specific drug targeting efficacy studies for developed drugs with known targets. (182)

1.5.4 OG cancer clonogenic models

The clonogenic approach was an early attempt to produce a high throughput 3D patient relevant drug screen with established PDX cells, embedding the cells in agar and measuring their growth into cancer clusters. Although the initial results were reported as having predictive value in the chemo-sensitivity testing of standard and experimental anticancer drugs, the assay did not provide a biologically active tumour microenvironment or any tumour stroma (205). And thus despite a later adaptation to include co-culture with a 2D seeded stromal layer, (204) its generalised applicability remained in question. Other attempts at assessing chemotherapeutic activity in 3D models with close-to-patient tissue assessed the survival of fresh tumour fragments embedded in the synthetic matrix polyHEMA, without a tumour stromal component or humanised microenvironment. However, where the tumour fragments did reliably culture, the assay was not predictive (206).

1.5.5 The Nottingham 3D-Tissue Growth Assay

The Nottingham three dimensional tissue growth assay (3D-TGA) uses multicellular co-cultures with a dispersion of tumour cells within a Matrigel scaffold. It has been used to study cellular

interactions within the 3D microenvironment, their growth patterns and response to chemotherapy. The model (originally described by Sasser et al (102)) has been developed in the Division of Preclinical Oncology (University of Nottingham) whereby patient tumour material is established and expanded as PDX. These close-to-patient cancer cells from the PDX are then grown in the 3D-TGA allowing multi-factorial pharmacological testing.(238)

The cancer cells are grown in the 3D-TGA in the presence of extracellular matrix and human mesenchymal stromal support, restoring paracrine interactions between tumour and stroma, and allows the cells to form the basic 'cell-cell' and 'cell-matrix' interactions that occur *in vivo* and are known to influence drug resistance. (102, 239). Importantly the assay only requires a limited amount of tumour material from the PDX to provide sufficient close-to-patient cells for pharmacological testing in the 3D-TGA, and by scaling to a 384 well plate allows numerous drugs and combinations to be tested simultaneously, unlike animal models which take weeks-months and require a large expansion of tumour material for implantation. Importantly this assay mimicking the tumour microenvironment is reproducible, reliably imaged and provides results that can be compared between assays and back to patients. So although it is not automated, it can be used to perform high-content drug screening (239). This is not a complex organotypic model and so could be criticised for not accurately representing the known layered tissue architecture of the oesophagus, or reproducing its air / fluid component, or the flexing of musculature of the gut tube providing a mixed tissue tension. However, these extra 3D complexities may not have an effect on the chemo-responsiveness of the primary OG tumour cells themselves. So although this 3D-TGA model may not be ideal for investigating

complex cellular interactions, carcinogenesis, invasion & metastasis; it is specifically designed to be more reliable and can reproducibly grow tumour cells, from different patients, and their response to toxic drugs can be quantified and compared in a setting incorporating elements of the TME which influence drug chemotherapy sensitivity and is therefore hypothesised to be more clinically predictive.

The Ex Vivo Cancer Pharmacology (EVPC), Division of Cancer and Stem Cells, University of Nottingham has built up extensive expertise in the application of 3D *in vitro* models for studying prostate, lung and colorectal cancer. By using early passage xenografted patient tumours it has already shown the important role of tumour stroma in drug sensitivity and the role it can in play in evaluating emerging drugs that are designed to specifically target tumours with specific mutations. For example it has shown that lung cancers with EGF mutation can be demonstrated to have a mutation-dependent sensitivity to targeted agents such as Erlotinib.(238)

1.5.6 Summary of OG cancer models

Multiple different methods of 3D spheroid culture, organotypic modelling and animal xenografts have been attempted to study oesophageal cancer. However, all of these models have critical differences with the *in vivo* disease and none provides an ideal model system for completely reflecting the complex 3D structure of the disease and its tumour–organ components in their entirety, whilst also providing a practical system for evaluation and study of a particular tumour characteristic or functional mechanism (174). The Nottingham 3D-TGA is a significant step forward in modelling the tumour microenvironment and chemo-therapeutic assessment; however, the tumour material required for the assay comes from a PDX which are immensely

challenging to establish (if at all) pre-chemotherapy, as the volume of tissue obtained by an endoscopic biopsy is tiny (and therefore the PDX establishment rate is negligible). I therefore focussed on a modified *in vitro* establishment, passage and expansion approach that could provide pre-chemotherapy close-to-patient tumour cells from the tiny endoscopic biopsies, for subsequent drug screening in the 3D-TGA.

1.6 *Ex vivo* chemotherapy drug evaluation

1.6.1 Clinical chemotherapy regimen

The clinically administered chemotherapy regimen comprises of 3 cycles of anthracycline, platinum and fluoropyrimidine, following the evidence from 2006 MAGIC trial, where patients were administered an ECF regimen - Epirubicin, Cisplatin and infusional 5-Fluorouracil. A complementary follow-on trial (56) showed that infusional 5-Fluorouracil can be safely substituted for an oral Fluorouracil pro-drug: Capecitabine (240). Given that both regimens have the same gross clinical efficacy (56), and are interchanged clinically, for purposes of clarity they will be referred to collectively as ECF chemotherapy in this study. The doses of this standard of care (SOC) chemotherapy consists of Epirubicin: 50mg/m^2 on Day 1 of each cycle only (i.e. every 21 days), Cisplatin: 60mg/m^2 on day 1 of each cycle only (i.e. every 21 days), and either Capecitabine: 625mg /m^2 twice daily tablets for 21 days, or 5 Fluorouracil: 200 mg/m^2/Day as a continuous intravenous infusion every day for 21 days/3 weeks.(4)

1.6.2 The challenge of measuring delivered drug concentrations in the dynamic patient *in vivo* state

It is widely acknowledged that the typical methods used to calculate the dose at which chemotherapy drugs are administered and monitored are not wholly accurate. The standardised method of drug dosage is based on body surface area (BSA), which is a mathematical formula based on the patient's height and weight, rather than a direct measurement of body mass. In fact the formula was originally developed from a 1916 study with only 9 human subjects to translate the equivalent dose from lab animals into humans(241). This dosage by BSA is widely accepted to be flawed, especially with the change in the body morphology of current society, however no

other functional or widely applicable method has been developed for universal use (242). There is a persistent variation up to 10 fold in the systemic chemotherapy concentration in difference patients dosed using the BSA formula.(242, 243)

This is not only because body morphology has changed with the trend towards obesity, but importantly because drug absorption and clearance are influenced by multiple factors such as age, gender, metabolism, disease state, organ function, drug-drug interactions, and genetics (244-246). This results in drug delivery only be estimated from population studies, and individualised patient studies have inevitably then shown that some patients being overdosed and some under-dosed (247).

The measurement of drug delivery and systemic chemotherapy concentration is measured by two pharmacokinetic parameters: the peak concentration (CMax) achieved in that specified area of the body and the Area Under the Curve (AUC) which represents the total drug exposure over time. The plasma CMax and AUC will be affected by patient age, metabolism, genetics and drug interactions, so are not universal across a given patient population. The CMax is usually employed to help understand the peak serum as this frequently relates to level of toxicity and the severity of the side effects experienced. Due to the metabolism and elimination of any drug, the recorded CMax will not represent the total drug exposure over time following administration (248). As a marker of total drug exposure, the AUC is generally considered to represent a better marker of chemotherapy drug dose received, however the pharmacodynamics of drug elimination are rarely linear, half-lives frequently vary between patients, and for most agents it is unclear below what threshold of concentration the drug stops becoming clinically efficacious. Therefore, although the AUC is a

useful measure of patient's overall drug exposure following dosing, it is not an accurate measure of the relevant concentration of chemo-active dosage the patient is being exposed to. Optimising plasma concentrations using these two measures is important to try and maximise drug delivery and survival outcomes whilst minimising the inevitable bystander organ toxicity(248). However, this further raises the question of the relevance of plasma concentration recordings when trying to understand the direct chemocidal effects on the tumour and the drug concentration within the tumour itself. Researchers have studied the intra-tumoural concentrations of chemotherapy drugs using micro-dialysis catheters, which have resulted in surprising findings of concentrations of drug both above and below the corresponding AUC plasma concentration (249). However, these studies are not numerous, have small numbers of participants and are often performed in different tumour tissue types and with markedly different dosing regimens than those for which the drug is used than OG cancer, and so it is difficult to know the relevance and significance of these reported concentrations given they are a snap shot of a few patients only and from a tissue where diffusing concentrations will be different from OG cancer.

1.6.3 The challenges of comparing population drug pharmacokinetics with static *ex vivo* cultures

Given the difficulty in obtaining an absolute figure for the delivered drug concentration that is representative across the patient population, pragmatism and caution must be employed when comparing the standard cytotoxic dose delivered between the two scenarios of dynamic *in vivo* patient tissue and static *ex vivo* 3D-cultures. To enable comparison there is a need to use an approximated but consistent measure that can be used between the two scenarios as a proxy measure of the concentration of chemo-active dosage. Given the lack of published data pertaining

to the intra-tumoural drug concentrations seen in OG cancer, the use of the intra-tumoural dose as a proxy measure for *ex vivo* equivalence is impractical.

If the AUC of total patient drug exposure was used for the *ex vivo* assays then the whole equivalent dosage concentrated within the shortened assay period would be consistently incomparably high, killing all living cells present, and resulting in all cancers declared sensitive to these disproportionately colossal levels of chemotherapeutic drugs.

The CMax is a reflection of the peak serum concentration of the drug and therefore the highest concentration that can be delivered to the tumour in the patient. Therefore when translated into the static *ex vivo* assay, although the CMax is higher than what would be consistently experienced *in vivo,* it would represent an accurate threshold above which any remaining *ex vivo* live tumour cells could be considered resistant, and directly comparable to the *in vivo* scenario.

For the purpose of this study the mean peak serum of the chemotherapy drugs will be sought from published pharmacodynamics studies taking into account the individual drugs different regimens, dosages, methods of delivery and half-lives. There will be an effort to match as closely as possible the published pharmacology data from regimens similar to that administered as the clinical standard for OG cancer. The CMax will be used as proxy value to definitively identify resistant tumours but below that there is a need to investigate the true correlation of *ex vivo* sensitivity to clinical response.

1.6.4 Epirubicin

Epirubicin is an anthracycline drug. Anthracyclines are anti-cancer compounds that were originally derived from Streptomyces and were established in the 1960s. The original anthracycline drugs e.g. doxorubicin, had dose dependent cardiotoxicity, and so analogues like epirubicin with lower toxicity were later developed.

Anthracyclines have multiple reported mechanisms of action: Intercalating between base pairs preventing DNA and RNA synthesis thus preventing replication; Generation of free radicals which cause damage to protein, cell membrane and DNA; Disruption of the histone release from chromatin stopping the DNA damage mechanisms; Inhibition of the enzyme topoisomerase II, stopping the unravelling of DNA and therefore blocking DNA transcription.

Epirubicin can be used against breast and ovarian cancer, gastric cancer, lung cancer and lymphomas. Both haematological malignancies and solid tumours can demonstrate primary and acquired resistance to anthracyclines.

Whilst many mechanisms for anathracycline resistance have been proposed, only the classic multidrug resistance (MDR) pump has been shown to contribute to resistance in clinical conditions, whereas evidence for the other mechanisms of resistance is still missing (250). This MDR mechanism (from the MDR-1 gene) is a P-glycoprotein transmembrane drug efflux pump that can extrude a wide range of anticancer drugs (251).

Conversely the thioredoxin protein could potentially be used as a biomarker for response to anthracycline treated OG cancer. Defective intra-cellular redox buffering systems are thought to play a role in the effectiveness of anticancer agents such as the

anthracyclines and platinum agents which are used in OG cancer. Drug effectiveness can therefore be affected by low levels of the redox protein, thioredoxin interacting protein, in its capacity buffering the effects the reactive oxygen species generated by these chemotherapeutics. In OG cancer exposed to chemotherapy, high thioredoxin interacting protein expression was an independent marker for improved disease specific survival, and particularly in anthracycline-based regimes (252).

As a mono-therapy it is administered at a dose of 60–90 mg/m^2, and at 50mg/m^2 as part of combination chemotherapy. Epirubicin is metabolised in the liver and excreted in a loosely dose related linear fashion (253). Despite its bolus administration over 3-5 minutes it has been reported with an up to five fold variation in subsequent drug exposure between individuals (254) and a mismatch between plasma concentration and intra-tumoural concentration(255, 256). In a study of patients undergoing surgery, for the administered dose of 20mg/m^2 the intra-tumoural, metastases and LN concentrations (~2.5 μM) were double the recorded plasma concentrations(249).

Combined pharmacokinetic studies of >150 patients, administering between 60-90 mg/m^2 of Epirubicin in each regimen, have recorded a close variation of max plasma concentrations following similar drug administration, of which the mean CMax (mean peak serum) Epirubicin is 4.5 μM. (254, 255, 257-259)

1.6.5 Cisplatin

Cisplatin is the original and most common of the platinum-based chemotherapy drugs, it was first synthesised in 1845, but its anti-cancer effects only realised in the 1960s by Rosenberg and

colleagues, before being marketed as Platinol® by Bristol-Myers Squibb.

The platinum complexes react *in vivo* in a process termed aquation where the two chloride ligands are slowly displaced by water. It subsequently binds to and causes crosslinking of DNA. This mode of action by crosslinking the purine bases on the DNA; interfers with DNA repair mechanisms, causing DNA damage, and subsequently inducing apoptosis in cancer cells.

Cisplatin is a highly effective drug and widely used against many solid malignancies including lung, ovarian, head and neck, breast, gastric and brain cancer. However, it is usually used in combination therapy with other chemotherapeutics as despite initial responsiveness, patient relapse is common with the cancer becoming resistant. Cisplatin resistance mechanisms proposed include changes in cellular uptake, drug efflux, increased detoxification, inhibition of apoptosis and DNA repair (99, 260).

It is administered intravenously as short-term infusion with normal saline and forced diuresis in an attempt to minimise the common nephrotoxic side effects seen by free radical species in the kidney during excretion.(261)

After intravenous administration Cisplatin quickly distributes across all tissues, with 90% of Cisplatin bound to plasma proteins. The remaining filterable, non-protein bound Cisplatin has a short biphasic half-life of 20 and 50 minutes. The elimination of the total quantity of platinum has tri-phasic half-lives of 14 minutes, and 4.6 hours and 53 days respectively. (261)

Cisplatin is frequently given as part of a combination regimen, administered as recurrent doses of 20mg/m^2 or single doses of up to 150mg/m^2 are given according to the cancer type and the

chemotherapy regime. Intra-tumoural concentrations are not grossly dissimilar to the administered plasma concentration, which reflects its wide tissue distribution.(262)

Studies into Cisplatin pharmacokinetics from doses between 25mg/m^2 and 150mg/m^2 have a similar CMax following their different regimen administrations with a resultant mean CMax (mean peak serum) Cisplatin of 4.31 μM (262-264). Interestingly in other targeted studies investigating intra-tumoural concentration of Cisplatin the mean measured intra-tumoural CMax is comparable at 3.9 μM. (264-266)

1.6.6 5-Fluorouracil

5-fluorouracil (5-FU) was patented in 1956 has been in use in clinical oncology since the 1970s, and is still the cornerstone of many gastrointestinal chemotherapy regimens. Fluorouracil can be used topically for actinic keratosis and basal cell carcinoma and systemically for breast, colorectal, oesophageal, gastric, pancreatic and skin cancer.

It is a pyrimidine analogue. It works through irreversible inhibition of the thymidylate synthase enzyme blocking synthesis of thymidine, so rapidly dividing cells die due to acute thymine deficiency(267). Modulation strategies, such as co-treatment with leucovorin and methotrexate, have been developed to increase the anticancer activity of 5-FU.

5-FU an S-phase-specific drug, so is predominantly effective in cycling cells, which represent only a small proportion of the tumour cell mass at any point in time (267). However, it only has a short half-life of 10 minutes and therefore, administration in clinical practice logically developed from delivery as a bolus injection into administering the drug as an infusion(268). Despite a relative reduction in the infusional drug dose to decease the

toxicity profile, administering 5-FU as an infusional therapy resulted in increased tumour response and significantly increased survival rates.(269)

Even as an infusion, 5-FU has marked variability in individual patient pharmacokinetic dose availability and therefore an identical dose maybe therapeutic in one patient and sub-therapeutic or toxic in another(270). This problem is compounded by the inaccuracy of dosing based on the current standard BSA formula. The limitations of BSA dosing and risks of chemo-toxicity from overdosing results in many patients receiving a sub-therapeutic dose (271). In an attempt to improve outcomes, one group used the labour-intense process of pharmacokinetically guided infusional dose adjustments to achieve steady state of the ideal therapeutic 5-FU plasma level of 4.2 μM, this showed improved therapeutic outcomes, but also increased toxicity(272).

In the *ex vivo* 3D assays the majority of the cells in culture will have undergone division with the high growth fraction and therefore there is no need to mimic the extended continuous exposure used in patients where the tumour growth fraction is smaller. Also, the issue of extended exposure is likely to be largely irrelevant as the short half-life of 5-FU in the patient is due to hepatic metabolism of the drug, and this drug inactivation through metabolism and subsequent excretion will not be present in the *ex vivo* assay.

1.6.7 Capecitabine

Capecitabine is an orally available fluorinated pyrimidine analogue, which reproduces the effects of parenteral continuous-infusion 5-FU, resulting in a more cost effective and acceptable delivery regimen for patients. It has largely replaced 5-FU as the pyrimidine component of previous 5-FU based chemotherapy

regimens, unless patients experience excessive grade 3-4 gastrointestinal toxicity (nausea and diarrhoea) with the Capecitabine.

Capecitabine can be considered as prodrug, which is activated in three steps to yield 5-FU. Higher levels of the enzymes involved in the transformation process to the active cytotoxic compound 5-FU are found in several tumours and the liver, compared with normal healthy tissue(273). This higher activity of the enzyme thymidine phosphorylase within tumours has been shown to produce three times higher levels of 5-FU in tumour tissue vs. healthy tissue and up to 8 times higher than plasma in isolated studies (274). Although there is interpatient variability of CMax and AUC of the resultant 5-FU metabolite between patients, it is slight in comparison to the interpatient variability of >85% seen with 5-FU.

When Capecitabine is administered at the 1250mg/m^2 per day dose given in OG cancer, plasma peak values of the terminal active metabolite of 5-FU have been described in separate reports as 7.4μM(274) and 2.3μM (275). The resultant mean CMax (mean peak serum) of 5-FU over the two different in use regimens (infusional or oral) is 4.6μM.

1.6.8 Novel emerging chemotherapeutics

One of the most common uses of *ex vivo* models is in the investigation and evaluation of novel emerging chemotherapeutics and their mechanisms. I therefore intend to assess the value of our potential 3D tumour model for this potential purpose with two different drugs – one drug where I will investigate the effect of the tumour microenvironment (PDE5 inhibitor) and another where I will assess drug efficacy (HDAC inhibitor).

1.6.8.1 Panobinostat

Epigenetic modification of DNA occurs by methylation and posttranslational histone modifications, with acetylation, methylation, and phosphorylation. Lysine acetylation leads to open chromatin that allows for gene transcription. This acetylation depends on the opposing activity of two enzyme groups: histone acetylases and histone deacetylases (HDACs). Reduced acetylation because of enhanced expression of HDACs may lead to transcriptional repression of tumour-suppressive pathways, including cell cycle regulators and DNA repair pathways leading to aberrant gene expression and the persistence of cancer cells(276). Overexpressed HDACs can therefore behave as oncogenes. (e.g. HDAC1 and HDAC2 regulate acetylation of the oncosuppressor p53, thus inhibiting its function(277)). Because of this HDAC inhibitors have been proposed as anticancer drugs.

Human HDAC can be grouped into four classes: either zinc-dependent HDACs (Class I, Class II, and Class IV) or the zinc-independent, Class III sirtuin enzymes. *In vitro* studies of the HDACi have demonstrated potent inhibitory activity against Class I, II, and IV HDAC enzymes. In cancer cells, HDAC inhibition can induce cell cycle arrest, differentiation, and induction of apoptosis, at a concentration where normal cells are not affected(278). It has been suggested that tumour cells are vulnerable in contrast to normal cells which have variation and redundancy in epigenetic regulatory mechanisms, whereas HDACs may be essential for key genes needed for growth of cancer cells(279).

HDAC inhibitors have shown potent pre-clinical anti-tumour activity, but so far only two agents, vorinostat and romidepsin, have become FDA licenced as short half-lives and toxicity at

higher doses limit the practicable translation into routine clinical practice (280). Panobinostat is a novel HDACi which has recently undergone accelerated FDA approval for use in multiple myeloma (281) (282). It is also in multiple phase II and phase III trials currently, as it has a broad spectrum of against common solid tumours (inc. Lung, GI and Head & Neck),(278) at a lower dose than the other current FDA/EMA-approved HDACi.(281). When Panobinostat went through successful Phase I dose escalation trials in Japan (283), it used a dose of 20mg/m^2 (which was higher than the 20nM originally seen to provide efficacy *in vitro*)(284).

Preclinical data suggests that study of panobinostat therapy in oesophagogastric cancer may also be useful as adjunct to other chemotherapies. Analysis of mRNA isolates from gastric cancer lines found that several genes indicative of anthracyclines resistance were down regulated after treatment with panobinostat (e.g. activation of *CITED2* (*Cbp/p300-interacting transactivator 2*) (285). This pre-clinical data suggests that if panobinostat could down-regulate expression of genes that mediate anthracycline resistance, this would increase sensitivity to these drugs. This encourages future study in this area where HDACi could act as chemo sensitizers for use with anthracyclines, such as Epirubicin in the treatment of oesophagogastric tumous.

I aimed to test Panobinostat in the oesophageal 3D-TGA, not only because it has been shown to be effective in a range of solid tumours (278), but because it has been shown to potentiate the action of anthracyclines(285) which are part of the current SOC therapy. This will also therefore allow us to evaluate the 3D-TGA as a potential platform for appraisal of new drugs.

1.6.8.2 Vardenafil

Vardenafil hydrochloride is a highly selective cyclic GMP-specific phosphodiesterase type 5 (PDE5) inhibitor usually used for the treatment of male erectile dysfunction. Normally during sexual stimulation, nitric oxide is released from nerve endings in the corpus cavernosum resulting in increased synthesis of cGMP concentrations in penile smooth muscle. This leads to smooth muscle relaxation thereby increasing blood to flow into the penis, ultimately resulting in an erection. The tissue concentration of cGMP is regulated by phosphodiesterases. The most prominent in the human corpus cavernosum is the cGMP-specific phosphodiesterase type 5. Vardenafil selectively inhibits PDE5, preventing the breakdown of cGMP and enhancing erectile function. (286)

Following the entry of PDE5i onto the market and their following increasingly widespread use, there were uncommon reports of incidental effects relating to fibrosis(287). These were noted more in particularly fibrosis dominant diseases such as in scleroderma and cystic fibrosis, which were investigated *in vitro* and *in vivo* (288, 289). These studies suggest that PDE5i at low concentrations (0.1 μM) can reduce pro-inflammatory and pro-fibrotic responses (downregulated TNF-α, IL-1β and IL-6 mRNA expression), whereas much larger (10 μM) drug concentrations could prevent fibroblast differentiation into α-SMA +ve myofibroblasts, through the disruption of transforming growth factor-beta1 (TGF-β1), a key growth factor for fibroblast function.

In cancer, hypoxia activates hypoxia-inducible factor 1 (HIF-1) and induces TGF-β expression. The TGF-β signalling which promotes myofibroblast/CAF activation, can be blocked by phosphodiesterase 5 (PDE5) inhibitors (290). It is therefore

hypothesised that by blocking the fibroblasts activation into CAFs, it will reduce the effects of CAFs on increased tumour aggression and drug resistance. The mechanistic role of stromal cells and the micro-environmental interactions within the tumour-organ contributing to chemo-resistance is increasingly becoming a key area for research and a crucial consideration for the development of active anticancer therapeutics (as detailed in the Introduction section 1.3). This is particularly true in OAC where inherent drug resistance to the traditional chemotherapeutics is frequent, and tumours frequently have a CAF-rich stroma.

I sought to evaluate the effectiveness of PDE5i drugs, which have been reported to interfere with myofibroblast CAFs in the TME, and so may have an effect on chemotherapy response (291). I therefore chose to evaluate the PDE5i drug Vardenafil, because of its known characteristic effects on CAFs *in vitro* (291)

It has been trialed at an *in vitro* dose of 20 - 50uM, because of its extensive clinical experience with well reported tolerability for use in sexual dysfunction and pulmonary hypertension. In clinical use a 20mg oral administration is rapidly absorbed and provides a Mean Peak Serum (CMax) of 15ug/L with a half-life of 4-5 hours and total elimination after 24 hours via hepatic metabolism(286).

1.6.9 Peak serum concentration of chemotherapy agents

Drug	Mean peak serum	Reported publications	Dose in reference
Epirubicin	4.5μM	(254, 255, 257-259)	50mg/m^2
Cisplatin	4.3μM	(262-264)	60 mg/m^2
Fluorouracil / Capecitabine	4.6μM	(272, 274, 275)	200 mg/m^2 & 625 mg/m^2
Panobinostat	1.5μM	(283)	20mg/m^2
Vardenafil	0.0267μM	(286)	20mg for ED
Vardenafil	50μM	(291)	*In vitro* for CAF inhibition

1.7 OG Cancer Characterisation

1.7.1 Overview

When patient tissue which is suspicious for malignancy is sent to the histopathology laboratory for analysis and characterisation, a number of standard histopathological features are used to make the diagnosis: Loss of differentiation (abnormal multi-cellular structure for that tissue type), High nucleus to cytoplasmic ratio with Cellular & Nuclear pleomorphism (size and shape of cells & nuclei), Nuclear hyperchromatism (dark staining nuclei due to increase in DNA) and High mitotic count (increased number of cells with abnormal mitotic forms).

Making a judgement about the malignant nature of a tissue sample is usually adequate using bright light microscopy on haematoxylin and eosin stained tissue. However, where there are single cells alone without a tissue structure, a judgement of malignant status becomes very difficult to make with certainty due to this lack of architecture, without which to make any comparative and objective judgement using the above standard histopathological features.

In this scenario, where only cytology rather than histology is available for analysis, immunohistochemistry techniques are employed to stain the single cells for markers that can indicate both the malignant nature of the cellular material and the tissue of origin.

Whilst the small tissue biopsies obtained at OGD from the patients in this study do have tissue architecture, any *in vitro* established material will be cellular growth and not have the *in vivo* tissue architecture. There is a vital requirement to correctly identify and characterise any newly established cells grown from the primary biopsy material using cytological

immunohistochemistry techniques, to ensure that they represent malignant OG cancer epithelial cells, rather than any adjacent normal cells. It would also be helpful to have the option to scrutinise the malignant nature of the cells by using aCGH to compare the DNA of the Patient Biopsies to the *in vitro* Feeder-layer established cells, but I don't have ready access to an aCGH machine. So on balance it was decided best pragmatic approach was to characterise their epithelial and malignant nature using immunohistochemistry (IHC), to check potential tumourigenicity by xenografting, and to examine for potential populations of Cancer Stem Cells using flow cytometry (FACS).

1.7.2 Candidate markers for malignant epithelial characterisation

1.7.2.1 E-cadherin

E-cadherin is a member of the larger cadherin superfamily of membrane glycoprotein adhesional molecules expressed by epithelial tissues. E-cadherin function is key for cell growth, development and maintaining epithelial structural integrity. It is frequently implicated in carcinomatosis, and reduced expression of e-cadherin correlates with infiltrative and metastatic phenotype in gastric carcinomatosis (292) and patients with e-cadherin positive cancers have a significantly improved survival rates (292, 293)

E-cadherin is seen reduced from normal oesophageal epithelial expression to 59 – 66% in OSSC, and this reduced expression correlates with tumour invasion and vascular invasion. (294, 295). Those patients with absent e-cadherin expression have a worse predicted prognosis (294-296)

1.7.2.2 Cytokeratin

Cytokeratin expression is different between OSSC and OAC. Using IHC, OSCC stains strongly for cytokeratin 5/6 in 95% of cases, whereas it is only stains weakly in 10% OAC only (297). Conversely >90% of OAC of the distal oesophagus stain positively for cytokeratin 7 & 19. Interestingly less than 45% of adenocarcinomas of the proximal stomach stain positively for cytokeratin 7 &19 (298).

1.7.2.3 Aneuploidy

The presence of aneuploidy in conjunction with other histopathological features is frequently used to distinguish normal from malignant cells, but it is not present universally throughout carcinomatous tissue.

In oesophageal cancer 56 -67% of tumours demonstrated aneuploidy using flow cytometry. This was found to correlate with aggressive behaviour of the malignant tumours, a higher histologic grading and worse survival rate. (299, 300). Aneuploidy was demonstrated in gastric cancer in 44 – 52%, with 80% of aneuploid tumours positive for expression of the EGF receptor. Although tumour ploidy status itself did not correlate with patient survival, those with aneuploidy and EGF-R expression were indicative of a worse prognosis. Despite this, multivariate analyses showed that the TNM stage remained the most important prognostic indicator(301, 302). Therefore in Conclusion aneuploidy alone is not a helpful marker of malignancy or aggressiveness in OG carcinoma tissue.

1.7.2.4 Epithelial cell adhesion molecule

Epithelial cell adhesion molecule (EpCam /CD326) is a transmembrane glycoprotein which is thought to primarily mediate epithelial-specific cell–adhesion interactions, but it is

also thought to be instrumental cell signalling, migration, proliferation and differentiation.

EpCam is exclusively expressed in normal epithelia and neoplasia or pre-malignant tissues derived from epithelia. It is also thought to be expressed on Cancer stem cells. EpCam positive malignant cells are not only detected in most primary adenocarcinomas but are also found in their metastases and malignant effusions. EpCam is never found on mesenchymal cells(303).

EpCam is frequently identified from phenotypical staining of fixed primary carcinoma tissue using IHC or cells harvested from malignant effusions using ICC. But it can also be identified and levels quantified using RT-PCR on snap frozen tissue, and by ELISA using patient serum (304, 305).

In many cancers (e.g. ovarian) high EpCam expression is linked to advanced stage of disease and worse prognosis. Thus EpCam has been highlighted as a potential diagnostic marker, prognostic indicator and therapeutic target.

Indeed, the first therapeutic EpCam targeting antibody treatment (intra-peritoneal catumaxomab) showed a benefit in the palliative treatment of EpCam positive malignant ascites, with overall survival and reduced need for ascitic drainage in patients with advanced gastric cancer (303).

EpCam in OG Cancer

Normal oesophageal or gastric epithelium is reported to be virtually negative for EpCam(306) and Barrett's Metaplasia, OAC and OSSC positive, with EpCam expressed at significantly higher levels.(303) Using IHC on TMAs Went et al showed that malignant gastric, GOJ, OSSC and OAC tissue stained strongly for EpCam, and the corresponding normal gastric and

oesophageal epithelial tissue only stained very marginally for EpCam (unlike cerebellar or intestinal smooth muscle tissue which is completely negative)(307). This marked difference in EpCam staining between malignant and normal OG tissue has been reported by others (304, 308) who demonstrated a consistently significant difference ($P < 0.001$). EpCam staining is not universal in OSCCs but is reported in 80% of cases (308). This difference between tumour and normal OG tissue has also been demonstrated using RT-PCR examination of snap frozen OG tissue of both OAC and OSCC with a significant difference in EpCam expression in comparison to normal ($p > 0.0001$). Indeed RT-PCR of EpCam expression can be used to accurately discriminate between normal oesophageal tissue, Barrett's oesophagus and oesophageal adenocarcinoma (305).

The level of EpCam expression in OG cancer patients and how this reflects on prognosis has been studied using both ELISAs of serum and IHC of primary tumour tissue. Interestingly, comparatively lower levels of positive EpCam expression correlated with poor prognosis and comparatively higher levels of positive EpCam expression correlated with improved prognosis and 5 year survival (304). This level of heterogeneity seen within the EpCam expression in tissue samples was not found to be an independent prognostic factor in a multivariate survival analysis, however the differing positive levels of EpCam expression detected in serum were found to be an independent prognostic factor (304).

The correlation of poor survival with a reduced level of positive EpCam expression is thought to reflect epithelial to mesenchymal transition (EMT) and the lack of EpCam expression on circulating tumour cells, as part of a dynamic context dependant adaption of EpCam expression during metastatic progression. An elegant

study by Driemel et al has shown in OG cancer that most primary tumours express high levels of EpCam, whereas the majority of disseminated tumour cells had low levels of EpCam expression, which was significantly associated with occurrence of lymph node metastasis and decreased overall survival of oesophageal cancer patients. *In vitro* studies showed down-regulation of EpCam was observed with a partial loss of the epithelial phenotype, decreased proliferation, but an increase in migration and invasion of these cells. This was validated *in vivo* where these highly positive EpCam cell populations promoted xenografted tumour growth(309).

In conclusion, EpCam is a positive marker of Barrett's and OG cancer and can be used to identify metaplastic and malignant cells from normal cells. Differing levels of EpCam expression correlate to the stage of tumour progression, and prognosis in OG cancer, in the context of anatomical setting. High levels of positive expression representing proliferative epithelial growth of the primary tumour and low levels of positive EpCam expression are associated with EMT, migration, invasion and metastatic dissemination.

1.7.2.5 p53

p53 is a multi-functional protein which is coded by the TP53 gene. It has a small number of structural domains but is disproportionately involved in a large number of complex interactions with different molecular species: proteins, DNA, RNA, and cellular metabolites. It sits within a complex feedback circuit of interconnecting functions which help to control cell growth and multiplication. In normal unstressed cells consistent low levels are maintained by its constant production and then subsequent degradation, facilitated by the MDM2 protein. MDM2

binds to p53 inactivating it, and then transports it from the nucleus into the cytoplasm.

Activation of the p53 protein occurs as a result of cellular stress, it accumulates in the nucleus, where it regulates the transcription of target genes. Activating stressors include DNA damage (e.g. UV), lack of ribonucleotides and uncontrolled expression of oncogenes. As activation occurs, two changes happen, there is a confirmation change in the structure of the p53 protein enabling it to regulate transcription, and its degradation half-life increases. Depending upon the type and severity of the stress experienced by the cell, the p53 activation will generate a cellular response including cell cycle arrest, DNA repair, differentiation, senescence and apoptosis (310).

p53 is known as a tumour suppressor as it has an anti-cancer function by maintaining genetic stability through a number of mechanisms. When DNA damage is detected, it can cause cell cycle arrest (at the G1/S point), allowing for potential DNA repair by activating the DNA repair proteins(311) followed by apoptosis if DNA repair is not possible (312). Also, it is involved in the senescence reaction to short telomeres, and inhibition of angiogenesis. p53 therefore is vital in maintaining the integrity of the genetic sequence by preventing proliferation of cells carrying damaged and potentially mutagenic DNA (313).

An alteration of the TP53 gene on chromosome 17p can occur by deletion or by mutation, and can be precipitated by exposure to mutagens such as radiation, chemicals or viruses. This will result in the p53 protein becoming dysfunctional and compromising its anti-cancer role, by prevention the vital DNA integrity check, allowing the accumulation of mutations, and increasing the prospect of the uncontrolled cell division integral to cancer (314).

As a result, somatic mutations in the TP53 gene are one of the most frequent alterations seen in human cancers. (315)

Unlike other tumour suppressors (which are commonly inactivated by frameshift or nonsense mutations) most TP53 mutations are missense and cause single amino-acid changes at many different positions (315).Even single missense mutations can be compromising, with a mild to serious functional spectrum of effect (316).

The resulting mutant p53 protein (which may differ from wild-type p53 by just one amino acid residue) is subsequently expressed at high levels. This is due to metabolic stabilization rather than overexpression (317) and with its prolonged half-life accumulates in the nucleus. These increased levels of p53 within the cell nucleus can be detected by immunohistochemistry (318).

Interestingly, as well as the loss of wild type suppressor function, there is suggested to be an oncologic effect seen by the nuclear accumulation of the mutant p53 (310). This oncogenic gain of function (GOF) has been seen where several hotspot mutants have been shown to cooperate with oncogenes such as RAS for cellular transformation (319).

Immunohistochemistry studies have shown that although over half OAC are reported to have a p53 mutation, non-dysplastic Barrett's oesophagus is mutation free (320, 321). Cohort studies have shown that those with dysplastic disease with loss of chromosome 17p have a significantly increased the risk of progression to cancer (322) This has been also demonstrated at a genetic level where p53 mutations are not present in non-dysplastic Barrett's (323).

Despite its prevalence and importance in confirming the carcinogenic process, the presence of p53 mutation has not been shown to be prognostic, or related to chemotherapy response in oesophagogastric cancer (324).

1.7.2.6 Trefoil Factor 3

Trefoil Factor 3 (TFF3) is a functional molecule, and is thought to be involved in the protection, maintenance and repair of the intestinal mucosa(325). It is found in the gastrointestinal mucosa both intra and extra-cellularly. TFF3 has been shown to be specific for cells with an intestinal phenotype,(326) and is a reliable marker of metaplastic change in the oesophagus.(327)

1.7.3 Cancer Stem Cells in OG cancer

1.7.3.1 Characteristics

Cancer stem cells (CSCs) are a population of undifferentiated tumorigenic cells responsible for tumour initiation, maintenance, and spreading to distant organ sites (328). CSC have been defined by the four key characterised that they demonstrate: chemo-resistance (329), multi-potency(330), tumorigenicity(331, 332), and stem gene expression(333, 334). Many also exhibit aldehyde dehydrogenase (ALDH) activity (335, 336).

Tumour initiation by CSCs is seen by their ability to form cancers when injected into immunodeficient mice (337). Following initiation, CSC provide tumour maintenance by their capacity to self-renew and their unlimited proliferation potential, dividing (sometimes asymmetrically, producing an identical daughter cell and a more differentiated cell(338)) to create the large number of differentiated cells that make up the bulk of the tumour(339).

To spread to different sites these cells display features of epithelial to mesenchymal transition (EMT) and trans-

differentiation (340, 341) to become circulating tumour cells (342) before seeding in distant organs. Unlike the rapidly proliferating differentiated tumour cells, CSCs are slow cycling and relatively quiescent. This protects them against traditional chemotherapeutics that are particularly directed toward killing rapidly dividing cells (343). CSC have other defence mechanisms against chemotherapeutics, including drug transporters and strong repair responses to DNA damage, when compared with differentiated daughter cells (344-346). This results in CSCs being characteristically radiotherapy and chemotherapy-resistant.(347)

1.7.3.2 Identification

Well-documented cell surface antigens are frequently employed to identify CSC within various malignancies, and the cells themselves can frequently be isolated by flow cytometry based on these cell surface markers (348-352). However, this relative clarity is not the case in OG carcinoma tissue. Although many of the traditional markers of CSC (seen in other solid tumours such as CD24, CD29, and CD133) are frequently up regulated this is not seen uniformly in OG cancer, others markers e.g. CD166 are present in both metaplasia as well as dysplasia and carcinoma, and others like CD34 have not been seen(353, 354), and it is frequently a heterogeneous picture. The CSC marker Lgr5 provides a good example of the lack of clarity: Lgr5 is generally considered to be intestinal stem cell marker and has been described in colon cancer, ovarian cancer and hepatocellular carcinoma (355). Using standard IHC, it has been shown to be present in 90-100% of OAC and 70% of Barrett's oesophagus, with the intensity of expression greater in carcinoma/dysplasia than Barrett's. In patients with OAC, high levels of intensely staining Lgr5 are associated with poor survival independent of stage of disease and treatment with neoCRT (356), which is

consistent with the notion that such stem cells are less sensitive to chemotherapy (357). However, the relative overlap in staining between Barrett's oesophagus and OAC means that the practical use of Lgr5 as a conclusive CSC marker in OAC is limited. Interestingly, the expression of Lgr5 does not change between OAC associated with Barrett's and OAC without Barrett's, and conversely OSSC does not appear to have cells which express Lgr5. (358)

ALDH activity has been studied in many cancers using its functional as an alternative CSC marker, rather than an expressed cell surface molecule. Aldehyde dehydrogenases (ALDHs) are a normal family of enzymes involved in detoxifying a wide variety of endogenous and exogenous aldehydes to weak carboxylic acids (e.g. cyclophosphamide or ethanol). ALDH isoforms are widely distributed in the body, with the highest levels unsurprisingly seen in the kidney and liver where a large proportion of routine detoxification occurs (336). ALDHs are involved in the biology of cancer stem cells as well as normal stem cells, with ALDH1 in particular used as a marker to identify and isolate both normal stem and cancer stem cells. ALDH1 has been shown to be a marker of CSCs in many types of solid tumours, including liver, pancreas, lung, prostate, bladder, ovary, breast, and colon. (359) By studying the ALDH1 levels in corresponding tumour and normal tissue ALDH1 can be used to identify CSCs in tissues that do not normally express ALDH1 at high levels, including breast, lung, colon, oesophageal and gastric epithelium, but understandably not from tissues that normally express ALDH1 at a high level like liver and pancreas (360). ALDH-positive cells in these cancers demonstrate the behaviours of CSCs. High levels of ALDH1 are associated with poor prognosis in breast (361), bladder(362) and prostate cancer patients (363). Furthermore patients with ALDH1 positive breast

cancers have worse survival after neoadjuvant chemotherapy, than patients with ALDH1-low tumours. And, in those who did not have a histopathological response following chemotherapy, the number of ALDH1 positive cells increased significantly (364). These ALDH1 positive cells are therefore more chemo-resistant than the other cell populations in these cancers. ALDH positive cells also appear to be highly tumorigenic, with tumour inoculation experiments in immunocompromised mice showing that only 500 ALDH positive breast cancer cells were needed to form a tumour, whereas inoculation with 50,000 ALDH1 negative cancer cells failed to form tumours.(361)

1.7.3.3 ALDH in OG cancer

Rather than use the traditional surface antigen markers of CSC which do not appear to apply in OG cancer, ALDH has recently been used by a number of groups to try and identify CSC in multiple OG cancer cell lines(365). It has been shown that OG cancer cell lines (EC 109, SCC) cultured in 3D spheroids have CSC populations with elevated ALDH, expressing increased levels of stem cell related genes (Nanog and Oct 4), and demonstrate higher chemo-resistance to Cisplatin with an upregulation of drug resistance genes (ABCG2 and MDR1). And from a large panel of expressed genes examined using microarray analysis, ALDH is specifically up regulated when cell lines grow in 3D culture conditions as the CSC population enriches (366).

Others have shown that selected highly positive ALDH cells from this EC109 OSCC line demonstrate other CSC like properties such as increased self-renewal, differentiation, tumour initiation, invasion and metastasis (367). Primary OSCC carcinomas in 165 patients have supported this finding, showing that highly positive ALDH cell populations were associated with worse tumour grade,

invasion, and metastasis; as well as poor patient outcomes and prognosis (367)

Studies have also been carried out on OAC cell lines (FLO-1, BE3, SKGT-4, JHESO and OCAP) showing that cell lines with a higher proportion of ALDH1 positive cells were more resistant to chemotherapy, with corresponding raised levels for stem cell signalling related genes: SOX9, Shh and Hes-1 which have been reported as resistance conferring genes. These lines with a higher proportion of the ALDH1 positive cells had a higher ability to form tumour spheres and which were again more resistant to chemotherapy. These ALDH1 positive cells also demonstrated a higher proliferation rate.(368)

Unlike staining for CD44 to predict response to neoadjuvant therapy (which was only moderately effective only where a lack of CD44 positive cells accurately distinguished those who would respond to therapy(369)), IHC staining of ALDH1 in pre-neoadjuvant therapy OG adeno ca biopsy tissue was able to distinguish between those with low levels of ALDH1 who subsequently had a good histopathological response to neoCRT, and those with high levels of ALDH1 who subsequently had a poor histopathological response to neoCRT. Although the numbers in this reported study are small, this is extremely promising and could potentially guide treatment when routinely administering neoCRT.(368)

1.7.3.4 CD44 in OG Cancer

By far the most promising classical marker of Cancer Stem Cells in OG cancer is CD44, but the available evidence is variable. CD44 is a transmembrane glycoprotein which has many isoforms dependant on alternative splicing and post-translational modification, resulting in a wide number of adhesion and signalling functions in both health and disease(370). Indeed,

particular splice variants (e.g. CD44v4–7) are thought to be directly involved in the metastatic spread of tumour cells(371).

CD44 has been reported as a marker of cells with CSC like properties in oesophageal(369, 372) and more particularly gastric adenocarcinoma in cell lines (350, 373), but reports of the presence of CD44 IHC staining in human tissue vary (369, 372, 374). When sorted for this well-known CSC marker, OG cancer cell populations from cell lines have readily formed tumours when transplanted into NOD-SCID immunocompromised mice (373, 374). However, when isolated from fresh human tissue these same cell populations have not consistently resulted in an increased tumour-initiating capacity or formed tumours at lower cell concentrations than unsorted populations.(353)

Conversely *in vitro* studies of OG squamous cancer cell lines (TE2 & TTn) in cultured 3D spheres do not demonstrate enhanced expression of the characteristic CSC markers (CD44, CD133, CD338), despite showing an upregulation of other indicators of cancer stem-ness(375), such as: increased stem cell related gene expression (Sox-2 and Nanog) using RT-PCR, greater chemotherapy drug resistance to Cisplatin and doxorubicin, expression of CA-9, a hypoxia surface antigen indicator of CSC induction and maintenance, increased activity of aldehyde dehydrogenase (ALDH)

Similarly, 'side populations' of OG cancer stem cells isolated from OG squamous cancer cell lines EC9706 and EC109 demonstrated the following stem-like properties without evidence of CD44 and other traditional stem cell markers: high clone formation efficiency, fifty times higher tumour forming capacity in immunodeficient mice, higher gene expression of the stem-cell related genes (OCT-4, SOX-2, BMI-2 & ZFX) and transporter

genes (ABCG2 and ABCA5) and Wnt and Notch signalling pathways genes.

This conflicting evidence has been well documented throughout other tumour types and in some cases different research groups have presented contradictory evidence on the expression of CD44 and its prognostic value (371, 376), which maybe due to true partial or variable involvement in the carcinogenesis process or alternative control of the mitogenic signals diving the CD44 splicing(370). However, where CD44 is overexpressed in intestinal cancer it is considered highly tumorigenic and marks out proliferative cells which behave in a cancer stem cell like fashion(377).

1.8 Study Outline

1.8.1 Study Rationale

There are over 8,000 new diagnoses of oesophageal cancer per year in the UK and near 500,000 worldwide.(3) Mortality remains high, with a 5-year overall survival of only 13%.(3) In the UK and much of Europe, routine treatment for potentially curable patients is neoadjuvant chemotherapy and resectional surgery followed by adjuvant chemotherapy.(4) However, the response rate to neoadjuvant chemotherapy is only 40%, so over half of patients do not benefit whilst suffering toxic chemotherapy-related side-effects.(5) A model to understand the mechanisms of chemo-resistance in tumours and that can potentially predict which patients are most likely to benefit from chemotherapy would provide a marked clinical advantage and an opportunity for personalised treatment of oesophageal cancer.(6)

Our group has previously described a pre-clinical tumour model (3D tumour growth assay, 3D-TGA) that allows chemotherapeutic drug testing in a more accurate and clinically-relevant setting, using 'close-to-patient' cells isolated from patient-derived xenografts.(238) Incorporating extracellular matrix and mesenchymal support restores both direct and paracrine tumour-stroma interactions which are known to influence drug resistance.(102, 239)

Here, I propose to develop a method to establish cultures of individual patient OG cancer cells derived from small pre-chemotherapy endoscopic biopsies, and then adapt the Nottingham 3D-TGA to grow these specific OG close-to-patient cancer cells in a 3D TME, and subsequently undertake pharmacological screening in an attempt to determine individual patient chemo-sensitivity.

1.8.2 Study Hypothesis

It is hypothesised that stromal elements of the TME have a role in modulating OG cancer chemo-sensitivity, and that by incorporating stromal cells into the 3D-TGA of a patients primary OG cancer cells it will influence the potential chemotherapeutic accuracy of the 3D assay, and that this may correlate correctly with clinical chemotherapy sensitivity of that patient's cancer.

1.8.3 Study Aims

The overall objective of the study is to determine whether an individual patient oesophago-gastric cancer 3D-Tumour Growth Assay can predict response to chemotherapy.

The individual aims are:

1) Establish individual patient primary cancer cells to grow patient relevant tumour tissue, within a clinically relevant timeframe.
2) Use these primary patient cells to create 3D models of individual patient cancers.
3) Use the assay to determine the response of the tumours to the standard neoadjuvant chemotherapy regimen, and
   a) correlate the predicted *ex vivo* response to the actual clinical response, as measured by the histopathological tumour regression grade.
   b) evaluate the 3D cancer model for the screening of potentially efficacious drugs that could be used against this highly resistant tumour type

1.8.4 Study Design

Following a histological diagnosis of OG Cancer, patients routinely undergo standard OG cancer endoscopic staging examinations, either at oesophagogastroduodenoscopy (OGD) or at endoscopic ultra-sound (EUS), or both. With informed

consent, chemo-naive tumour biopsies and matched blood samples will be taken at this endoscopy for research. The tumour will be grown *ex vivo* and then analysed in the 3D-TGA to predict individual chemotherapy response. If staged for treatment with curative intent, patients subsequently undergo routine neoadjuvant chemotherapy (3 cycles of anthracycline, platinum and fluoropyrimidine) before definitive surgical resection of their oesophageal tumour.

A matching chemotherapy-exposed tumour specimen will be collected at surgical resection. All resected tumours will be examined by dedicated team of Consultant Gastrointestinal Histopathologists, and allocated a TRG from 1-5. The clinical response to chemotherapy will then be related to the predicted 3D-TGA chemotherapy response, to assess the accuracy of the 3D model. The chemotherapy-exposed tumour collected at surgical resection will also be analysed in the 3D-TGA, to examine if the chemo-sensitivity of the remnant tumour has evolved following exposure to the neoadjuvant chemotherapy regimen.

2 Materials and Methods

Unless otherwise stated, all reagents and chemicals were purchased from Sigma Aldrich LTD (Pool, UK) and all tissue culture reagents were purchase from ThermoFisher (Stafford, UK).

2.1 Tissue Collection

2.1.1 Patient identification

Endoscopic tumour biopsies (REC: 10/H0401/80) and fresh surgical specimens (REC: 10/H0405/6) were collected with informed consent from patients at the Nottingham University Hospitals NHS Trust in 2014-2015, and used in accordance with National Research Ethics Service approval.

Patients with biopsy confirmed OG cancer at any regional hospital were added to the list of patients to be discussed at the central Nottinghamshire multi-disciplinary team (MDT) meeting. This happened weekly and had at least one member of each sub-specialty team attending: surgery, oncology, pathology and radiology. Minutes were taken and distributed. Patients who met criteria for inclusion in the study were identified from this weekly meeting: patients must have had operable OG cancer, intended for treatment with curative intent.

Patients then had their staging investigations planned. This involves a combination of CT, PET-CT, EUS and laparoscopy with gastroscopy (lap & gas). Biopsies of tumour for the study were obtained endoscopically at the EUS and Lap & Gas procedures as appropriate.

Patient identification and subsequent progress along the diagnostic, staging and treatment pathway was confirmed and discussed with the Upper GI Specialist Nurse. Communication

was maintained with the medical secretaries and PAs who organise clinic appointments and the staging procedures. Individual patient variances and caveats were identified, and provision was made for non-routine cases e.g. severe oesophageal stenosis, learning difficulties, anti-coagulation.

The identified patients attended outpatient clinic to be informed of their diagnosis, and offered further investigation and treatment as recommended by the MDT. After the selected patients had been informed of their diagnosis, a study letter was sent out to the patients introducing the research and explaining that they would be met by a member of the research team at the time of their further staging investigations.

Regular liaison with the endoscopy departments at both campuses of the Nottingham University Hospitals NHS Trust was undertaken to identify the times of the planned EUS procedures, so that the research staff could be present to meet patients and enrol them in the study.

For EUS biopsies, the identified patients were met at the relevant endoscopy department and introduced to the aims and purpose of the research and given an information leaflet. If the patient was happy to donate tissue, then they were enrolled in the study and consent was taken.

For lap & gas biopsies, patients were offered dates on set hospital operating lists, which when confirmed were then obtained from the medical secretaries, so that the research staff could attend. On the day of the procedure, patients were met at the elective admissions lounge (EAL) and consent for study participation was obtained.

The necessarily brief overview of sample collection outlined above is a disarmingly simplified summary. The process of

patient identification and following them (as an external member of the direct clinical team) through their staging investigations to enrol them in the study and obtain primary patient tumour samples was a time consuming and testing process. This is due to the number of different potential pathways of investigation and treatment, re-presentations at MDT and multiple different clinicians and staff involved in organising their care. Despite the best liaison and preparation with the clinical staff, plans for patient investigation and treatment were re-arranged at short notice for multiple unexpected reasons (e.g. broken EUS scopes, theatre list over-runs, clinician cross-cover, list cancellations or weekend initiative lists) which frequently disrupted potential research enrolment and sample collection.

2.1.2 Tissue collection

Up to eight chemo-naïve tumour biopsies per patient were taken when patients underwent routine endoscopic staging examinations by their treating clinicians: principally Mr Parsons, Dr Ragunath, Mr Welch & Mr Catton. These were designated OBX1 (patient 1), OBX2 (patient 2) etc. These were either at the oesophagogastroduodenoscopy (during lap & gas in theatre) or at EUS (in the endoscopy department), or during both which resulted in two sets of chemo-naïve samples from the same patient (designated for example as OBX5**(i)** for first biopsy, OBX5**(ii)** for second biopsy). A corresponding blood sample was drawn and placed in EDTA tubes and clotting tubes for later extraction of serum and plasma. If disease stage allowed treatment with curative intent, patients subsequently underwent routine neoadjuvant chemotherapy before definitive surgical resection where if possible a matching chemotherapy-exposed tumour specimen was collected (designated as **OES**5).

One of the endoscopically obtained chemo-naive tumour biopsies was stored in RNA*Later*® for future genetic analysis, one was placed into 10mls of Normal Buffered Formalin (NBF) for later formalin fixed paraffin embedded (FFPE) histological analysis. The other 6 live biopsies or surgical material were placed into a universal tube containing 10mls of Tissue Transfer Medium (Dulbecco's modified eagle's medium with 10% foetal bovine serum, 0.2M L-glutamine, 5mls Antibiotic/Antimicotic, (10,000 units/mL penicillin, 10 mg/mL streptomycin and 25 µg/mL amphotericin B; A5955 Sigma-Aldrich), 1 µg/ml hydrocortisone, 7.5 µg/ml insulin at 4^{o}C.)

These tumour samples and blood were labelled and placed on ice in a tissue transfer box, and then transported back to the University of Nottingham EVPC laboratory, at the Queens Medical Centre, Nottingham. At the EVPC laboratory, the bloods (EDTA tubes and clotting tubes) were centrifuged at 500g for 5-10min in a sealed rotor. Plasma and serum was aliquoted into 2ml Corning cryovials and stored at -80^{0}C.

The tissue samples (< 5mm) placed in RNA*later* (1.8ml RNA*later* in 2ml Corning cryovials, at room temperature) were left to soak in RNA*later* at 4^{0}C overnight before transfer to -80^{0} for long-term storage.

The tissue placed in neutral buffered formalin (20 volumes of formalin to tissue) for FFPE analysis was kept at room temperature (RT). Tissues were allowed to fix for at least 1 day (the formalin penetrates 1mm per hour) before processing and paraffin embedding using the standard protocol.

Samples of the live tissue were snap frozen. Either biopsies or cut samples of the main tumour (<1cm) were placed into 2ml

Corning cryovials, which were immediately placed into liquid nitrogen and then stored at -80^{0}C.

Other samples of the live tissue underwent viable cryopreservation. Primary tumour, biopsies, normal tissue or fresh xenograft tissues were cut into small (1-2 mm^3) pieces. These are collated and ~10 pieces of similar sized tissue were assembled into clumps (~10mm in diameter) and placed into cryovials containing 1ml cold freezing medium (90% (v/v) RPMI-1640 medium, 10%(v/v) DMSO). These were incubated on ice for 1h, before transfer to a Nalgene Freezing Container (containing 250ml propan-2-ol), at room temperature. This was then placed at -80^{o}C for 25 min, before transfer to -20^{o}C freezer for 10 min. The samples in the Nalgene Freezing Container were subsequently returned to the -80 ^{o}C freezer for 35 min. Finally the vials were removed from the Nalgene Freezing Container and were transferred to the -150 ^{o}C freezer.

To re-animate the samples, the frozen cryovials were thawed in a 25^{0}C water bath until last ice crystal had just disappeared (~2min). The cryovial contents was then placed into 10mls of cold sterile saline or PBS and incubated on ice for 30min. The universal tube containing the tissue in saline was centrifuged at 500g for 1 min, before the saline was aspirated and a further 10ml cold sterile saline or PBS was added. This was again held on ice for 30min, before repeat centrifuge at 500g for 1 min and saline aspiration. The live tissue was now ready for analysis and experimentation and could be disaggregated for *in vitro* cell line establishment or xenografted for *in vivo* tumour establishment (see detailed explanation of method in following section). Note that the first disaggregation from cryopreserved tissue tends to just yield dead cells, and therefore the tissue needs to undergo multiple disaggregation cycles (~3) and the cellular supernatant

plated out in separate 6 well plates to avoid live cells being overwhelmed by the toxic environment which results from high volumes of apoptotic or dead cellular material from the early disaggregation cycles.

2.2 Tissue Culture

A standard method for successfully establishing primary tumour cell cultures from diverse patient cancer tissue has been developed by the Ex Vivo Cancer Pharmacology (EVPC) laboratory (191) from the original method published by Liu et al (172). The key alterations from this original published method include the use of the J2 clone of random-bred Swiss mouse 3T3 cells for the feeder-layer, and the use of mitomycin C to induce irreversible growth arrest of these feeder cells, rather than irradiation as originally described (see materials and methods 2.2). Protocol adjustments were required for different tissue types, for example overnight digests with extra enzymes are required for some particularly fibrous tissue samples (191).

2.2.1 Tissue disaggregation

The purpose of tissue disaggregation is to mechanically and enzymatically disperse the biopsies to produce a viable single cell suspension for culture of the fibroblasts and epithelial cells, which can then grow up on a layer of supporting feeder cells in a tailored ROCKi supplemented medium (172).

On arrival at the laboratory, the surgical tumour material was dissected and the majority of this live tumour tissue was finely-minced using a 12 blade surgical scalpel in a plastic petri dish, before disaggregation.

The minced tissue sample was washed with Hank's Balanced Salt Solution (H6648 without CaCl or $MgSO_4$) supplemented with 5mls of the previously described Antibiotic/Antimicotic (A5955 Sigma-Aldrich); this medium is abbreviated to HBSS/AA from herein. The tissue was allowed to settle and then medium aspirated (if the medium appeared to contain cells, this was harvested and put into culture as a pre-digest sample).

The minced tumour was enzymatically disaggregated in 10mls of dispase/collagenase solution (Type II collagenase (100 U/ml, Dispase (2.4 U/ml), in HBSS/AA without calcium or magnesium). If the sample was particularly fibrous the addition of 100U/ml hyaluronidase helped to generate a single-cell suspension. The sample was then incubated at 37°C under constant rotation for 2 hours.

Cells were removed at 1-2 hourly intervals: After removing from the constant rotation, the undigested material was allowed to settle out. The cell suspension was carefully removed (retaining the minced tissue) and pipetted into a sterile universal; then topped up with RPMI medium (RPMI-1640, 10% FBS, 0.2M L-glutamine). A further 10ml dispase/collagenase solution was added to the remaining undigested material and incubated at 37°C with rotation for a further hour to digest the remaining tissue.

Progressive diameter nylon cell strainers were used (100µm (BD 352360), 70µm (BD 352350), 40µm (BD 352340)) with RPMI dilutions to remove debris from the cell solution, and the RPMI/cell suspension solution was subsequently centrifuged at 500g for 5min. The media was aspirated off, and if the cell pellet appeared 'contaminated' with red blood cells, 1ml of red blood cell lysis buffer (4.14g ammonium chloride, 0.5g potassium bicarbonate, 0.018g EDTA, dissolved in dH2O to a total volume of 500 ml, adjusted pH to 7.35 with 0.1 M NaOH, filtered and aliquoted) was added for 1min, before re-suspending in 10ml RPMI medium and re-centrifuging the sample at 500g for 5min to produce a new cell pellet.

After the third digest, any remaining tissue was mashed through a 70µm nylon mesh cell strainer, and then the previously

outlined steps were performed to produce a cell pellet, which can then be grown on a feeder layer.

2.2.2 Preparation of feeder layer

The J2 clone of random-bred Swiss mouse 3T3 cells was employed to provide feeder support for the epithelial cells (173, 378). The cells were maintained by twice weekly passaging and not allowing to remain at confluence. Fresh low passage cells were thawed every 2 months, as with prolonged passaging the cells start to senesce or undergo spontaneous transformation and are not recommended for use above P20. Following routine cell culture at 37°C in a 5% CO_2 incubator, the cells were harvested and counted each week from a near confluent T75 flask (approx. 3 – 6 x 10^6) and re-seeded in T75 flasks as required with 1.0 - 2.0 x 10^5 cells in each, and maintained in the J2 Medium (DMEM, 4mM L-Glutamine 10% heat inactivated adult bovine serum). Foetal bovine serum was avoided for the culture of 3T3 J2 as it is rich in nutrients and gave an advantage to the faster growing cells in the population.

The temporary addition of mitomycin C (10 μg/ml) (MMC) was used to irreversibly inhibit proliferation of the flask of growing 3T3 J2 cells. Medium was removed from T225 flask so that only 10mls remained, 200μl of mitomycin C (500μg/ml) was added in 10ml of medium (10μg/ml). It was incubated for 2hrs at 37°C, ensuring that the medium covered the cells, with rocking of the flask every hour to ensure adequate mixing of the MMC containing medium and cellular exposure. The cells were then washed thoroughly with 15ml of HBSS and this step was repeated twice to ensure that all residual MMC had been discarded. Cells were then trypsinised, harvested, spun and re-suspended in fresh J2 medium.

Following the repeated washings, the MMC treated cells were re-seeded in the J2 Medium. The optimal density of the feeder layer was 1.0-1.5 x 10^6 cells per T75 flask or one-quarter confluent, so each MMC treated flask was split approximately 1:4. i.e. 1x T225 was seeded into 4x T225 or 12x T75 or ~10x 6-well-plates.

The feeder cells could be used that day (plated 2 hours prior to seeding the epithelial cells) or preferably prepared 1 day before they were required. The feeder layer cells were not be prepared more than 3-4 days before use, because the feeder cells would start to degenerate from this point.

2.2.3 Establishment and expansion of primary cells

Six-well plates were established with a pre-seeded feeder layer of MMC-treated J2 cells (Swiss 3T3 cells, Howard Green lab, Harvard Med School) in Dulbecco's modified Eagle's medium (DMEM) supplemented with 10% foetal bovine serum (DMEM/FBS), in a modification of the originally described method (172). The DMEM/FBS medium was removed and the feeder cell layer washed with HBSS. The freshly disaggregated OG primary cells pellets were re-suspended in F Medium (3:1 (v/v) F-12 Nutrient Mixture (Ham)–Dulbecco's modified Eagle's medium (Invitrogen), 5% defined foetal bovine serum, 0.4 μg/mL hydrocortisone (Sigma-Aldrich), 5 μg/mL insulin (Sigma-Aldrich), 8.4 ng/mL cholera toxin (Sigma-Aldrich), 24 μg/mL adenine (Sigma-Aldrich), supplemented with epidermal growth factor (EGF) (10 ng/mL epidermal growth factor (Invitrogen)), RhoKinase inhibitor (ROCKi) (10 μmol/L ROCKi Y-27632 (Enzo LifeSciences)), and 5mls Antibiotic/Antimicotic, (10,000 units/mL penicillin, 10 mg/mL streptomycin and 25 μg/mL amphotericin B; A5955 Sigma-Aldrich).This tumour material was then plated onto the J2 feeder cells in the supplemented F-Medium, and placed in a 5% CO_2 incubator at 37°C.

The OG primary cells were given 48 - 72 hours to establish before re-examination using bright light microscopy. The floating dead cells and debris in solution were aspirated and discarded, and the cells were re-fed fresh F-Medium. All wells were re-examined every 48-72 hours, and microscopically selected areas of epithelial establishment or fibroblast growth were marked on the flask. Subsequently, the tissue culture 6 well plate (or subsequent 25 or 75cm^2 flask) was examined under a low power microscope to assess the degree of confluence of the cell monolayer every 48 hours.

Media colour was also assessed as it contains phenol red which is an indicator of pH (yellow at acidic pH, purple at alkaline pH and red at neutral). This acts as a good indicator of cell growth or contamination: when cells grew and multiplied they produce acidic metabolites that decrease the pH, therefore either the cell line could be approaching confluence, or the flask of cells was demonstrating high acidity with low numbers of epithelial cells, and could be an indicator of bacterial cell or fungal contamination.

Depending on the cellular growth rate, primary flasks exhibiting <75% confluence could be re-fed with growth media and >75% confluence were split to reduce cell numbers and crowding.

Re-feeding was performed by aspiration of the used medium from the flask using an un-plugged sterile Pasteur pipette attached to a vacuum line, and cells were swiftly re-covered with 2-3mm depth of medium (pre-warmed to room temperature). Flasks were replaced in the incubator (37ºC, 5% CO_2).

Splitting was performed by aspiration of the used medium from the flask using an un-plugged sterile Pasteur pipette attached to a vacuum line, followed by the addition of TrypLE™ Express. The

plates / flasks were incubated at 37ºC for ~5 minutes or until 90% of the cells detached from the flasks with intercurrent observation under an inverted microscope to determine cell detachment. The flask was gently tapped to detach all the cells, and a sterile pipette was then used to remove the cell suspension to a sterile universal tube which was then topped up with (serum-containing) medium to neutralise the effects of the TrypLE™ Express, and was centrifuged at 1500rpm for 5 minutes. The cell pellet was re-suspended in 10ml growth medium and counted in a Neubauer haemocytometer at this point if they were for use in experimentation or cryopreservation. If the cells were to be re-seeded for growth and sample expansion they were placed into a new flask(s) at ~1-2x10^6 cells per T75 and the flask was re-filled with growth medium (~15ml / T75) before being replaced in the incubator (37ºC, 5% CO_2).

Differential trypsinization was used to remove any excessive fibroblast growth which was preventing expansion of the fledgling epithelial cell colonies. The stripped cancer associated fibroblasts (CAFs) were re-suspended in PCA Medium (500mls Dulbecco's Modified Eagle Medium (DMEM), 100mls heat inactivated Foetal Bovine Serum, 6ml 0.2 M sterile L-glut, 6ml 100x AA, 0.6ml 1mg/ml hydrocortisone in ethanol, 0.45ml 10mg/ml bovine insulin in 1% glacial acetic acid), and re-seeded in sterile T75 flasks in the absence of a J2 feeder layer, to expand the CAFs as a separate population. This process of differential trypsinization was performed on multiple occasions throughout the establishment and growth phase to generate an enriched epithelial population. As the epithelial and CAF cell colonies established and grew, they were re-fed with supplemented F-Medium or PCA Medium respectively and transferred to progressively larger tissue culture flasks (pre-seeded with a J2 feeder layer for the epithelial cells) until the

point of sub-confluence in a T225 tissue culture flask. From this early passage tumour material, the malignant epithelial cells and CAFs were harvested and could then be characterised, used for pharmaco-therapeutic experimentation or cryopreserved for future analysis.

This same disaggregation and tissue establishment process was used for the chemo-exposed tumour collected at surgical resection; however, the greater volume of tissue obtained allowed for additional samples to be snap frozen, viably cryopreserved, and preserved in formalin for future immuno-histochemical analysis

Agarose embedding of the *in vitro* cultured individual patient OG cancer cell lines was performed once the cells had been pre-fixed. The harvested epithelial cells were re-suspended in 10mls of Normal Buffered Formalin (NBF) for 10 mins, before being twice washed in PBS, spun down and re-suspended. This pre-fixed cell pellet was then mixed with 100-200ul of liquid agarose (2% agarose in PBS) at 60^{o}C, and then pipetted onto the top of a plug of pre-gelled agarose (contained within the conical tip of a 0.6ul sized Eppendorf) on ice. After the agarose-cell suspension had cooled and gelled, the tip of the Eppendorf containing the initial plug layer of agarose was amputated using a scalpel blade. The pellet of gelled agarose embedded cells was then gently pushed out of the barrel of the Eppendorf tube (using the plunger of a 1ml hypodermic syringe) and placed into a universal tube containing NBF where the further fixation process continued over the next 24 hours before it was then embedded and processed in the usual fashion.

Cryopreservation of cells was performed by detaching the epithelial OG cancer cells from the feeder-layer in the usual manner with TrypLE™ Express, washing and centrifuging to a

pellet before re-suspension in supplemented F-Medium with an addition of 10% DMSO at a concentration of 8-10x10^6 cells / ml. The 10% DMSO solution is toxic and therefore this cell suspension was swiftly aliquoted in 1ml portions into pre-labelled cryovials and was placed in a Nalgene Freezing Container (containing 250ml propan-2-ol), at room temperature. This was stored directly in the -80^{o}C freezer before transfer to the -150^{o}C cell storage freezer in the following 24-48 hours.

Cryo-preserved cell recovery was performed by first preparing a T75 flask for the *in vitro* culture, with a feeder layer, seeded no longer than 48 hours previously. The J2 medium was discarded and the T75 flask filled with supplemented growth medium, and then warmed in a 5% CO_2 incubator at 37^{o}C for 15 minutes to prepare an optimum environment for arrival of the re-animated cells. The selected primary cell line was then removed from the -150^{o}C freezer and immediately transferred to the water bath, and agitated gently until it was 90% defrosted. Using sterile technique, the 1ml cell suspension was pipetted into the pre-warmed medium in the T75 with its feeder-layer. The medium was gently washed from side to side in the flask to mix the newly re-animated cells with the growth medium. The T75 plate was incubated overnight, and after microscope examination the following morning was subsequently re-feed with fresh medium.

2.3 Patient-Derived Xenografts

Individual patient cancer epithelial cells ($2x10^6$ cells) were admixed (in a 2:1 tumour: stroma ratio) with low passage bone marrow-derived mesenchymal stem cells (hMSCs) ($1x10^6$ cells) (ScienCell) in 100 µl medium and suspended in 100 µl cold Matrigel (BD Biosciences, Germany). This was injected subcutaneously into the right and left flanks of sex-matched 6-8 weeks old MF-1 / CD-1 nude, SCID or RAG immunocompromised mice (Harlan), depending upon the laboratory availability.

Animal procedures were carried out with ethical approval under UK Home Office Licence (PPL 40/3559) in accordance with the 3R's framework for humane animal research. Tumour growth from the cell injections was monitored by calliper measurements, until they had reached the maximum acceptable size, when tumours were surgically removed under anaesthesia and were portioned for histological examination, cryopreservation and re-implantation.

2.4 Characterisation

2.4.1 Immunohistochemistry

Tissue and the agarose embedded patient cancer cells were formalin fixed and paraffin embedded (FFPE) before 4µm thickness sections were cut for both H&E and immunohistochemistry (IHC) analysis. IHC was essential for characterising the *in vitro* established patient cancer cells as tissue architecture is absent and therefore characterisation by H&E alone unreliable.

Optimisation was undertaken carefully to ensure characteristic staining of the control tissue and thus subsequent study samples in comparison to the background stroma. The optimisation assay results are displayed (appendix). Following optimisation, staining was undertaken in batches for each antigen with the corresponding negative controls, in line with previous reports in the published literature, and detailed below (Table 3).

Slides were de-paraffinised and underwent heat induced epitope retrieval. Following equilibration in phosphate-buffered saline (PBS) the endogenous peroxidase activity was blocked by incubating slides in a solution of hydrogen peroxide in PBS. Endogenous proteins were blocked with the serum corresponding to the secondary antibody, before incubation with the primary antibody in question. Amplification and visualisation was then performed either with streptavidin-biotin-peroxidase or horseradish-peroxidase (HRP) technique with diaminobenzidine (DAB), which becomes visible as a brown precipitate. Finally, slides were counter-stained with haematoxylin before mounting.

Sections were viewed with a Leica DMLB Bright-field Microscope (Leica-microsystems, Milton Keynes, UK) and images acquired with Leica QWin Standard v3 software. The presence of any

characteristically stained cells was considered positive with respect to negative controls, and confirmed by a second blinded individual.

Table 3. Particulars of each immunohistochemistry technique

Stain	Species & specificity	Clone & supplier	Epitope retrieval	Endogenous peroxidase	Non-specific binding site block	Primary antibody	Secondary antibody	Amplification and visualisation	Method-ological References
Cytokeratin	Mouse monoclonal	clone MNF116, DAKO, M0821	10mM Trizma base & 1mM anhydrous EDTA (pH 9.0) 98°C for 20mins	1% H_2O_2 in PBS for 5mins	20% rabbit serum in PBS for 10mins	1:50 in PBS for 30mins at RT	Biotinylated polyclonal rabbit anti-mouse at 2 µg/mL. (DAKO, E0354)	Avidin-Biotin-Complex (ABC) for 20mins (Peroxidase standard, Vector Laboratories)	(297, 298, 366)
ALDH1A1	Rabbit monoclonal	EP1933Y, Abcam, ab52492	10mM Citric Acid (pH 6.0) 98°C for 30mins	1% H_2O_2 in PBS for 10mins	20% swine serum in PBS for 20mins	1:100 in PBS for 60mins at RT	Biotinylated polyclonal swine anti-rabbit at 1/300. (DAKO, E0353)	Avidin-Biotin-Complex (ABC) for 20mins	(365, 366, 368)

EpCam	Mouse monoclonal	clone Ber-EP4, DAKO, M708201	Preheated DAKO Target retrieval Solution (S1700) at 98°C for 40mins, and allow to slowly cool to RT for 20mins	3% H_2O_2 in PBS for 10mins	20% rabbit serum in PBS for 30mins	1:100 in PBS for 60mins at RT	Rabbit anti-mouse HRP at 1/100 (DAKO, P0161)		(304, 307, 308, 375, 379)
p53	Mouse monoclonal	clone DO-7, DAKO, M700101. (binds mutant and wild type protein)	10mM Trizma base & 1mM anhydrous EDTA (pH 9.0) 98°C for 20mins	0.5% H_2O_2 in PBS for 10mins	20% rabbit serum in PBS for 30mins	1:25 in PBS for 30mins at RT	Rabbit anti-mouse HRP at 1/100 (DAKO, P0161)		(380-383)
CD44	Mouse monoclonal	clone DF1485, DAKO, M708201	10mM Citric Acid (pH 6.0) 98°C for 20mins	1% H_2O_2 in PBS for 10mins	20% rabbit serum in PBS for 30mins	1:25 in PBS for 30mins at RT	Rabbit anti-mouse HRP at 1/100 (DAKO, P0161)		(350, 353, 369, 372, 375)

Vimentin	Mouse monoclonal	clone V9, DAKO, M0725	10mM Citric Acid (pH 6.0) 98°C for 20mins	1% H_2O_2 in PBS for 10mins	20% rabbit serum in PBS for 20mins	1:50 in PBS for 30mins at RT	Rabbit anti-mouse HRP at 1/100 (DAKO, P0161)		
Anti-Trefoil Factor 3 (TFF3)	Mouse monoclonal	Abcam, UK, ab57752	10mM Citric Acid (pH 6.0) 98°C for 20mins	1% H_2O_2 in PBS for 10mins	20% rabbit serum in PBS for 20mins	1:75 in PBS for 60mins at RT	Biotinylated polyclonal rabbit anti-mouse at 2 µg/mL. (DAKO, E0354)	Avidin-Biotin-Complex (ABC) for 20mins	(326, 327, 384)

2.4.2 Flow cytometry

Following validation of the protocols and optimisation of stains with the known control cell line of OE33, the expanded individual patient tumour epithelial cells were stained with anti-human HLA-class 1, Cytokeratin, EpCam, CD44 and ALDH and corresponding isotype control according to the below detailed methods for intra-cellular and extra-cellular staining. Cells were then washed and fixed in 2% formaldehyde before being analysed on a LSRII flow cytometer (Becton Dickinson), equipped with 488 nm and 633nm lasers. Data was analysed with Weasel software Version 3.0.2 (The Walter and Eliza Hall Institute of Medical Research, Melbourne, Australia).

2.4.2.1 Intracellular staining with directly conjugated antibodies (Cytokeratin)

The primary OG cancer cells to be analysed were harvested using trypsin, which was then neutralised with PCA medium. These were centrifuged, supernatant discarded, pellet vortexed and re-suspend in 10-20ml of wash buffer (PBS with 2% BSA), then centrifuged, supernatant discarded, pellet vortexed and then re-suspended in 1ml of fix buffer (PBS with 3.7% formaldehyde), before it was incubated for 20mins on ice. 19ml of wash buffer was added, then centrifuged, supernatant discarded, pellet vortexed and then re-suspended in Saponin buffer (PBS with 0.5% Saponin, 2% BSA). It was then incubated for 20mins on ice.

An aliquot of 50μl of cells (approx. $2x10^5$ cells, but can be anywhere from $2x10^4$-$2x10^6$) per test was placed into each 1.5ml micro-centrifuge tube. Every cell line needed 4 tubes: Unstained, Isotype Control plus secondary antibody, Secondary antibody only and Test antibody with secondary antibody.

The primary antibody or isotype control antibody was added (see below table with optimised and matched concentrations) and a matched volume of saponin buffer was added to the unstained sample and secondary only sample. The antibody was mixed well with cells by gentle pipetting, before incubation on ice in the dark for 30mins.

Subsequently 1ml of wash buffer was added, and centrifuged (5mins 3,000rpm), supernatant discarded and pellet vortexed. The pellet was re-suspend in Saponin buffer and secondary antibody added, with a matched volume of saponin buffer added to the unstained sample, before incubation on ice in the dark for 30mins. The secondary antibody was removed by adding wash buffer, centrifuging (5mins 3,000rpm), supernatant discarded and pellet vortexed. It was then re-suspend in 500ul of fixation buffer, transferred to a FACS tube with a lid, kept in the fridge, and analysed within 24 hours.

Table 4. Particulars of Flow Cytometry Intra-cellular Antibodies						
Antibody	**Company**	**Cat #**	**Target/ Control**	**Target species**	**Fluorophore**	**Concentration /Test**
Primary	DAKO	M0821 clone MNF116	Cytokeratin	Human (cross-reactive)	unlabelled	Dilute in saponin buffer to a final conc of 6.8uL /mL
Isotype	BD biosciences	554121	Cytokeratin	Mouse IgG	Unlabelled	Diluted in saponin buffer to match conc cytokeratin Ab
Secondary	ThermoFisher		Anti-Mouse IgG	Goat	AF488	Dilution of 1/200 in saponin Buffer

2.4.2.2 Surface staining with directly conjugated antibodies (HLA, EpCam, CD44)

The OG cancer cells were harvested for analysis from the feeder cell culture as usual (keeping time of exposure to trypsin to a minimum, to prevent further stripping of the cell surface molecules). The trypsin was then neutralised with medium containing serum, centrifuged, supernatant discarded, pellet vortexed and re-suspended in wash buffer (PBS with 2% BSA kept at 4°C) at $4x10^6$ /ml. 50μl of cells were aliquoted ($2x10^5$) per test into a 1.5ml micro-centrifuge tube (Eppendorf tube). NB: cell number can be anywhere from $2x10^4$-$2x10^6$, and every cell line needs 3 tubes: Unstained, Isotype Control and Test antibody stain. Throughout all buffer and cells were kept cold to prevent internalisation of antibody.

The primary antibody (HLA, EpCam, CD44), or isotype control antibody was added according to the optimised concentrations outlined (Table 4) and a matched volume of wash buffer added to unstained samples. When dual and triple staining, the antibodies were premixed and added at the same time, ensuring that the antibody was well mixed with the cells by gentle pipetting, before then incubated on ice in dark for 30mins. Subsequently 1ml of wash buffer was added, centrifuged (5mins 3,000 rpm), supernatant discarded and pellet vortexed.

The pellet was re-suspend in 500ul of fixation buffer (PBS with 3.7% formaldehyde) before transferred to a FACS tube with lid and kept in fridge before it underwent analysis in the following 24 hours.

Table 4. Particulars of each flow cytometry technique						
Antibody	**Company**	**Cat #**	**Target**	**Clone / Isotype**	**Fluorophore**	**Volume /test**
Primary	BD Biosciences	560533	CD44	Hu	PE-Cy7	1μl
Isotype	BD Biosciences	560542	CD44 (560533)	Mouse IgG2b	PE-Cy7	1μl
Primary	Cell Signalling technology	5447	EpCam	VU1D9	AlexaFluor 647	1μl
Isotype	Cell signalling technology	4843	EpCam	Mouse (MOPC 21) IgG1	AlexaFluor 647	1μl
Primary	AbD Serotec	MCA81PE	HLA ABC	W6/32	RPE	10uL
Isotype	AbD Serotec	MCA929PE	HLA ABC	IgG2a	RPE	10μl

2.4.2.3 Intra-cellular enzyme induced fluorescence with ALDH substrate conversion

The levels of the enzyme aldehyde dehydrogenase (ALDH) within the cells were investigated using the commercial ALDEFLUOR™ kit. This works using the activated Aldefluor Reagent, BODIPY-aminoacetaldehyde (BAAA), which is a non-toxic substrate for ALDH, which diffuses into intact and viable cells. In the presence of ALDH, BAAA is converted into BODIPY-aminoacate (BAA), which is fluorescent. Active efflux is prevented by an efflux inhibitor in the Aldefluor Assay Buffer and therefore the fluorescent reaction product is retained inside the cells.

The amount of this fluorescent reaction product is proportional to the ALDH activity in the cells and can then be measured using a flow cytometer. A specific inhibitor of the ALDH enzyme, diethylaminobenzaldehyde (DEAB), is used to control for background fluorescence, and acts as a surrogate isotype control.

One should always expect some staining overlap between Antibody and DEAB enzyme inhibitor control due to background staining. The stain therefore doesn't separate out into easy homogeneous populations on the histogram, but as expected it is clear on the dot plot.

The exact method from the commercial ALDEFLUOR™ kit instructions was followed, including optimization. It was tested on FLO 1 and OE33 at multiple concentrations as per manufacturer's instructors to get the clearest staining at the lowest concentration. The BAA (fluorescent reaction product) stained with most clarity (in contrast to the standard non-efflux inhibited background fluorescence) at a concentration of $2x10^5$ for OE33 and $5x10^5$ for FLO-1.

The literature reports positive staining for FLO-1 (368) as a control, but I have also shown that OE33 stains identically for ALDH as FLO-1, and so OE33 can therefore be used instead as the internal control for ALDH, and universally as a control for all of the chosen antibodies, as all of the other stains already use OE33 as the positive control.

Table 5. Details of antibodies and controls used for flow cytometry and IHC							
Antibody:	**Method:**	**Company:**	**Product number:**	**Animal origin:**	**Reacts to:**	**Clone status:**	**Conjugation:**
Cytokeratin	IHC	DAKO	M0821	Mouse	Anti-human.	Monoclonal: MNF116	
	Flow cytometry	DAKO	M0821	Mouse	Anti-human	Monoclonal: MNF116	needs secondary Ab
	Negative control	BD Pharmingen	554121	Mouse IgG1, κ Isotype Control		Monoclonal: MOPC-21	
	secondary Antibody Fluoro-stain	Invitrogen	A-11001	Goat IgG (H+L) Antibody	Anti-Mouse		Alexa Fluor® 488
NB: I have used DAKO clone mnf116, it reacts with cytokeratin 5, 6, 8, 17 and also 19.							
EpCam	IHC	DAKO	M0804	Mouse	Anti-human.	Monoclonal: Ber-EP4	No
	Flow cytometry	Cell signalling technology	5447	Mouse	Anti-human	Monoclonal: VU1D9	AlexaFluor 647 – Red (using blue laser)
	Isotype control	Cell signalling technology	4843	Mouse IGg1		MoPC-21	AlexaFluor 647 – Red (using blue laser)

CD44	IHC	DAKO	M7082	Mouse	Anti-human.	Monoclonal: DF1485	No
	FACS	BD Pharmingen	560533	Mouse	Anti-human	Monoclonal: G44-26 (also known as C26)	PE-Cy7
	Isotype control	BD Pharmingen	560542	Mouse	Anti-human	IgG2b	PE-Cy™7
Aldehyde dehydrogenase (ALDHA1)	IHC	Abcam	ab52492	Rabbit	Anti-human	Monoclonal: EP1933Y	No
	FACS	StemCell technologies	01700	ALDEFLUOR™ assay kit	ALDH Enzyme	-	Green
	Isotype control	Diethylaminobenzaldehyde (DEAB), a specific inhibitor of ALDH, is used to control for background fluorescence and provide an isotype.					

2.4.3 Immunofluorescence

Immunofluorescence (IF) staining of was performed on the cancer cell clusters once extracted from the 3D-TGA. On day 7, cell clusters from the 3D-TGA were extracted using the standard method,(185) performed by the careful removal of obvious medium with 200μL pipette, addition of 13uL of Dispase (120 units/mL) to each well and incubated for 20 mins at 37°C.

A large area on each of the polyscene IHC slides was marked with a Pap pen, and slides were then placed on a metal IHC tray with lid. A pipette using a P200 tip was set at 25uL and was used at the bottom of the well to loosen the BME, whilst being careful not to introduce bubbles. The contents from all wells was then pipetted onto a single slide per 3D condition. The flat part of a bent pipette was used to smear the cellular mixture into a thin layer (if necessary). As the excess liquid evaporated and the volume starts to reduce and dry around the edges, it was flooded with formaldehyde (1:10 PBS dilution of 36% stock formaldehyde). The formaldehyde solution fixed the cells for 20 mins, before it was tapped off and the slides were immediately frozen in a pre-cooled slide box. These could stay frozen for months, before then being stained as a batch.

Immuno-staining was performed as previously reported(238) and following optimisation (appendix), with Trefoil Factor 3 (TFF3, Abcam), anti-mouse AlexFluor488 (ThermoFisher Scientific) and mounted in Prolong Gold Anti-fade containing DAPI (ThermoFisher Scientific).

The slides were defrosted in a PBS bath (or with PBS on top of slide) to prevent dehydration, and then washed twice with PBS to remove formaldehyde and the slide thoroughly remarked with the PAP pen. At no point were the slides let dry out.

The slides were then covered with Blocking solution (20% goat serum, 2% goat F(ab')2 anti-mouse IgG and 20% rabbit serum, in permeabilisation buffer) for 90 mins at room temperature (RT). [The purpose of the anti-mouse F(ab')2 fragments is to block against immune-reactive mouse IgG species in the BME. The additional rabbit serum is to help stop non-specific binding of the secondary, as the primary & secondary antibody are mouse & rabbit respectively.] The excess blocking solution was then tapped off (do not wash) before adding primary antibody and isotype control. The primary antibody (TFF3, abcam, ab57752, conc: 0.45mg/ml) was diluted 1/25 in permeabilisation buffer (2% BSA, 0.2% Triton X-100, 0.05% Tween-20, and 10% rabbit serum in PBS) for an end concentration of 18μg/ml. The negative (isotype) control (mouse IgG1, DAKO, X0931) was diluted in permeabilisation buffer to match the primary antibody end concentration of 18μg/ml. These slides were then incubated in humid conditions for 2 hours at room temperature.

Following this staining the slides were then washed three times in PBS baths to thoroughly remove primary antibody. The secondary antibody (Rabbit anti-mouse AlexaFluor(R)488, Lifetechnologies A21204) was diluted 1 in 1000 in permeabilisation buffer, and then applied to the slides which underwent incubation for one hour, in the dark at RT in a humid environment. The slides were then washed three times with fresh PBS.

Slides were mounted using Prolong gold glue, with DAPI (blue) by adding 1 drop of mount to the slide and carefully place coverslip on top. The coverslip was pressed on to remove bubbles, but using gentle pressure to avoid snapping it. These were left to harden (non- humid, 4°C in the dark for 24-48 hours) and then sealed at the edges with nail varnish. If the

DAPI glue didn’t set, the sides were stored at RT in a dark drawer for 24-48hrs before sealing with nail varnish, and subsequent longer term storage at 4°C.

Fluorescent Microscope imaging was performed with the slides upside down. Immunofluorescent images of the stained clusters were obtained with the Nikon Eclipse Ti-E microscope and NIS Elements Advanced Research Software.

2.5 Three-Dimensional Tumour Growth Assay

The individual patient's epithelial cells, were co-cultured in the three-dimensional tumour growth assay (3D-TGA) with or without human mesenchymal stem cells (hMSC) (#7500, ScienCell, CA, USA) in a Cultrex® basement membrane extract (BME) (Trevigen, MD, USA), using a serum-free medium, with a pH and glucose reflective of human tissue values. The original 3D-TGA method was adjusted to take account of the specific requirements needed to allow growth of OG cancer cells, as is outlined in Results Chapter 2, with the final methodology outlined here.

2.5.1 OG cancer 3D-TGA method

To setup the 3D-TGA, the appropriate number of Cultrex® Basement Membrane Extract (BME) without phenol red (3432-005-01) aliquots were placed on ice to thaw slowly. Key equipment (multichannel pipette tips, pipette-boy 10ml pipettes, pre-marked up universal tubes, troughs, pre-marked up falcon tubes) was corralled and pre-cooled to -20°C to avoid premature gelling of the BME when it is handled whilst performing the cell seeding.

A low-adherent, black-walled, clear-bottom, 384-well plate (Corning, New York, USA) was cooled at 4°C. 50µl of TGA medium (F medium with 10 ng/mL EGF, and 10 µmol/L ROCKi Y-27632) was added to all outer wells. The plate warmer (VWR 460-3253 & 460-3238) was set to 37°C, and multichannel pipette programmed.

OG cancer cells and the stromal cells (hMSCs) were harvested, the cells were centrifuged into a pellet and re-suspend in TGA medium and stored on ice. Cells were counted with a Neubauer haemocytometer and the number and concentrations of tumour

cells and hMSCs were calculated per close-to-patient cancer cell culture. To seed 2 plates per cell culture (one with and without co-cultured hMSCs), approximately $6x10^6$ OG cancer cells were needed in total.

Although it is possible to seed more than one cell culture into the 3D-TGA 384 plate at a time, it was recommended to perform each separately rather than in tandem, to prevent cells waiting on ice for prolonged periods and losing some of their viability.

$6.25x10^3$ tumour cells +/- addition of 2.083 $x10^3$ mesenchymal cells (3:1 tumour: stroma ratio) per well for the 384 well plate were admixed. These were then centrifuged (5min, 500g) into a pellet, the suspending medium aspirated taking extreme care not to disturb the pellet, and then underwent vigorous tapping and vortexing. Using a pre-cooled 10ml pipette, the cell pellet was re-suspend in 6mLs neat BME (13μl/well, x1.5 for excess) by gently pipetted up and down to mix, without introducing bubbles. This BME cell suspension mix was carefully transferred to a trough on ice, to allow swift accurate seeding using a pre-cooled multichannel pipette.

A 12.5μl/well cell suspension was seeded into the wells in the 384 well plate on ice taking caution to avoid bubbles. The plate was gently tapped and rocked to ensure the BME was evenly spread on a level at the bottom of wells. A hypodermic syringe needle was used if necessary to pop any significant bubbles. The BME cell suspension within the plate was then warmed to 37°C on the plate warmer, which allowed the BME to gel with the cells in suspension. The whole plating process was then repeated for the second condition (+/-hMSCs). Once the BME was gelled and cells embedded in the 3D matrix, a 3D Growth medium overlay of 12.5μl per well was used for cell cluster nutrition. The 384-

well plate was gently tapped to ensure an even spread of medium at the bottom of each well and then placed in a 5% CO_2 incubator (37°C) for 1hr to allow the cells to rest.

Cellular metabolism and growth was assessed throughout the period of the assay with an alamarBlue® cell fluorescence assay (ThermoFisher Scientific, Loughborough, UK). A baseline reading was obtained following the establishment of the 3D-TGA. The alamarBlue® was diluted 1:10 in TGA medium and added 25μl / well of Day 0 growth wells. (NB it is a 1:5 dilution of 12.5μl / well for the drug well overlays, as there is an additional 12.5μl / well pharmaceutical compound overlaid so final alamarBlue dilution is always 1:20). The 3D-TGA 384 well plate was then incubated at 37°C (5% CO_2) for exactly 60 minutes, before the signal was measured on a fluorescent plate reader (excitation 560 nm, emission 588 nm, Flex Station II, Molecular Devices) with SoftMaxPro software.

To enable separate assessment of the co-cultured stromal cells within the 3D-TGA, hMSCs were generated which constitutively expressed the red fluorescent protein mCherry. The mCherry-labelled hMSC component of the 3D-TGA was concurrently measured by the fluorescent plate reader (excitation 553 nm, emission 613 nm) to allow separate assessment of this component of the 3D-TGA.

To assess the standard growth pattern of the cancer cell clusters over the 7 days of the assay, alamarBlue readings and the corresponding mCherry readings were taken on Day 0 and every 48 hours following: on Day 3 (D3), 5 (D5) and 7 (D7).

Plates were incubated for 72 hours (3 days) to allow cells to establish within the extracellular matrix and form cell clusters. These were then treated with increasing concentrations of the

chemotherapy drugs as a 12.5µl medium overlay per well, to enable endpoint drug sensitivity (see later section explaining this in depth). An aliquot of 12.5µL of TGA medium was added to each of the remaining D5 and D7 growth microscopy/florescence wells as a surrogate drug overlay.

On day 7, following 96 hours (4 days) exposure to the chemotherapeutics, progress of the pharmaceutically treated and baseline growth wells was assessed using a 12.5µl per well alamarBlue 1:5 dilution overlay (achieving a final alamarBlue dilution of 1:20 in each well), as these had already had a surrogate drug layer of medium added. Exactly one hour after the alamarBlue was administered to the plates the signal was measured using the fluorescent plate reader.

Following the final (D7) alamarBlue reading, assay endpoint microscopy and 3D photography were undertaken to obtain images of mCherry hMSCs and OG Epithelial cells where they had grown into 3D cancer clusters over the 7 day period. After completion of the alamarBlue flex-station readings and the serial microscopy, the cancer cell clusters were harvested for the performance of fluorescent staining (which is outlined in a further section).

2.5.2 Measurement of growth and cytotoxicity with alamarBlue

Assessment of growth is performed using the alamarBlue® cell fluorescence assay which is based on the ability of metabolically active cells to convert the reagent into a fluorescent and colorimetric indicator. Damaged and non-viable cells have lower innate metabolic activity, and generate no or very low signal, whereas those growing and dividing cells will have a high signal, and therefore this acts as a surrogate marker for cancer cell

proliferation. The dye itself has low toxicity, is generally safe for cells, and it is a very standard and accepted technique in cell culture for assessing cell growth. Care should be taken not to presume that alamarBlue universally represents growth, as it is also influenced by the level of metabolic activity of the cells within the well, however this evaluation of growth can be easily checked by microscopy visual assessment of cellular proliferation within the wells.

2.5.3 Formulation of TME RPMI

Tissue Micro-Environment amended Roswell Park Memorial Institute (TME RPMI) Medium was obtained upon request from ThermoFisher and consisted of phenol red free RPMI (ThermoFisher #11835105), altered to pH 6.8, with 6mM D-glucose.

2.5.4 Formulation of Base Media and additional Growth Factors

The culture conditions used by the Clevers group for organoid growth used a basal cell culture medium (Base Media), optimised for Human Intestinal Stem Cell (HISC) growth and with additional growth factor supplementation for the growth of Barrett's. This was used to aid the development and optimisation of the 3D-TGA culture conditions for primary patient OG carcinoma cells. The following tables describe the components (Table 6) and supplements (Table 7) in this media.

Table 6. Base Media Formulation					
Reagent name	**Supplier**	**Cat No.**	**Solvent**	**Stock soln**	**Final conc**
Advanced DMEM/F12 (4°C)	Invitrogen	12634-010		500ml	
HEPES (powder)	Invitrogen	15630-056	DW	1M	10mmol/L
GlutaMAX-I (Room temperature)	Invitrogen	35050-038		200 mM	2 mM
Penicillin /Streptomycin (-20 °C)	Invitrogen	15140-122		10000 / 10000 U/mL	100/100 U/mL
B27 (-20 °C)	Invitrogen	17504-044		50 x	1x
N-Acetylcysteine (powder)	Sigma-Aldrich	A9165-5G	DW	500 mM	1 mM

Table 7. Additional Growth Factors					
Reagent name	**Supplier**	**Cat No.**	**Solvent**	**Stock solution**	**Final conc**
Recombinant Human EGF (-80)	Invitrogen	PHG6045	PBS/BSA	500 µg/mL	50 ng/mL
Recombinant Human Noggin (-20 °C)	Peprotech	120-10C	PBS/BSA	100 µg/ml	100 ng/ml
human recombinant R-spondin1 (-20 °C)	Peprotech	120-38	PBS/BSA	1 mg/ml	1 µg/ml
Recombinant Human Wnt-3a (-20 °C)	rndsystems	5036-WN-010	PBS	10 µg/ml	100 ng/ml
Human recombinant FGF10 (-20 °C)	Peprotech	100-26	PBS/BSA	100 µg/mL	200 ng/mL
[Leu15]-Gastrin I human (-20 °C)	Sigma-Aldrich	G9145	PBS/BSA	100 µM	1 nM
TGFβi A-83-01 (-20 °C)	Tocris	2939	DMSO	500 µM	2 µM
ROCKi Y-27632 (-80 °C)	Enzo	ALX-270-333M025	PBS	10 mM	10 µM

2.5.5 Generation of mCherry hMSCs

Low passage hMSCs were seeded in 6-well plates ($2x10^5$ cells/ well) and left to adhere overnight before being transduced with mCherry (Clontech Lentiviral X containing mCherry under the control of CMV_{IE} promoter), according to the manufactures instructions. Transduced cells were selected by exposing cells to puromycin at a concentration shown to kill parental cells (1μg/ml). Selection was maintained for a week. Surviving cells were expanded, expression of mCherry determined by flow cytometry, and aliquots of the low passage mCherry-labelled hMSCs cryopreserved for subsequent use.

2.5.6 Bright field imaging

Serial bright-field and immunofluorescent images of the co-cultured mCherry-labelled hMSCs and cancer cell clusters were obtained at day 0 and 7, using a Nikon Eclipse Ti-E microscope with Hoffman Modulation Contrast. Forty z-stacks were taken throughout the depth of the well, and extended depth of field projection picture was produced using the Nikon NIS Elements software, allowing a condensed view of the three-dimensional profile of the cancer cell clusters.

2.5.7 Chemotherapeutic pharmacology

Once established at day 3 cancer cell cultures were then treated with increasing concentrations of the chemotherapy drugs as a media overlay, to enable endpoint drug sensitivity at day 7.

Chemotherapy drugs were retrieved from the secure poisons cupboard or fridge, and 4 wells of a 10 fold dilution series were made up in a 96 well dilutions plate using TGA medium for each drug and combination (5 wells are required for Vardenafil due to the broad variation of concentrations that encompass the endpoint tissue concentrations seen in use). All drugs and their

dilutions were prepared together as a complete batch individually and in their combinations (Table 8 and Table 9).

These progressive drug dilutions were then added as a 12.5μl media overlay, to each of the x6 duplicate 3D-TGA wells for that drug concentration condition. The administration of chemotherapy to the 3D-TGA was performed for all drugs, combinations and at each of the dilutions as a large batch using an automated multi-channel pipette to ensure that chemotherapy exposure is uniform across all conditions (+/- hMSCs), taking extra care with the 5th dilution for the Vardenafil. The 3D-TGA plate was then returned to the incubator.

For the measurement of cytotoxicity, it is commonplace to display a control 'kill curve' of the solvent (e.g. DMSO) in which the cytotoxic agent is dissolved to show that the result seen is from the cytotoxic agent and not solvent. This is because many of the classic drug solvents (e.g. DMSO) are cytotoxic in their own right. In this study, the drugs used were sourced directly from the hospital pharmacy or manufacturer in non-toxic liquid preparation form ready for human injection. The concentrate drug was then diluted to its stock concentration using the standard serum free TGA medium, (Table 8) before subsequent 10 fold dilutions (Table 9) to produce drug concentrations that mirrored endpoint tissue concentrations and were applied to the 3D-TGA to assess cytotoxicity. The drug vehicle used is a tissue culture media which does not have an incidental cytotoxic side-effect, and therefore classical control kill curves for the solvent are not warranted. Nonetheless, a matched growth control condition with just TGA media was included in every assay as an internal control.

Table 8. Calculations of the final concentrations of drug to be delivered in the 3D-TGA as a media overlay (as 1/3 of the total well volume) from stock concentrations

	Stock conc	Top final conc (uM)	Mw	[Stock] (mg/ml)	[Stock] (M)	[Stock] (mM)	Dilution to give 3x top Conc	Vol (ul) to add to 1ml
Epirubicin	2mg/ml	200uM	580	2	0.003448	3.448276	5.747126	174.00
Cisplatin	1mg/ml	200uM	301.1	1	0.003321	3.321156	5.53526	180.66
5-FU	25mg/ml	10000mM	130.1	25	0.19216	192.1599	6.405329	156.12
Panobinostat	2mg/ml	10uM	349.44	2	0.005723	5.723443	190.7814	5.2416
Vardenafil (Bayer) *in vivo*	1mg/ml	1uM	561.52	1	0.001781	1.78088	593.6268	1.68456
Vardenafil (S'ton) *in vitro*	1mg/ml	100uM	561.52	1	0.001781	1.78088	5.936268	168.456

Table 9. Calculations of the drug the combinations in serum free medium, for serial 10 fold dilutions which encompass the endpoint tissue concentrations

	Top final conc (uM)	Drug 1 (ul in 1ml)	Drug 2 (ul in 1ml)	Drug 3 (ul in 1ml)	Drug 4 (ul in 1ml)	Serum free media (ul)
Epirubicin	200	174				826.00
Cisplatin	200	181				819.34
5-FU	10000	156				843.88
Epi/Cis	200/200	174	181			645.34
Epi/5-Fu	200/10000	174	156			669.88
Cis/5-Fu	200/10000	181	156			663.22
Epi/Cis/5-Fu	200/200/10000	174	181	156		489.22
Panobinostat	10	5.24				994.76
Epi/Cis/5-FU/Panobinostat	200/200/10000/10	174	181	156	5.24	483.98
Vardenafil *in vitro*	100	168				831.54
Epi/Cis/5-Fu / Vardenafil *in vitro*	200/200/10000/100	174	181	156	168	320.76

2.5.8 Calculation of chemo-toxicity

Following the addition of drugs to the cancer cell clusters in the 3D-TGA, the chemo-toxic effect was calculated as a percentage of the matched untreated control. IC_{50} curves were generated for the drugs both individually and in combination, as previously described (238, 385). The previously outlined mean peak serum concentration achieved in patients for each drug was compared with the IC_{50} values, and chemo-response was thus defined as sensitive, borderline (+/- 10% of the mean peak serum), or resistant.

2.5.9 Statistical analysis

Two-way ANOVA was performed to compare the different parameters among the different groups when assessing the relative efficacy of the drug combinations. Difference between groups was only considered to be significant if there was no overlap between the 95% confidence interval about the median.

The paired and un-paired t-test was used to calculate the significance of difference between parametrically distributed groups, and Mann-Whitney U test between non-parametric and independent groups, with a significance level of $p < 0.05$.

Statistics were computed with GraphPad Prism 5 Software (San Diego, CA, USA) and plotted with mean values, and error bars for standard deviation.

3 Results 1: Establishment and Characterisation of primary OG cancer cells

3.1 Overview & Aim

Tissue specimens were transferred from the hospital to the laboratory, processed and disaggregated to produce a cellular suspension (Materials and Methods 2.2.1). *Ex vivo* tumour cells were then expanded using a supporting feeder layer system. From this early passage material, the tumour epithelial cells and cancer-associated fibroblasts (CAFs) were expanded, harvested and characterised. Characterisation was vital to investigate whether they represent malignant OG cancer epithelial cells, rather than any adjacent normal cells, their similarity to the patient tissue from which they were derived and the presence of any other potential features, such as CSC populations.

The aim was to develop and subsequently refine a new methodology for establishing individual patient OG tumour cell cultures in the laboratory, which has never previously been reported.

These close-to-patient OG cell cultures were formalin-fixed for IHC analysis to study their origin and phenotype, xenografted to study tumorigenicity and analysed by flow cytometry to investigate the presence of CSC sub populations.

3.2 Results

3.2.1 Establishment of *ex vivo* OG cancers

The small volume OG cancer biopsies taken at endoscopy, did not readily establish using the standard method, and so a number of adjustments and refinements to the routine method were employed, which enabled malignant cell establishment. The technique was more challenging to perform reliably due to the exceedingly small portions of tumour tissue obtained at biopsy in comparison to the physical pieces of tumour received from tumour resections.

An initial cohort of 30 patients and their biopsy tissue was used in this method development phase of the study and did not generate patient cancer cells. The results of these challenges and adjustments made (e.g. alterations to disaggregation, supplementary antibiotics) during the establishment phase are detailed below.

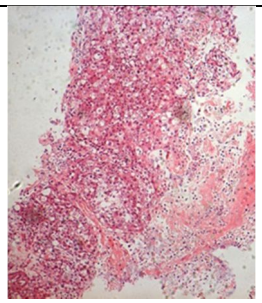
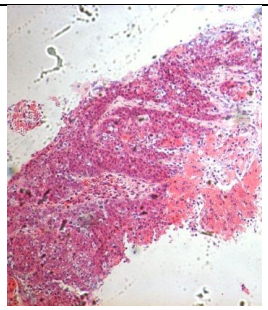
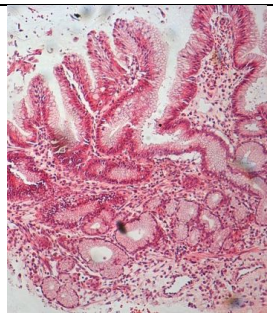
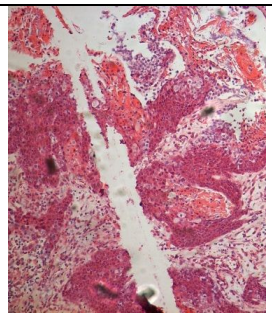
3.2.1.1 Tissue transfer media

When endoscopy lists occasionally ran late and transfers were delayed from the hospital site back to the laboratory at a different location, it resulted in extended transfer times of up to 24-48 hours. Despite being suspended in 10mls of Hanks Balanced Salt Solution (HBSS) as transfer medium at 4^{o}C before being transported on ice, the delay significantly reduced the cellular viability (of the later disaggregated cells) to 25-50%.

Three alternative tissue transfer media were trialled in an attempt to improve the conditions within which these fragile tumour biopsies were being held and increase cellular viability, particularly when transfer timelines were stretched. The original medium (HBSS) was compared to the 'in-house' prepared PCA Medium (500mls Dulbecco's Modified Eagle Medium, 100mls heat

inactivated Foetal Bovine Serum, 6ml 0.2 M sterile L-glut, 6ml 100x AA, 0.6ml 1mg/ml hydrocortisone in ethanol, 0.45ml 10mg/ml bovine insulin in 1% glacial acetic acid), and 2 commercial tissue transfer media: Hibernate A (BrainBits LLC), and MACS solution (Miltenyibiotec).

At 48 hours post biopsy, HBSS provided the least effective tumour tissue preservation and cellular viability, as measured by trypan blue exclusion assay (Table 10). PCA medium provided adequate viability and tissue quality, but both commercial products were superior. Tumour tissue was histologically slightly better preserved in MACS solution; however, cellularity in Hibernate A and MACS solution was broadly equivalent (Table 10). In the interests of pragmatism, (given that tissue transfer from endoscopy to the laboratory was usually prompt) the routine tissue transfer media was changed to PCA Medium, which combined cost effectiveness with improved cellular viability, particularly if the tissue transfer times were extended.

Table 10. Comparison candidate tissue transfer media				
Transfer solution	Histology	Tissue quality	Cellular viability (48 hrs)	Price (100mls)
HBSS		Poor	25–50%	£1
PCA		Good	60–80%	£10
Hibernate A		Excellent	70-80%	£35
MACS		Excellent	70-90%	£57

3.2.1.2 Disaggregation

Initial disaggregation with dispase and collagenase resulted in poor viability as measured by trypan blue exclusion assay. Switching to a 60 minute disaggregation from the original 2-4 hours resulted in cells with typically >70% viability and so 60 minutes incubation was used for all further work.

Originally, the superfluous cellular clumps and connective tissue debris was progressively broken up and filtered using fine strainers (100uM > 70uM > 50uM) to produce populations of single cells within the disaggregation solution. However, switching to filtering the disaggregated cellular solution only once with a 70um filter resulted in a 15% increase in cellular yield, in the progressive trials using 4 different samples. Whilst this was a somewhat small increase, any increase in cell numbers was paramount given the relatively small overall number of cells (maximum 0.3 $x10^6$ total cells per sample) that was generated from disaggregating the biopsies.

3.2.1.3 Microbial and fungal contamination

The principle challenge encountered during the establishment phase of the close-to-patient OG cancer cells was microbial and fungal contamination. 18 of the cell cultures were irreversibly contaminated and had to be discarded, despite the routine use of media supplemented with antibiotic / antimycotic (AA) (penicillin, streptomycin and amphotericin B) to store the human cancer tissue from the point of biopsy, tissue transfer, disaggregation and growth in *in vitro* culture.

Given the nature of the tissue sample's origin within the chronic bacterial colonised gut, there was constant vigilance for potential bacterial contamination of the *in vitro* cultures. Suspicious growth in one or more of the 12 wells of the 6-well plates (used

in the initial plating and incubation following disaggregation) occurred in 45% of patient samples. Eradication was performed by the immediate addition of 2mls Distel disinfectant solution (Tristel Ltd, UK) to the suspicious well in an attempt to prevent any cross-infection, between both different wells of the newly establishing cells and other OG cancer cells within that incubator. However, on two discrete occasions, bacterial contamination was not identified and contained at an early stage, and the other primary patient OG cancer cells (that were previously growing well) became irreversibly contaminated and had to be discarded, losing 7 and 5 of the close-to-patient OG cancer cell cultures respectively.

Six of the primary patient cancer cell cultures failed to establish due overwhelming fungal contamination. Fungal oesophagitis is a well-recognised complication of oesophageal cancers, and was reported as present visually during 9 of the endoscopic procedures. However, evidence of fungal load at endoscopy did not have any correlation with subsequent growth of fungus within *in vitro* tissue culture. Given the evident fungal growth despite the routine presence of the anti-mycotic Amphotericin B within the culture media, two additional antimycotics: Nystatin and Fluconazole were trialled in an attempt to salvage the primary biopsy derived cells. However, the addition of Nystatin was abandoned as in both cases where it was trialled, it precipitated out of solution over a 24-48 hour period and killed >60% of the 3T3-J2 feeder layer cells, which in turn prevented the epithelial cells from establishing in culture. Fluconazole was trialled according to reported doses, as an alternative second line anti-mycotic agent following some positive reports of use in tissue culture in the published literature (386, 387). However, whilst Fluconazole not affect the 3T3-J2 feeder layer cells, it failed to eradicate the fungal growth, and therefore the routine

addition of a second anti-mycotic to the primary tissue culture media was halted. In addition to overt bacterial contamination, ongoing low-level fungal contamination was also present despite anti-fungal treatment, and one close-to-patient OG cancer cell culture (which initially appeared to be contamination free) was discarded following a late fungal overgrowth following cancer cell sample's re-animation after cryopreservation.

3.2.1.4 Cell senescence following cryopreservation

Following re-animation after cryopreservation, all of the close-to-patient cell cultures appeared to be more fragile (than growth prior to cryopreservation), grew less quickly (2-4 times the previous passage timeframe) and died more easily in the previous permissive environment. From the patient cohort used for the novel method development phase, 5 individual patient cancer cell cultures were lost and 6 patients cancer cell cultures were also lost from the patient cohort that was due to go onto chemotherapy evaluation. The brittle behaviour evidenced by the re-animated close-to-patient OG cancer cells recurrently hampered growing substantial numbers of the primary patient cells following cryopreservation, which prevented the ready performance of further experiments which requires consistent cell culture growth and available cell numbers.

3.2.1.5 Success at establishing primary OG cancer close-to-patient cells

Following the initial (30 patient) method development phase from which close-to-patient cells were not generated, this refined OG cancer method for primary *in vitro* cancer cell establishment was used for the following 40 patient's endoscopic chemotherapy-naïve tumour biopsy samples. This resulted in more reliable close-to-patient cell culture establishment with a characteristic 2D visual growth pattern that was similar to all of

the OG cancer close-to-patient cell cultures (Figure 2). The epithelial cancer cells only established in islands and grew where there was close contact with the pre-seeded feeder cells (Figure 2A). Once the close-to-patient epithelial cells had established and started expanding into larger colonies (on the base of the plastic cell culture plate), intra-tumoural cellular heterogeneity became apparent, with cells of different sizes, shape and granularity (Figure 2B).

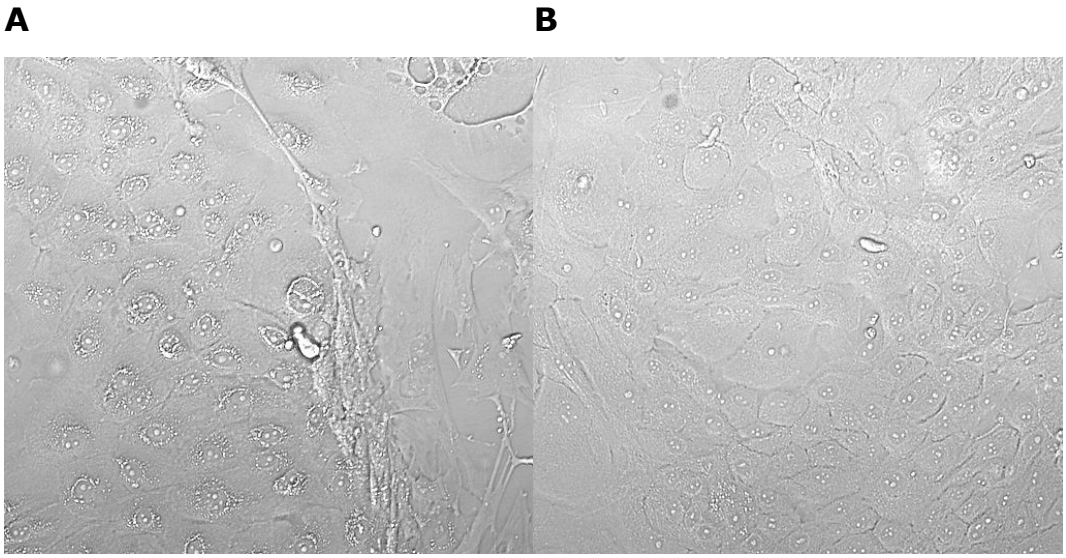


Figure 2. Appearance of primary close-to-patient cell cultures using Feeder Layer system

The morphology of established OG epithelial cells growing on a feeder layer in ROCKi supplemented tissue culture was examined with bright field microscopy. **(A)** The physical proximity between the epithelial cancer cells (rounded shape, left of picture), and the feeder J2 cells (vertically orientated linear cells, right of picture). **(B)** The heterogeneity of the epithelial cancer cells.

From this 40 patient cohort, samples from twelve patients were not useable due to technical reasons (e.g. low level infection, contamination, or non-recovery from cryopreservation) leaving a subsequent group of 28 patients with primary cells available for use, and an *in vitro* establishment rate of 70% (Table 11).

Table 11. Success of establishing *in vitro* close-to-patient cells from biopsies and the paired resected tumours

Origin of tissue	**Establishment of *in vitro close-to-*patient cells from patient tumour**	
	No. of patients	Patient cell cultures established
Pre-chemo biopsy	40	28 (70%)
Matched post-chemo tumour tissue	25	15 (60%)

The tumour biopsies from which the 28 individual close-to-patient cell cultures were established were collected from patients early in their diagnostic and staging pathway. There was no apparent difference in oncological or demographic characteristics between those patient's tumour biopsies that did (n=28) and did not (n=12) establish *in vitro*. (Table 12). The clinical characteristics of these 28 patients and tumours which did establish are described (Table 13).

Table 12. Oncological and Demographic Characteristics			
Characteristics		**Primary cells established**	**Primary cells not established**
Patients		n=28	n=12
Gender		F= 7, M = 21 Ratio: 0.33	F = 3, M = 9 Ratio: 0.33
Age (mean)		66	69
Charleson comorbidity score (mean)		1.4	1.6
Performance status (mean)		0.5	0.6
Known Barrett's		6 (21%)	5 (33%)
Histology		Adeno: 20 Squamous: 7 Linitus: 1	Adeno: 10 Squamous: 1 Linitus: 1
Site of tumour		Gastric: 1 (3%) GOJ: 13 (46%) (Siewert I:7, II:5, III:2) Oesoph: 14 (46%)	Gastric: 2 (17%) GOJ: 8 (66%) (Siewert I:4, II:2, II:2) Oesoph: 2 (17%)
Pre-chemo / staging TNM	cT (mean)	3	3
	cN (mean)	1	1
Tumour Regression Grade where available (mean)		4	4

Table 13. Clinical Characteristics of the 28 patients from which cell cultures were established

Patient ID	Gender	Age	Oncologist	Surgeon	Barrett's	Tumour from teeth	Site	Siewert	Histology	cTNM	Past Medical History	Drug History	Family History	Smoking History	Alcohol History	Performan	Palliation
OBX9	F	53	1	1	y	34-40	GOJ	II	Adeno	T3 N2	nil	nil	nil	nil	nil	0	
OBX10	F	71	1	1	y	30	GOJ	I	Squam	T3 N0	COPD, hypothyroidism	omeprazole, throxine	nil	nil	nil	1	
OBX18	M	45	1	1	n	39-42	GOJ	II	Adeno	T3 N0	nil	nil	nil	20 per day	nil	0	
OBX24	M	78	4	4	n	35-40	Lower Oes		Adeno	T2 N1	OA	Paracetamol, codeine	nil	nil	nil	1	Supra-clavic Met
OBX25	M	75	4	4	n	37-40	Lower Oes		Adeno	T3 N1	MI	Ramipril, bisoprolol, simvastatin, warfarin	nil	nil	nil	0	
OBX26	M	73	1	2	y	30-34	GOJ	I	Squam	T2 N0	Prostate Ca, HTN, partially sighted, aspergillosis	Atenolol, LHRH agonists, aspirin, NKDA	nil	20 per day	Mod	1	Syncronous lung lesions

OBX29	M	60	4	3	n	37-43	GOJ	II	Adeno	T3 N1	Cardiomyopathy, AF. Frailty	Warfarin, bisoprolol, ramipril	nil	nil	Mod	1	Cardiac failure
OBX33	M	59	2	1	n	30-36	Lower Oes		Squam	T2 N0	nil	nil	nil	nil	nil	0	
OBX34	M	64	4	1	n	42-50	GOJ	III	Adeno	T2 N0	T2DM, hypertension	Ibersartan, BFZ, iron, atorvastatin, omeprazole	nil	nil	nil	0	
OBX37	F	73	1	4	n	29-31	Lower Oes		Squam	T3 N3	Hypertension	Perindopril, fortjuice,	nil	nil	Mod	0	Inoperable
OBX39	M	85	1	2	n	38-39	GOJ	I	Adeno	T2 N0	COPD, right lower lobe collapse, CKD stage 3, hypertension, anaemia	Inhalers, cocodamol, felodipine, carbocisteine, ferrous sulphate, ramipril, lansoprazole, simvastatin, NKDA	nil	Ex heavy 20 years ago	nil	1	Synchronous bronchial and upper tract urological ca
OBX40	M	61	2	2	n	36	GOJ	I	Adeno	T3 N0	Hypertension, COPD, previous AKI, clubbed foot	NKDA, lisinopril, inhalers	nil	nil	nil	1	
OBX41	F	80	3	3	y	37-42	GOJ	II	Adeno	T3 N0	Op right ankle, benign breast op, Frailty	Gluconate, omeprazole, lolmesartan, netafim, dihydrocodeine	Father - Lung Ca	nil	nil	2	Frail

OBX42	F	54	1	3	n	29-31	Lower Oes		Squam	T2 N0	Anorexia	Cod liver oil, sertraline, fortisips	nil	nil	nil	1	
OBX44	M	67	2	3	n	35-40	GOJ	I	Adeno	T3 N0	Hypertension, hypercholesterol	nil	nil	nil	nil	0	
OBX45	F	51	1	1	n	25-30	Upper Oes		Squam	T3 N0	Sarcoid	nil	nil	nil	nil	0	
OBX46	F	61	1	3	n	25-35	Mid Oes		Squam	T2 N0	Severe deoression, hemicolectomy	Chlorpromazine, nitrazepam, anti-depressants	nil	nil	nil	1	
OBX47	F	74	1	4	n	20	Upper Oes		Squam	T3 N2	Hypertension, COPD, breast Ca, (mastectomy & radiotherapy)	Salbutamol, simvastatin, tiotropium, BFZ, betahistine, lansoprazole	nil	nil	nil	1	Advanced COPD & Frail
OBX53	M	58	2	1	n	35-41	GOJ	II	Adeno	T3 N2	Hypertension, varicose veins	Amlodipine, ramipril, bendroflumethiazide	nil	nil	nil	1	
OBX54	M	74	2	2	n	39-40	Lower Oes		Adeno	T2 N1	bilateral knee OA, back pain, angina	GTN spray	nil	Stop 2010	nil	1	
OBX57	M	56	2	3	n	37-40	GOJ	I	Adeno	T2 N0	Asthma, IBS, hypertension	Symbicort, salbutamol, atrovent, omeprazole, ramipril	nil	nil	nil	0	positive peritoneal washings

OBX59	M	72	4	3	y	28-40	GOJ	I	Adeno	T3 N2	Asthma, AF	Digoxin, warfarin	Sister – kruken berg ca	nil	nil	0	
OBX6	M	59	2	1	n	20	Mid Oes		Adeno	T3 N1	COPD	inhalers	nil	20 a day	nil	1	thoracic node - inoperable
OBX64	M	65	2	3	n	45	GOJ / Gastri	III	Linitis	T3 N2	Ulcerative colitis	Lansoprazole, loperamide,	nil	Stop 2006	nil	1	Joint decision
OBX65	F	49	3	2	n	32	Lower Oes		Squam	T2 N0	nil	nil	nil	nil	nil	0	
OBX70	M	77	1	3	y	35-39	Lower Oes		Adeno	T3 N0	CKD, HTN, TURP, Hiatus hernia	Lansoprazole, Amlodipine, Losartan	nil	nil	nil	1	
OBX71	M	55	1	3	n	35-40	Lower Oes		Adeno	T3 N2	Reflux, spinal surgery	omeprazole	nil	nil	nil	0	
OBX73	M	62	1	1	n	37-39	Lower Oes		Adeno	T3 N1	nil	nil	nil	nil	nil	0	

For clinical reasons, two-thirds of these patients did not undergo the full curative therapy regimen, and so did not have a clinical chemotherapy response to compare with the *ex vivo* result. This resulted in a final group of 12 samples from nine patients who were entered into the study (Figure 3) and subsequently underwent full characterisation and chemotherapeutic analysis.

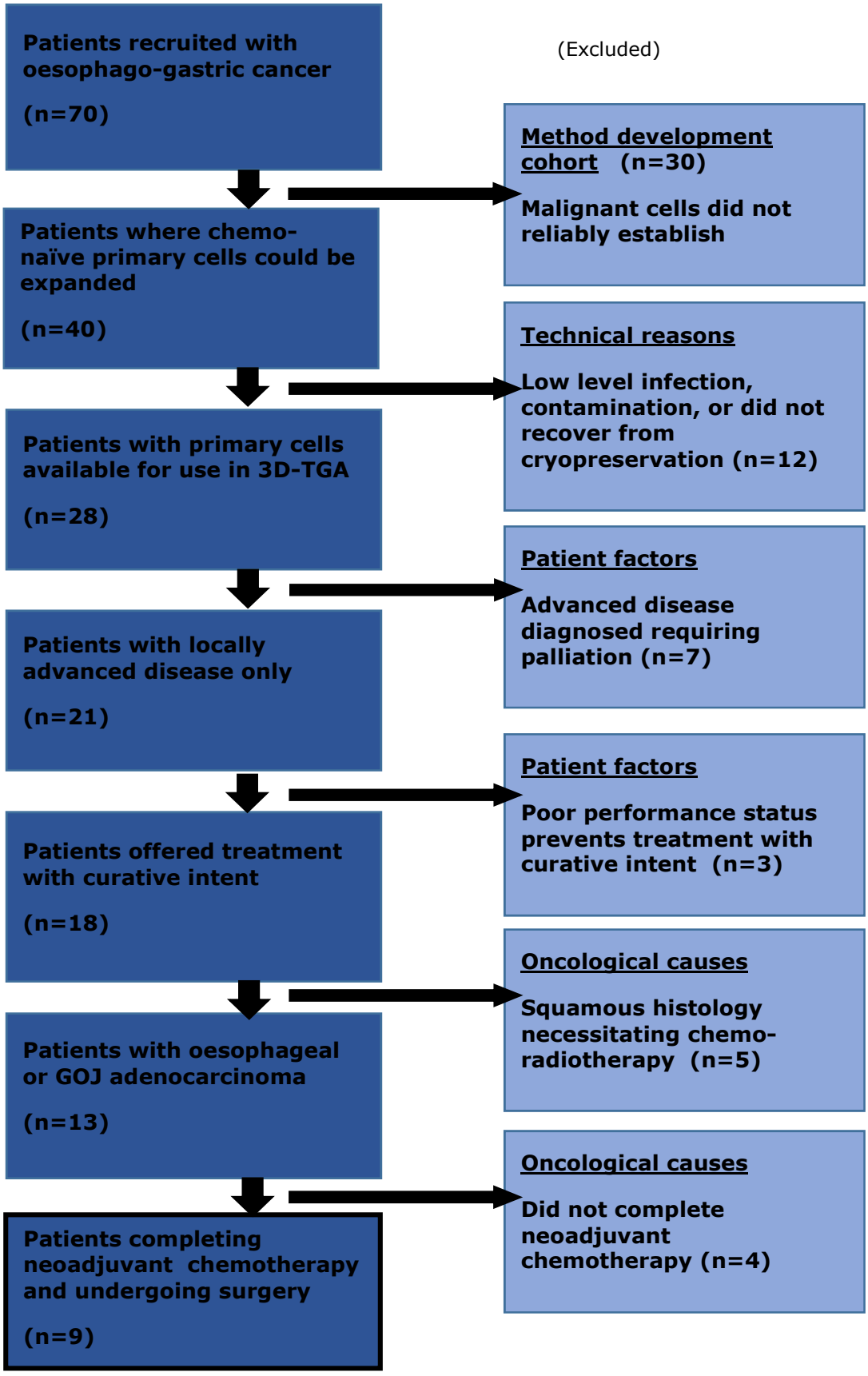


Figure 3. Flow chart demonstrating application of Inclusion Criteria to recruited Study Patients

3.2.2 Immunohistochemistry Characterisation

There is no standalone molecular marker that can be used to individually identify OG cancer cells, and therefore a pragmatic group of markers was applied to make an informed scientific judgement on the characterisation of the established cells.

Evidence of epithelial status was established by examining for cytokeratin staining. I used DAKO clone mnf116 (which reacts with cytokeratin 5, 6, 8, 17 and 19) as this clone shows an especially broad pattern of cytokeratin reactivity with human epithelial tissue and will identify near 100% of all squamous and adenocarcinomas of the oesophagus(297, 298). Specific staining for cytokeratin 7 (CK7) was not employed at this point, as unlike oesophageal adenocarcinoma, gastric adenocarcinoma only is positive in 50% of cases and oesophageal SCC is negative for CK7 (380). This therefore would have made the broad identification of epithelial cells grown from OG cancer biopsies (particularly at the GOJ) difficult. Once the cells were shown to be of epithelial origin by staining positively with cytokeratin (DAKO clone mnf116), further characterisation was then employed.

EpCam staining was used to identify cells of a transformed columnar phenotype, with the metaplastic (weaker) and dysplastic (stronger) staining confirming they are separate from the adjacent squamous epithelium of the normal oesophagus (303, 304, 307). Distinct EpCam staining in oesophageal samples is strongly suggestive of the neoplastic phenotype, but can be confirmed by p53 staining, as oesophageal p53 staining is not found in non-dysplastic Barrett's Oesophagus(320, 321, 323).

The antibody chosen for the identification of p53 was clone DO-7 (DAKO M700101) which binds an epitope between amino acids

19 to 26 recognising both the mutant and wild type protein. This clone was chosen as it has been shown to be the most sensitive and specific for p53 labelling in contrast with other comparative p53 antibodies clones in use (388). In normal cells, the wild-type p53 protein is relatively unstable and has a short half-life, and therefore is present in such low quantities that it is undetectable by immunochemical techniques (389, 390). In tumour cells, the mutant p53 has a much longer half-life, and so accumulates creating a stable target for detection (317). The antibody binds the stabilised mutant p53 protein within the nucleus as large amounts of it accumulate, which can then be visualised with immunohistochemistry. This therefore enables a strong and discrete nuclear staining pattern, diffusely labelling the mutational p53 protein across a tissue (391). In this study samples were considered positive if they displayed the classical nucleic staining pattern, but also demanded that more than 20% of nuclei were positive, in clusters or scattered through the tissue.

CD44 and ALDH were chosen as the most representative markers of cancer stem cells (CSC) in OG cancer currently recognised in the literature (see Introduction 1.8.3).

The close-to-patient cells were embedded in agarose and then underwent formalin fixation and paraffin embedding (FFPE) before analysis by immunohistochemistry alongside all biopsy , resectional material and matched Xenograft where available.

All of the 28 primary biopsy derived cell cultures and 15 resection derived patient cell cultures stained strongly positive for cytokeratin as did their corresponding biopsies and resection specimens.

Five of the 28 cancers were squamous cell carcinomas and were not characterised further. IHC analysis of the remaining patient tissue specimens showed two of the patient tissues (OBX16 & OBX61) did not stain positively for EpCam and therefore likely represented the adjacent normal oesophageal mucosa that had been mistakenly biopsied. The corresponding established cells did not stain positively for EpCam either. The remaining tumour specimens all stained were positive for EpCam, and they also demonstrated correspondingly EpCam positive cell cultures.

The 17 tumour samples with their corresponding close-to-patient cells from the 9 suitable patients who met the study inclusion criteria were all characterised further. An example of staining results are shown in Figure 4, and all results in Table 14. All 17 of these patient tissues (that were cytokeratin and EpCam positive) also stained convincingly for p53. This confirmed respectively the epithelial nature of the cells, their derivation from transformed metaplastic columnar-type epithelium (rather than adjacent normal squamous oesophageal epithelium); and neoplastic phenotype.

The potential oesophageal cancer stem cell (CSC) markers CD44 (369, 372) and ALDH (366, 368) were present in 11/17 (64.7%) and 13/17 (76.5%) of the samples respectively, and both were present in 9/17 (52.9%) of the samples (Table 14). Expression in the primary patient tumour was reflected in the corresponding close-to-patient cells, suggesting maintenance of cells with a CSC-like phenotype in culture (Figure 4). Although numbers are small, the presence of ALDH and CD44 (either individually or together) did not relate to stage of disease, pre- or post-chemotherapy tissue status, the TRG, or *in vitro* growth.

The clinical features of the original primary tumour in the human – i.e. histological subtype, stage, grade, TRG, prognosis had no

clear relation to the expression of these proposed CSC markers, however, this was unsurprising given the small numbers involved (Table 13 and 14).

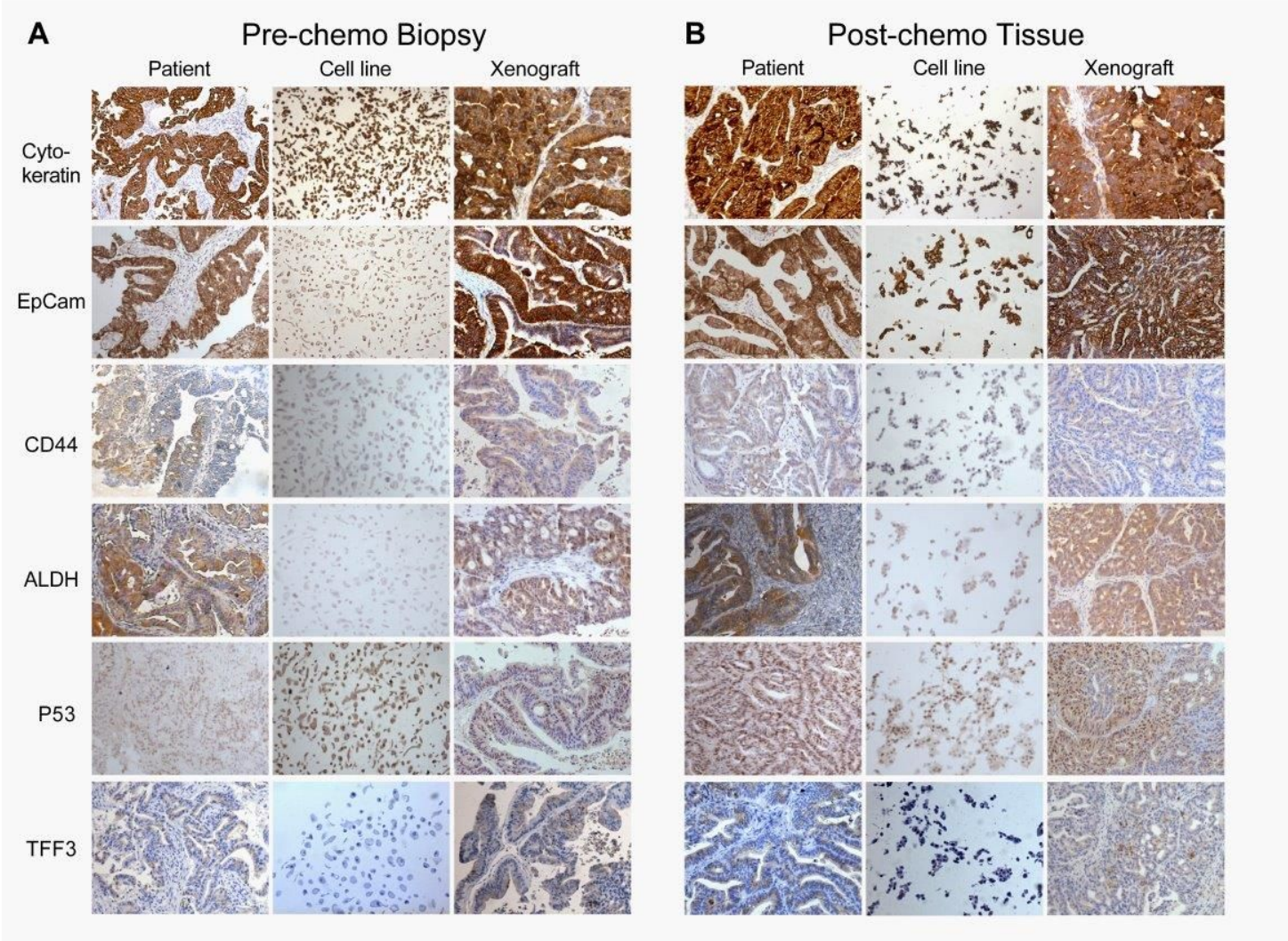
There was a marked difference in the expression of the TFF3 molecule, which despite being present throughout the primary patient tissue, was never expressed intra or extra cellularly in the corresponding Feeder-layer established cells.

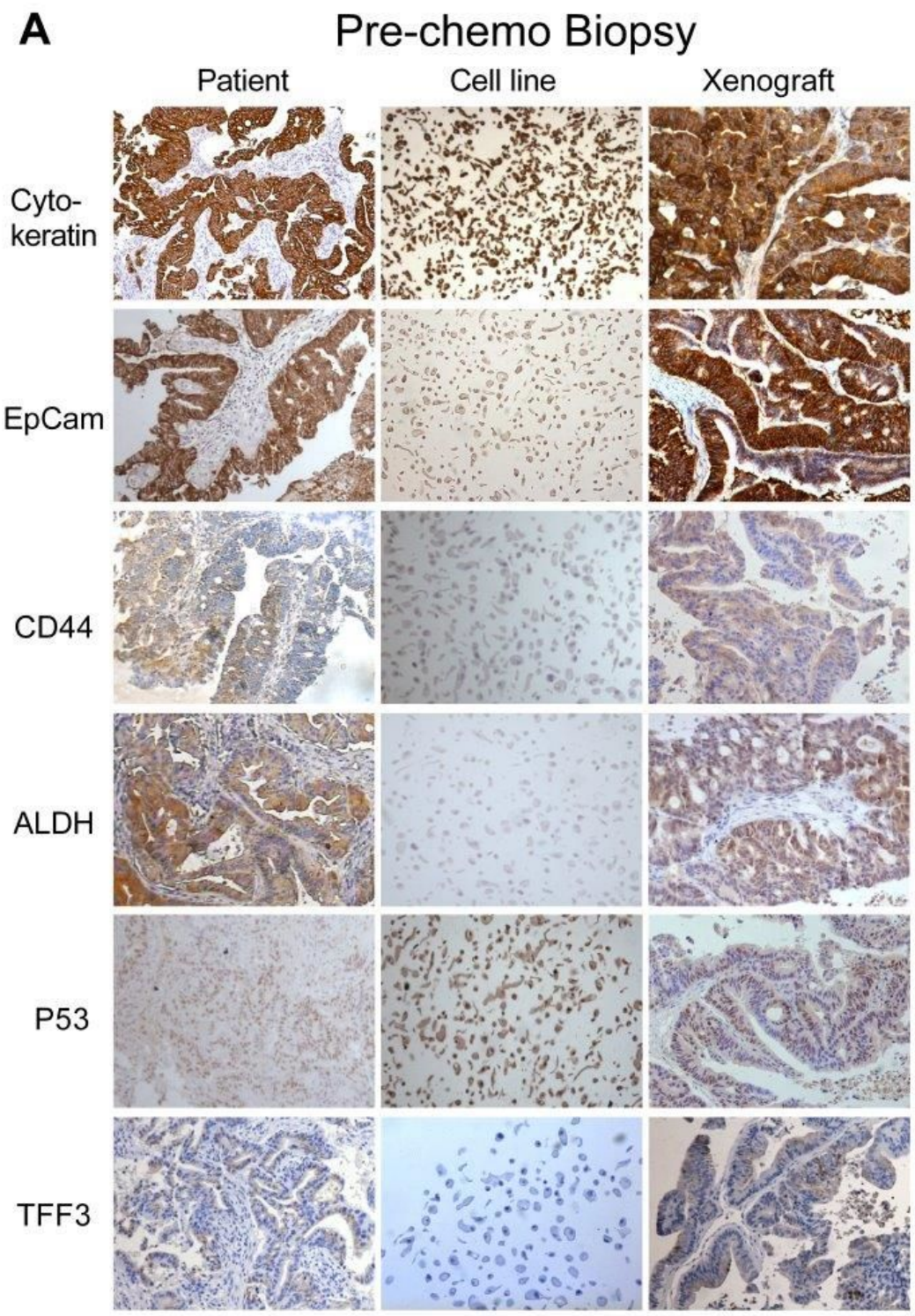
Table 14. Histological characteristics of each patient, and corresponding close-to-patient cells, pre & post chemotherapy

IHC Tissue			**Patient Tissue**						**Patient Cell Culture**					
Patient ID	Sample ID	TRG	Cyto	EpCam	CD44	ALDH	p53	TFF3	Cyto	EpCam	CD44	ALDH	p53	TFF3
Oes1B	OBX70	1	+	+	-	+	+	+	+	+	-	+	+	-
Oes2B	OBX71	3	+	+	-	-	+	+	+	+	-	-	+	-
Oes3B	OBX18	3	+	+	-	+	+	+	+	+	-	+	+	-
Oes4B	OBX9	4	+	+	+	+	+	+	+	+	+	+	+	-
Oes4R	OES125		+	+	+	+	+	+	+	+	+	+	+	-
Oes5B(i)	OBX53	4	+	+	+	+	+	+	+	+	+	+	+	-
Oes5B(ii)	OBX53(ii)	4	+	+	+	+	+	+	+	+	+	+	+	-
Oes5R	OES141		+	+	+	-	+	+	+	+	+	-	+	-
Oes6B(i)	OBX59	4	+	+	-	+	+	+	+	+	-	+	+	-
Oes6B(ii)	OBX59(ii)	4	+	+	+	+	+	+	+	+	+	+	+	-
Oes6R	OES145		+	+	+	-	+	+	+	+	+	-	+	-

Oes7B(i)	OBX25(i)	5	+	+	+	+	+	+	+	+	+	+	+	-
Oes7B(ii)	OBX25(ii)	5	+	+	+	+	+	+	+	+	+	+	+	-
Oes7R	OES127		+	+	+	+	+	+	+	+	+	+	+	-
Oes8B	OBX73	5	+	+	-	-	+	+	+	+	-	-	+	-
Oes8R	OES148		+	+	+	+	+	+	+	+	+	+	+	-
Oes9B	OBX44(ii)	4	+	+	-	+	+	+	+	+	+	-	+	-

Footnote: Abbreviations: **B**: chemo-naïve biopsy sample, **R**: chemo-exposed resection sample, **(i)**: first biopsy **(ii)**: second biopsy, cyto: cytokeratin.


A
Pre-chemo Biopsy
Patient
Cell line
Xenograft
B
Post-chemo Tissue
Patient
Cell line
Xenograft
Cyto-keratin
EpCam
CD44
ALDH
P53
TFF3


A
Pre-chemo Biopsy
Patient
Cell line
Xenograft
Cyto-keratin
EpCam
CD44
ALDH
P53
TFF3

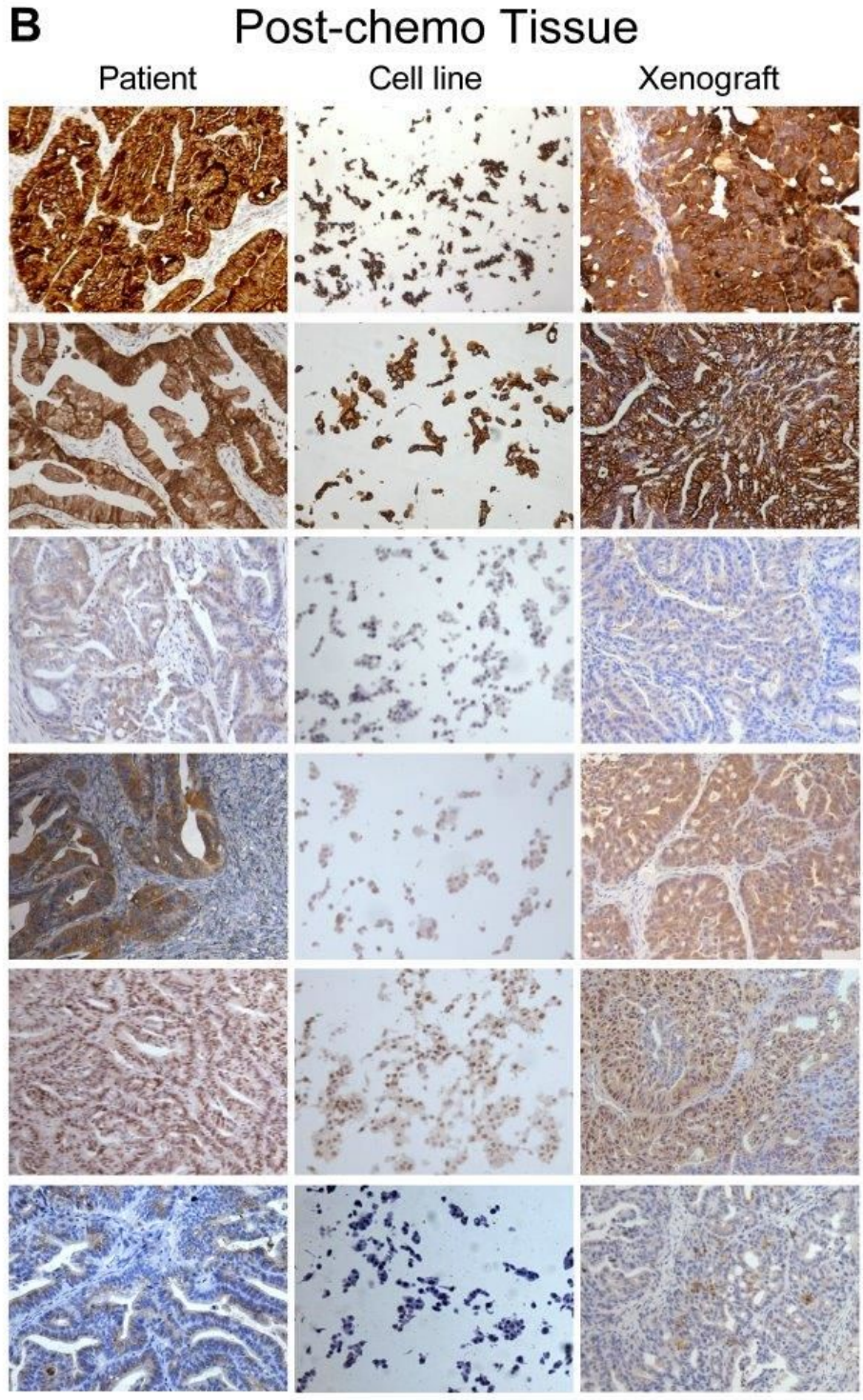


Figure 4. Histological characterisation of the patient's cancer, corresponding close-to-patient cell line and xenograft tissue

IHC analysis of **(A)** pre-chemotherapy biopsy and **(B)** matched post-chemotherapy tumour tissue, and their subsequently generated close-to-patient cells and xenograft model, all from patient Oes7. FFPE sections were stained with antibodies against Cytokeratin, EpCam, CD44, ALDH, P53 and TFF3, using standard IHC techniques and visualised with Leica DMLB bright-field microscope at x10 magnification.

3.2.3 Patient-Derived Xenografts

The patient-derived cancer cells were subcutaneously injected into 6-8 weeks old MF-1 / CD-1 nude, SCID or RAG mice (according to availability) in an attempt to form patient-derived xenografts (PDX) as a means to assess tumorigenicity of the close-to-patient cell cultures.

26 of 28 potentially suitable biopsy derived close-to-patient cell cultures were engrafted within immunocompromised mice. 50% (n=13) of the immunocompromised mice did not develop tumours at the injection sites. In the 13 that did develop tumours at the injection site, only 4 (15% of the original 26 biopsy derived close-to-patient cells) and 3 (25% of the 12 resection derived close-to-patient cells) were human epithelial cell tumours from the injected cellular material (Table 15). The other 9 tumours that developed did not stain positively for cytokeratin unlike the cells that were injected and appear to be reactive inflammatory growths of potential murine origin.

Where the close-to-patient cells did not form a PDX, the process was repeated one further time with a new immunocompromised mouse, and on 3 occasions this resulted in the formation of a PDX, representative of the original patient tumour.

These PDX underwent passage to increase the overall tumour volume, but also immunohistochemical (IHC) analysis to verify their similarity to the original patient tissue and the close-to-patient cells (Table 16).

An example of staining results are shown in Figure 4 and all results in the PDX histology table (Table 16). All seven of the individual PDXs (4 biopsy and 3 resection derived) had the same phenotypic characteristics confirmed by IHC: cytokeratin, EpCam and P53, and confirmed their phenotypic lineage derived from

the individual *ex vivo* close-to-patient cells of malignant human oesophageal tissue.

Pictures of the H&E and cytokeratin stained slides of the original tumour and the matching xenograft tissue was shown to a blinded Consultant Histopathologist (IS, Nottingham University NHS Trust), who independently verified the identification of carcinoma in the xenograft samples. These were not graded.

Expression of the potential CSC markers of CD44 and ALDH was the same in the PDX tissues as it was in the original patient tissue. However, CD44 expression was different in two of the patients: OES127 and OES141. In these particular patients, expression was present in the primary patient tissue, not apparent in close-to-patient feeder layer culture, and then present again in the close-to-patient cell derived PDX. This result was carefully repeated to ensure accuracy (rather than methodological error) and can also be seen to occur with the control cell line, OE33 (Table 16).

TFF3 was present in all of the primary patient cancer tissue, but absent in the feeder layer culture of the close-to-patient cancer cells, however expression was universally restored in all of the tumour xenografts (Table 16, Figure 4).

Table 15. Primary patient cell cultures and PDX establishment

	Establishment of *in vitro* primary patient cell cultures from patient tumour material		**Establishment of *in vivo* PDX from *in vitro* primary patient cell cultures**	
	Patients enrolled	Close-to-patient cancer cell cultures established	Patient cell cultures engrafted	Patient-derived xenografts established
Pre-chemotherapy biopsy	70 (inc. method development cohort n=30)	40 (57%)	26	4 (15%)
Matched post-chemotherapy tumour tissue	25	15 (60%)	12	3 (25%)

Table 16. PDX Histology: characteristics of each patient where a PDX was generated, and corresponding close-to-patient cells and patient-derived xenograft

IHC Tissue	Patient Tissue						Patient Cell Culture						Patient-Derived Xenograft					
Sample ID	Cyto	EpCam	CD44	ALDH	p53	TFF3	Cyto	EpCam	CD44	ALDH	p53	TFF3	Cyto	EpCam	CD44	ALDH	p53	TFF3
OE33 (control)							+	+	-	-	+	-	+	+	+	+	+	+
OBX18B	+	+	-	+	+	+	+	+	-	+	+	-	+	+	+	-	+	+
OES127R	+	+	+	+	+	+	+	+	-	+	+	-	+	+	+	+	+	+
OBX53B	+	+	+	+	+	+	+	+	+	+	+	-						
OES141R	+	+	+	-	+	+	+	+	-	-	+	-	+	+	+	+	+	+
OBX25(i)B	+	+	+	+	+	+	+	+	+	+	+	-	+	+	+	+	+	+
OBX25(ii)B	+	+	+	+	+	+	+	+	+	+	+	-	+	+	+	+	+	+
OES127R	+	+	+	+	+	+	+	+	+	+	+	-	+	+	+	+	+	+
OBX40B	+	+	+	+	+	+	+	+	+	+	+	-	+	+	+	-	+	+

Footnote: Abbreviations: **B**: chemo-naïve biopsy sample, **R**: chemo-exposed resection sample, **(i)**: first biopsy **(ii)**: second biopsy, cyto: cytokeratin.

3.2.4 Flow cytometric identification of potential cancer stem cells

Flow cytometry was performed on the close-to-patient cancer cell cultures to try and identify any sub-populations of cancer stem cells within each sample (as marked by ALDH and CD44), and then for each particular patient cell culture, relate the CSC population to chemo-sensitivity, and PDX engraftment rates, as other groups have reported for OG cancer cell lines (372, 373, 375, 392).

Seven of the available patient neoadjuvant chemotherapy naïve biopsy obtained and established primary close-to-patient cancer cultures (OBX) were examined (OBX25, 9, 71, 76, 53, 59, 61) . A single primary close-to-patient cell culture established from chemotherapy exposed resectional material (OES 127) was also studied and was derived from the same patient as OBX 25. The standard oesophageal adenocarcinoma cell line OE33 and the 3T3 J2 feeder-layer cells were also examined as internal controls. All of the cells were stained and measured for expression of Cytokeratin, EpCam, HLA, CD44 and ALDH.

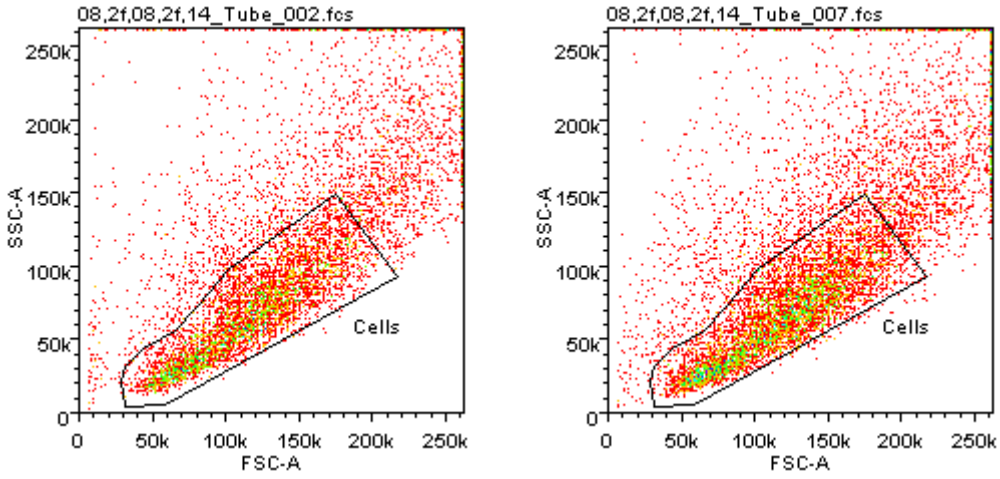
A single patient-derived OG cancer cell culture (OBX 25) was used from herein as an example to demonstrate the development and collation of the flow cytometry results.

3.2.4.1 Cytokeratin

OBX25 cells were examined for the intracellular presence of cytokeratin. A graph of Forward scatter (size) vs Side scatter (granularity) to delineate the main distribution of live cells is shown, with the same selective gate used for both the antibody and the isotype control (Figure 5A). These dot-plots were displayed as a histogram of the ungated and gated populations, which effectively demonstrates the stained and unstained populations of cells (Figure 5B). From these histograms, a

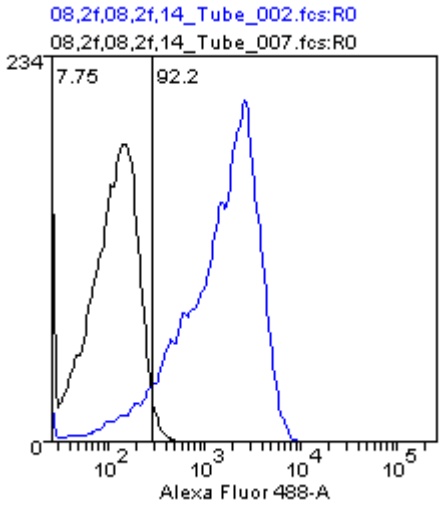
median fluorescence was calculated and a ratio of antibody staining to the isotype control was calculated.

A



Cytokeratin antibody Isotype control

B



Median Fluorescence of gated populations:

Isotype = 126,

Cytokeratin = 1947

Ratio: 15.5

Figure 5. Cytokeratin (AF 488)

Individual close-to patient cells (OBX25) were stained for cytokeratin and examined using flow cytometry. **(A)** A plot of forward scatter against side scatter allowed gating of live cells. **(B)** A histogram was used to compare the cytokeratin stained and isotype control populations, and a ratio was produced.

3.2.4.2 HLA

The primary patient cells were established and grown using a feeder-layer system comprised of 3T3-J2 cells which are murine in origin, and which despite careful differential trypsinization during harvesting, a small proportion of these will contaminate the overall population of the human patient derived cells. Given that the aim of this investigation was looking for a sub-population of human cells, to avoid any confusion it was important to exclude any residual small population of 3T3-J2 cells. Therefore to ensure that all the cells being examined were human, the samples were stained for the human Major Histocompatibility Complex (MHC), which is the Human Leukocyte Antigen class I (HLA). (Figure 6)

The plots demonstrate that the examined cell population almost universally stained HLA class I positive, which demonstrates that despite the seemingly crude technique of differential trypsinization, it does effectively separate out the human epithelial cells from the murine feeder layer cells.

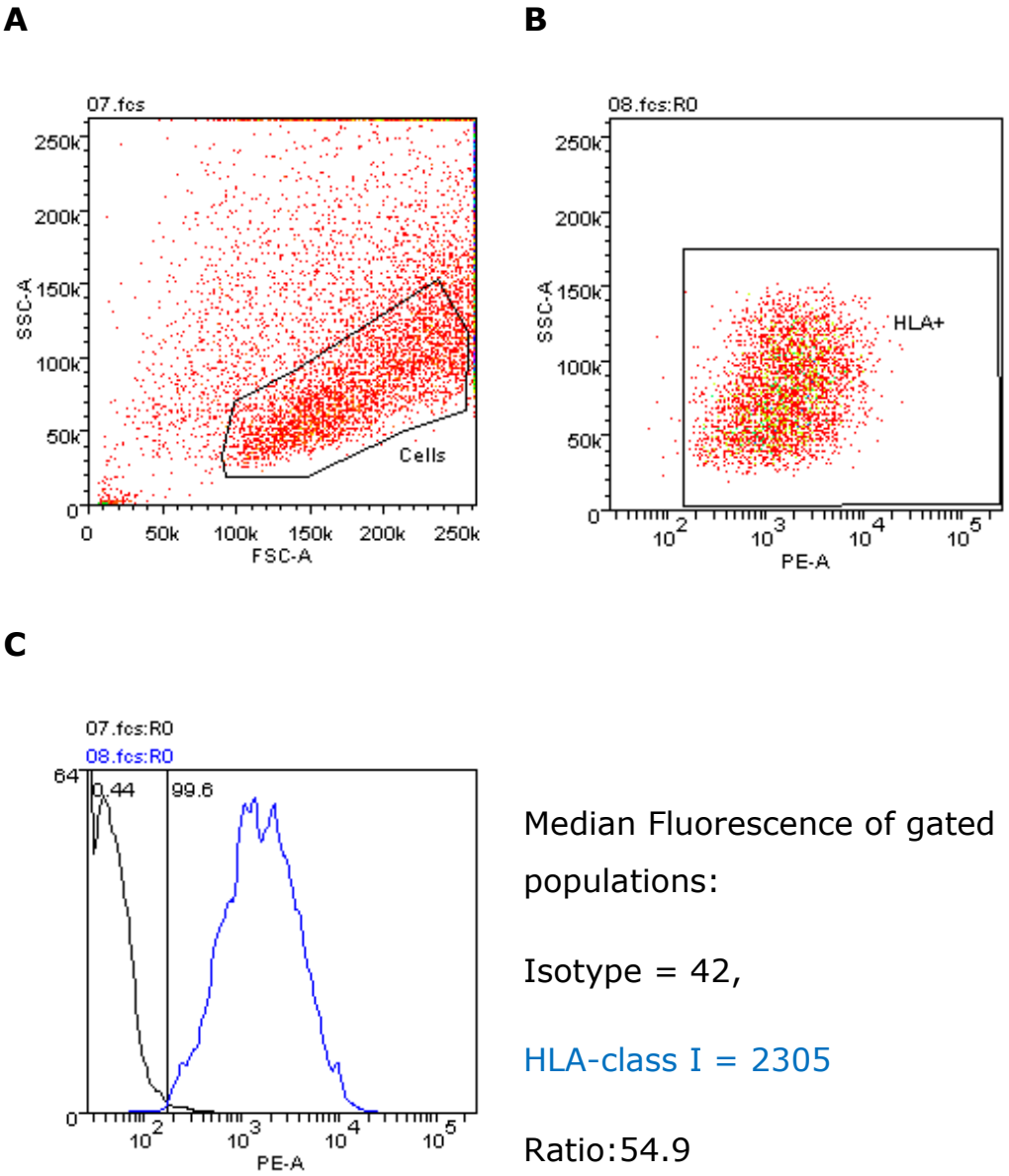
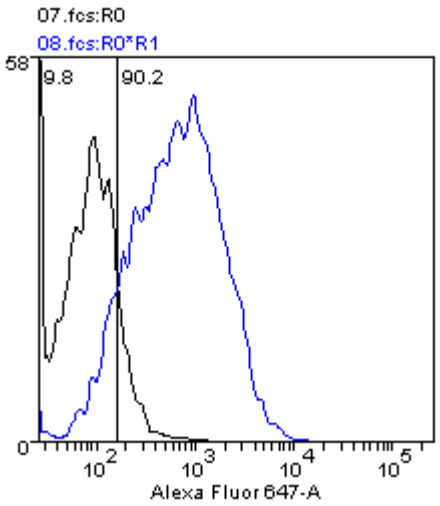


Figure 6. HLA class I (PE-A)

Individual close-to-patient cells (OBX25) were stained for HLA class I and examined using flow cytometry. **(A)** A plot of forward scatter (FSC) against side scatter (SSC) allowed gating of live cells. **(B)** A plot of HLA (PE-A) against SSC identifies the HLA positive cell population within the sample **(C)** A histogram was used to compare the HLA stained and isotype control populations and a ratio can be produced.

3.2.4.3 EpCam

The expression of EpCam was measured on OBX25 close-to-patient cells, (Figure 7) demonstrating a that the population was EpCam positive.



Median Fluorescence of gated populations:

Isotype = 102,

EpCam = 1056

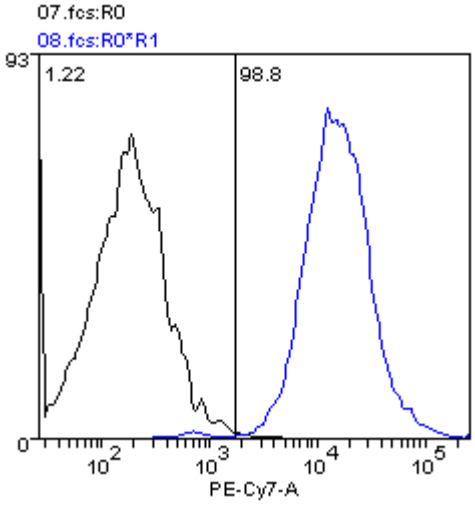
Ratio: 10.6

Figure 7. EpCam (AF 647)

Individual close-to patient cells (OBX25) were stained for EpCam and examined using flow cytometry. Following gating for the live and HLA+ cell populations, a histogram was used to compare the EpCam (AF 647) stained and isotype control populations and a ratio was produced.

3.2.4.4 CD44

The expression of CD44 was measured on OBX25 close-to-patient cells, (Figure 8) demonstrating a clearly staining CD44 group.



Median Fluorescence of gated populations:

Isotype = 251,

CD44 = 20145

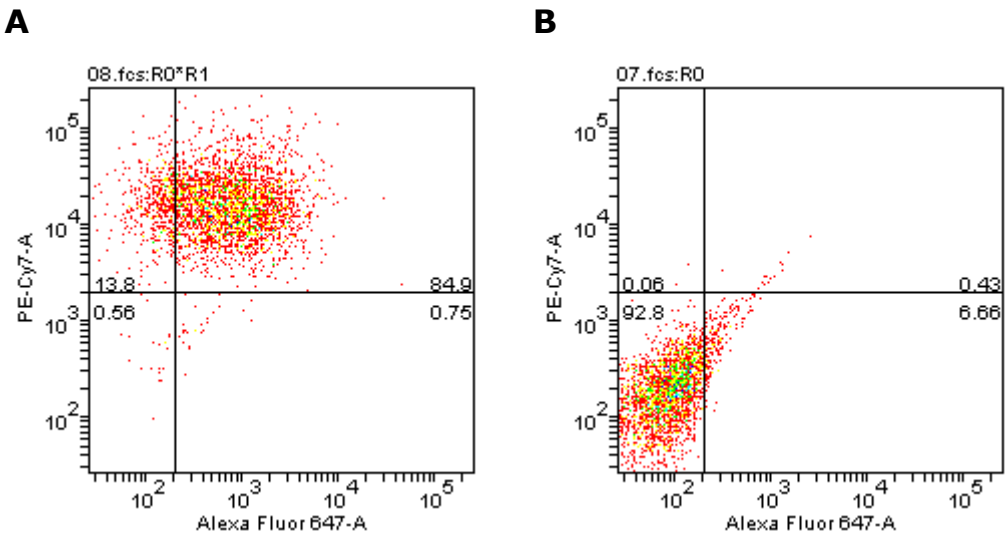
Ratio: 80.3

Figure 8. CD44 (PE-Cy7)

Individual close-to patient cells (OBX25) were stained for CD44 and examined using flow cytometry. Following gating for the live and HLA+ cell populations, a histogram was used to compare the CD44 (PE-Cy7) stained and isotype control populations and a ratio was produced.

3.2.4.5 EpCam and CD44+ cell sub population

The expression of EpCam and CD44 was measured on OBX25 close-to-patient cells, (Figure 9) showing that the cells were EpCam positive and the whole population was CD44 positive. There was therefore no particular 'subgroup' of CD44+ potential CSC that could be identified.



EpCam (x-axis: AF 647) Isotype control

CD44 (y-axis: PE-Cy7)

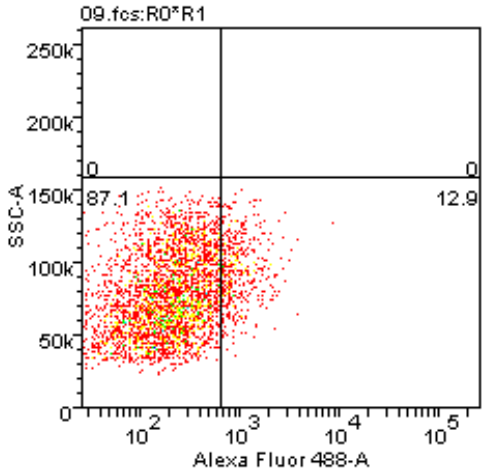
Figure 9. EpCam (AF 647) vs CD44 (PE-Cy7)

Individual close-to patient cells (OBX25) were stained for EpCam and CD44 and examined using flow cytometry. Following gating for the live and HLA+ cell populations, a plot of EpCam (AF 647) against CD44 (PE-Cy7) was used to compare **(A)** the EpCam/CD44 cell population in comparison to **(B)** the isotype controls.

3.2.4.6 ALDH

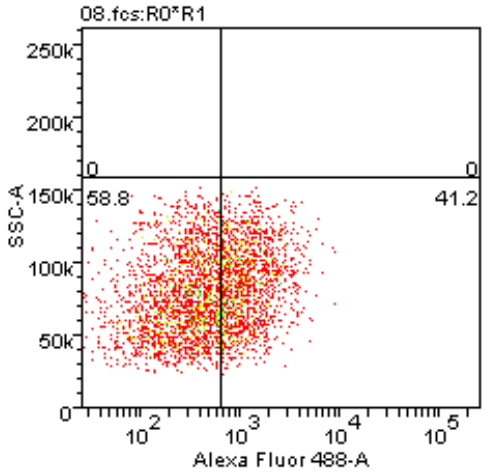
The presence of ALDH (as determined by staining for its active enzymic activity) was measured on OBX25 close-to-patient cells, (Figure 10) showing that the overall cell population had inherent ALDH activity (Figure 10A). By plotting the EpCam positive cell population (Fig 10C) it could be demonstrated that ALDH was present within these OG cancer cells. To identify whether these same cells with ALDH also expressed CD44 these were also plotted (Figure 10E), demonstrating the ALDH activity throughout this cell group. There was no 'subgroup' of ALDH+/CD44+ potential CSC that could be identified from this close-to-patient cell culture.

A



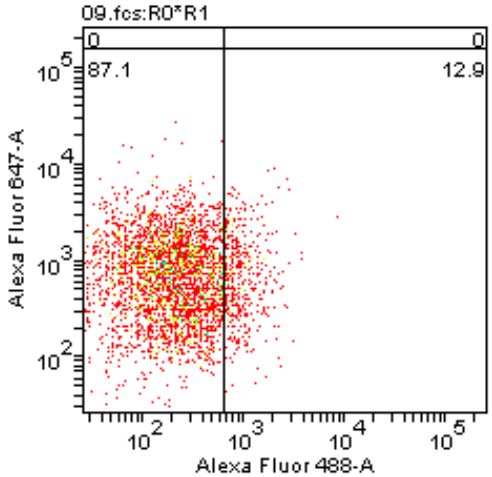
ALDH

B



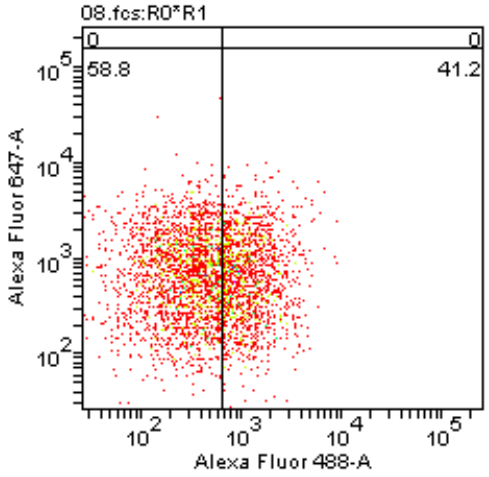
Isotype

C



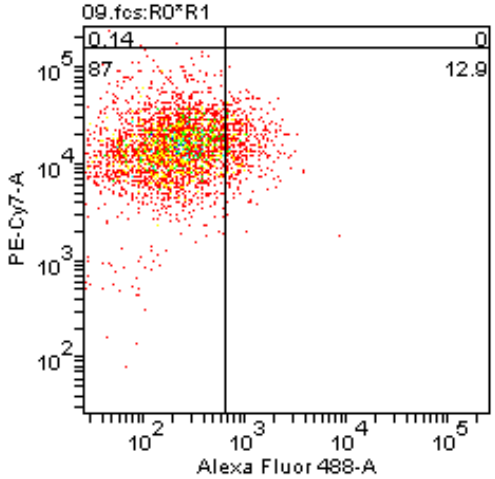
EpCam and ALDH

D



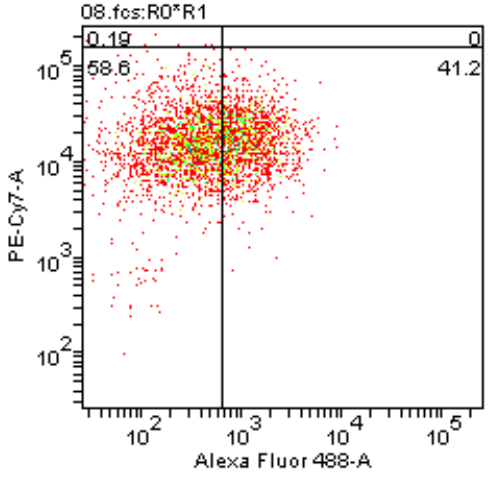
Isotype

E



CD44 and ALDH

F



Isotype

Figure 10. ALDH (AF 488)

Individual close-to patient cells (OBX25) were stained for ALDH (AF 488) and examined using flow cytometry. Following gating for the live and HLA+ cell populations, **(A)** a plot of ALDH (AF 488) against SCC was used to examine the ALDH (AF 488) population in relation to **(B)** the isotype control, **(C)** a plot of ALDH (AF 488) against EpCam (AF 647) was used to examine the EpCam/ALDH cell population in relation to **(D)** the isotype control, **(E)** a plot of ALDH (AF 488) against CD44 (PE-Cy7) was used to examine the CD44/ALDH cell population in relation to **(F)** the isotype control.

3.2.4.7 Overall evaluation of CSC marker presence within the close-to-patient cells

The results from all 8 of the examined close-to-patient cell cultures (127, 25, 9, 71, 76, 53, 59, 61) and 2 comparator cell lines (OE33 , 3T3-J2) were collated and plotted as a bar chart for each stain (Figure 11).

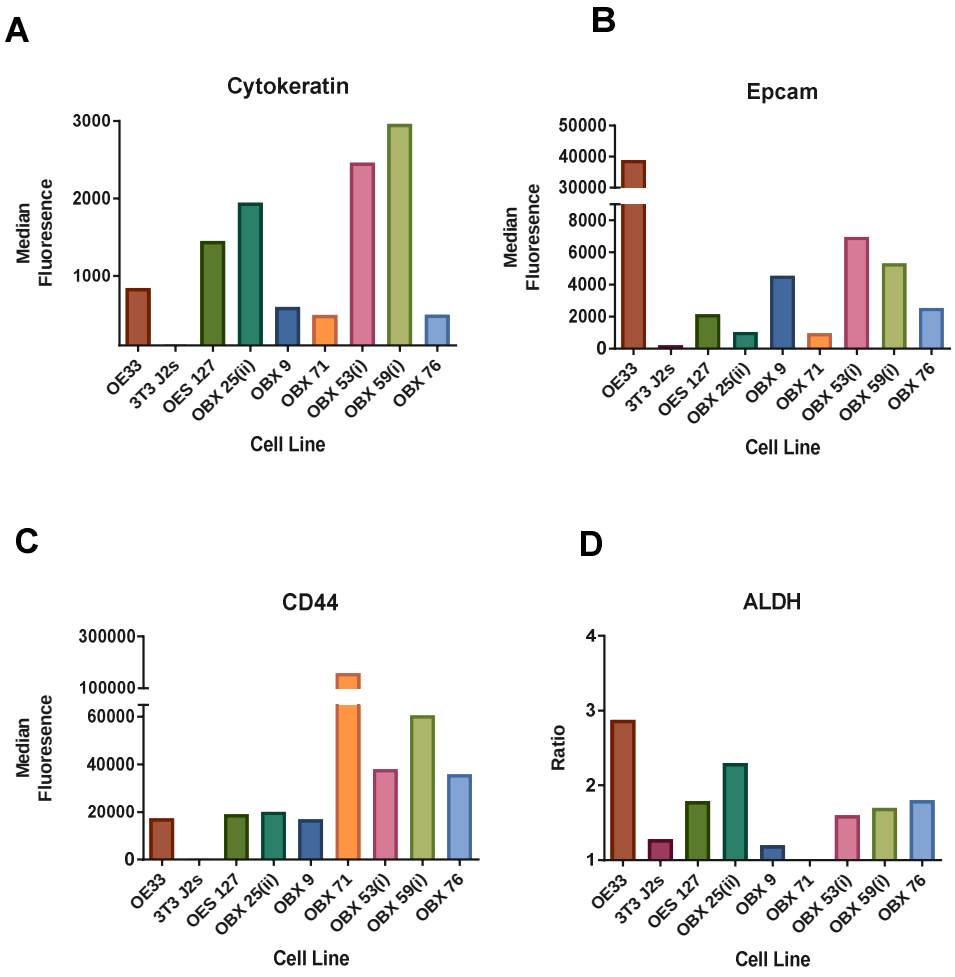


Figure 11. Summary of flow cytometry characterisation of the close-to-patient cancer cell cultures

Cells from 7 close-to-patient cell cultures and two control cell lines (OE33 - positive, 3T3-J2 -negative) were stained and analysed, on a LSRII flow cytometer (Becton Dickinson). Positive staining was based on the cut-offs from the individual corresponding isotype controls. Following initial gating on the population of HLA positive cells, the following staining levels were measured and plotted on bar charts. **(A)** cytokeratin, **(B)** EpCam and **(C)** CD44, and **(D)** ALDH.

Analysis of the scatter plots revealed that the sample analysed for OBX 61 was more debris than live cells and therefore the signal from staining does not represent a meaningful result, and so was not included in the overall analysis. The remaining 7 individual close-to-patient cancer cell cultures all displayed varying morphology from patient to patient when examined in the flow cytometer. Unlike the small and homogeneous appearance of the standard cell lines of OE33 and 3T3 J2, the individual patient cancer cultures were on average were of a much larger and more granular appearance, but also had a broad heterogeneous size spectrum.

The standard cell line OE33 being used for baseline comparison stained positively with a fluorescence result as previously documented in the literature. The 3T3 J2 cells stained negatively for cytokeratin and EpCam, consistent with previous reports.

Despite all of the cancer cell cultures staining positively for Cytokeratin and EpCam, there was no standard level or pattern of staining fluorescence that was replicated over the 7 patient-derived cell cultures. However, the primary cell cultures from the same patient, OBX25 and OES127 displayed a similar pattern of staining to one another. Overall levels of fluorescence staining of the potential OG cancer CSC markers of CD44 and particularly ALDH were variable between patient cultures.

The heterogeneity seen in this result is possibly a reflection of the wide variance seen in, and between, individual patient's cancers, which express the potential CSC markers such as CD44 and ALDH in a heterogeneous fashion. And, indeed the literature contains contradictory reports of the markers' clinical relevance and predictive value (Introduction: section 1.7.3.3/4). This reported clinical variation therefore supports the hypothesis that these newly established close-to-patient cell lines are more patient-representative, than the homogeneous clonal features frequently seen in traditional cancer cell lines.

When examining the scatter plots of the 7 patient-derived cell cultures for these 2 potential CSC markers, there was generalised staining amongst the whole cell group and no discrete sub groups of cells staining positively or negatively, and therefore no indication of the presence of a specific sub-population of CSC.

3.3 Conclusions

Conclusions of Chapter 3: Establishment and Characterisation of primary OG cancer cells.

A method for the *ex vivo* establishment and growth of individual patient OG cancers from small endoscopic biopsies has been described. This is a significant adaption of the originally reported cellular reprogramming method described for growing keratinocytes, as it allows individual patient cancers to be grown.

The presence of cytokeratin, EpCam, and p53 confirmed the established close-to-patient cancer cells as derived from a neoplastically transformed oesophageal epithelium, and can therefore be used in a representative fashion to study each patient's cancer in the *ex vivo* setting.

The formation of PDX from these close-to-patient cells demonstrates their tumorigenicity, and also confirms their malignant OG status through the PDX histological morphology and staining.

The fairly consistent pattern of expression of CD44 and ALDH as potential markers of a sub-population of CSC, throughout the different tissue settings (patient, 2D close-to-patient cells and PDX) suggests a maintenance of the individual characteristics and heterogeneity of that patient's cancer.

The successful establishment and characterisation of primary OG cancer cells is an important step forward as it allows more clinically relevant research using close-to-patient cells (rather than cell lines), and gives the potential for individual patient personalised investigations, including assessment of potential chemotherapeutic sensitivity.

4 Results 2: OG Cancer 3D-TGA Optimisation

4.1 Overview & Aim

Once the individual patient's malignant epithelial cells were established and expanded, using the feeder-layer system, we next aimed to establish a 3D model which would allow drug screening. In particular, we wanted to investigate the role of the mesenchymal stromal component of the tumour microenvironment on oesophageal cancer cell growth in a 3D assay. Here, the oesophageal cancer cells established in the feeder layer system would be co-cultured with mesenchymal stem cells (MSCs), to provide more relevant TME conditions for the primary patient OG cancer cells to grow. Potential cancer cell proliferation was measured using the alamarBlue® cell fluorescence assay.

We chose to adapt the previously described 3D-TGA, which hitherto used close-to-patient cells derived as PDXs, to screen drugs (238). This required much optimisation of the assay so that the feeder layer derived cells (which had not previously been used in this assay), from chemo-naive oesophageal cancer, could proliferate to form cancer cell clusters within the 3D environment, and pharmaceutical evaluation could subsequently occur.

4.2 Results

4.2.1 Growth using the standard baseline 3D-TGA

Preceding work growing xenograft-established patient cancers (180, 238) and cancer cell lines (239) in the 3D-TGA provided a baseline methodological framework for attempting the growth of malignant OG epithelial cells in 3D. This standard baseline method, to which the subsequent refinements are compared, involved the following conditions: growth of the cells in a 384 well plate, at a density of 6250 cells/well, suspended in Cultrex BME diluted to 3mg/ml, using the adapted TME RPMI media (phenol red free RPMI, altered to pH 6.8, 6mM D-glucose).

Condition	Standard
Time	5 days
BME conc	3mg/ml
Supplementary ROCKi	No
Media	TME RPMI
Serum	None
Additional Growth Factors	No
Re-feeding	No
Epithelial, Stromal cell (3:1) co-culture	hMSCs

Growth of OBX6, OES112, OES111 and OES110 cells was assessed for 5 days, in the presence of hMSCs, using the standard PDX 3D-TGA conditions. These close-to-patient cancer cell cultures, established using the 2D Feeder-layer method, did not establish in the 3D-TGA and grow successfully (Figure 12).

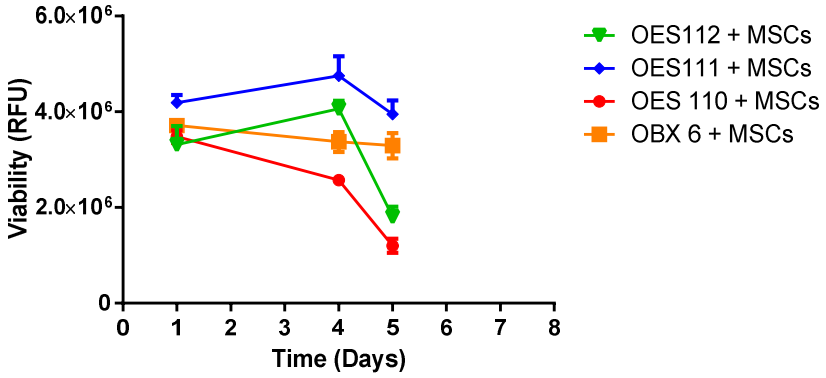


Figure 12. OG cancer primary cells do not grow in the standard baseline 3D-TGA conditions

OES112, OES111, OES110 & OBX6 grown in the 3D-TGA using baseline conditions, for 5 days in the presence of hMSCs.

Given the poor performance of the standard PDX 3D-TGA method when applied to OG primary cells, a series of variations to the standard PDX 3D-TGA conditions were carried out to optimise the technique and permit growth of these new primary patient oesophageal cells in the 3D-TGA.

4.2.2 Alteration of BME concentration and ROCKi supplementation

Alterations to the 3D-TGA were considered and then trialled with reference to other published methods for growing primary patient cells in a 3D model (as outlined in the Introduction, Table 2). The 3D assay was revised to:

a) be performed over a longer 7 day time period,
b) examine varying concentrations of BME; contrasting 2D culture with no BME (0mg/ml), to the standard 3D conditions of 3mg/ml BME and 3D with 6mg/ml BME.
c) the supplementary use of ROCKi, as this was present in the feeder layer culture from which the growing cells are obtained.

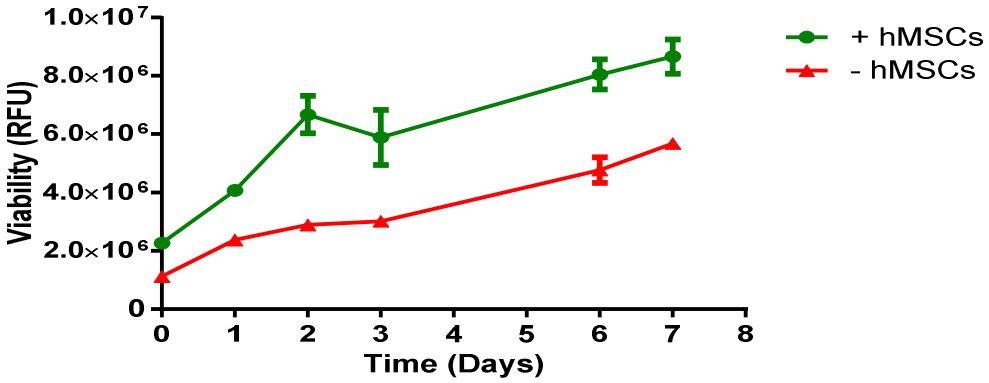
The change in conditions is summarised below:

Condition	Standard	Experimental change 1
Time	5 days	**7** days
BME conc	3mg/ml	**0, 3, 6** mg/ml
Supplementary ROCKi	No	**Yes / No**
Media	TME RPMI	TME RPMI
Serum	None	None
Additional Growth Factors	No	No
Re-feeding	No	No
Epithelial, Stromal cell (3:1) co-culture	hMSCs	hMSCs

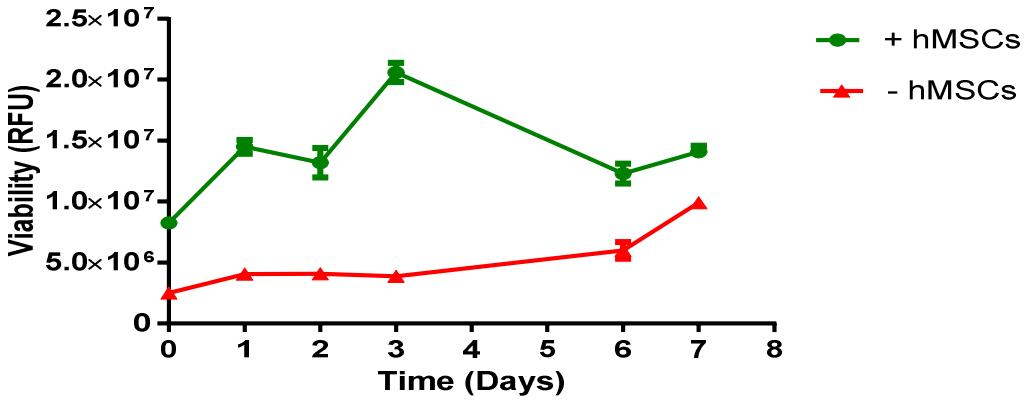
The 3D-TGA was performed for 7 days using OBX11 with BME at 3 different concentrations (growth in a monolayer without BME (0mg/ml) vs 3D models with 2 BME concentrations (3 and 6 mg/ml), in the presence of ROCKi, with hMSCs as a supporting stromal component.

It demonstrated that the primary patient OG cells OBX11 grows more quickly as a 2D monolayer (BME conc of 0mg/ml) than in 3D in the TGA at 3 or 6 mg/ml. The 3D-TGA at a 3mg/ml BME concentration demonstrates initial growth then falters. The 3D-TGA at a 6mg/ml BME concentration shows initial excellent growth, before growth plateaued (Figure 13).

A



B



C

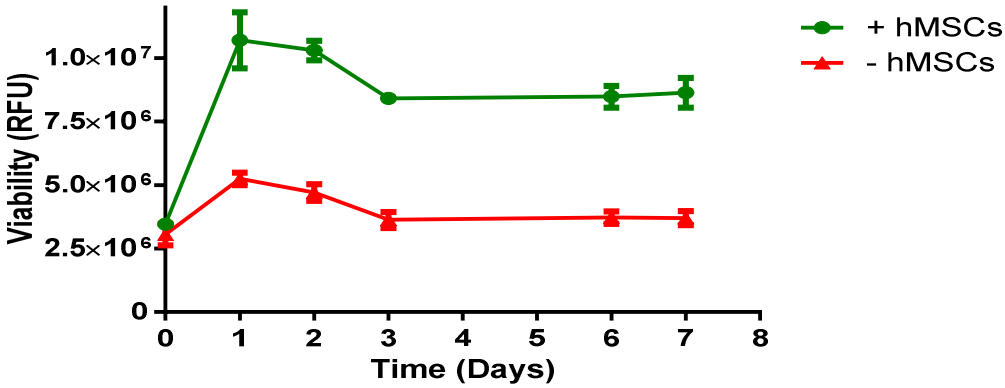


Figure 13. OG cancer growth in the TGA with BME concentration of 0, 3 and 6mg/ml

OBX11 was grown in the 3D-TGA using modified conditions with BME at **(A)** 0 mg/ml, **(B)** 3mg/ml, **(C)** 6mg/ml, for 7 days, with and without hMSC co-culture.

The 3D-TGA cultures were examined by brightfield microscopy (Figure 14), which demonstrated that at the lower BME concentration (3mg/ml) a proportion of the 3D seeded cells (Figure 14A) were dropping out of the matrix to the bottom of the wells and growing on the plastic base of the well (Figure 14B). Therefore, although at 3mg/ml the assay was set-up in 3D, the results of the assay are potentially reflecting a surrogate 2D environment. At the higher BME concentration (6mg/ml) the OG cancer cells appear to stay within the 3D matrix environment (Figure 14C), and not drop to the bottom of the well (Figure 14D).

This finding is not unprecedented; an increased BME matrix concentration of 6mg/ml and above has been preferentially used with some tumour cell lines (NCI-H460 & PC-3M-luc-C6) (239) where higher BME concentrations were required to prevent the tumour cells falling out of the 3D matrix.

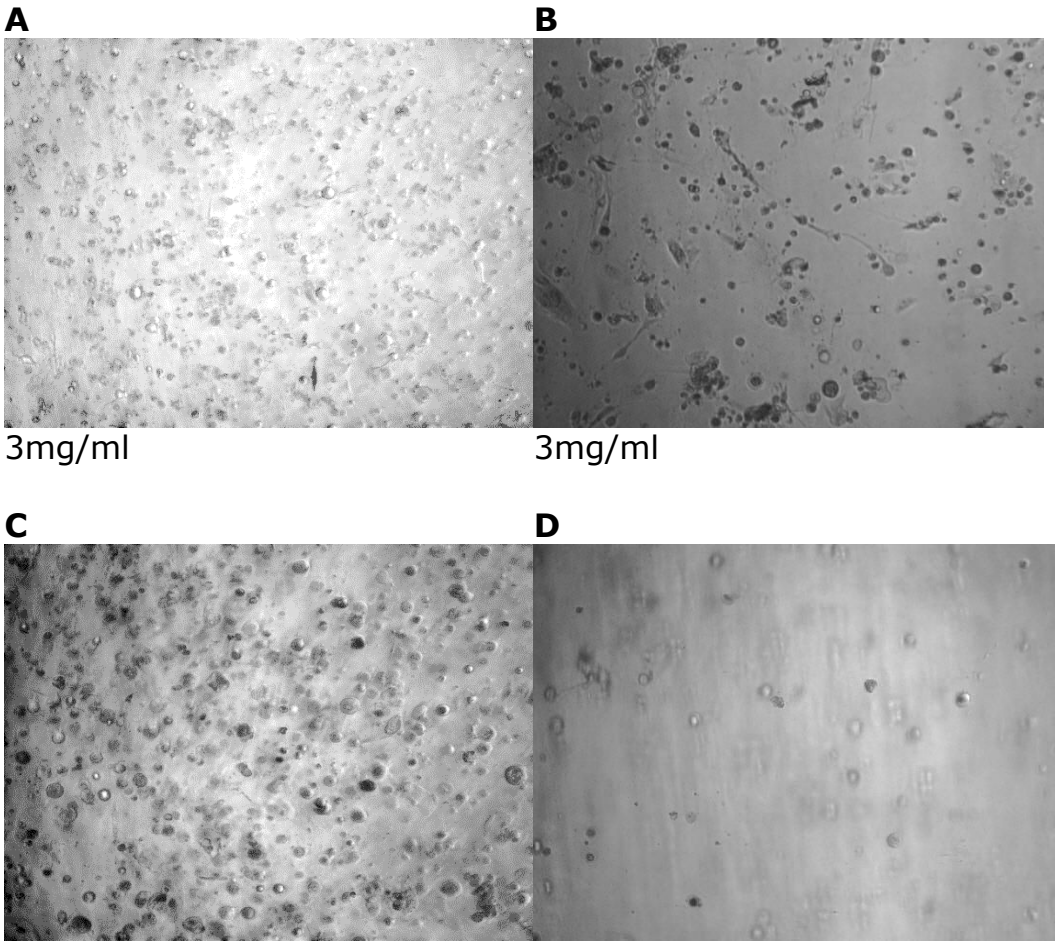


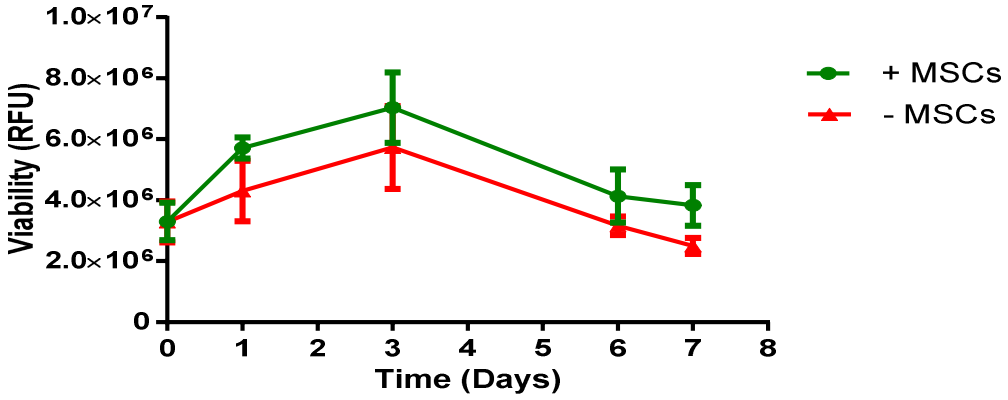
Figure 14. Primary patient OG cancer cells are not suspended in the 3D matrix at a 3mg/ml BME concentration

OBX11 was grown in the 3D-TGA using modified conditions with BME at 3mg/ml and 6mg/ml. **(A, C)** Images are condensed multilayer focussed bright-field image showing a typical 3D-TGA well with cell seeding density within the 3D matrix. **(B, D)** Images are single level brightfield microscopy images from the base of the 3D TGA well.

The 3D-TGA was repeated using a different OG cancer cell culture (OBX9) again examining the effect of BME concentrations (3mg/ml, 6mg/ml) in the presence of ROCKi (experimental conditions as per 'Experimental change 1'). This demonstrated that the primary patient OG cells OBX9 grows better in the 3D-TGA at a BME concentration of 6mg/ml rather than 3mg/ml

(Figure 15). However, the 6mg/ml BME concentration again demonstrates a plateaued period before finally declining (Figure 15B). This may demonstrate that the 3D assay would benefit from an even stiffer matrix using higher concentrations of BME. The outlier result was at the BME 6mg/ml concentration without MSCs, which hasn't demonstrated any tangible growth. This resulted from a technical plating mistake, which occurred as manual user error during the 3D plating.

A



B

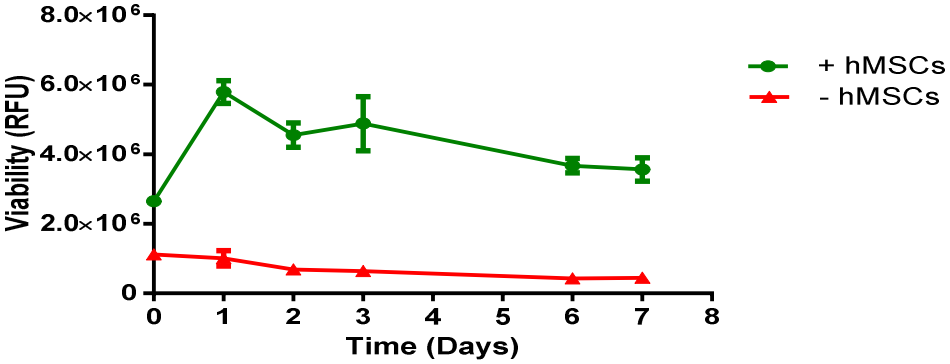


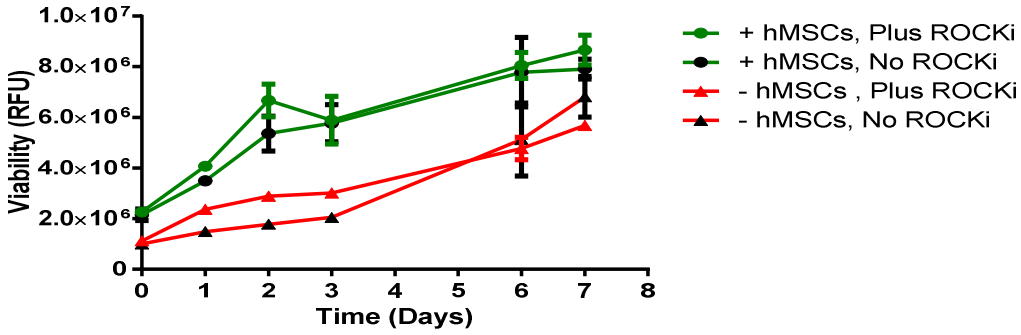
Figure 15. OG cancer exhibits different growth in the 3D-TGA with BME concentration of 3mg/ml and 6mg/ml

OBX9 was grown in the 3D-TGA using modified conditions with BME at **(A)** 3mg/ml and **(B)** 6mg/ml for 7 days, with and without hMSC co-culture.

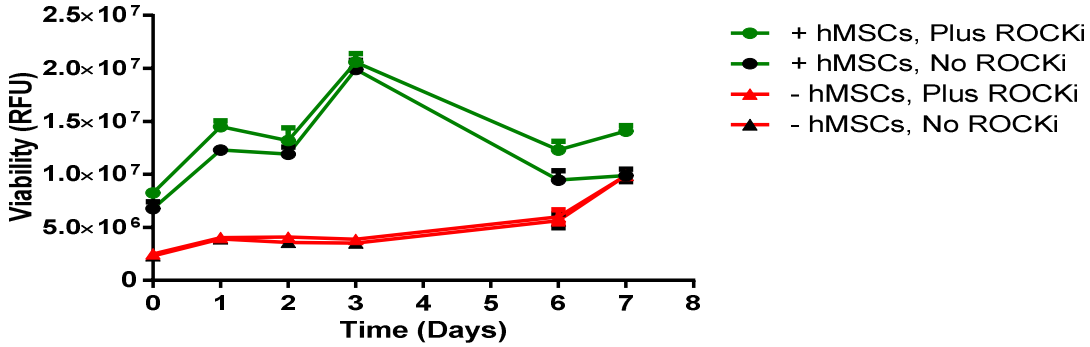
Alongside the investigation of BME concentration, the 'experimental changes 1' also examined the effect of ROCKi supplementation. The 3D-TGA assay was performed using OBX11 and OBX9 with and without ROCKi, for 7 days, with BME at different concentrations, with and without hMSCs. This demonstrated a small advantage of continuing the supplementation with ROCKi, but the significance of this was unclear where the cells had stopped growing by day 7 (Figure 16). The most promising prolonged 3D growth was seen at the higher BME concentration (6mg/ml) and appeared to benefit from ROCKi supplementation (Figure 16C,E).

The stromal co-culture effect of hMSCs was variable throughout the assays: co-culture stimulated overall growth for OBX11 at 6mg/ml (Figure 16C), but alternatively was providing additive growth for OBX9 at 3mg/ml (Figure 16D). However, the true effect of hMSC co-culture was unlikely to become clear until the overall underlying assay conditions allowed the epithelial cancer cells to grow in a reliable and reproducible fashion.

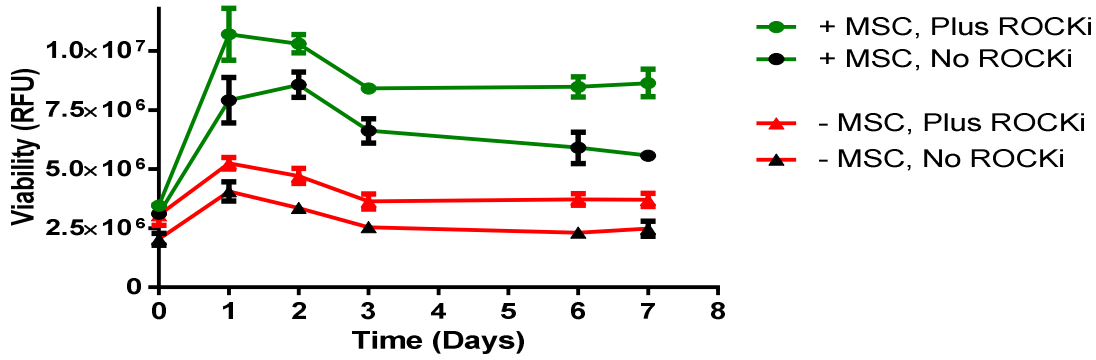
A


1.0×10⁷
8.0×10⁶
6.0×10⁶
4.0×10⁶
2.0×10⁶
0
Viability (RFU)
0 1 2 3 4 5 6 7 8
Time (Days)
+ hMSCs, Plus ROCKi
+ hMSCs, No ROCKi
- hMSCs , Plus ROCKi
- hMSCs, No ROCKi

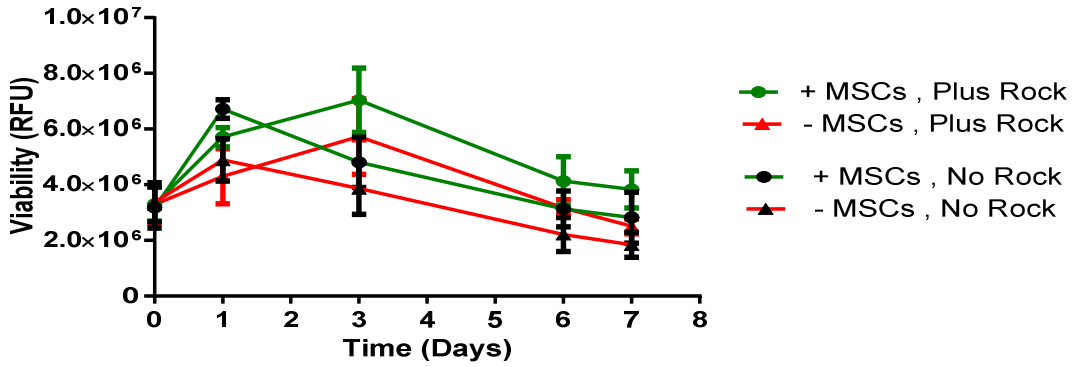
B


2.5×10⁷
2.0×10⁷
1.5×10⁷
1.0×10⁷
5.0×10⁶
0
Viability (RFU)
0 1 2 3 4 5 6 7 8
Time (Days)
+ hMSCs, Plus ROCKi
+ hMSCs, No ROCKi
- hMSCs, Plus ROCKi
- hMSCs, No ROCKi

C


1.0×10⁷
7.5×10⁶
5.0×10⁶
2.5×10⁶
0
Viability (RFU)
0 1 2 3 4 5 6 7 8
Time (Days)
+ MSC, Plus ROCKi
+ MSC, No ROCKi
- MSC, Plus ROCKi
- MSC, No ROCKi

D



E

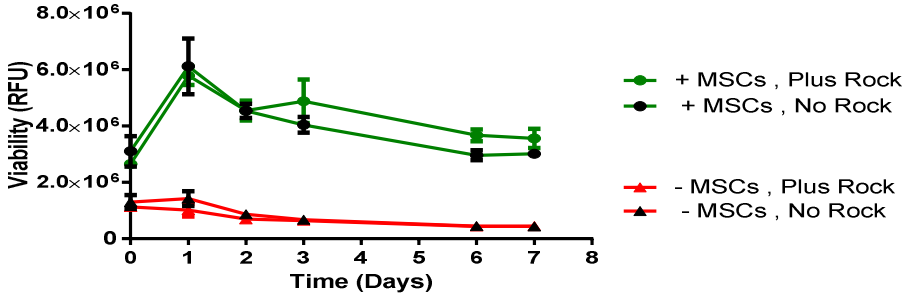


Figure 16. Presence of ROCKi in the 3D-TGA can affect OG cancer growth at different BME concentrations

Two different patient's OG close-to-patient cancer cells (OBX9 & OBX11) are grown in the 3D-TGA using modified conditions for 7 days, with and without hMSC co-culture, with BME at different concentrations: OBX11 **(A)** BME: 0mg/ml, **(B)** BME: 3mg/ml, **(C)** BME: 6mg/ml. And OBX9 **(D)** BME: 3mg/ml and **(E)** BME: 6mg/ml.

To further understand the effect of ROCKi within the 3D cultures this assay was run with a further OG cancer cell culture (OBX25), maintaining the same (experimental change 1) conditions and BME concentration at 6mg/ml (Figure 17). This demonstrated similar results to the other 2 OG cancer patient cell cultures - the presence of ROCKi within the 3D-TGA assay had a small but positive effect on the growth (of OBX11, OBX9 and OBX25), particularly at a BME concentration of 6mg/ml. This effect was

not marked, or universal across environments, or consistent throughout the time period.

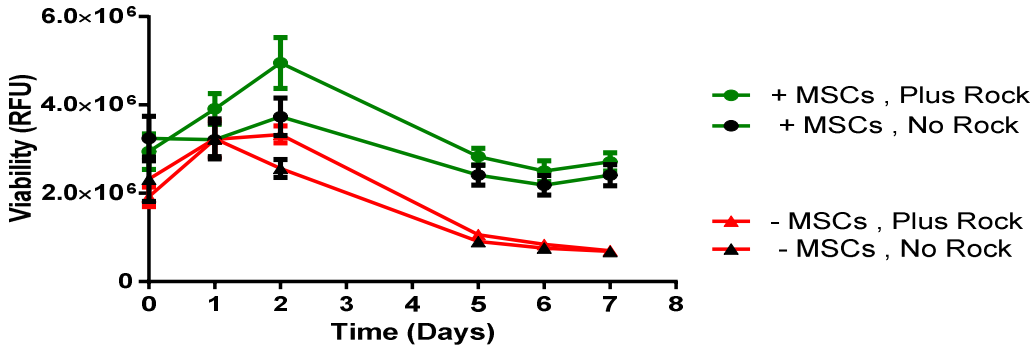
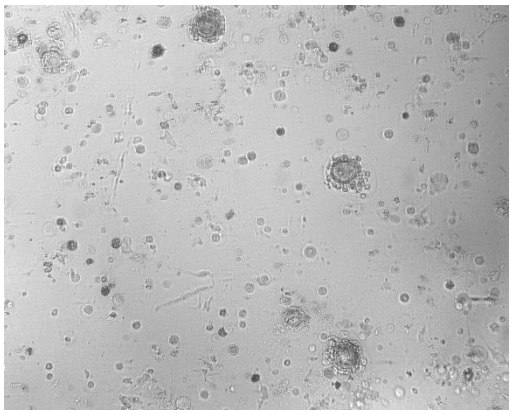


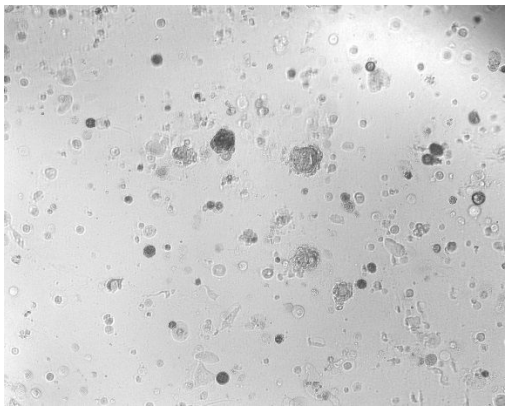
Figure 17. Presence of ROCKi slightly increases OG cancer growth in the 3D-TGA with BME concentration of 6mg/ml

OBX25 was grown in the 3D-TGA using modified conditions with BME at 6mg/ml, for 7 days, with and without hMSC co-culture.

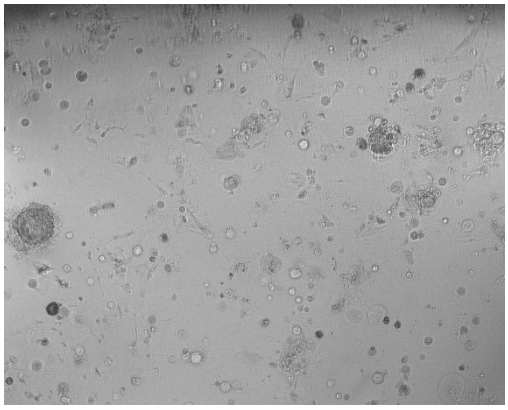
The 3D-TGA cultures were examined by brightfield microscopy, and at the BME concentration of 6mg/ml only, they were found to form infrequent cancer cell clusters.



OBX9



OBX 25



OBX 11

Figure 18. Primary patient OG cancer cells form infrequent clusters in the 3D matrix at a 6mg/ml BME matrix concentration in the 3D-TGA

OBX9, OBX11 and OBX25 are grown in the 3D-TGA using modified conditions with BME at 6mg/ml, presence of ROCKi and hMSC co-culture. Images obtained with bright-field microscopy show a typical 3D-TGA well with infrequent cell clustering within the 3D matrix.

4.2.3 Adjustment of media, timescale and re-feeding

The 3D assay conditions were revised (with respect to the observations from experimental changes 1), to have routine supplementary ROCKi and a minimum BME concentration of 6mg/ml. Following advice from colleagues who had seen a similar benefit from using higher concentration BME in a parallel setting, a 12mg/ml BME was subsequently trialled(191).

Due to the poor prolonged growth observed in the 'experimental changes 1' 3D assays, the 'experimental changes 2' examined the effect of different media, growth time periods and the potential for re-feeding the 3D-Assay. The 3D assay encompassing 'experimental changes 2' was therefore performed over a 7-10 day time period, with 12mg/ml BME matrix, routine ROCKi supplementation, and with or without stromal cells; and examining an extended growth timeline with re-feeding, and the effects of different growth media, serum and additional growth factors.

The 3 different growth media examined were:

- *TME RPMI*:
  phenol red free RPMI, altered to pH 6.8, 6mM D-glucose. (see Materials and Methods for formulation)

- *F.Media*:
  F12/DMEM, defined FBS, hydrocortisone, insulin, cholera toxin, adenine, EGF. (see Materials and Methods for formulation)

- *Base Media (BM) and additional Growth Factors (Add GFs)*:
  DMEM/F12, HEPES, GlutaMAX-I, B27 serum-free substitute, N-Acetylcysteine. The culture condition used by the Clevers group for organoid growth, of basal cell culture medium optimised for Human Intestinal Stem Cell (HISC) by the full Growth Factor supplementation required the growth of Barrett's: EGF, noggin, R-spondin1, Wnt-3A, FGF10, Gastrin, TGFβi A-83-01, ROCKi Y-27632. (see Introduction, and Materials and Methods for formulation)

The change in conditions are summarised:

Condition	Standard	Experimental change 2
Time	5 days	**7 - 14** days
BME conc	3mg/ml	12 mg/ml
Supplementary ROCKi	No	Yes
Media	TME RPMI	**BM & F.Media**
Serum	None	**Yes**
Additional Growth Factors	No	**Yes**
Re-feeding	No	**Yes**
Epithelial, Stromal cell (3:1) co-culture	hMSCs	hMSCs

The 3D-TGA was performed for 7 days initially using OES145 with and without hMSC co-culture, examining the 3 different media: TME RPMI, Base Media with additional Growth Factors (BM + Add GFs), and F.Media. It demonstrated that both F.Media and Base Media support progressive and consistent OG cancer cell growth in the 3D-TGA. However, the TME RPMI used in the standard baseline assay did not, and mirrored the previous growth results when using this media (seen in the 3D assays of 'experimental change 1'). The F-media supports marginally better growth than the BM+GFs Media (Figure 19).

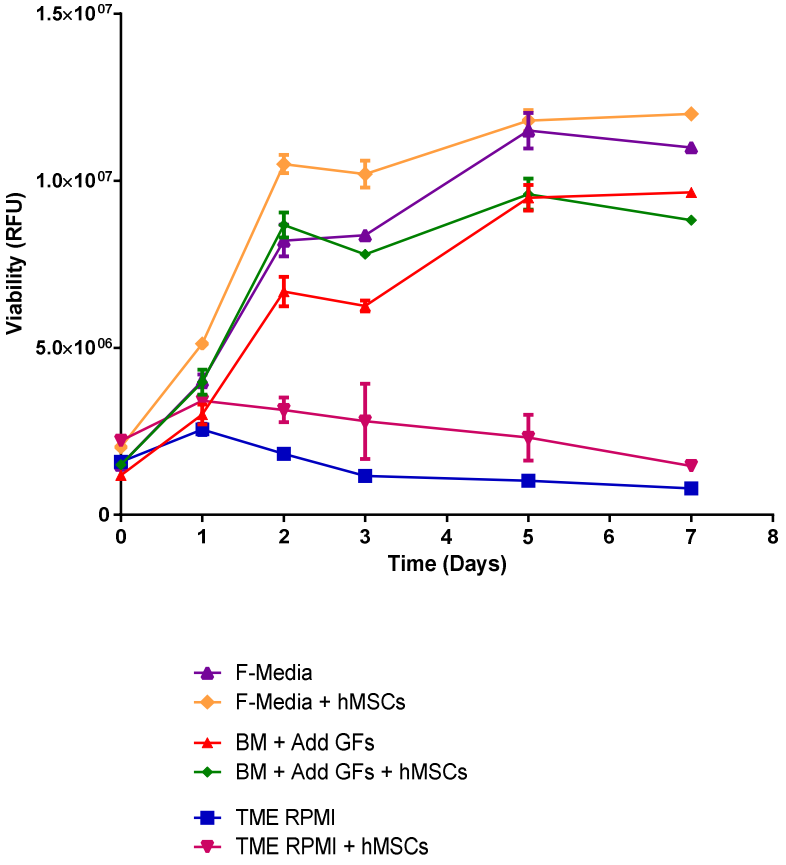
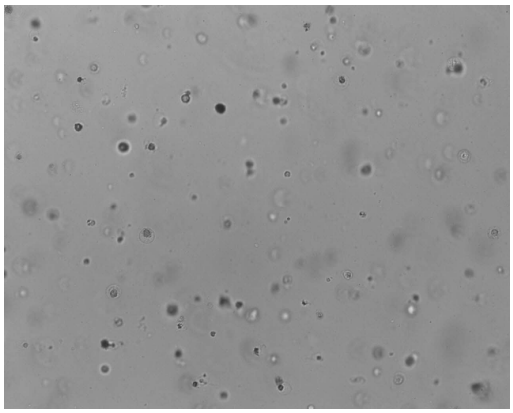


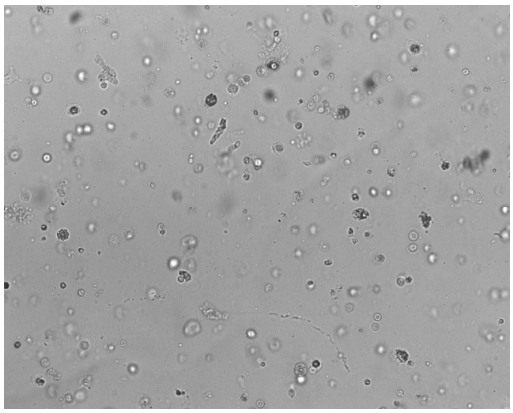
Figure 19. F.Media and Base Media, but not TME RPMI media, support OG cancer growth in the 3D-TGA

OES145 was grown in the 3D-TGA using modified conditions with BME at 12mg/ml, in the presence of ROCKi, for 7 days, with and without hMSC co-culture, in three different culture media: F-Media, Base Media with additional growth factors (BM + Add GFs) and TME RPMI.

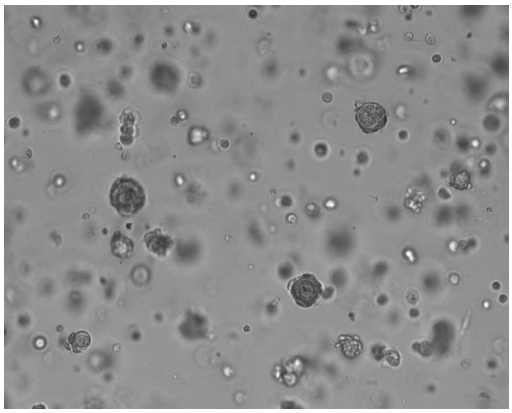
The six different conditions of the 3D-TGA cultures were examined by brightfield microscopy and showed increased clustering for OG cancer cells seeded in the conditions of BM and F.Media, in comparison with the original TME RPMI media (Figure 20). This was consistent with the growth measured by alamarBlue (Figure 19). There was no clear difference in cluster formation when OG epithelial cells are grown with or without hMSCs.



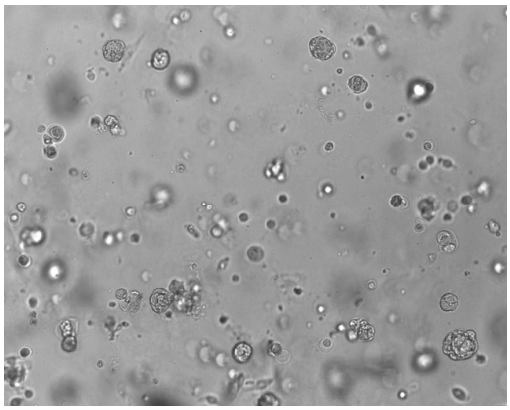
TME RPMI



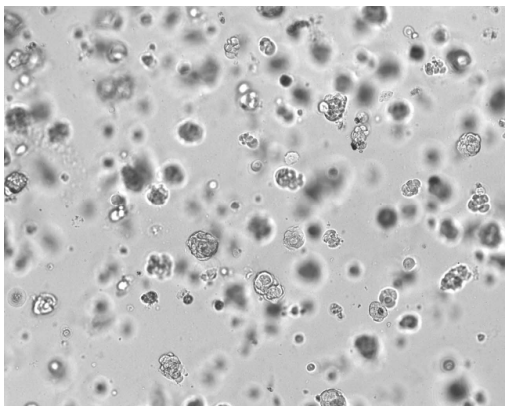
TME RPMI +hMSCs



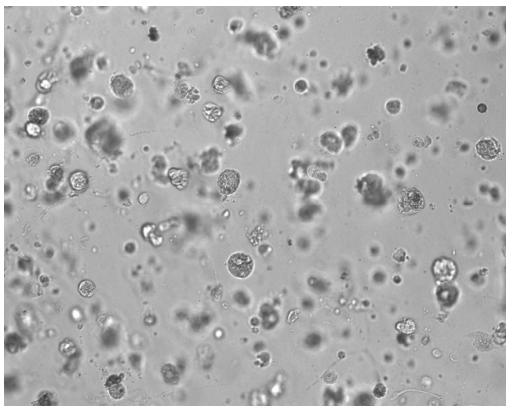
F-Media



F-Media +hMSCs



BM + Add GFs



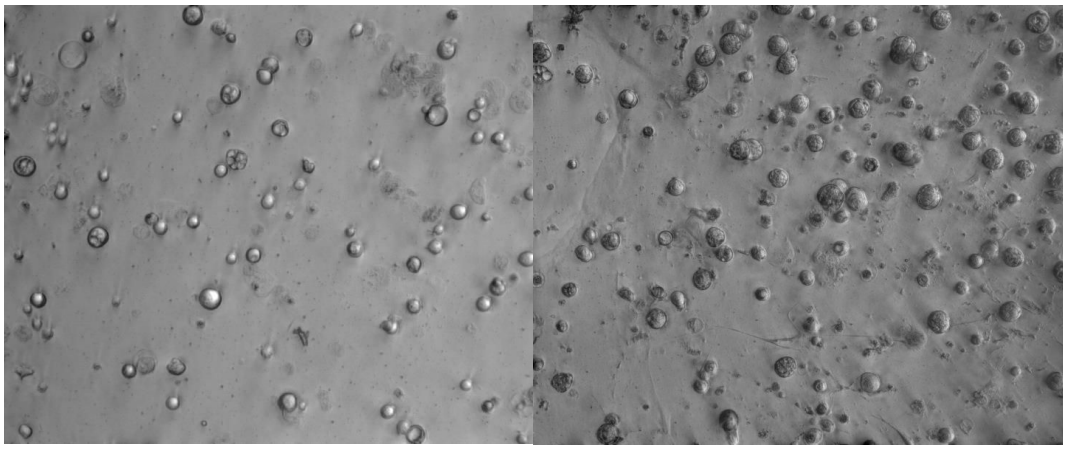
BM +Add GFs +hMSCs

Figure 20. Primary patient OG cancer cells grow in cancer cell clusters in the 3D matrix, with Base Media and F.Media but not TME RPMI

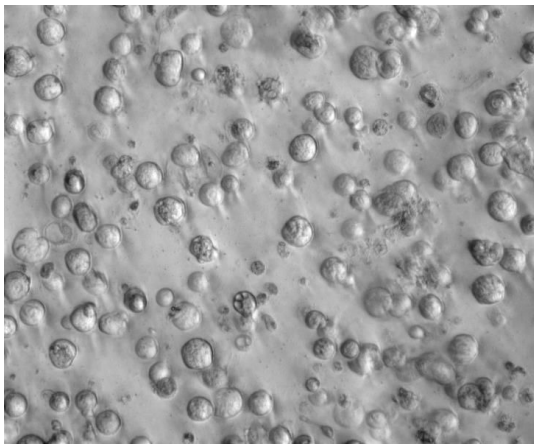
OES145 was grown in the 3D-TGA using modified conditions with 3 different media, with and without stromal co-culture. Images of a typical 3D-TGA well were captured on day 10 using the x10 objective on the Nikon 2D bright-field microscope.

To examine the cell growth in the 3D-TGA, from seeding as a single cell suspension into forming cancer cell clusters, the cells were examined using serial microscopy (Figure 21). This showed growth and cluster formation occurs progressively over 10 days. The multi-cellular clusters form consistently from the individually seeded cells in a reproducible fashion throughout wells.

The structure and formation of the cancer cell clusters in the 3D-TGA was examined using progressive powered microscopy objectives (Figure 22). This showed both BM and F.Media provide growth conditions which allowed the formation of discrete, spherically shaped, multi-cellular clusters.



Day 0 Day 5



Day 10

Figure 21. Primary patient OG cancer cells exhibit progressive clusters formation and growth over a 10 day time period

OES145 was grown in the 3D-TGA using modified conditions (using the BM media + add GFs in this example), without stromal co-culture. Serial images of a typical 3D-TGA well were captured using condensed multilayer focussed bright-field microscopy at the x10 objective on the Nikon bright-field microscope.

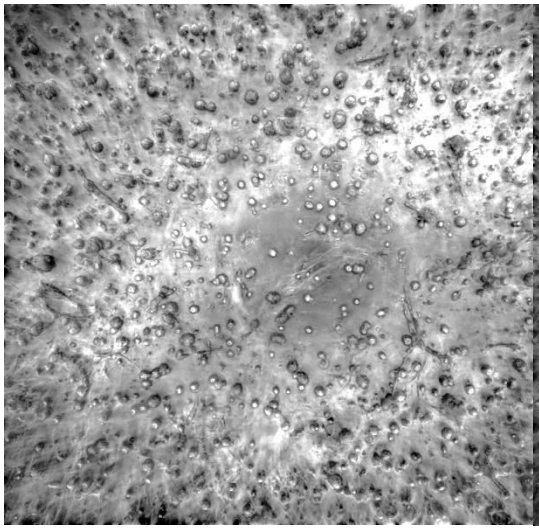
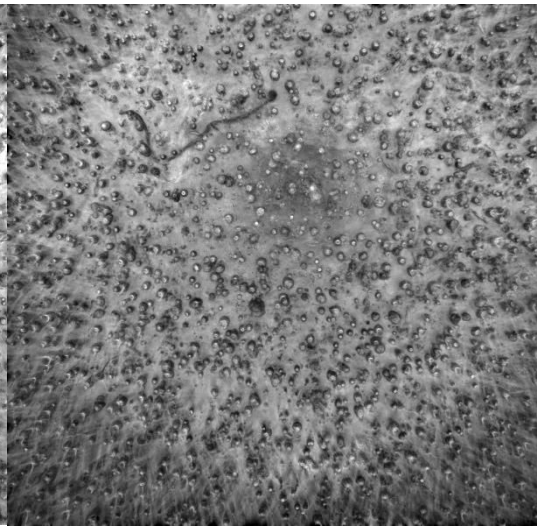
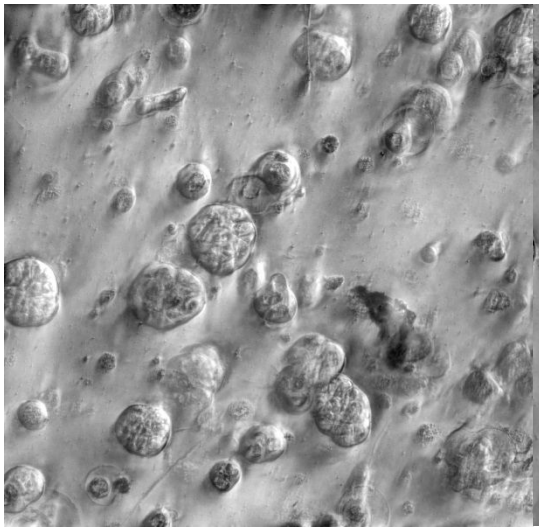
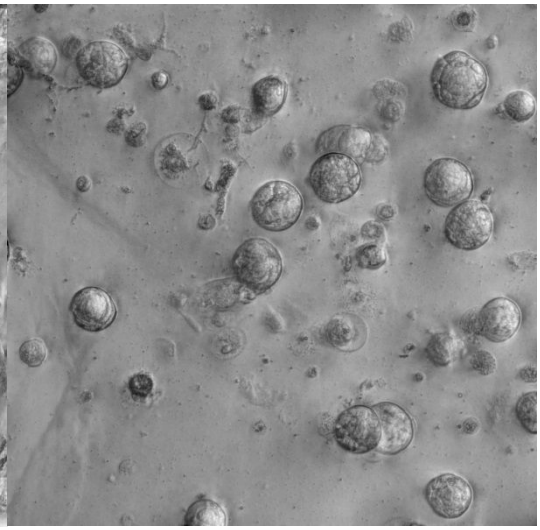
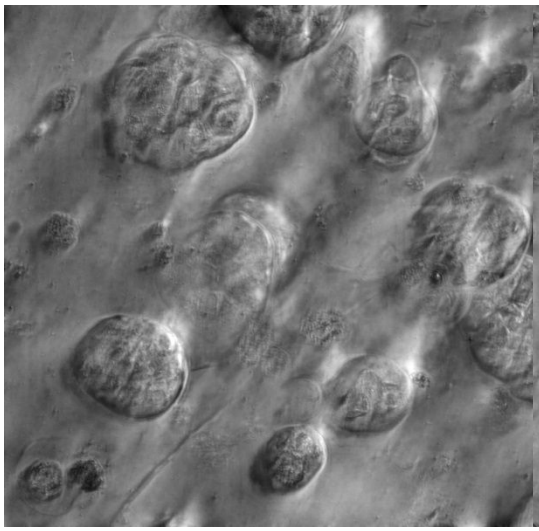
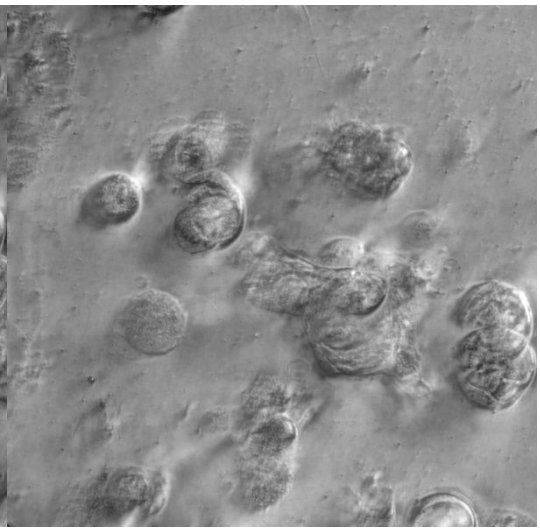
F-Media +hMSCs	BM +Add GFs +hMSCs
	
x4 objective	x4 objective
	
x20 objective	x20 objective
	
x40 objective	x40 objective

Figure 22. Primary patient OG cancer cells exhibit multicellular cluster formation

OES145 was grown with hMSC co-culture in the 3D-TGA using modified conditions, over a 10 day period, in BM media and F.Media. Images of a typical 3D-TGA well were captured using condensed multilayer focussed bright-field microscopy at progressively powered objectives on the Nikon bright-field microscope.

The 3D-TGA examining the conditions set out in 'experimental changes 2' was continued for a further 7 days to a total of 14 days to investigate the optimum timescale for cancer cell cluster growth (Figure 23A) and any potential role for re-feeding in prolonging the 3D cancer cluster growth (Figure 23B).

The two other published methods for re-feeding cancer cell clusters with more media (as outlined in the introduction) are performed every 3-5 days, either by sucking out the residual media and re-feeding, or by just adding further media on top of the culture. And therefore these two methods of re-feeding were trialled at Day 5 and then growth followed to Day 14, for the two media (Base Media, and F.Media) where active cancer cell cluster growth had been identified during the preceding 5 days of the assay (Figure 23B). The experimental results suggest that the 3D cultures did marginally better when not re-fed, although this was only apparent to day 7, and all growth of cultures declined by day 12. The poor results from re-feeding may be explained in part by the technical issues encountered with re-feeding in the small wells of a 384 well plate. This would therefore suggest that there was no benefit from re-feeding the 3D-TGA (when in a 384 well plate format) and an optimum timescale for the assay would be 7 days, which would then allow any assessment of drug cytotoxicity during active cell cluster growth.

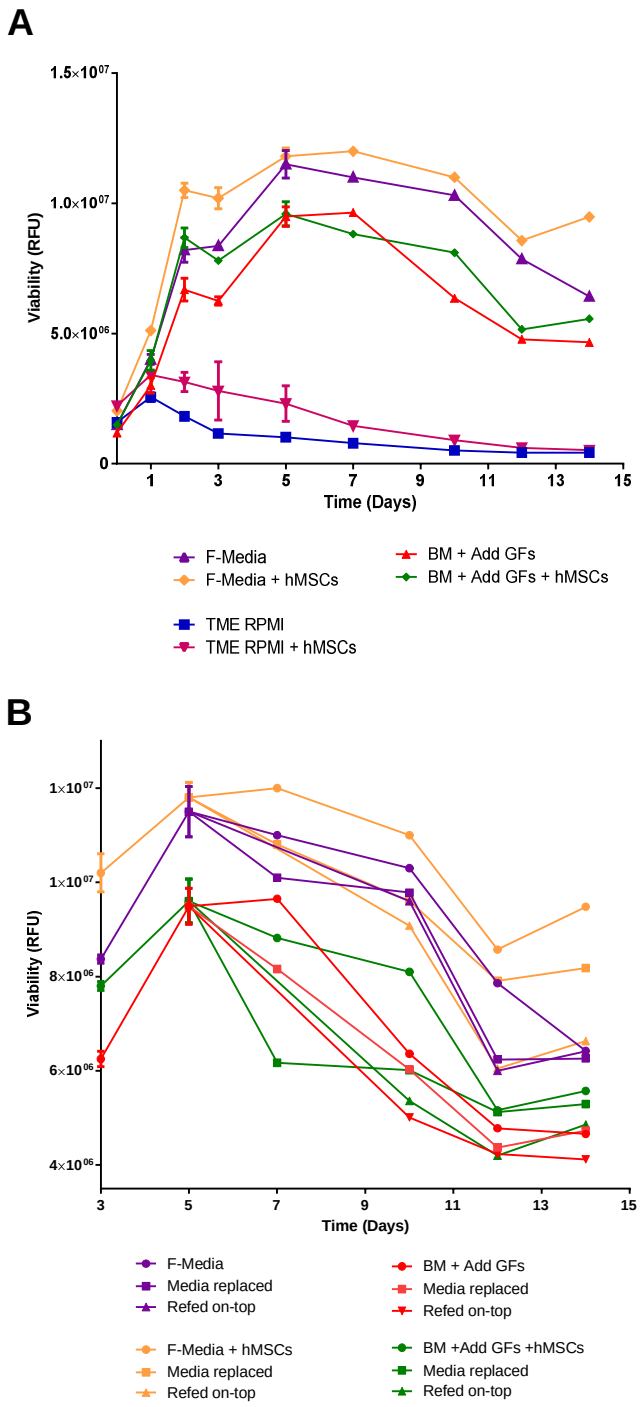


Figure 23. Growth pattern in the 3D-TGA over an extended time period with different media and re-feeding

OES145 was grown in the 3D-TGA using modified conditions with BME at 12mg/ml, in the presence of ROCKi, with and without hMSC co-culture, in three different culture media. **(A)** Growth was measured over a 14 day period. **(B)** Where 3D-TGA growth was confirmed at Day 5, each different condition was then either: monitored only (baseline), or media replaced, or media refed on-top.

The assays performed with 'experimental changes 2' demonstrated that increasing the BME concentration to 12mg/ml supported 3D growth and cluster formation of the close-to-patient cells, however this increased concentration was not directly compared to 6mg/ml. F-Medium and BM + Add GFs (but not TME RPMI) both promoted the growth of close-to-patient OG cancer cells. This growth was consistently seen to day 7, and re-feeding the assay did not provide any benefit.

4.2.4 Evaluation of supplementary serum, growth factors and stromal co-culture

The 3D assay conditions were revised (with respect to the observations from experimental changes 2), to use BME at a concentration of 12mg/ml with an assay time length of 7 days, with either F.Media or BM.

F.Media contains bovine serum, which despite being 'defined Foetal Calf Serum' still contains some unspecified non-human growth factors, and therefore results in a non-humanised tumour micro-environment in the 3D-TGA. The next variables examined were firstly the necessity for serum in the F-Media, and secondly the effect of hMSC co-culture on the perceived epithelial cancer growth measured by an overall alamarBlue reading for the whole co-culture.

The change in conditions are summarised below:

Condition	Standard	Experimental change 3
Time	5 days	7 days
BME conc	3mg/ml	12 mg/ml
Supplementary ROCKi	No	Yes
Media	TME RPMI	**BM / F.Media / serum deplete F.Media**
Serum	None	**Yes / No**
Additional Growth Factors	No	**Yes / No**
Re-feeding	No	No
Epithelial, Stromal cell (3:1) co-culture	hMSCs	**MMC hMSCs / mCherry hMSCs**

The 3D-TGA was performed for 7 days using OBX53 with and without hMSC co-culture, to define the necessity of serum within the assay by examining 3 different media conditions: Base Media plus GFs, F.Media +/- defined foetal calf serum. This demonstrated that the serum deplete F-media growth was equivalent to that of the BM +GFs condition with or without hMSC co-culture (Figure 24).

Two close-to-patient cell lines (OES145: Figure 19; OBX53: Figure 24) have demonstrated progressive growth over a 7 day time period in these 3D-TGA conditions, suggesting that these modified 3D-TGA conditions (used 'experimental change 3') maybe applicable across the wider patient cohort of close-to-patient cells.

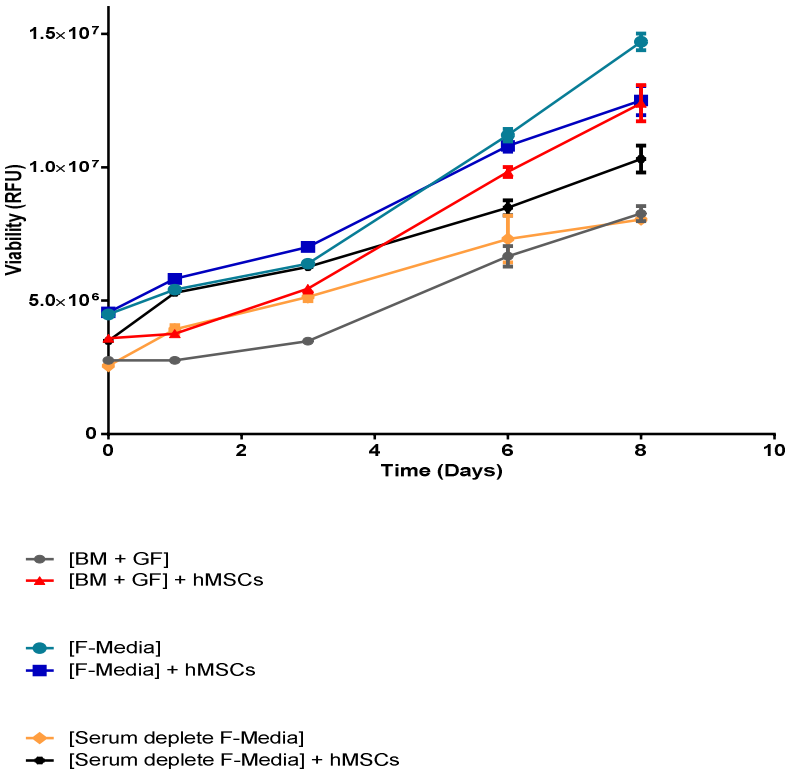


Figure 24. F.Media without foetal calf serum adequately supports OG cancer growth in the 3D-TGA

OBX53 was grown in the 3D-TGA using modified conditions with BME at 12mg/ml, in the presence of ROCKi, for at least 7 days, with and without hMSC co-culture, in three different culture media.

The 3D-TGA was again performed (using the 'experimental change 3' conditions), examining fluorescently transduced and growth arrested hMSCs in co-culture to explore the effect of hMSCs in their perceived growth enhancement of OG epithelial cell cancer clusters. hMSCs stably expressing mCherry, allowed the measurement of their growth separate to the overall measurement of all of the co-cultured cells in the well by alamarBlue signal. In addition, hMSCs were either left alive in the assay, or pre-treated with mitomycin-C to induce growth

arrest as a way to ensure hMSC growth was not overly contributing to the overall alamarBlue signal.

The 3D-TGA demonstrates that hMSC growth arrest did not reduce the signal observed in the alamarBlue assay, indicating the values are not being skewed by excessive hMSC growth in the 3D-TGA (Figure 25). This demonstrates that the observed epithelial cell growth was being stimulated by the presence and interactions of hMSCs rather than by hMSC growth.

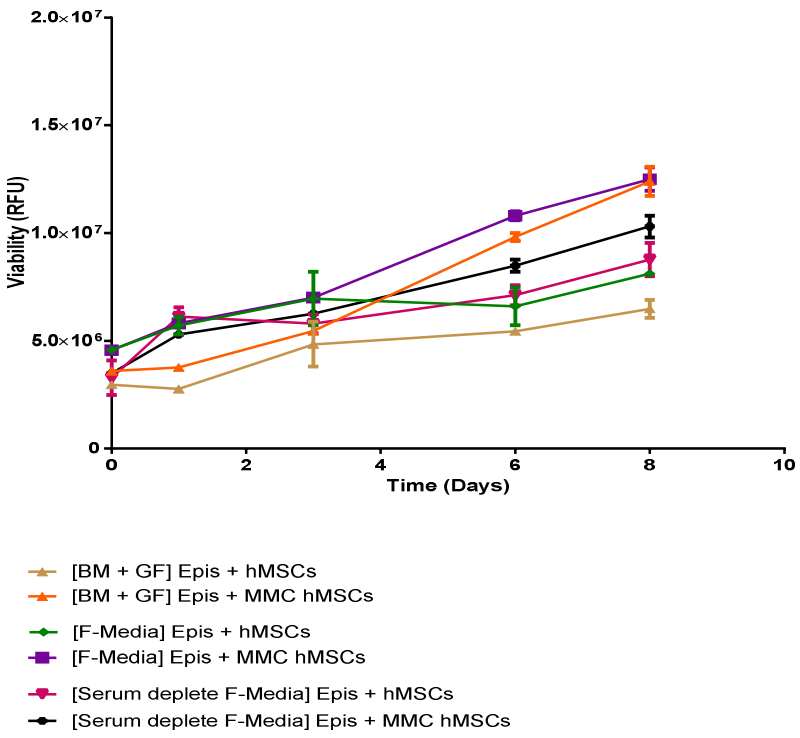


Figure 25. Co-cultured hMSCs do not require MMC growth arrest to prevent excessive hMSC growth in the 3D-TGA

OBX53 was grown in the 3D-TGA using modified conditions, with hMSCs and MMC hMSCs co-culture, in three different culture media, as measured by alamarBlue.

The 3D-TGA assay also had hMSCs in culture alone, to examine whether a particular media condition or additive growth factor enhanced or prevented the survival of hMSCs (Figure 26). It demonstrated an overall minor growth of hMSCs in a 3D matrix (with the 'experimental change 3' conditions), which was not affected by growing in different media.

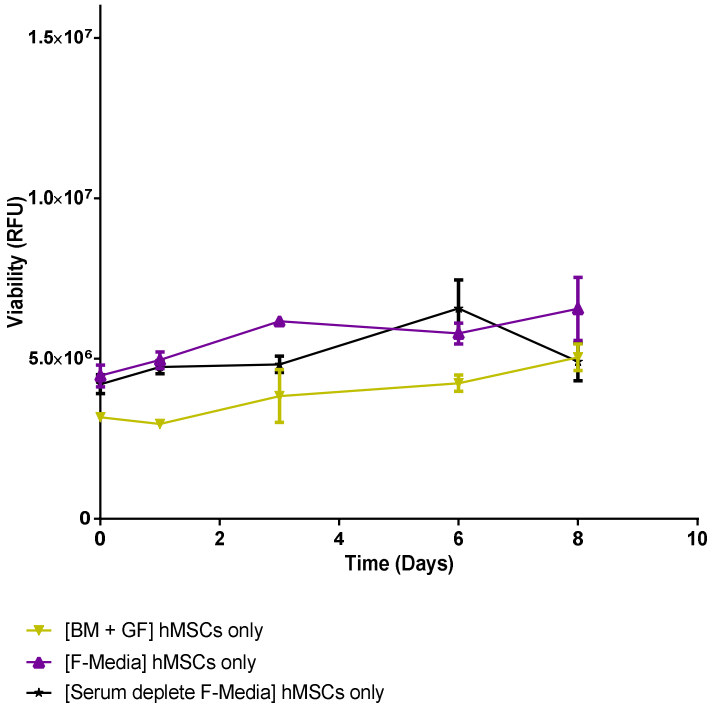


Figure 26. There was no difference in the growth of hMSCs in the 3D-TGA, as measured by alamarBlue

hMSCs are grown alone in the 3D-TGA using the modified conditions, in three different culture media, measured by alamarBlue.

The mCherry transduced hMSCs in this 3D-TGA assay enabled a parallel method of assessing growth of this cellular component directly (Figure 27). The 3D-TGA demonstrated no increase in mCherry signal in different conditions when grown with epithelial cells or subject to growth arrest by pre-treatment with MMC, and

it also shows no difference in growth between different media conditions. It also demonstrates that measuring hMSC growth in the 3D-TGA assay by their constitutively expressed mCherry fluorescence signal matched the result for hMSC growth measured with alamarBlue.

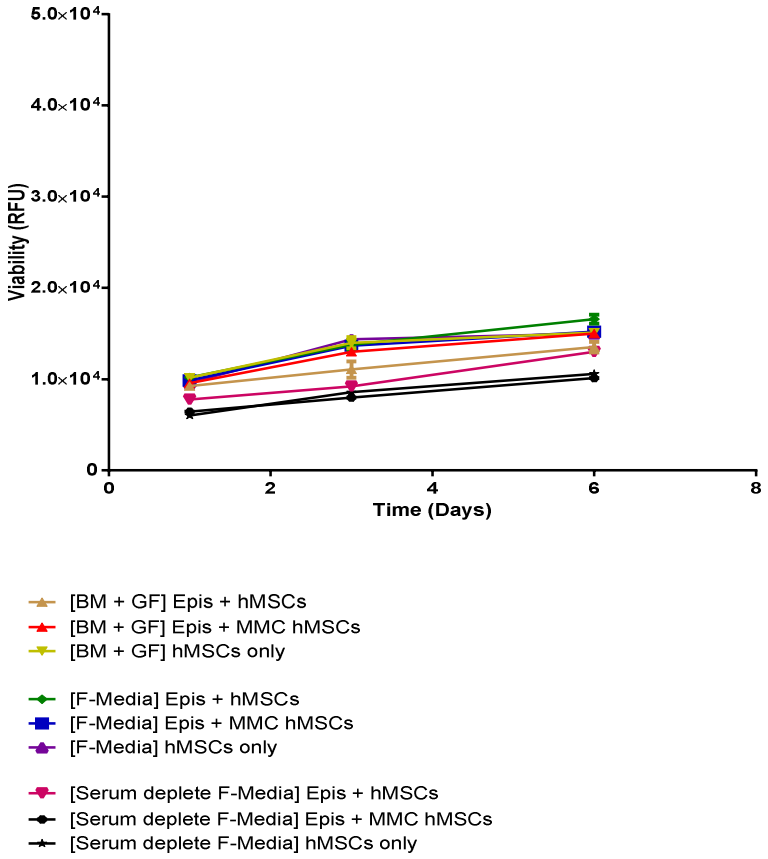


Figure 27. 3D-TGA co-cultured hMSCs in all media conditions demonstrate the same minimal growth as when growth arrested or when grown alone, as measured by mCherry fluorescence

hMSCs in co-culture with OBX53, MMC hMSCs in co-culture with OBX53, and hMSCs alone are grown in three different culture media, in the 3D-TGA, as measured by their constitutive mCherry fluorescence.

To examine the development of cancer cell clusters in conjunction with mCherry hMSC co-cultures, in different media conditions, the OG cancer cell clusters were examined using fluorescence microscopy (Figure 28). This demonstrated that in all three media conditions (regardless of the presence of serum) the seeded epithelial cells are starting to form cancer cell clusters on D3 and this was taking place in conjunction with the mCherry hMSC stromal cell component. When co-cultured, the hMSC cellular component are not evenly distributed throughout the well (as they are following initial seeding), but found in distributed in conjunction with the developing epithelial cancer clusters, which can be seen where the cherry colour is preferentially pictured in juxtaposition with the developing cancer cell clusters (Figure 28).

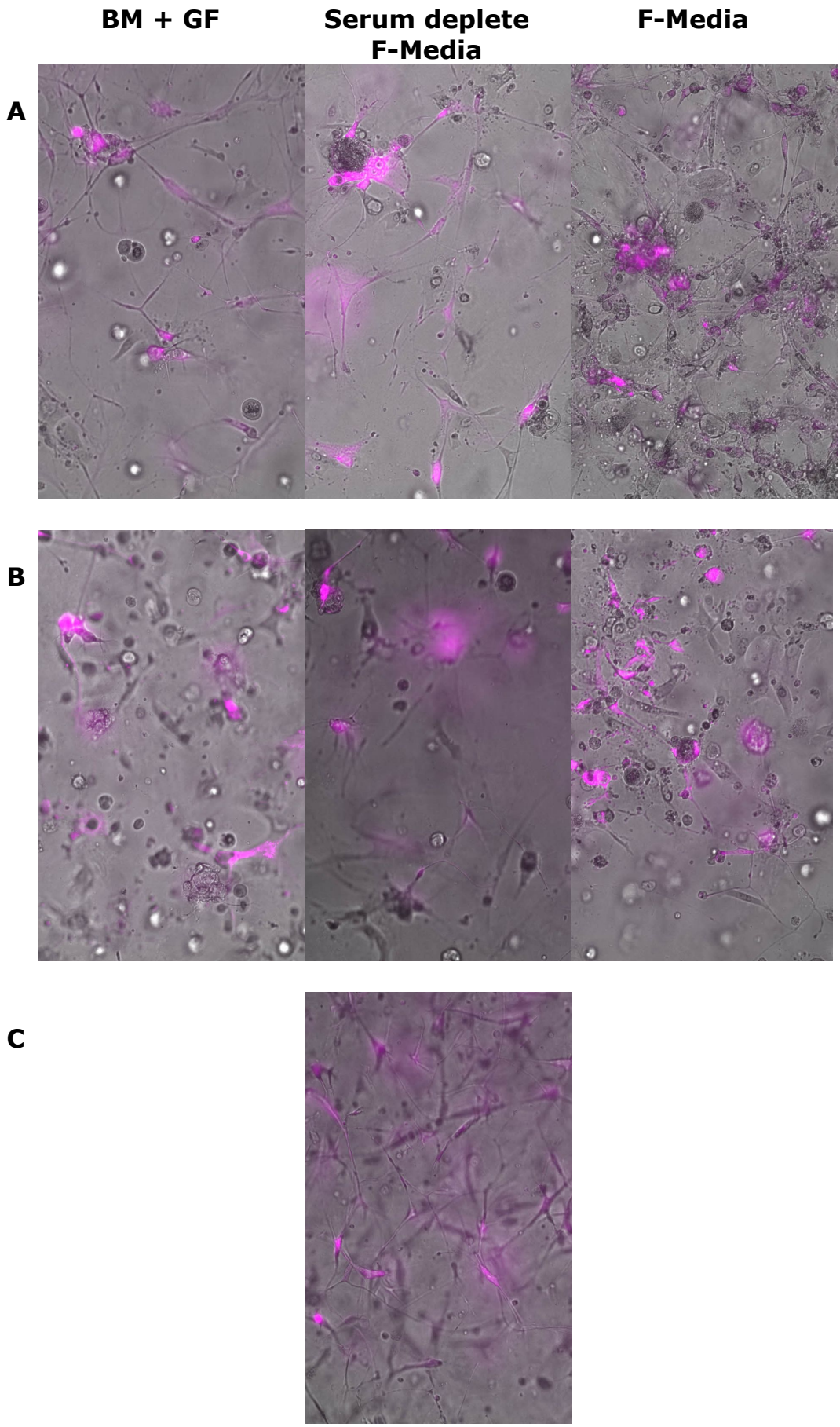

BM + GF
Serum deplete F-Media
F-Media
A
B
C

Figure 28. Primary patient OG cancer cells grow in cancer cell clusters in the 3D matrix, in conjunction with the co-cultured mCherry hMSCs

OBX53 was grown in the 3D-TGA using modified conditions with 3 different media (Base Media, Serum deplete F.Media and F.Media), with **(A)** hMSC co-culture, **(B)** MMC hMSC co-culture and **(C)** hMSCs alone. Images of a typical 3D-TGA well were captured on Day 3 using the x10 objective on the Nikon 2D bright-field microscope, with fluorescence capture.

To examine the cellular composition of the of co-cultured cancer cell clusters in the 3D-TGA, the OG cancer cell clusters were extracted from the 3D culture matrix of the remaining wells, immuno-fluorescence stained and examined using immunofluorescence microscopy (Figure 29). This demonstrated a 3D multi-cellular composite structure, combining both epithelial cells (green) and hMSCs (cherry). Fluorescent in-assay microscopy and ex-assay immunohistochemical staining of the co-cultured cells demonstrates that there is a physical interaction between the hMSCs and the developing epithelial cell clusters.

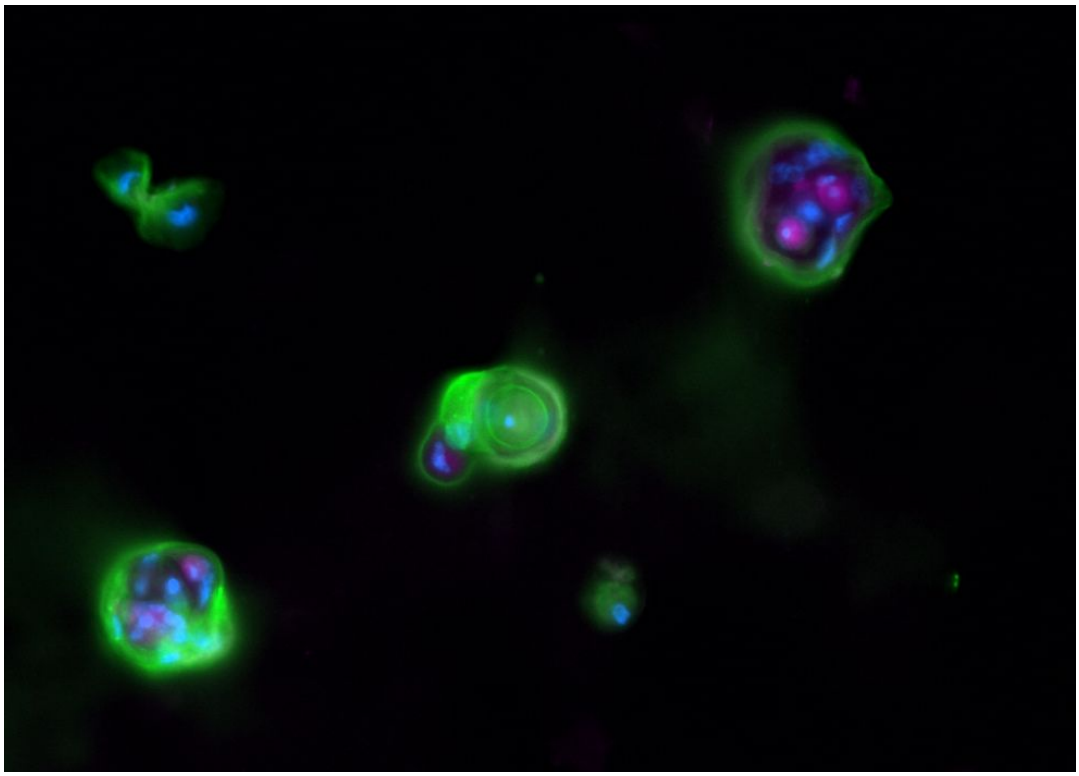


Figure 29. OG cancer cells co-cultured in the 3D-TGA with hMSCs form composite clusters of multi-cell types

OBX53 was grown in the 3D-TGA using modified conditions with hMSC co-culture. Cancer cell co-cultures were extracted from the 3D-TGA on Day 7 and immuno-stained on glass slides. The epithelial cells have been identified with EpCam and stained green, all cell nuclei appear blue from staining with DAPI, and the hMSCs appear red from their constitutively expressed mCherry protein. Images were captured using a x20 objective on the Nikon 2D bright-field microscope, using stepwise fluorescence capture.

Based on the above data of similar growth rates of the close-to-patient cells in the different media, the serum deplete F.Medium was selected as the media of choice for the further 3D-TGA experiments. Not only was it preferable to aim for a more humanised microenvironment (without foetal calf serum), and uses less supplementary additives and additional GFs than the BM, but also keeps consistency from the feeder-layer culture.

The experimental data also showed that formal growth arrest of the hMSCs with MMC is not necessary. The relatively little hMSC growth in the 3D-TGA will not substantially alter the measurement of epithelial growth (by whole well alamarBlue assessment). It was concluded that it is the hMSCs presence and interactions within the assay which are growth supportive of the epithelial cells, not a measurement of additive hMSC cell growth to the alamarBlue growth signal.

The data obtained from measuring hMSC growth with mCherry expression allowed successful co-existing monitoring of the hMSC cells whilst still co-cultured with the epithelial cells. This demonstrates the mCherry signal can be used successfully to monitor the fractional proportion of hMSC growth when in co-culture.

4.2.5 Cell functionality within the 3D-TGA

Previous IHC staining (in Chapter 3) of the individual OG cancers either as patient tissue, *in vitro* cells or *in vivo* PDX has demonstrated variable expression of TFF3, suggesting that the return to a functional cell phenotype is dependent upon the microenvironmental setting within which the tumour cells are grown. To assess the potential tumour cell functionality within the 3D-TGA growth TME, the OG cancer cell clusters were extracted and underwent immunofluorescent staining for TFF3 (Figure 30). Unlike in 2D feeder-layer culture, the same close-to-patient cancer cells produced TFF3 when growing in co-cultured clusters in 3D culture, suggesting that these 3D-TGA conditions are enabling a return of cell functionality.

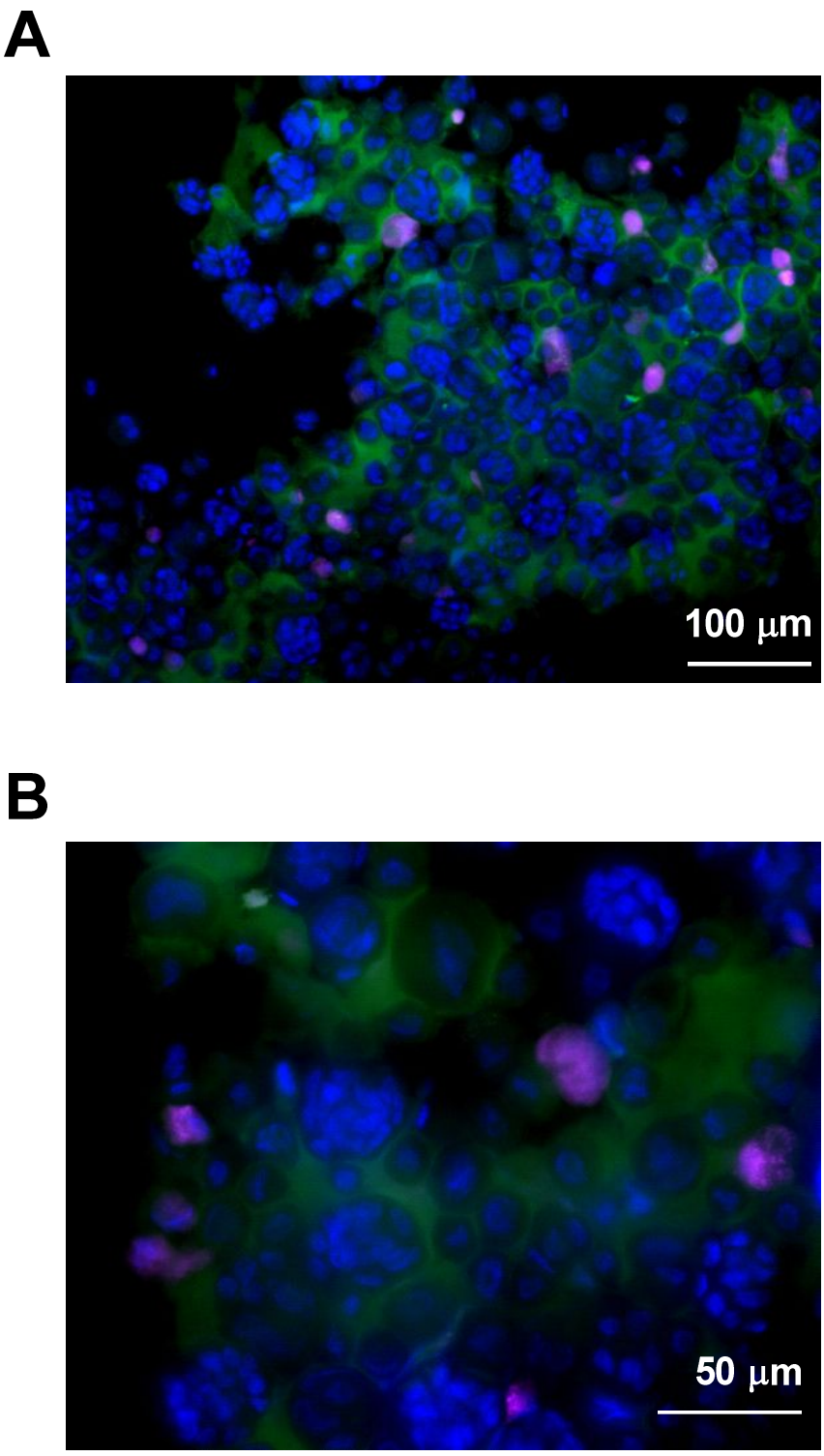


Figure 30. OG Cancer Cells express TFF3 when cultured in the 3D-TGA in the presence of hMSCs

OES145 Cell clusters with mCherry-labelled hMSCs (purple) at day 7 were extracted to glass slides and stained with anti-TFF3-AlexaFluor488 (green) and counter-stained with DAPI (blue), and imaged by fluorescence microscopy at x20 **(A)** and x40 **(B)** magnification.

4.2.6 Finalised assay conditions and use for chemotherapeutic drug evaluation

The 3D assay conditions were revised (with respect to the observations from experimental changes 3), to use serum deplete F.Medium and mCherry hMSCs.

The proposed final conditions for performing the OG cancer 3D-TGA in a 384 well plate, with 6250 cells/well, were therefore:

Condition	Standard	Final conditions
Time	5 days	7 days
BME conc	3mg/ml	12 mg/ml
Supplementary ROCKi	No	Yes
Media	TME RPMI	F.Media
Serum	None	No
Additional Growth Factors	No	No
Re-feeding	No	No
Epithelial, Stromal cell (3:1) co-culture	hMSCs	mCherry hMSCs

To confirm these OG 3D-TGA culture conditions and investigate the use of the assay for pharmacological evaluation of the individual cancers, the 3D-TGA was performed for 7 days using OES145 with and without mCherry hMSC co-culture.

Evaluation of baseline epithelial cell and hMSC growth, and cluster development was performed by alamarBlue (Figure 31), mCherry fluorescence (Figure 32) and serial microscopy (Figure 33).

The proposed final OG 3D-TGA growth conditions are confirmed as successfully supporting primary close-to-patient OG cancer cell culture growth (Figure 31). The stromal co-culture component of the 3D-TGA doesn't grow significantly and therefore does not alter the growth measurement of the epithelial cancer cell clusters (Figure 32).

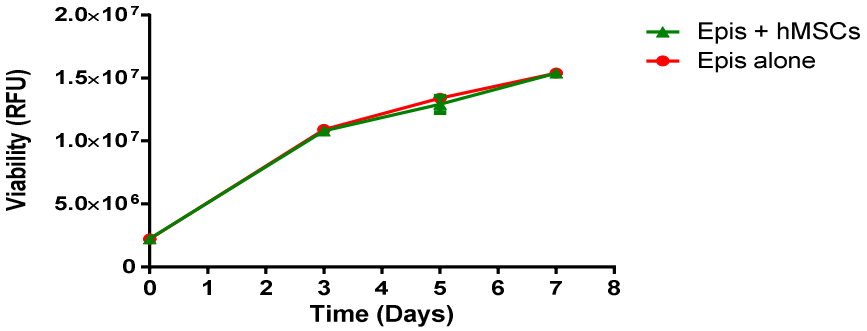


Figure 31. Endorsement of the modified conditions that support OG cancer growth in the 3D-TGA

OES145 was grown in the 3D-TGA using the modified conditions for 7 days, with and without mCherry hMSC co-culture.

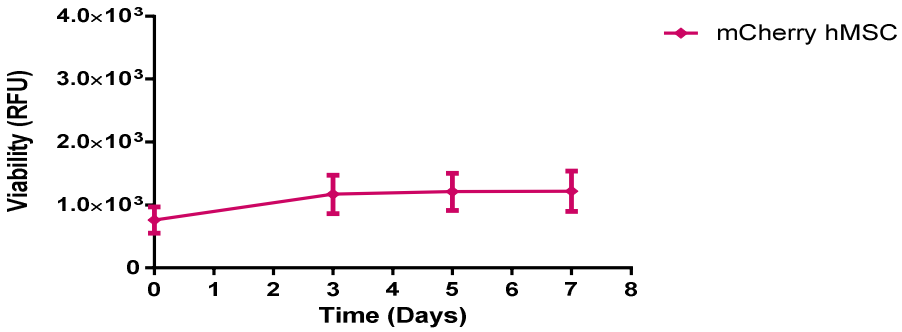
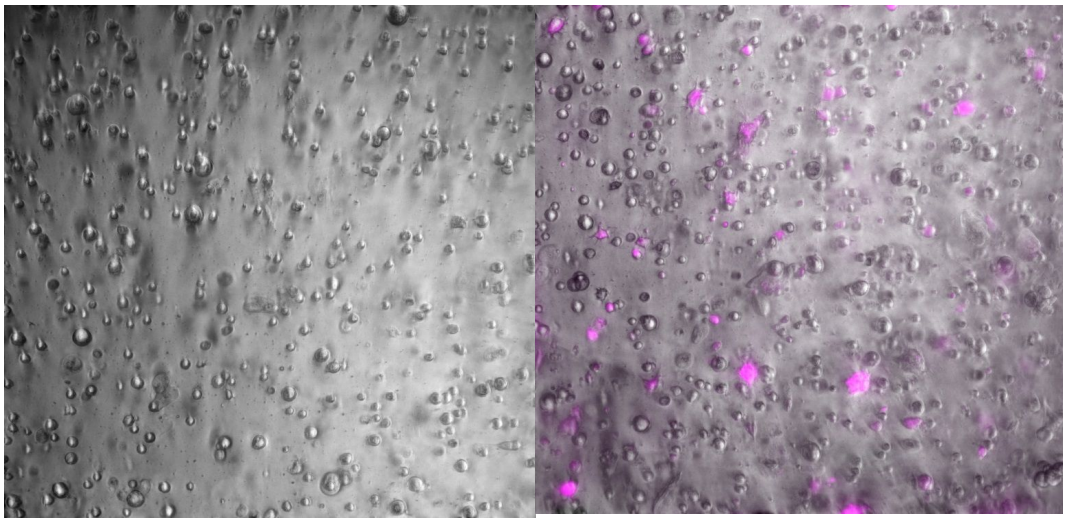


Figure 32. mCherry hMSCs in 3D-TGA co-culture have consistently plateaued growth pattern

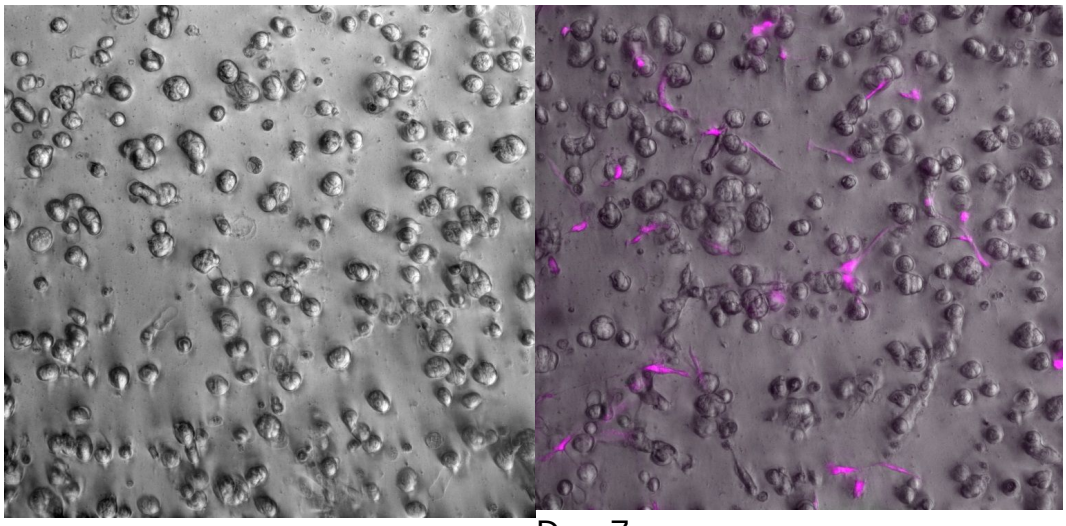
The growth of mCherry hMSC co-culture component of the OES145 3D-TGA was measured separately from the OG epithelial cancer cells by monitoring the constitutively expressed hMSC cell fluorescence.

To examine the growth from seeding as a single cell suspension into cancer cell clusters in the 3D-TGA, the OG cancer cell clusters were examined using start (day 0) and endpoint (day 7) microscopy (Figure 33). These images demonstrate the progressive growth and cluster formation that takes place in the 3D-TGA under these supportive growth conditions. The images show that the cluster formation was consistent and reproducible, which is of paramount importance to chemotherapeutic testing reliability.

Epis alone **Epis + mCherry hMSCs**



Day 0 Day 0



Day 7 Day 7

Figure 33. Primary patient OG cancer cells in the 3D-TGA exhibit reproducible cancer cell growth and cluster formation

OES145 was grown with mCherry hMSC co-culture in the 3D-TGA using the proposed final conditions, over a 7 day period. Images of a typical 3D-TGA well were captured using condensed multilayer focussed fluorescent microscopy using the x10 powered objective on the Nikon bright-field microscope.

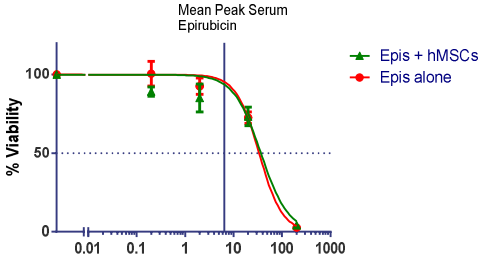
This OG 3D-TGAs use for assessing chemotherapeutic drugs was evaluated, with application of drugs as a media overlay on day 3 (Figure 34). The standard of care drugs ECF (Epirubicin, Cisplatin, 5-Fluorouracil) chemotherapy were used, to establish evidence of chemo-sensitivity. The chemotherapy doses tested in the 3D-TGA were at a range of concentrations that encompassed the endpoint tissue concentrations seen in the human (mean peak serum concentrations) and compared to the inhibitory concentration (IC_{50}) required for chemo-toxicity *in vitro*. The drugs were simultaneously tested both individually and in combination, to show if a chemotherapy agent was providing the principle chemo-toxic effect and if there was evidence of a combinational response to the drugs. These assays were also run with and without hMSC stromal support to investigate the influence of stromal support in the TME on the chemo-resistant phenotype.

This assay shows that when the chemotherapeutics are given individually, the concentration required to reach the IC_{50} was significantly greater than any concentration that could be safely administered clinically (Figure 34). By administering the chemotherapeutics in doublet combinations, the concentration at which the chemotherapeutics achieve the IC_{50} was significantly reduced, but for this cancer, it is still greater than the mean peak serum achieved in patients. This suggests that at clinically

administered concentrations, these doublet drug combinations would not provide an adequate chemotherapeutic effect for this patient. A combination of all 3 drugs (ECF: as it would be administered clinically) further decreases the overall IC_{50}, which for this primary patient cancer, was below the mean peak serum level which at these chemotherapeutics that are administered (Figure 34). This suggests that this particular OG cancer (OES145) may be sensitive to this combination chemotherapy in the clinical setting.

Co-culture of the cancer epithelial cells with stromal cells demonstrates an effect on the chemotherapeutic sensitivity of this cancer to individual drugs at their higher concentrations, as demonstrated by a change in the IC_{50}. However, this was less pronounced when the cancer is exposed to doublet chemotherapy and even where there does appear to be a difference in the IC_{50}, this is not statistically significant as the 95% confidence interval overlaps. Indeed when triplet chemotherapy was administered, the increased chemo-resistance demonstrated by the co-cultured cancer cells is minor and again statistically insignificant for this patient's cancer (Figure 34).

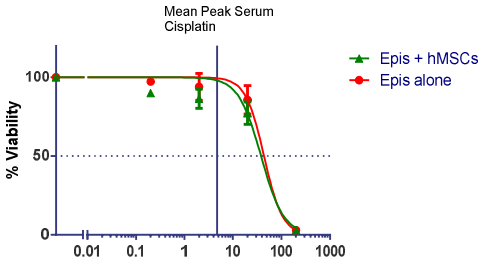
Epirubicin



	Epis alone	Epis + hMSCs
IC50	33.74	36.70

	Epis alone	Epis + hMSCs
IC50	28.13 to 40.47	27.67 to 48.67

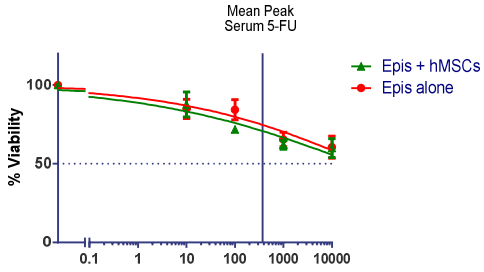
Cisplatin



	Epis alone	Epis + hMSCs
IC50	43.62	37.86

	Epis alone	Epis + hMSCs
IC50	32.72 to 58.14	27.91 to 51.37

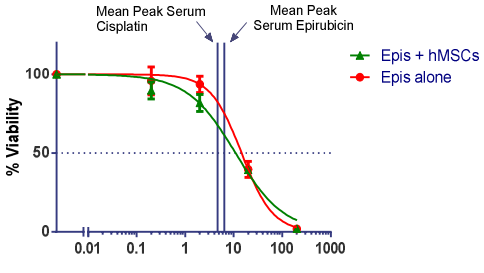
5-FU



	Epis alone	Epis + hMSCs
IC50	46551	31929

	Epis alone	Epis + hMSCs
IC50	14663 to 147793	10410 to 97930

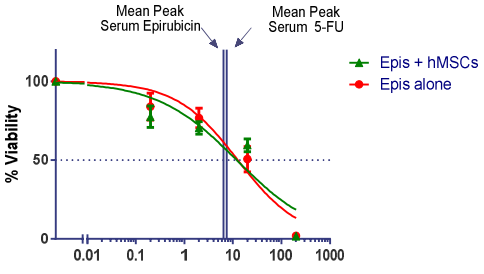
Epirubicin / Cisplatin



	Epis alone	Epis + hMSCs
IC50	14.59	10.93

	Epis alone	Epis + hMSCs
IC50	12.72 to 16.72	9.108 to 13.12

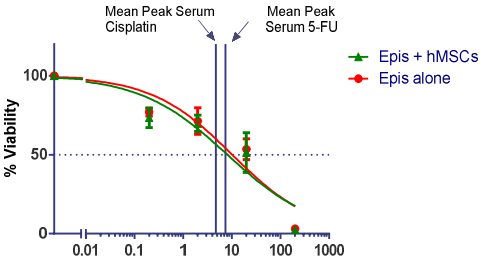
Epirubicin / 5-FU



	Epis alone	Epis + hMSCs
IC50	12.73	12.09

	Epis alone	Epis + hMSCs
IC50	8.406 to 19.29	6.938 to 21.07

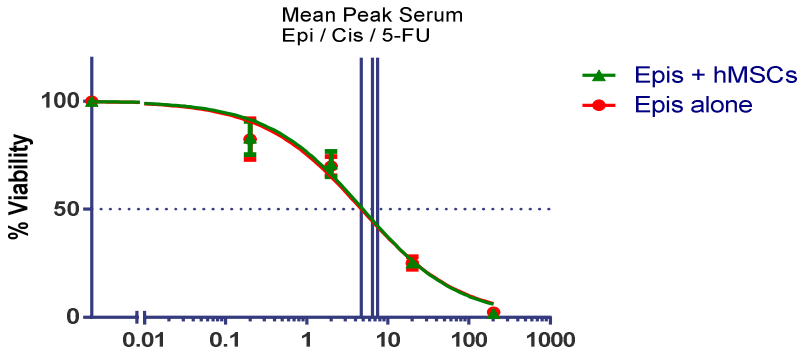
Cisplatin / 5-FU



	Epis alone	Epis + hMSCs
IC50	10.23	8.146

	Epis alone	Epis + hMSCs
IC50	6.244 to 16.75	4.607 to 14.40

ECF (Epi/Cis/5-FU)



	Epis alone	Epis + hMSCs
IC50	4.721	4.933

	Epis alone	Epis + hMSCs
IC50	3.691 to 6.038	3.911 to 6.220

Figures 34. Primary patient OG cancer cells in the 3D-TGA exhibit a dose response effect when exposed to increasing concentrations of chemotherapeutics

OES145 was grown with mCherry hMSC co-culture in the 3D-TGA. Chemotherapeutics (Epirubicin, Cisplatin and Fluorouracil) were added at a range of doses, individually and in their combination on day 3 and resultant growth (relative to untreated wells) measured on day 7. The mean peak serum concentration of that drug administered clinically is demonstrated by a solid vertical bar. The IC_{50} is marked with a horizontal dashed line, and the calculated value and confidence interval for each drug and combination is recorded in the table below each graph.

4.3 Conclusions

The standard Nottingham 3D-TGA for use with PDX cellular material required significant alterations so that it could be used for the successful and reliable growth of the primary close-to-patient OG cancer cells.

This has involved adjusting a number of parameters including the concentration of the basement membrane extract, ROCKi supplementation, media type, serum supplementation and use of additional growth factors. Stromal cell co-culture has been carefully examined to prevent confounding of the measurement of epithelial growth or cytotoxicity.

Fluorescent imaging of these cancer cell clusters has been performed, demonstrating the multi-cellular structure of these cancer cell clusters, with the different co-cultured cell types interacting within the cancer cluster.

Achieving consistent progressive cellular growth over an extended timescale with reproducible cluster formation has been important as a basis to allow the subsequent performance of reliable drug testing.

5 Results 3: Chemotherapeutic Evaluation using the OG Cancer 3D-TGA

5.1 Overview & Aim

The platinum based ECF chemotherapy regimen, which was administered clinically to the patients of this study, was assessed in the 3D-TGA, so a direct chemotherapeutic evaluation could be made.

The novel histone deacetylase inhibitor (HDACi) drug, Panobinostat, was also assessed to evaluate the 3D-TGA as a potential platform for appraisal of new drugs. This would allow assessment of potential new drug efficacy as monotherapy or in combination with the current SOC, for potential translation into clinical practice.

I also chose to evaluate the PDE5i drug Vardenafil in combination with ECF therapy, in models both with and without hMSC stromal support to evaluate any additional chemo-therapeutic effect the drug may bring to bear by interfering with the tumour microenvironment. I hypothesised that the PDE5i would only show a change in overall chemo-sensitivity within those 3D-TGA models incorporating hMSCs, as the PDE5i are thought to interfere with the stromal cells and their ability to promote a pro-tumorigenic TME, rather than be directly chemo-toxic to the epithelial cancer cells themselves.

5.2 Results

5.2.1 Study group and Demographics

Inclusion criteria for sample growth and subsequent characterisation and pharmacological assessment in the 3D-TGA were required, to ensure that the study population were all undergoing the same standardised curative chemotherapy regimen, that could be reproduced in the 3D-TGA in a standardised fashion, allowing an accurate comparison between *in vivo* and *ex vivo* results. The clinical inclusion criteria

- oesophageal adenocarcinoma (lower 1/3 and GOJ)
- completion of 3 full cycles of ECF neoadjuvant chemotherapy without dose reductions
- definitive surgery and TRG assigned

resulted in a final group of 12 samples from nine patients who were entered into the study (Figure 3), and underwent detailed chemotherapeutic analysis. Patient factors (e.g. advanced disease requiring palliation) and oncological causes (e.g. non-completion of chemotherapy) were the most common cause of study exclusion.

Five of these nine patients had a matched, chemotherapy-exposed resected tumour established *in vitro* which also underwent chemo-sensitivity analysis. The baseline demographic, surgical and oncological details for these nine patients with samples established from chemotherapy-naïve biopsies who met these inclusion criteria were recorded (Table 17). They have a similar distribution of grade and aggressiveness, and are similar to a standard clinical cohort presenting with disease amenable to neoadjuvant chemotherapy and surgery with curative intent.(57)

Table 17. Patient demographics, tumour staging and treatment

Patient ID	Demographics & Diagnosis					Chemotherapy & Surgery					Histopathology & Tumour Regression				
	Gender	Age at diagnosis	Tumour site	Barretts present	cTNM (all M0)	Cycles of NeoA ECF	Neo dose reduction	Neo cycle delay	NeoA complication	Procedure	pTNM (all M0)	Positive / Resected Nodes	Involved margins	Stage	TRG
Oes1	M	77	Lower third	yes	T3 N0	3	no	nil	none	ILO	T0 N0	0/12	no	0	1
Oes2	M	55	Lower third	yes	T3 N2	3	no	nil	none	ILO	T3 N1	2/30	no	IIIA	3
Oes3	M	45	GOJ	no	T3 N0	3	no	nil	none	ILO	T4a N1	1/23	no	IIIC	3
Oes4	F	53	GOJ	no	T3 N2	3	no	nil	none	ILO	T4a N0	0/7	CRM+	IIIA	4
Oes5	M	58	GOJ	no	T3 N2	3	no	nil	none	ILO	T3 N3	8/18	CRM+	IIIC	4
Oes6	M	72	GOJ	yes	T3 N2	3	no	1 week	Diarrhoea, N+V, fatigue	ILO	T3 N0	0/16	CRM+	IIB	4
Oes7	M	75	Lower third	no	T3 N1	3	no	2 week	AKI, mucositis	ILO	T3 N0	0/22	no	IIB	5
Oes8	M	62	Lower third	no	T3 N1	3	no	nil	Neutropenia, N/V 3rd cycle	ILO	T3 N2	4/17	CRM+	IIIB	5
Oes9	M	67	GOJ	no	T3 N0	3	no	nil	PPE	ILO	T3 N3	12/18	CRM+	IIIC	4

Footnote: Abbreviations: GOJ: gastro-oesophageal-junction, cTNM: clinical Tumour, Node & Metastasis at initial staging, Neo: Neoadjuvant chemotherapy, ECF: Epirubicin, Cisplatin, 5-FU, N/V: nausea & vomiting, AKI: acute kidney injury, PPE: Palmar-Plantar Erythrodysesthesia, ILO: Ivor-Lewis Oesophagectomy, pTNM; pathological TNM histologically at resection, CRM+: circumferential resection margin positive, TRG: Mandard tumour regression grade.

5.2.2 Pathological features and clinical correlation

Mean age on presentation was 63 years, with a male predominance 89% (n=8) and similar cTNMs of T3 N0-2 within the group, and stages IIB to IIIC. The proportion (33%, n=3) of chemotherapy sensitive tumours (TRG 1-3), was broadly comparable to that seen in clinical practice (40%) (57). There was no significant difference between the mean time (26 and 21 days for the TRG 1-3 and TRG 4-5 cancers respectively) to develop each patient tumour into an established *in vitro* patient cancer cell culture of sufficient volume for laboratory experimentation (>1 $x10^7$ cells).

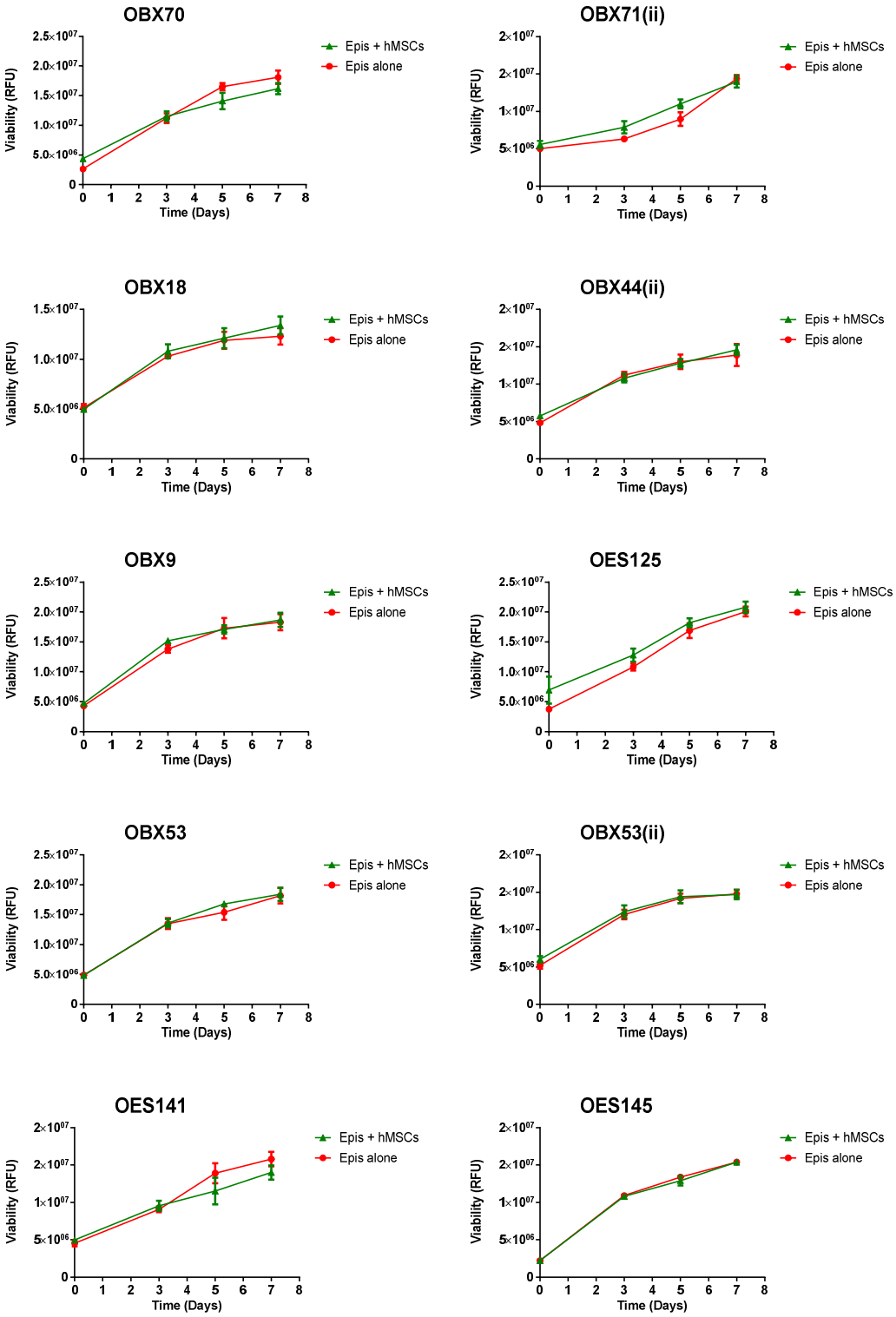
5.2.3 Growth, cluster formation and hMSC co-culture

All 12 samples from the 9 study patients grew in the 3D-TGA in a similar fashion consistent with the work in Chapter 4 (Figure 35A). Although all were similar to the method development growth curves, there was some variation in growth rate between the different patient cultures.

The growth of the hMSCs was consistently minimal compared to the cancer cells (Figure 35B) and so as anticipated did not affect overall growth measurement by alamarBlue. In co-culture, the cancer cell clusters displayed a small but significant increase in growth ($p<0.05$) compared to those without mesenchymal support (Figure 35C).

After establishment in the matrix, the close-to-patient cells developed into cancer cell clusters (Figure 35D,E), however (as with growth rates) there was some variation in the size and density of cluster formation.

A


OBX70
OBX71(ii)
OBX18
OBX44(ii)
OBX9
OES125
OBX53
OBX53(ii)
OES141
OES145
Viability (RFU)
Time (Days)
Epis + hMSCs
Epis alone

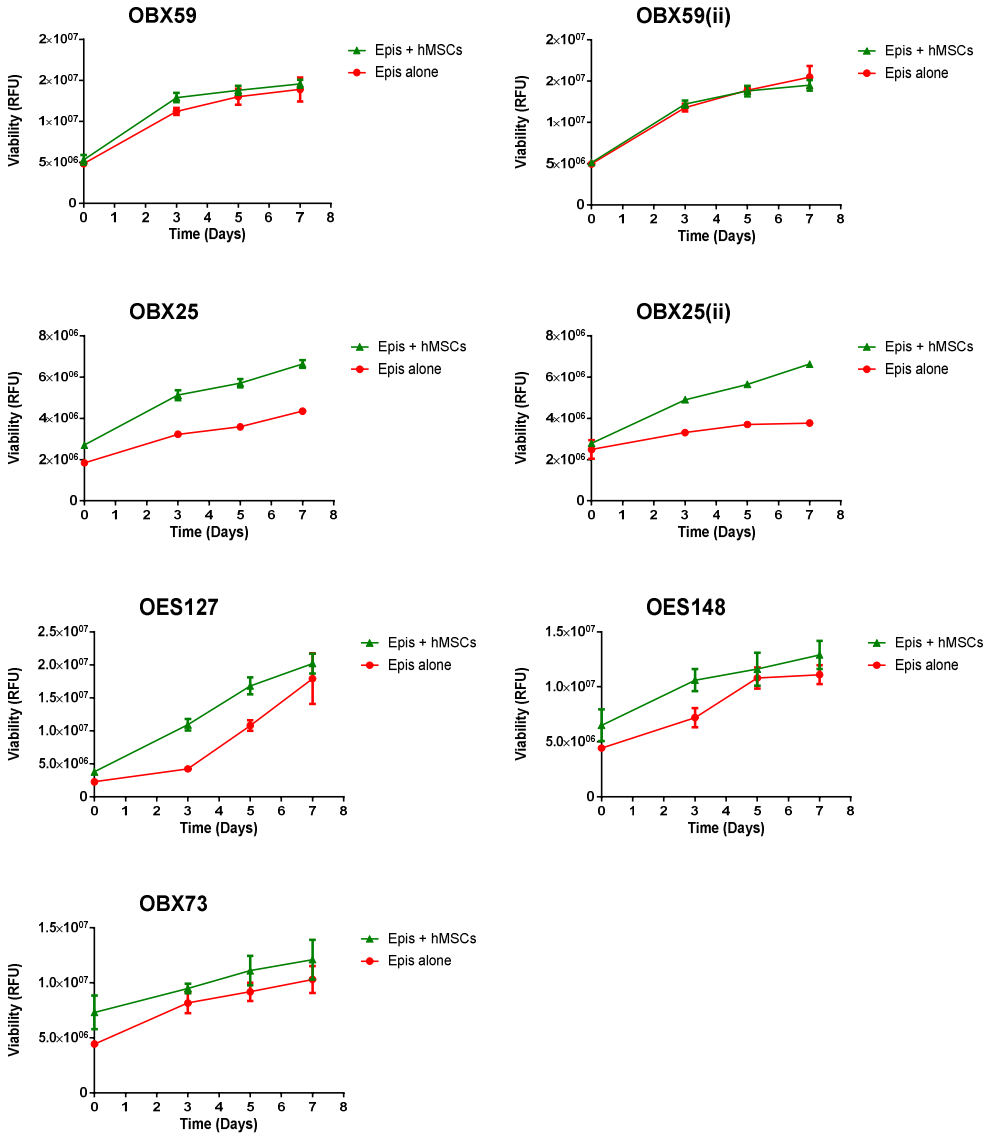


Figure 35. Growth in the 3D-TGA

OG tumour cells were seeded in 3D-TGA with and without hMSCs. Growth of close-to-patient cells was determined in 3D-TGA over the 7 day assay using the alamarBlue assay. **(A)** Progressive growth of tumour cells was monitored in 6 replicate wells immediately after establishment in 3D (day 0) and on days 3, 5 and 7.

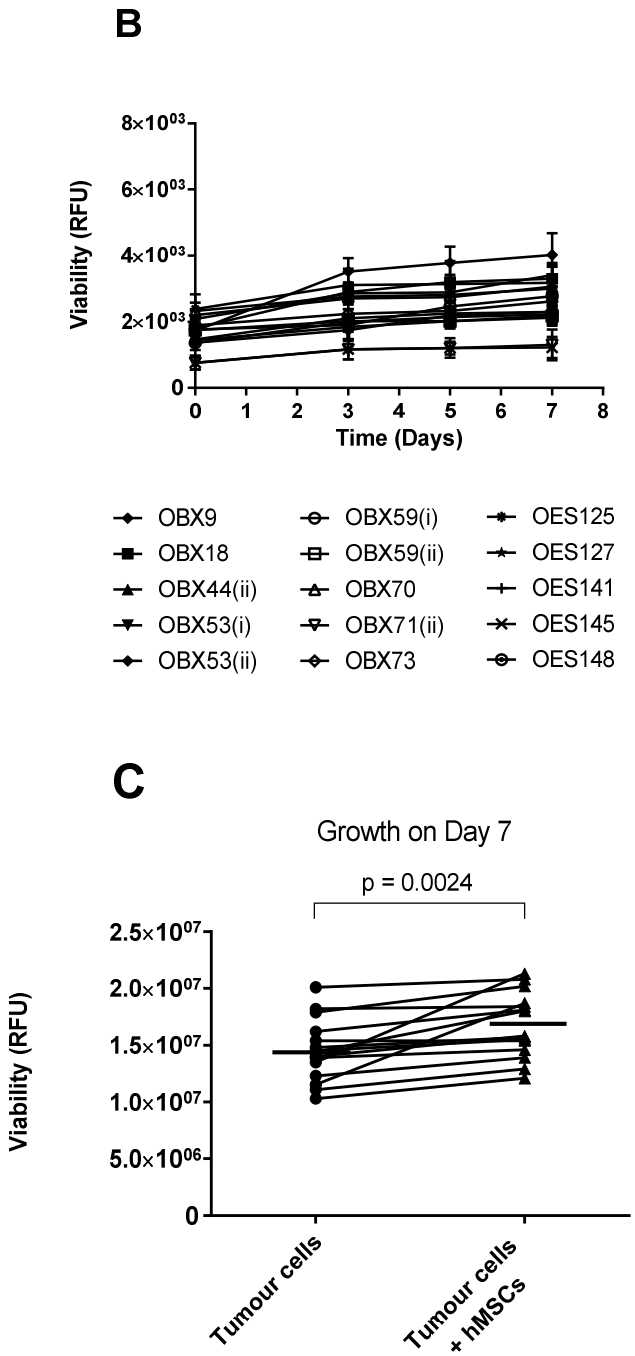


Figure 35. Growth in the 3D-TGA (continued)

(B) Growth of the mCherry-labelled hMSC stromal component of the 3D-TGA was measured independently from the epithelial cancer cluster growth, using the mCherry fluorescent signal. **(C)** The day 7 mean peak values from the growth curves were plotted in pairs, demonstrating a small but significant increase in growth in the models that incorporate mesenchymal support.

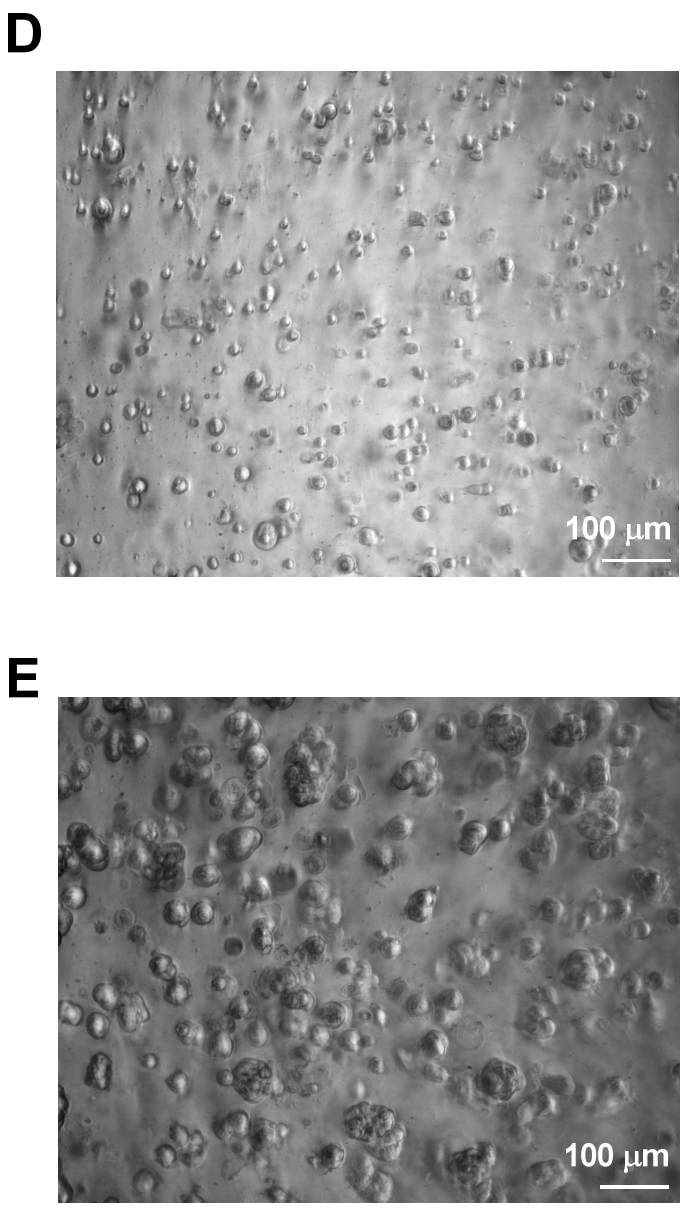


Figure 35. Growth in the 3D-TGA (continued)

(D, E) 3D cultures of live cells were imaged by wide-field microscopy with DIC at day 0 (D) and day 7 (E). Images are extended depth of field projection of multiple z-stacks taken of Oes141.

5.2.4 Application of chemotherapeutic drugs to the 3D-TGA and evaluation of sensitivity and resistance

The chemotherapy drugs Epirubicin, Cisplatin and 5-Fluorouracil were added to the 3D-TGA OG cancer clusters as monotherapy, doublet combinations, and as the triplet ECF combination which is administered clinically. This allowed evaluation of the efficacy of the individual drugs, their combinations, and the contribution of the individual drugs to the overall ECF chemotherapeutic effect.

An example patient OG cancer (OBX 18) is shown undergoing chemotherapeutic evaluation in the 3D-TGA. When the 3D-TGA was used to assess chemo-sensitivity, dose-dependent responses were observed (Figure 36A,B,C). Monotherapy with Epirubicin and Cisplatin provide a more progressive chemotherapeutic dose-response to increasing concentrations with a higher slope factor, whereas fluorouracil demonstrates a more linear relationship, with a lower slope factor. The steeper Hill-slope (for Epirubicin and Cisplatin) would suggest that these drugs are more potent (393), with corresponding individual drug mean IC_{50} values for Epirubicin, Cisplatin and 5-fluorouracil of 27.8, 27.9 and 67.7 respectively. The dose-response curve changes slightly with dual therapy administration, and shows a graphical profile encompassing both the steeper and shallower dose-response relationships, suggesting that both drugs are exerting a chemotoxic effect on the cells, and this is in line with the increased chemo-toxicity displayed by dual therapy (Figure 36D,E,F). Triple drug therapy with Epirubicin, Cisplatin and Fluorouracil in combination demonstrates a standard dose-response relationship, with a classical Hill slope (Figure 36G). These dose response curve shapes were replicated to a greater and lesser extent across all the OG cancer clusters evaluated in

the 3D TGA, suggesting that the mode of drug action in combination is similar.

By comparing the point at which IC_{50} is reached for each drug with the mean peak serum concentration at which the drug is administered clinically, it can be seen that when administered as monotherapy this OG cancer was resistant to all three drugs individually (Figure 36A,B,C). However, when administered as dual and then triple drug therapy a profile of potential sensitivity to this chemotherapy regimen emerges, which is modified by tumour cell co-culture. The individual patient cancer IC_{50}s and associated confidence intervals were calculated for all patients and drug combinations, and displayed a wide variation between different patients. These variations and comparisons are examined and reported in the following results.

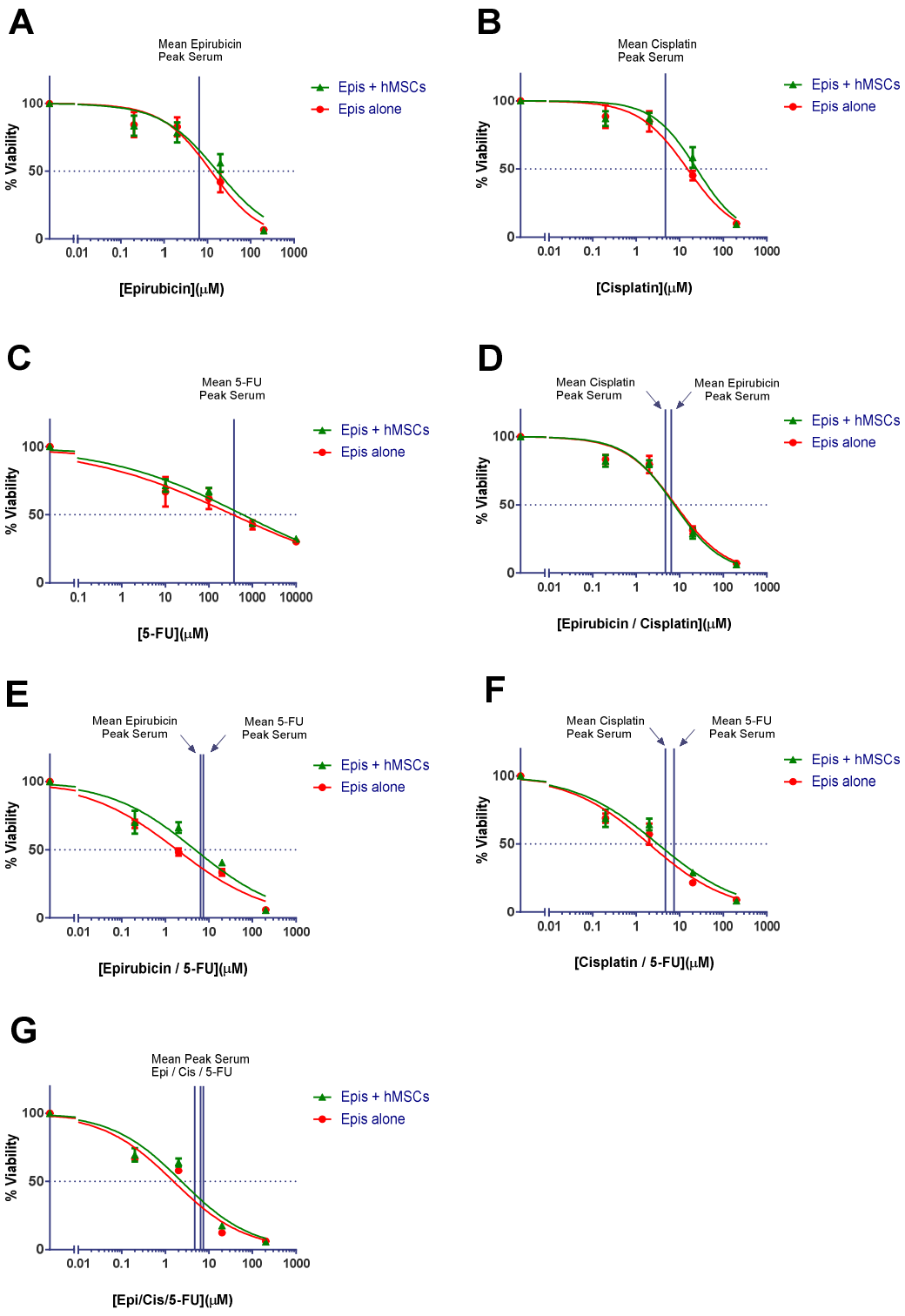

A
Mean Epirubicin Peak Serum
Epis + hMSCs
Epis alone
% Viability
100
50
0
0.01
0.1
1
10
100
1000
[Epirubicin](μM)
B
Mean Cisplatin Peak Serum
Epis + hMSCs
Epis alone
% Viability
[Cisplatin](μM)
C
Mean 5-FU Peak Serum
Epis + hMSCs
Epis alone
% Viability
0.1
1
10
100
1000
10000
[5-FU](μM)
D
Mean Cisplatin Peak Serum
Mean Epirubicin Peak Serum
Epis + hMSCs
Epis alone
% Viability
[Epirubicin / Cisplatin](μM)
E
Mean Epirubicin Peak Serum
Mean 5-FU Peak Serum
Epis + hMSCs
Epis alone
% Viability
[Epirubicin / 5-FU](μM)
F
Mean Cisplatin Peak Serum
Mean 5-FU Peak Serum
Epis + hMSCs
Epis alone
% Viability
[Cisplatin / 5-FU](μM)
G
Mean Peak Serum Epi / Cis / 5-FU
Epis + hMSCs
Epis alone
% Viability
[Epi/Cis/5-FU](μM)

Figure 36. Evaluation of individual patient OG cancer 3D-TGA chemotherapeutic sensitivity

Chemo-sensitivity of OBX18 close-to-patient cancer cell clusters was determined in 3D-TGA, in 6 replicate wells, after 4 day exposure to drug combinations at a range of concentrations, using the alamarBlue assay to measure viability. Viability curves were generated and IC_{50} values calculated using GraphPad Prism. Error bars represent one standard deviation. **(A, B, C) Monotherapy.** Viability curve for Epirubicin, Cisplatin and 5FU monotherapy respectively. The horizontal broken line indicates the IC_{50}, and the vertical line represents the mean peak serum concentration in patients. **(D, E, F) Dual therapy.** Viability curves for the dual combinations of all three drugs: Epirubicin, Cisplatin and 5FU monotherapy. The horizontal broken line indicates the IC_{50}, and the vertical line represents the mean peak serum concentration in patients. **(G) Triplet combination therapy.** Viability curve for all three drugs (Epirubicin, Cisplatin and 5FU) administered together. Again, he horizontal broken line indicates the IC_{50}, and the vertical line represents the mean peak serum concentration in patients.

5.2.5 Single drug and combination chemo-toxicity profiles for the patient cohort

Each individual patient's monotherapy, dual combination therapy and triple drug chemo-toxicity IC_{50} profiles, with and without hMSC co-culture were compiled (Figure 37).

This allows comparison of individual patient's cancers particular chemotherapeutic sensitivities and variation across the cohort as is seen with different clinical responses to chemotherapy.

Also, by examining each drug individually, and their combinations in the 3D-TGA, it is possible to put together a more comprehensive picture of drug efficacy, including their individual contribution to the overall effect of the ECF regimen.

Patient ID	Sample ID	Epirubicin		Cisplatin		5-Fluorouracil		Epi/Cis		Epi/5-FU		Cis/5-FU		ECF		TRG	Panobinostat + ECF	
hMSCs		-	+	-	+	-	+	-	+	-	+	-	+	-	+		-	+
Oes1B	OBX70	9.1	8.6	14.3	26.7	12.4	34.0	3.8	4.1	1.6	2.8	1.7	2.4	1.5	1.9	1	1.4	1.3
Oes2B	OBX71(ii)	9.9	32.4	7.0	31.8	6.0	12.9	4.8	11.4	2.9	9.5	1.7	9.1	1.7	3.4	3	0.4	2.3
Oes3B	OBX18	12.2	17.0	15.1	24.6	7.1	12.1	8.0	7.5	1.8	4.8	2.0	3.2	1.5	2.4	3	1.2	2.2
Oes4B	OBX9	33.7	22.6	37.5	35.8	14.7	25.2	9.3	5.9	7.6	12.5	5.0	5.9	4.6	5.2	4	4.4	3
Oes4R	OES125	47.1	38.4	39.7	43.0	14.4	27.2	26.8	20.3	4.4	7.6	3.7	6.0	3.4	5.0		4.3	3.8
Oes5B(i)	OBX53	14.9	18.3	19.3	26.5	7.8	32.6	5.2	6.8	3.6	7.0	2.6	5.5	1.8	5.1	4	1.5	2.1
Oes5B(ii)	OBX53(ii)	24.6	25.2	8.5	12.9	9.6	13.1	5.2	5.8	3.5	5.1	2.5	5.1	2.5	5.0		1.6	3.5
Oes5R	OES141	47.8	61.0	39.9	37.0	31.4	122.4	24.2	19.5	13.6	32.1	4.4	8.1	5.3	6.1		4.5	5.3
Oes6B(i)	OBX59	38.3	37.8	37.8	50.0	9.6	75.5	26.2	35.2	6.9	12.2	3.0	7.9	3.5	6.9	4	3.8	4.7
Oes6B(ii)	OBX59(ii)	41.3	50.1	28.2	33.0	11.7	54.4	6.7	7.4	5.6	11.3	3.1	5.6	3.2	5.6		3.3	4.8
Oes6R	OES145	33.7	36.7	43.6	37.9	931.0	638.6	14.6	10.9	12.7	12.1	10.2	8.1	4.7	4.9		3.8	3.7
Oes7B(i)	OBX25	12.0	12.9	9.7	15.8	11.0	23.4	4.9	5.2	2.6	5.0	2.2	6.0	2.3	5.2	5	1.8	3.3
Oes7B(ii)	OBX25(ii)	15.2	15.4	13.0	18.5	24.3	32.7	6.3	6.0	3.5	7.9	3.2	7.2	2.0	5.8			
Oes7R	OES127	17.6	15.9	9.0	12.5	6.4	65.6	7.0	13.0	5.3	7.4	5.1	6.8	4.1	6.0		3.3	4.9
Oes8B	OBX73	40.2	41.9	57.4	60.6	25.2	65.1	22.8	35.5	16.2	32.3	10.6	25.1	6.0	13.8	5	3.6	5.9
Oes8R	OES148	39.4	37.3	47.8	55.0	17.2	40.8	16.7	31.9	11.1	20.5	8.0	17.3	3.5	10.0		2.8	4.8
Oes9B	OBX44(ii)	35.2	45.6	47.3	60.1	11.4	96.5	36.1	40.7	4.7	22.6	6.7	10.0	7.9	10.1	4		

Figure 37. Panel of Response to Chemotherapy Agents

Each individual patient's cancer cells were grown in the 3D-TGA with (+) or without (-) the presence of hMSCs, and then underwent pharmacological assessment, to obtain individual patient 3D-TGA IC_{50}s, for mono and combination chemotherapy. The patient cancer cell clusters were classified as sensitive (green), borderline (orange), or resistant (red) by comparison of IC_{50} values to mean peak serum concentrations achieved in patients at the doses used in UK clinical practice.

5.2.6 Drug efficacy increases in combination

Individual drugs at the concentrations delivered to patients were never effective (Figure 37). Chemotherapy efficacy increased in combination, with mean IC_{50} values of Epirubicin/Cisplatin and Epirubicin/Fluorouracil of 15.7 and 12.5 respectively. The most effective drug doublet was Cisplatin/5-Fluorouracil, with a mean IC_{50} of 8.2, and thus it would seem that doublet chemotherapy combinations with Epirubicin are less effective. For triplet chemotherapy, further addition of Epirubicin to the Cisplatin/Fluorouracil (CF) doublet provided an overall marginal gain, with a mean IC_{50} of 6.0; 1.4-fold lower for the ECF triplet than the CF doublet ($p<0.05$) (Figure 38).

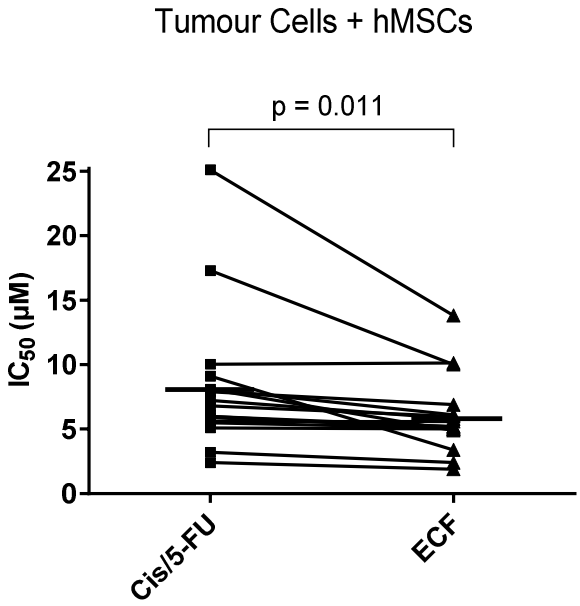


Figure 38. Sensitivity to Cisplatin/5-FU doublet compared to ECF triplet chemotherapy.

Chemo-sensitivity of close-to-patient cancer cell clusters was determined in 3D-TGA, to doublet and triplet drug combinations at a range of concentrations, using the alamarBlue assay to measure viability. IC_{50} values from viability curves were calculated using GraphPad Prism.

5.2.7 Effect of hMSCs on drug sensitivity

The 3D-TGA model demonstrates significantly higher chemo-resistance in the models incorporating mesenchymal support in a drug and patient dependent manner (Figure 37).

Using the clinical combination of ECF, sensitivity to chemotherapy agents was significantly reduced when mesenchymal cells were incorporated into the assay ($p = 0.0001$) (Figure 39).

When the drugs were examined individually, this co-culture induced chemo-resistance was not observed with Epirubicin monotherapy, and co-culture induced resistance greatest with Fluorouracil. The effect of co-culture on chemo-resistance became more pronounced when doublet and then triplet chemotherapy was administered (Figure 40). The significance of the magnitude of mesenchymal induced chemo-resistance increases and is maximal with the triplet combination chemotherapy.

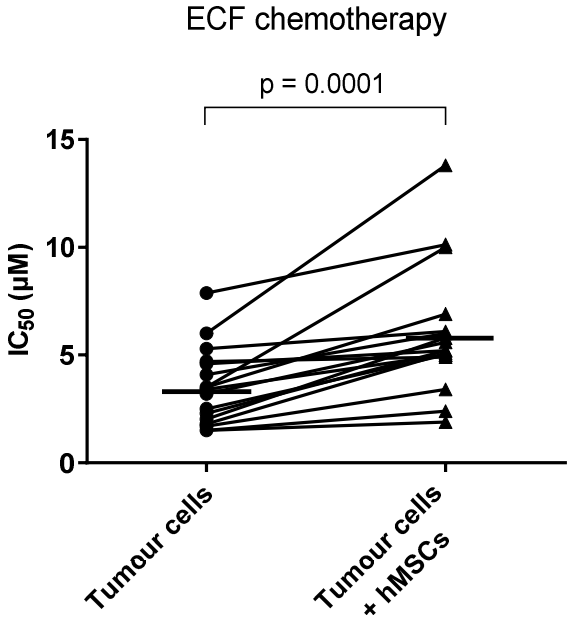


Figure 39. Sensitivity to ECF chemotherapy in the presence and absence of hMSCs

Chemo-sensitivity of close-to-patient cancer cell clusters was determined in 3D-TGA with and without hMSC co-culture, to the ECF drug combination at a range of concentrations, using the alamarBlue assay to measure viability. IC_{50} values from viability curves were calculated using GraphPad Prism. Horizontal lines represent mean IC_{50}s for each group.

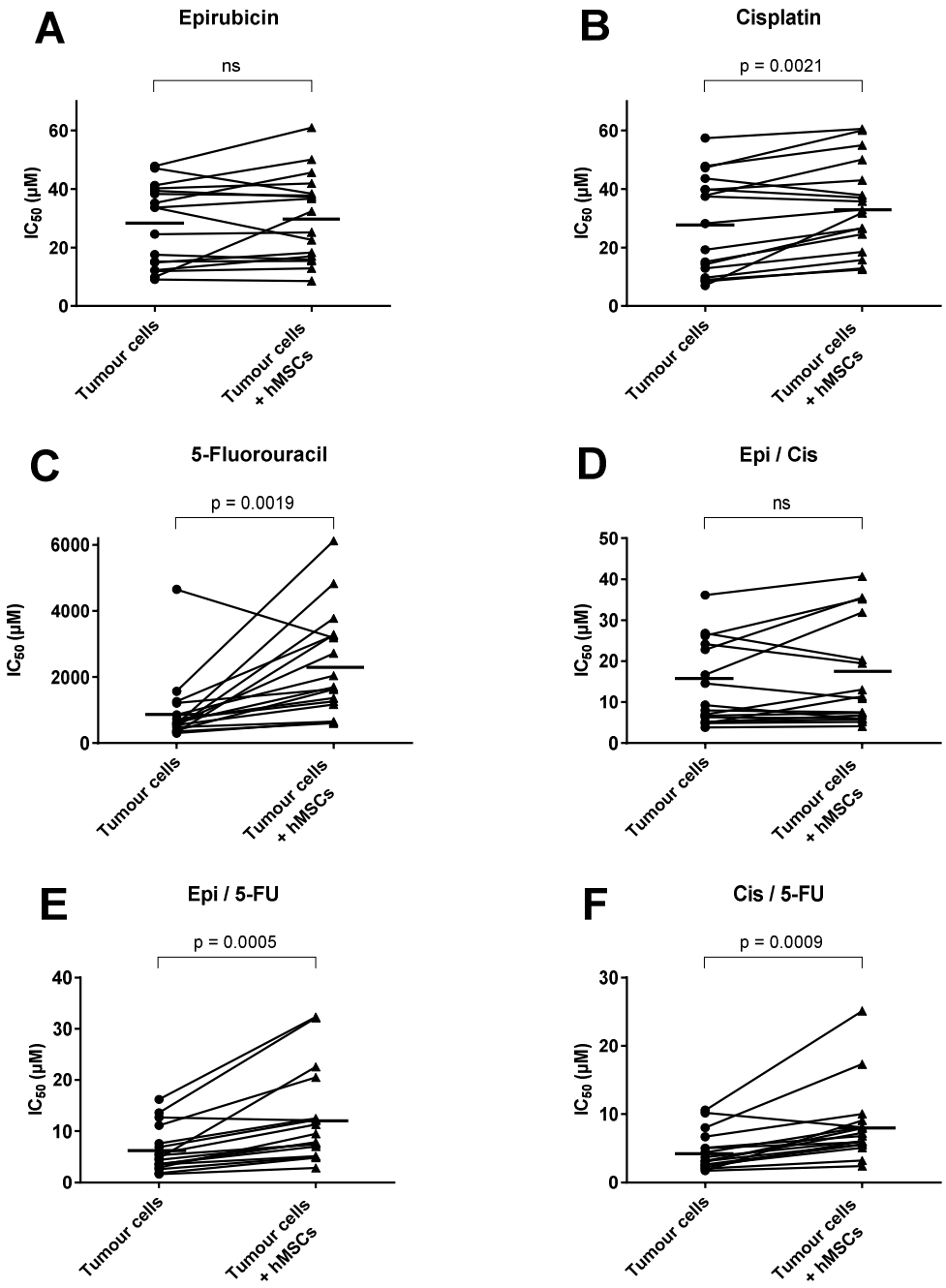


Figure 40. Influence of mesenchymal co-culture upon chemo-toxicity for individual and drug combinations

Sensitivity of close-to-patient cells was determined in 3D-TGA, after 4 day exposure to drug combinations at a range of concentrations, using the alamarBlue assay to measure viability. Viability curves were generated and IC_{50} values plotted using GraphPad Prism. Sensitivity to the SOC chemotherapy drugs alone (**A, B, C**), and their doublet combinations (**D, E, F**) was observed for cancer cells grown with and without co-culture with mesenchymal support.

5.2.8 The 3D-TGA using close-to-patient cells with mesenchymal cell co-culture accurately models clinical chemo-sensitivity

To investigate whether the *ex vivo* finding reflected the clinical chemotherapy response, correlation between the IC_{50}s of the individual patient cells grown in the 3D-TGA were compared with the patient's TRG (Figure 37).

When mesenchymal support was present, 100% (n=14) of the TRG 4-5 cancers had IC_{50}s higher than the mean peak serum threshold, and 100% (n=3) of the TRG 1-3 cancers had IC_{50}s lower than the mean peak serum threshold (Figure 41).

This prediction of chemotherapy response was only observed when mesenchymal cells were added to the model. Without mesenchymal cells incorporated in the 3D-TGA, the assay had no predictive value: although all of the TRG 1-3 cancer IC_{50}s remained lower than the mean peak serum with a positive predictive value and specificity of 100%, only 18% (n=3) of the TRG 4-5 cancers had IC_{50}s higher than the mean peak serum threshold, resulting in a negative predictive value of 23% and sensitivity of 17%.

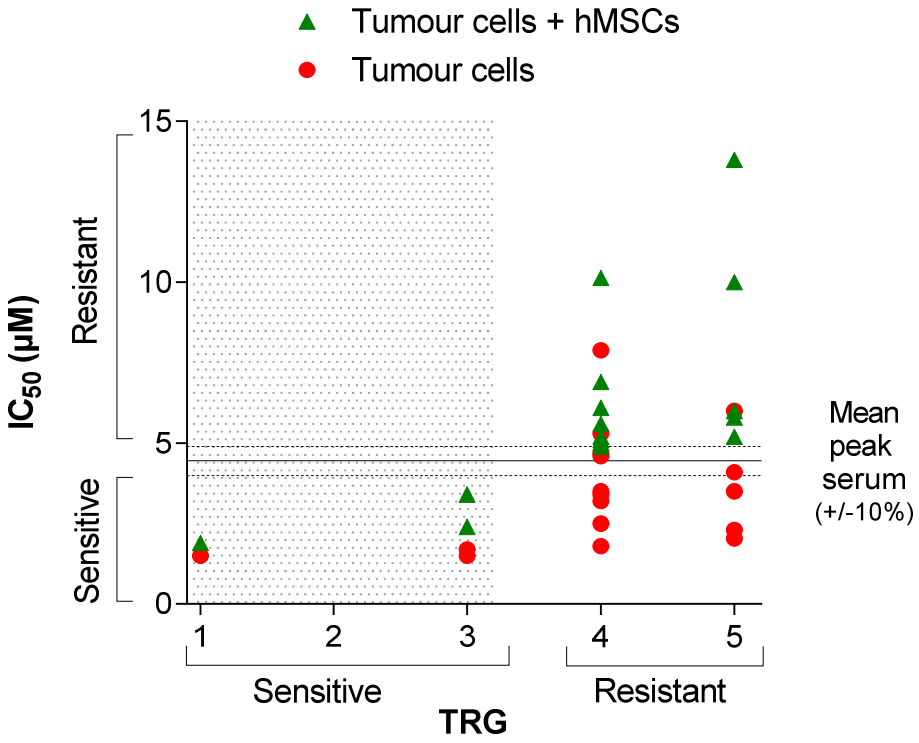


Figure 41. The *ex vivo* 3D-TGA co-culture chemotherapy response correlates accurately with the histopathological chemotherapy response for individual patients

Chemo-sensitivity of close-to-patient cancer cell clusters was determined in 3D-TGA, to ECF chemotherapy, at a range of concentrations, using the alamarBlue assay to measure viability. The Predicted chemo-sensitivity based on 3D-TGA IC_{50} measurement of ECF treatment is compared with the clinical response as reported by the TRG. The 3D-TGA IC_{50} data points, above the mean peak serum delivered to patients, are designated as resistant to chemotherapy. Data points that lie within 10% of the mean peak serum are defined as borderline.

5.2.9 Chemo-sensitivity was unchanged pre and post neoadjuvant chemotherapy

The *ex vivo* chemo-sensitivity of OG cancer samples obtained pre and post neoadjuvant chemotherapy was compared. The patients with matched samples obtained pre- (chemo-naïve) and post- (chemo-exposed) neoadjuvant chemotherapy were all from patients (n=5) with TRG 4-5 cancers, with remnant tumour bulk at surgical resection. Analysis showed no significant difference in IC_{50} chemo-sensitivity in the 3D-TGA, before or after neoadjuvant chemotherapy, whether they were grown with or without mesenchymal support (Figure 42).

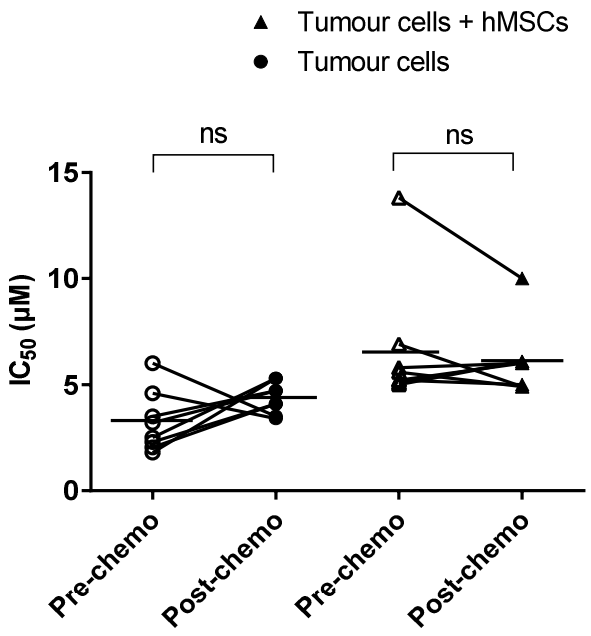


Figure 42. OG cancer chemosensitivity pre and post neoadjuvant chemotherapy is unchanged, whether modelled with or without hMSCs.

Chemo-sensitivity of close-to-patient cancer cell clusters was determined in 3D-TGA, to ECF chemotherapy at a range of concentrations, using the alamarBlue assay to measure viability. Sensitivity pre- and post-neoadjuvant chemotherapy is compared, in 3D-TGA models with or without hMSCs. IC_{50} values from viability curves were calculated using GraphPad Prism.

5.2.10 The novel HDACi Panobinostat provides enhanced chemo-sensitivity

The novel emerging HDACi Panobinostat was also assessed to evaluate the 3D-TGA as a potential platform for appraisal of new drugs, and examine whether HDACi could be effective against oesophagogastric carcinoma.

Panobinostat as a monotherapy was an effective chemotherapeutic *in vitro*, with a very small but significantly increase in chemo-resistance ($p<0.05$) exerted by mesenchymal co-culture (Figure 43A). When Panobinostat was combined with the SOC triplet ECF chemotherapy (Figure 43B), mesenchymal co-culture again provided a significantly increased chemo-resistance ($p<0.005$). However, this increase in chemo-resistance was less pronounced than that seen with the conventional ECF chemotherapy alone. Examples of individual patient cell line chemosensitivity dose-response to the conditions is shown below the overall results (Figure 43C,D,E,F). Patient lines chosen specifically to demonstrate those with and without a marked response to the mesenchymal co-culture.

The addition of Panobinostat to the ECF triplet when tumour cells were cultured alone was modest (Figure 44A); however, in co-culture this resulted in significantly enhanced drug efficacy ($p<0.005$), with the mean IC_{50} of ECF chemotherapy dropping from 6.02 to 3.70 (Figure 44B). Again, examples of individual patient cell lines dose-response is shown, and again demonstrates the variation in chemotherapeutic response to the same regimen by different patient's cell lines (Figure 44C,D,E,F). Whilst the results visually would suggest that there may be a synergistic (rather than additive) effect occurring between the Panobinostat and potentially the epirubicin from the ECF chemotherapy, this would need to be examined arithmetically

using the chou-talalay method, for which there is not enough data available at this juncture.

Of the 5 patients (12 samples) that were ECF-resistant, only 2 samples remained resistant when subjected to ECF + Panobinostat in combination (Figure 37). And, despite the increase in chemo-resistance seen by mesenchymal co-culture, the IC_{50}s for the individual patient cancers remained within achievable serum concentrations and were thus still classified as potentially chemotherapy sensitive (Figure 37). Therefore, despite co-culture induced increased chemo-resistance, in combination with ECF chemotherapy Panobinostat provides enhanced chemo-sensitivity.

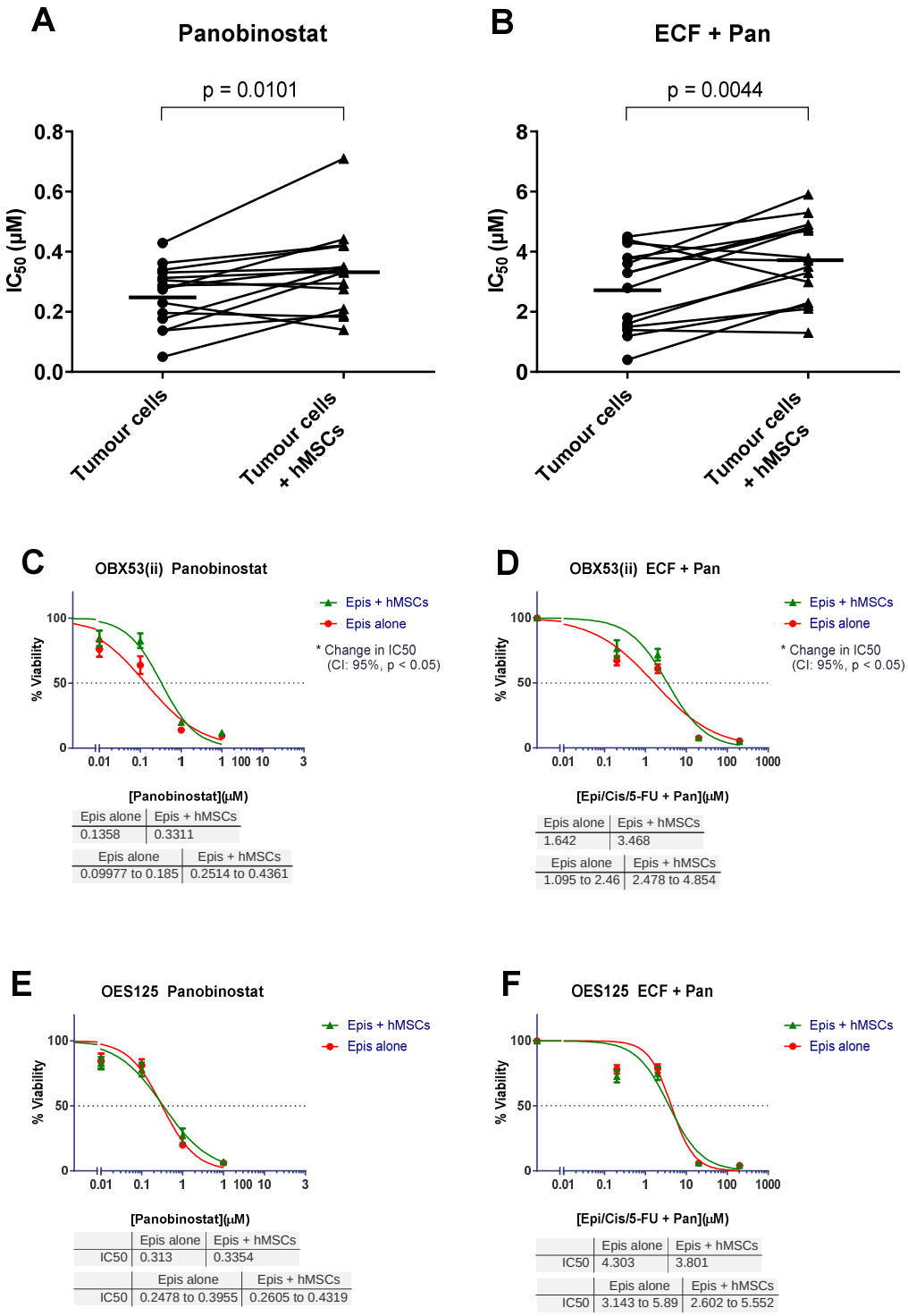


Figure 43. Combining ECF chemotherapy with Panobinostat provides enhanced chemo-sensitivity: Examination of the effect of stromal cell co-culture

Sensitivity of close-to-patient cells was determined in 3D-TGA, with and without mesenchymal cell co-culture, after 4 day exposure to ECF and Panobinostat drug combinations. Viability curves were generated

and IC_{50} values determined using GraphPad Prism. Horizontal lines represent mean IC_{50}s.

Overall sensitivity of all of the patient cell lines to Panobinostat alone (**A**) and in combination with standard of care ECF chemotherapy (**B**) was determined for assays with and without mesenchymal cell co-culture. Statistical significance calculated using paired t-test.

Examples of the individual patient cell lines different responses contributing to the reported overall effect of the chemotherapeutic conditions are shown. OBX53(ii) demonstrates a significant change in chemosensitivity to Panobinostat alone (**C**) or in combination with ECX (**D**) when co-cultured with or without hMSCs, whereas OES125 does not demonstrate any change in chemosensitivity (**E**) and (**F**) to either of these drug combinations by additional hMSC co-culture.

Statistical significance is determined by the arithmetic variance between the calculated IC_{50}s and their distinct 95% confidence intervals which have no overlap.

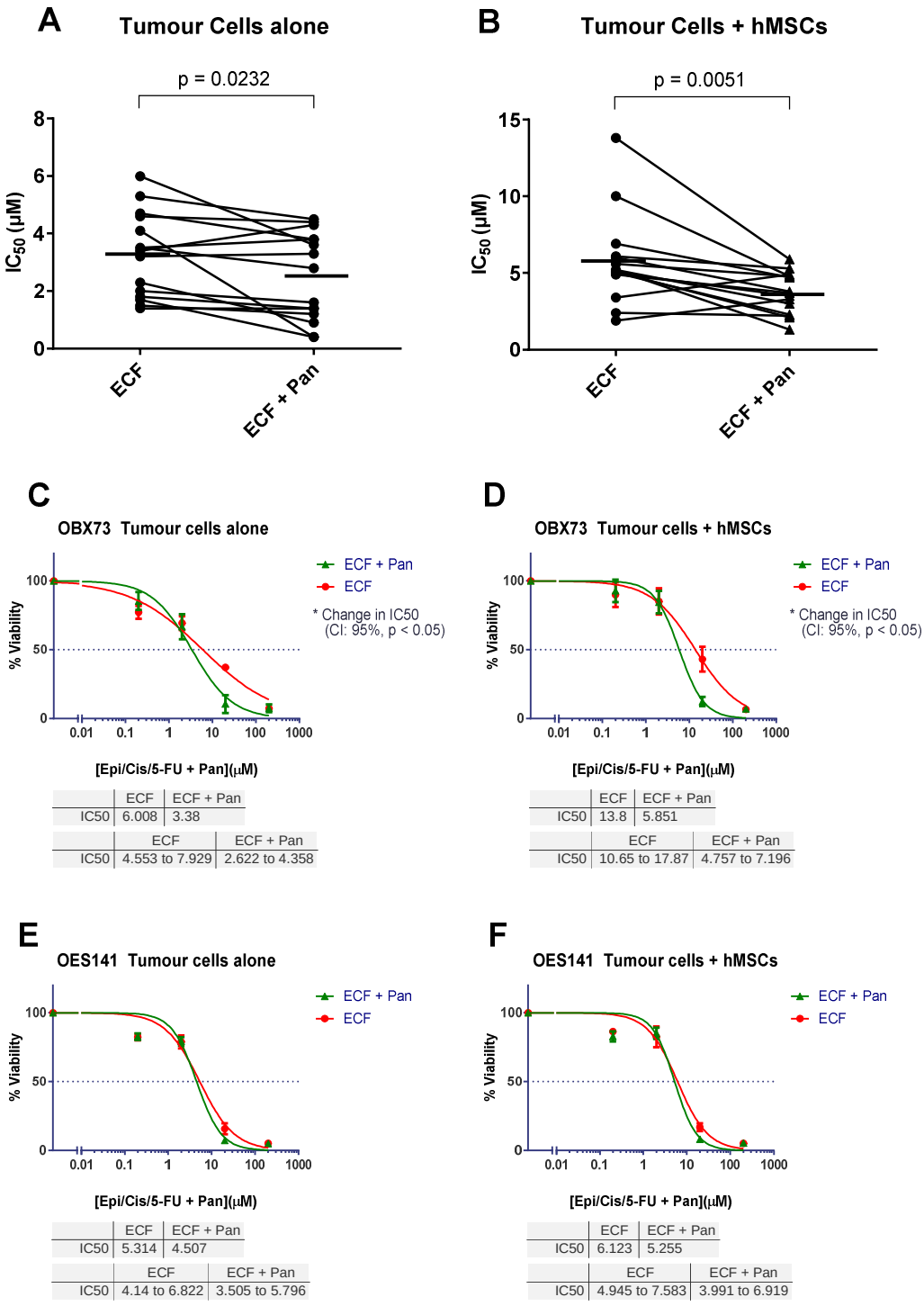


Figure 44. Combining ECF chemotherapy with Panobinostat provides enhanced chemo-sensitivity: Examination of the effect of ECF combination with Panobinostat

Sensitivity of close-to-patient cells was determined in 3D-TGA, with and without mesenchymal cell co-culture, after 4 day exposure to ECF and Panobinostat drug combinations. Viability curves were generated

and IC_{50} values determined using GraphPad Prism. Horizontal lines represent mean IC_{50}s.

Overall sensitivity of all of the patient cell lines either cultured as Tumour cells alone (**A**) or Tumour cells co-cultured with hMSCs (**B**) was determined for assays with and without the addition of Panobinostat to SOC ECF chemotherapy. Statistical significance calculated using paired t-test.

Examples of the individual patient cell lines different responses contributing to the reported overall effect of the chemotherapeutic conditions are shown. OBX73 demonstrates a significant change in chemosensitivity to ECF when exposed to additional Panobinostat whether tumour cells are cultured alone (**C**) or with hMSCs (**D**), whereas OES141 does not demonstrate a significant change in chemosensitivity with (**E**) or without co-culture (**F**) when exposed to additional Panobinostat.

Statistical significance is determined by the arithmetic variance between the calculated IC_{50}s and their distinct 95% confidence intervals which have no overlap.

5.2.11 Administration of PDE5i drugs alone exhibit no chemotoxic effect

The PDE5i drug Vardenafil was evaluated in combination with ECF therapy, in models both with and without hMSCs. PDE5i drugs have been reported to interfere with the function of the stromal component of the TME. Vardenafil specifically has been shown to prevent the activation of fibroblasts into α-SMA-positive cancer associated fibroblasts (CAFs) *in vitro* (291). Given the significant increase in chemo-resistance demonstrated in the 3D-TGA by co-culture with stromal cells, I hypothesised that the addition of the PDE5i drug Vardenafil may prevent activation of the hMSCs into activated CAF-like stromal cells within the assay, and thus may affect the interaction between the epithelial cells and stromal component of the 3D-TGA and potentially disrupt the co-culture induced chemo-resistance currently demonstrated.

9 patients with a total of 17 evaluable samples underwent global drug screening with the ECF SOC, of which 8 of these patients with 15 samples were also evaluated with addition of the PDE5i to the ECF chemotherapy regimen.

When the 3D-TGA models of OAC were exposed to PDE5i alone, there was no chemo-toxic effect seen in any of the 15 models, either when co-cultured with or without hMSC stromal support. A direct comparison of any change in growth with or without co-culture, following exposure to even extreme concentrations of PDE5i was not feasible, as recording an IC_{50} (or an IC_{75}) was not possible with the lack of observed toxicity from the drug (Figure 45A). When hMSCs were grown alone in the 3D-TGA without epithelial cancer cells and similarly exposed to the PDE5i Vardenafil, again no toxic effect was observed (Figure 45B).

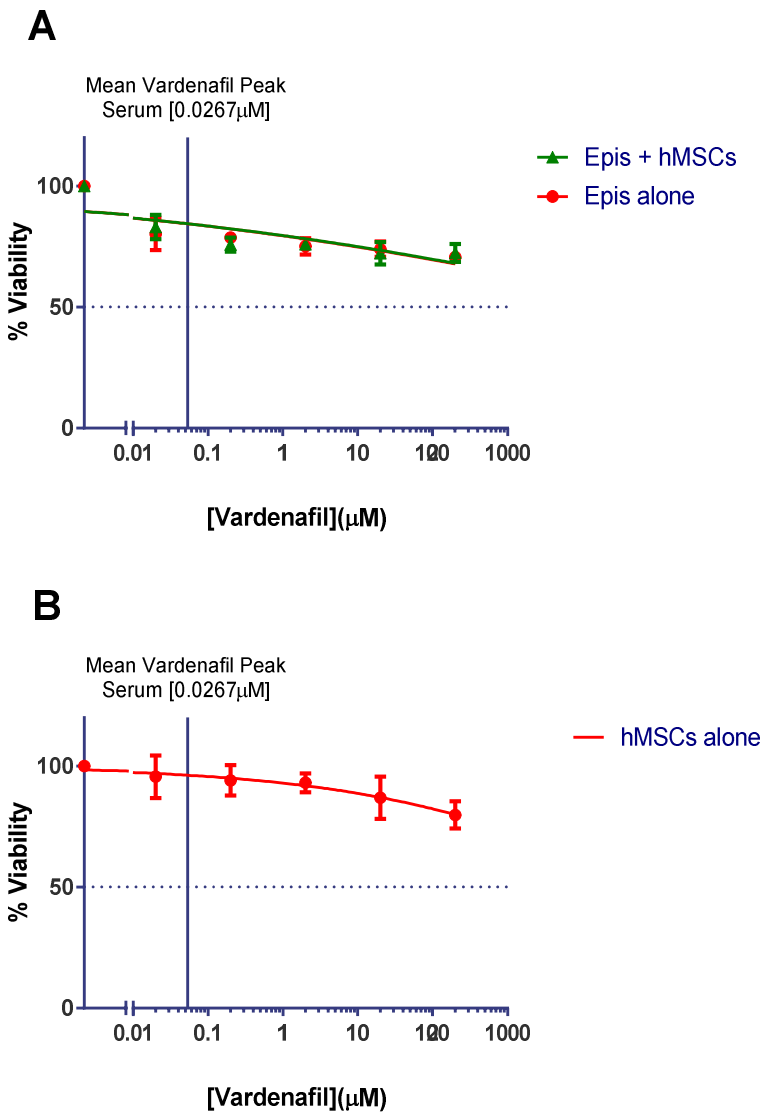


Figure 45. Cells grown in the 3D-TGA do not demonstrate chemo-toxicity upon exposure to increasing concentrations of the PDE5i Vardenafil

The chemo-sensitivity of OBX18 cancer cell clusters to Vardenafil was determined in 3D-TGA, in 6 replicate wells, after 4 day exposure to drug combinations at a range of concentrations, with and without hMSC co-culture using the alamarBlue assay to measure viability. Viability curves were generated and IC_{50} values calculated using GraphPad Prism. Error bars represent one standard deviation. **(A)** OAC OBX18 epithelial cells are grown in the 3D-TGA with and without hMSC co-culture before exposure to increasing concentrations of Vardenafil. **(B)** hMSCs are grown without epithelial cancer cells in the 3D-TGA before exposure to increasing concentrations of Vardenafil.

5.2.12 Mesenchymal co-culture induced ECF chemotherapy resistance affected by the administration of the PDE5i Vardenafil

Two example patient's cancer cell lines are used to demonstrate the alternate effects of administration of the PDE5i Vardenafil upon mesenchymal co-culture induced ECF chemotherapy resistance (Figure 46 and 47).

The individual patient OG cancer OBX53(ii) demonstrated a significant mesenchymal co-culture-induced ECF chemotherapy resistance (Figure 46B) and so is used as an example to demonstrate the effect of addition of the PDE5i drug Vardenafil to the standard ECF chemotherapy. The PDE5i addition exhibits a chemo-toxic effect and reverses the previously exhibited stromal induced chemo-resistance (Figure 46C).

This additional chemotoxic effect from the PDE5i administration does not occur in the absence of stromal co-culture (Figure 46D) suggesting that the PDE5i drug is acting upon the stromal component of the 3D-TGA co-culture model.

This individual patient's cancer cells are resistant to treatment with conventional ECF chemotherapy clinically (with a TRG of 4) and also chemo-resistant in the 3D model with stromal co-culture, with an *ex vivo* an IC_{50} of 4.977 (Figure 46E). However, when the patient's co-cultured cancer is treated with the PDE5i drug Vardenafil in addition to the standard ECF chemotherapy, the cancer cells were found to be sensitive to the chemotherapy, at a clinically-relevant dose with an IC_{50} of 2.105 (Figure 46E).

In contrast, although the individual patient OG cancer OBX59(i) also demonstrates a significant mesenchymal co-culture induced ECF chemotherapy resistance (Figure 47B) the addition of PDE5i does not exhibits a chemo-toxic effect and continues to exhibit

stromal induced chemo-resistance (Figure 47C). Therefore when the OBX59(i) patient's epithelial cells are co-cultured with hMSCs, addition of PDE5i to the SOC ECX chemotherapy does not have any effect on chemo-sensitivity (Figure 47E), and the IC_{50} remains greater than the mean peak serum clinically administered to patients.

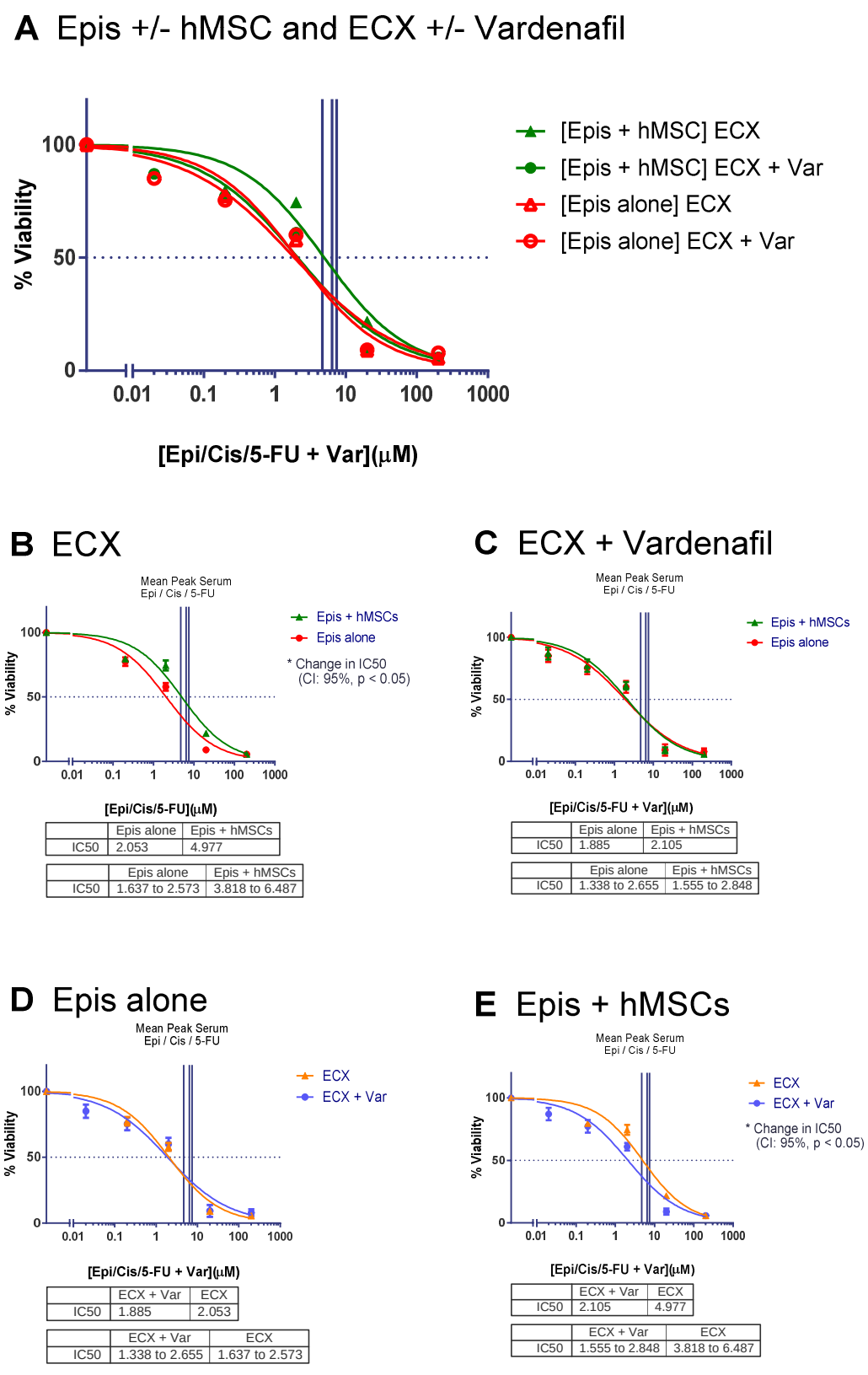


Figure 46. The alternate effects of PDE5i on close-to-patient cells demonstrating hMSC co-culture induced chemo-resistance to ECX chemotherapy: Addition of the PDE5i agent Vardenafil can increase chemo-sensitivity.

Close-to-patient OAC cells are cultured in the 3D-TGA with and without hMSC co-culture, before exposure to the standard of care chemotherapy agents Epirubicin, Cisplatin and Fluorouracil with and without the presence of the PDE5i drug Vardenafil.

(**A**) OBX53(ii) demonstrates dose-response to all chemotherapeutic conditions. **(B)** Resistance to ECX chemotherapy is significantly increased with hMSC co-culture. **(C)** Increased chemo-resistance with hMSC co-culture is no longer observed by the addition of PDE5i to ECX chemotherapy. **(D)** When epithelial cells are grown alone without hMSC co-culture, no change in chemotherapy sensitivity is seen by the addition of PDE5i to ECX chemotherapy. **(E)** When epithelial cells are co-cultured with hMSCs, addition of PDE5i to ECX chemotherapy results in a significant increase in chemo-sensitivity.

Statistical significance is determined by the arithmetic variance between the calculated IC_{50}s and their distinct 95% confidence intervals which have no overlap.

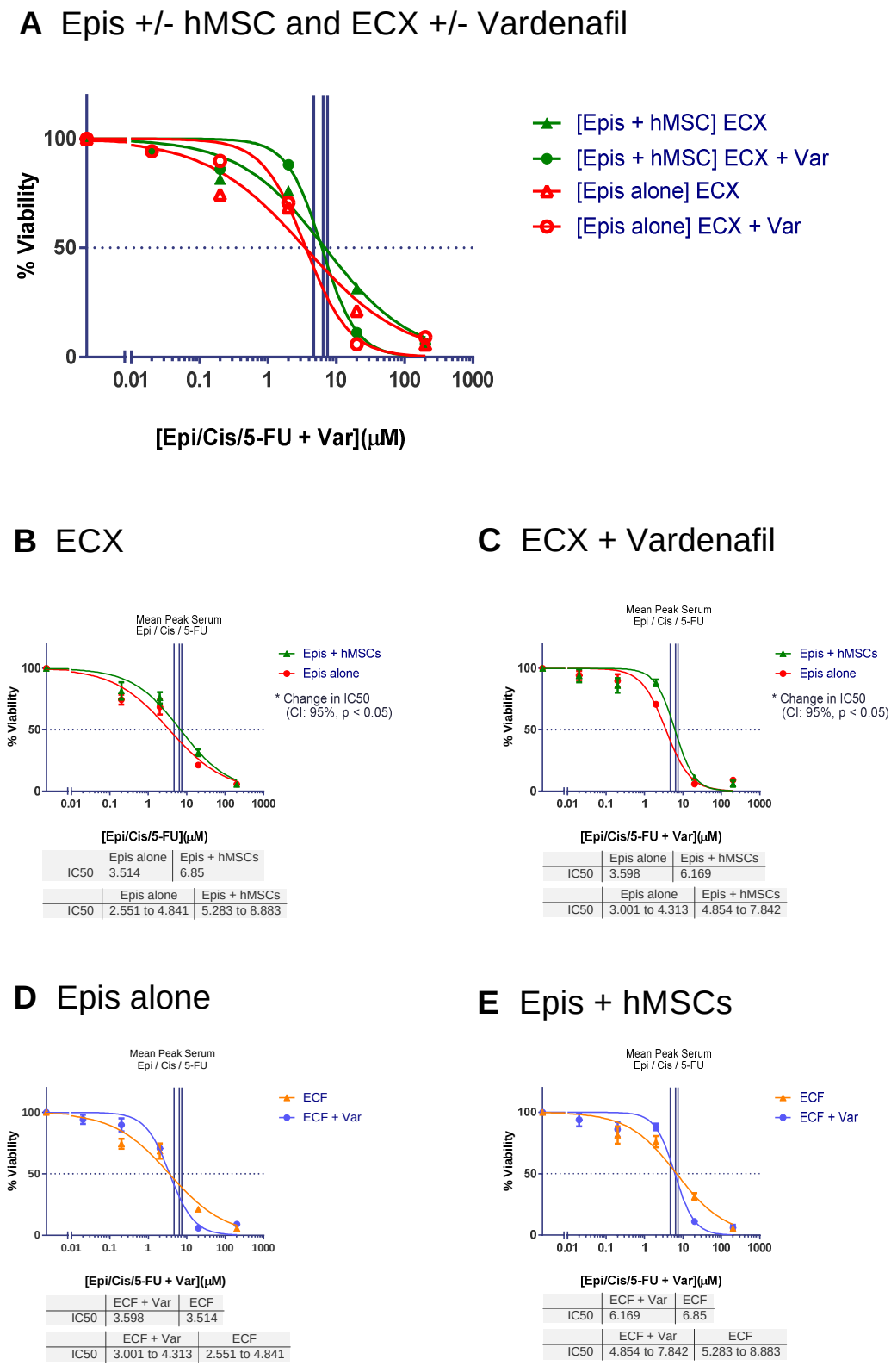


Figure 47. The alternate effects of PDE5i on close-to-patient cells demonstrating hMSC co-culture induced chemo-resistance to ECX chemotherapy: Addition of the PDE5i agent Vardenafil can have no effect upon chemo-sensitivity.

Close-to-patient OAC cells are cultured in the 3D-TGA with and without hMSC co-culture, before exposure to the standard of care chemotherapy agents Epirubicin, Cisplatin and Fluorouracil with and without the presence of the PDE5i drug Vardenafil.

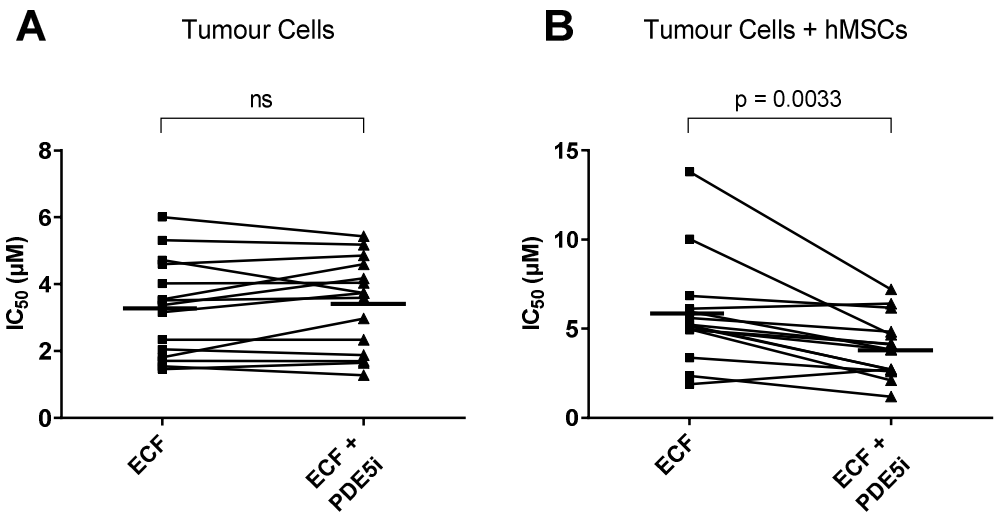
(**A**) OBX59(i) demonstrates dose-response to all chemotherapeutic conditions. **(B)** Resistance to ECX chemotherapy is significantly increased with hMSC co-culture. **(C)** Increased chemo-resistance with hMSC co-culture remains significant and is not affected by the addition of PDE5i to ECX chemotherapy. **(D)** When epithelial cells are grown alone without hMSC co-culture, no change in chemotherapy sensitivity is seen by the addition of PDE5i to ECX chemotherapy. **(E)** When epithelial cells are co-cultured with hMSCs, addition of PDE5i to ECX chemotherapy does not have any effect on chemo-sensitivity.

Statistical significance is determined by the arithmetic variance between the calculated IC_{50}s and their distinct 95% confidence intervals which have no overlap.

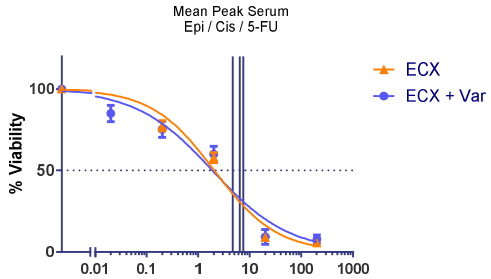
5.2.13 The addition of PDE5i to ECF chemotherapy overall increases chemo-sensitivity in the presence of stromal co-culture

When all of the patient's OG cancers were evaluated, addition of PDE5i to the SOC ECF regimen did not change the overall chemo-sensitivity in the 3D-TGA assay without hMSC stromal support (Figure 48A). However, when mesenchymal cells were incorporated into the assay, the addition of PDE5i provided an overall significant decrease ($p=0.0033$) in IC_{50} chemo-resistance (Figure 48B). Examples of individual patient cell line chemosensitivity dose-response to the conditions is shown below the overall results and demonstrates that the effect exerted by the PDE5i was patient specific (Figure 48D & F), with these patient lines chosen specifically to best demonstrate the alternate effects seen.

The addition of PDE5i to ECF chemotherapy overall reduced the effect of hMSC co-culture induced chemo-resistance (Figure 49A and B), but this change was marginal ($p=0.036$), with patient specific variations in the magnitude of the IC_{50} change, which did not fully negate the chemoresistant effect of hMSC co-culture. Examples of individual patient cell line chemosensitivity dose-response to the conditions is shown below the overall results and demonstrates that the effect exerted by the PDE5i was patient specific, with a marked (Figure 49D), partial (Figure 49F) or absent (Figure 49H) reduction in chemo-resistance. These 3 patient lines were chosen specifically to best demonstrate the variable effects seen in comparison to their similar hMSC co-culture induced chemo-resistance profiles (Figure 49C,E,F).



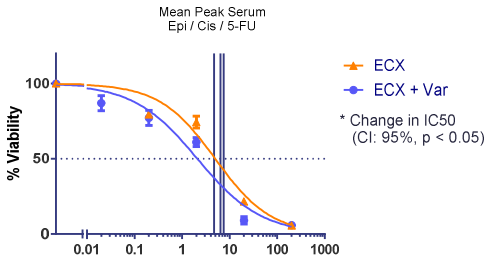
C



	ECX + Var	ECX
IC50	1.885	2.053

	ECX + Var	ECX
IC50	1.338 to 2.655	1.637 to 2.573

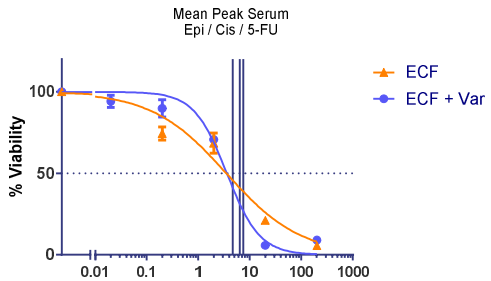
D



	ECX + Var	ECX
IC50	2.105	4.977

	ECX + Var	ECX
IC50	1.555 to 2.848	3.818 to 6.487

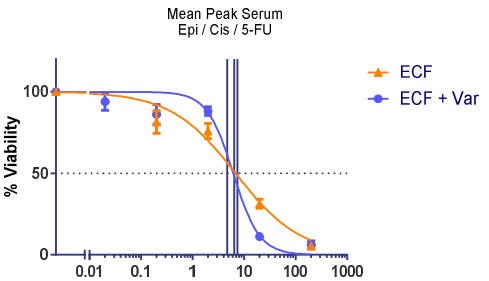
E



	ECF + Var	ECF
IC50	3.598	3.514

	ECF + Var	ECF
IC50	3.001 to 4.313	2.551 to 4.841

F



	ECF + Var	ECF
IC50	6.169	6.85

	ECF + Var	ECF
IC50	4.854 to 7.842	5.283 to 8.883

Figure 48. Combination therapy of ECF chemotherapy with a PDE5i provides enhanced chemo-sensitivity in the presence of hMSC co-culture: Examination of the effect of ECF combination with PDE5i

Sensitivity of close-to-patient cells was determined in 3D-TGA, with and without mesenchymal cell co-culture, after 4 day exposure to ECF and Vardenafil (PDE5i) drug combinations. Viability curves were generated and IC_{50} values determined using GraphPad Prism. Horizontal lines represent mean IC_{50}s.

Overall sensitivity of all of the patient cell lines either cultured as Tumour cells alone (**A**) or Tumour cells co-cultured with hMSCs (**B**) was determined for assays with and without the addition of PDE5i to SOC ECF chemotherapy. Statistical significance calculated using paired t-test.

Examples of the individual patient cell lines different responses contributing to the reported overall effect of the chemotherapeutic conditions in (**A**) and (**B**) are shown. There is no change in chemosensitivity following the addition of PDE5i to ECF chemotherapy when tumour cells are cultured alone for either OBX53(ii) (**C**) or OBX59 (**E**). However, when tumour cells are co-cultured with hMSCs the addition of PDE5i to the SOC ECF chemotherapy significantly changes chemosensitivity for patient cell line OBX53(ii) (**D**) but not for OBX59 (**F**).

Statistical significance is determined by the arithmetic variance between the calculated IC_{50}s and their distinct 95% confidence intervals which have no overlap.

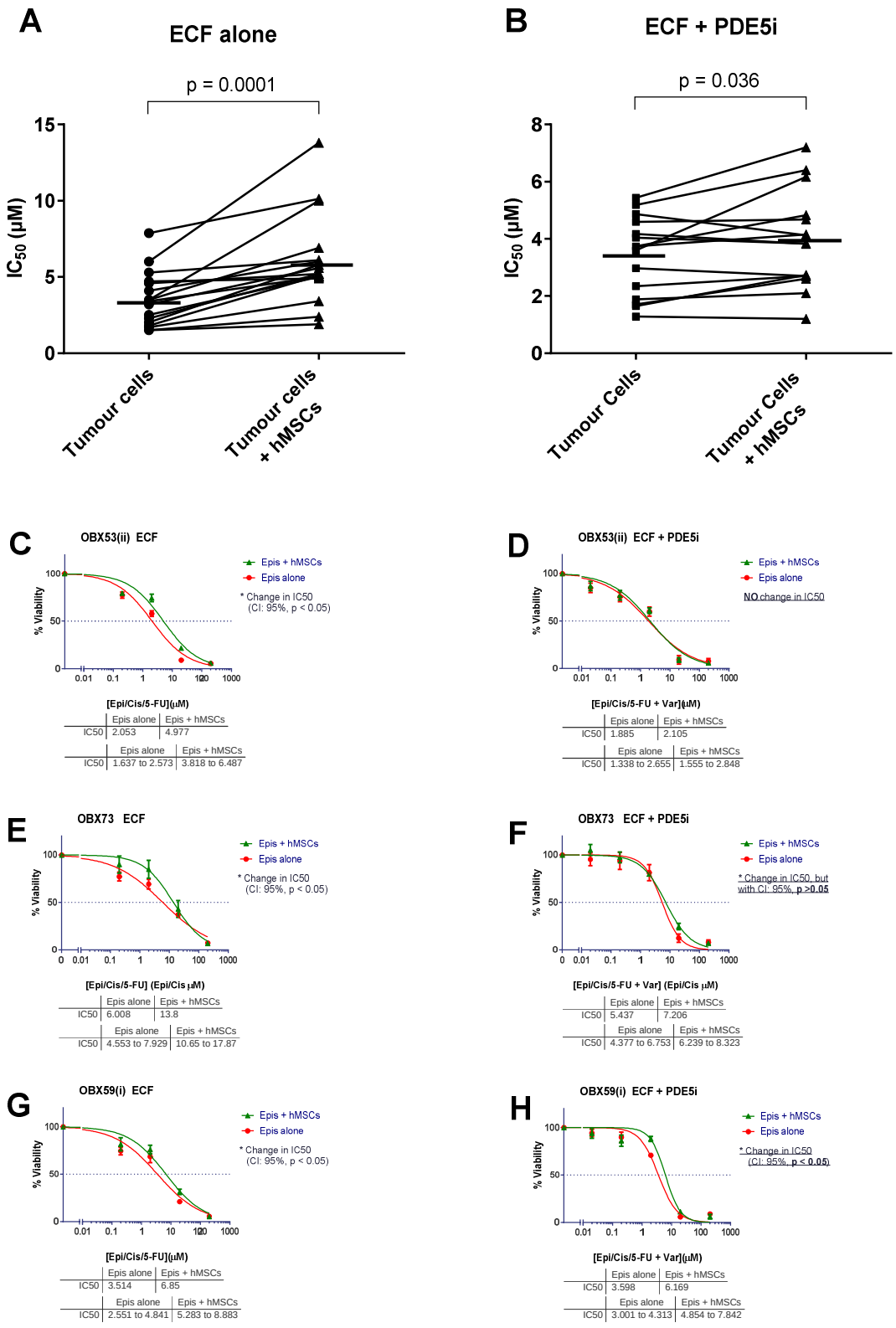


Figure 49. Combination therapy of ECF chemotherapy with a PDE5i provides enhanced chemo-sensitivity in the presence of hMSC co-culture: Examination of the effect of stromal cell co-culture.

Sensitivity of close-to-patient cells was determined in 3D-TGA, with and without mesenchymal cell co-culture, after 4 day exposure to ECF and Vardenafil (PDE5i) drug combinations. Viability curves were generated and IC_{50} values determined using GraphPad Prism. Horizontal lines represent mean IC_{50}s.

Overall sensitivity of all of the patient cell lines to ECF alone (**A**) and ECF in combination with PDE5i (**B**) was determined for assays with and without mesenchymal cell co-culture. Statistical significance calculated using paired t-test.

Examples of the individual patient cell lines quite different responses contributing to the reported overall effect of the chemotherapeutic conditions in (**A**) and (**B**) are shown. When exposed to ECF chemotherapy, all three patient cell lines (OBX53(ii)(**C**), OBX73(**E**), and OBX59(i)(**G**)) show a similar pattern of significantly increased resistance to chemotherapy when co-cultured with hMSCs. However when treated with PDE5i in addition to ECF, the increased chemo-resistance from hMSCs co-culture is altered for each patient line. With addition of PDE5i OBX53(ii)(**D**) demonstrates no change chemo-resistance from co-culture, OBX73(**E**) demonstrates a reduced non-significant ($p>0.05$) change in chemo-resistance, however OBX59(i)(**H**) is unaffected by the addition of the PDE5i and continues to demonstrate a significant ($p<0.05$) increase in chemo-resistance from hMSC co-culture.

Statistical significance is determined by the arithmetic variance between the calculated IC_{50}s and their distinct 95% confidence intervals which have no overlap.

Given the apparent patient specific efficacy of PDE5i, these reductions in IC_{50} need correlation with the patient serum levels to evaluate whether this change in IC_{50} might alter patient chemo-response.

Five patients (with a total of 12 tumour samples) undergoing chemo-sensitivity & PDE5i analysis had chemo-resistant tumours based on both the 3D-TGA and histological assessment (Mandard TRG 4 or 5). The addition of PDE5i to the SOC chemotherapy changed in the absolute IC_{50} value in 9 of the 12 chemo-resistant tumour samples to reduce the IC_{50} below the mean peak serum chemotherapy threshold seen in patients, indicating that 75% would potentially no longer be chemo-resistant in response to this combination therapy with PDE5i (Figure 50).

Patient ID	Sample ID	ECF		TRG	ECF + PDE5i
hMSCs		-	+		+
Oes1B	OBX70	1.5	1.9	1	2.7
Oes2B	OBX71(ii)	1.7	3.4	3	2.6
Oes3B	OBX18	1.5	2.4	3	1.2
Oes4B	OBX9	4.6	5.2	4	4.1
Oes4R	OES125	3.4	5.0		3.8
Oes5B(i)	OBX53	1.8	5.1	4	2.7
Oes5B(ii)	OBX53(ii)	2.5	5.0		2.1
Oes5R	OES141	5.3	6.1		6.4
Oes6B(i)	OBX59	3.5	6.9	4	6.2
Oes6B(ii)	OBX59(ii)	3.2	5.6		4.8
Oes6R	OES145	4.7	4.9		4.2
Oes7B(i)	OBX25	2.3	5.2	5	2.7
Oes7B(ii)	OBX25(ii)	2.0	5.8		x
Oes7R	OES127	4.1	6.0		3.8
Oes8B	OBX73	6.0	13.8	5	7.2
Oes8R	OES148	3.5	10.0		4.7
Oes9B	OBX44(ii)	7.9	10.1	4	x

Figure 50. The comparative efficacy of combination therapy of ECF chemotherapy and PDE5i across the cohort of patient OG cancers

Each individual patient's cancer cells were grown in the 3D-TGA with (+) or without (-) the presence of hMSCs, before combination chemotherapeutic assessment. The patient cancer cell clusters were classified as sensitive (green), borderline (orange), or resistant (red) by comparison of IC_{50} values to mean peak serum concentrations achieved in patients at the doses used in UK clinical practice.

5.2.14 Adjunctive PDE5i therapy only demonstrates efficacy for individual patients

Although there is an overall significant difference in chemo-toxicity by addition of PDE5i to ECF chemotherapy, the difference is small and when examining individual confidence intervals, they often overlap, bringing into question the true additional chemo-toxic effect of the drug in the clinical setting.

To accurately describe a significant change in IC_{50} when comparing drug regimens for each individual patient cancer, the confidence intervals (CIs) for each calculated absolute value of IC_{50} are displayed (Figure 51, column 'PDE5i effect (c/i)'). Confidence intervals do not overlap in only 4 of the 12 chemo resistant tumour samples i.e. 3 of the 5 patients (60%), and thus would demonstrate less efficacy from addition of the PDE5i (Figure 51, column 'PDE5i (crude effect)' vs 'PDE5i effect (c/i)').

It is important to note that an additional 2 of the patient cancer samples (OBX18, OBX73) displayed a significant change in their IC_{50} when additionally challenged with PDE5is (without overlapping CIs) but this did not result in a change in their chemo-sensitivity status, because they were already classed as chemo-sensitive (OBX18), or still remained above the threshold for chemo-resistance (OBX73).

PDE5i only changed chemo-sensitivity in the presence of hMSC driven chemo resistance. All 4 of the chemo-resistant tumour samples that became chemo-sensitive (without IC_{50} CI overlap) on addition of the PDE5i had an hMSC influenced chemo resistance i.e. in the 3D-TGA these 4 cancer samples were initially deemed sensitive to SOC chemotherapy. However, when co-cultured with hMSCs they became chemo-resistant, but when exposed to the SOC chemotherapy & PDE5i all 4 of these cancer

samples became sensitive to chemotherapy again (Figure 51, column 'IC_{50} change + hMSCs (c/i)' vs 'PDE5i effect (c/i)').

However, this effect was not demonstrated in reverse: PDE5i did not universally reverse the influence of stromal induced chemo-resistance. 8 of the 12 chemo-resistant tumour samples had a significant stromal influence on their chemo-resistance (without IC_{50} CI overlap), but only 4 of these 8 were significantly affected by addition of PDE5i changing their IC_{50}s (with correct CIs) to demonstrate a change to borderline or potential sensitivity to chemotherapy.

The addition of PDE5i to SOC chemotherapy only significantly alters the chemo-resistance influence of hMSC co-culture in half of those with co-culture-induced chemo resistance, and therefore across the whole patient cohort, the overall increase in chemo-resistance seen by stromal co-culture is not reversed by a routine addition of PDE5i to ECF chemotherapy ($p=0.036$) (Figure 47B).

	ECF		ECF + Var		TRG	ECF: Epis alone	95%CI		ECF: Epis +hMSCs	95%CI		IC50 change + hMSCs (c/i)	Sen / B / Res (crude)	Var + ECF: Epis +hMSCs	95%CI		Epis + hMSCs: ECF + Var	PDE5i (crude effect)	PDE5i effect (c/i)
Stroma	-	+	-	+		IC_{50}	lower	upper	IC_{50}	lower	upper			IC_{50}	lower	upper			
OBX70	1.5	1.9	1.6	2.7	1	1.462	0.965	2.213	1.889	1.294	2.759	n	S	2.736	1.944	3.851	S	n	n
OBX71(ii)	1.7	3.4	1.7	2.6	3	1.709	1.334	2.190	3.363	2.569	4.402	y	S	2.609	1.905	3.573	S	n	n
OBX18	1.5	2.4	1.3	1.2	3	1.541	1.100	2.159	2.358	1.661	3.348	n	S	1.196	0.851	1.651	S	n/a	y
OBX9	4.6	5.2	4.9	4.1	4	4.603	3.577	5.925	5.222	4.393	6.209	n	R	4.120	3.476	4.883	B	y	**n**
OES125	3.4	5.0	4.2	3.8	4	3.376	2.412	4.564	4.972	3.873	6.382	n	R	3.823	3.057	4.780	S	y	**n**
OBX53	1.8	5.1	3.0	2.1	4	1.818	1.202	2.749	5.132	4.026	6.541	y	R	2.703	1.596	2.693	S	y	y
OBX53 (ii)	2.5	5.0	1.9	2.1	4	2.053	1.637	2.573	4.977	3.818	6.487	y	R	2.105	1.555	2.848	S	y	y
OES141	5.3	6.1	5.2	6.4	4	5.314	4.140	6.822	6.123	4.945	7.583	n	R	6.401	5.320	7.702	R	n	n
OBX59	3.5	6.9	3.6	6.2	4	3.514	2.551	4.841	6.850	5.283	8.882	y	R	6.169	4.854	7.842	R	n	n
OBX59(ii)	3.2	5.6	3.7	4.8	4	3.161	2.317	4.312	5.609	4.636	6.785	y	R	4.831	4.066	5.741	B	y	**n**
OES145	4.7	4.9	3.7	4.2	4	4.721	3.691	6.038	4.933	3.911	6.220	n	R	4.159	3.010	5.747	B	y	**n**

OBX25	2.3	5.2	2.5	2.7	5	2.343	1.746	3.145	5.193	3.592	7.507	y	R	2.695	1.743	4.164	S	y	**n**
OBX25(ii)	2.0	5.8			5	2.036	1.532	2.706	5.799	3.807	8.835	y	R	x	x	x		x	x
OES127	4.1	6.0	4.0	3.8	5	4.021	3.455	4.679	5.959	4.745	7.485	y	R	3.834	3.127	4.700	S	y	y
OBX73	6.0	13.	5.4	7.2	5	6.008	4.553	7.929	13.80	10.66	17.87	y	R	7.206	6.239	8.323	R	n	y
OES148	3.5	10.	4.6	4.7	5	3.545	2.431	5.171	10.03	7.645	13.17	y	R	4.674	3.860	5.658	B	y	y
OBX44(ii)	7.9	10.			4	7.887	6.737	9.235	10.13	8.193	12.52	n	R	x	x	x		x	x

Figure 51. The efficacy of the co-culture dependant ECF and PDE5i combination chemotherapy should be considered with respect to the IC_{50} confidence intervals

Each individual patient's OG cancer cells were grown in the 3D-TGA with or without the presence of hMSCs before combination chemotherapeutic assessment with ECF and Vardenafil. The individual IC_{50}s, for the combinations and the associated confidence intervals are detailed. The patient cancer cell clusters were classified as sensitive (green), borderline (orange), or resistant (red) by comparison of IC_{50} values to mean peak serum concentrations. The potential change in clinical chemo-sensitivity by the addition of PDE5i addition is detailed.

5.3 Conclusion

The OG 3D-TGA using close–to-patient cells allowed effective evaluation of chemotherapeutics on individual patient cancers. The method allows individual drugs and combinations to be evaluated, and trends in chemo-sensitivity across drug types and between patients to be appraised.

Epithelial cell co-culture with hMSCs within the 3D-TGA enhanced the OG cancer cell growth and significantly increased the observed *ex vivo* chemo-resistance to the standard-of-care chemotherapy, demonstrating the important role of the tumour microenvironment in modulating chemotherapy response.

The *ex vivo* OG 3D-TGA evaluation of chemo-response in the presence of stroma correctly reflected the clinical chemo-sensitivity, with an accurate correlation between the 3D-TGA predicted chemo-resistance and actual clinical response.

The OG 3D-TGA was used for the evaluation of novel emerging drugs. Panobinostat enhanced the chemo-sensitivity in combination with ECF, and proved efficacious in otherwise chemo-resistant tumours. Evaluation of the stromal targeting PDE5i drug Vardenafil demonstrated enhanced overall chemo-sensitivity, but a meaningful clinical effect was limited to a sub-set of those patient's cancers with hMSC stromal co-culture induced chemo-resistance.

6 Discussion

6.1 Summary of research

Following the development of a novel method of establishing cancer cells from small biopsies of individual patient oesophageal cancers, I have assessed growth and chemo-toxicity in a tumour micro-environment (TME)-relevant 3D assay which enables multi-drug chemo-sensitivity testing, and screening of novel drugs.

Mesenchymal co-culture had a significant effect; enhancing growth and chemotherapy drug resistance in the 3D model, resulting in accurate prediction of chemo-sensitivity for individual patients.

The oesophageal 3D-TGA also allows individual and novel drugs to be evaluated, trends in chemo-sensitivity between patients to be appraised, and analysis of the effect of the TME on tumour growth and drug resistance, which could prove a useful target for future therapy.

6.2 Establishment and Characterisation

The development of a method for the repeated establishment of *ex vivo* cultures of individual patient OG carcinoma cells is a novel achievement, which has not been reported before in the scientific literature.

6.2.1 Establishment of *ex vivo* OG cancer cells

The transfer of tissue to the laboratory in PCA media over extended timelines may have made a difference to establishment rates, however this is unclear, as the speed at which the endoscopic biopsies were transferred to the laboratory rarely extended to >24 hours as the efficiency of the patient selection, endoscopy and transfer processes improved. However, the experimental results clearly show the fragility of the OG cancer biopsy material, and the effect on viability caused by transfer solution, which has been reported in other tumour types(394).

Many other particularly fibrous tissue types have benefited from varying multi-step and extended enzymic disaggregation to produce a cellular solution from the tumour tissue (169, 191). However, the OG cancer biopsies disaggregated easily following a reduced time period of enzyme exposure, and indeed less exposure to the disaggregating enzymes actually increased cellular viability. It could be postulated that this is due to the soft and fragile architecture of OG tumour biopsies from the exophytic surface of the tumour within the lumen of the oesophagus. This variation in technique is in common with other reports that disaggregation methodology has to be tissue dependant to achieve best results(395).

The true prevalence of bacterial contamination of the initial cancer cell cultures could be less than suspected, as to prevent potential cross-contamination, confirmation of bacterial contamination not waited upon, before any suspicious looking

cultures were discarded and the well within the 6wp treated with disinfectant. In future studies an automated contamination alert system could be used (such as the BacT/ALERT®3D automated culture system) which would prevent unnecessary loss of initially suspicious cultures which were pre-emptively discarded, but not actually contaminated(396).

The prevalence of oesophageal candidiasis amongst healthy individuals is rare, at less than <1% (397). However, in contrast, yeast colonization is common in patients with cancer (57%), and is clinically evident in 20%-30% of those with cancers of the upper aero-digestive tract. (398) Given the high level of occult fungal colonisation, it is therefore unsurprising that patients without visual evidence of oesophageal candidiasis at endoscopy could still go on to suffer fungal contamination *in vitro*, and that there was no correlation between the *in vivo* and *in vitro* settings. Clinically the vast majority of infections are caused by C. albicans, but one third are caused by non-C. albicans strains (e.g. C. glabrata) which display increased resistance to anti-fungals (398). Despite broad sensitivity to amphotericin B and nystatin, anti-fungal resistance is the most common in the first-line azole drugs (fluconazole / itraconazole / ketoconazole) in up to 28% of cases.(398) This pattern of azole resistance *in vivo* may have been mirrored in our *in vitro* samples where the addition of fluconazole to the cultures did not exert a significant additional fungicidal effect. However, the true nature of any azole resistance was not formally investigated, and alternatively it has been reported that Fluconazole is not effective in tissue culture where there is a particularly heavy fungal load, and no competing microbes within that environmental niche due to the sterile conditions and AA supplementation (386, 387). The ongoing low-level fungal contamination despite continued anti-mycotic supplementation and a cycle of cellular cryo-

preservation and re-animation raises the possibility that despite macroscopic fungal clearance, spores persist. Alternatively, this close-to-patient cell sample could have become cross contaminated due to technical error during the cryo-preservation, re-animation process, subsequently overwhelming the established cancer cell culture.

The 'cell senescence following cryopreservation' negative growth phenomenon which was observed, may have been caused by damage inflicted by the freezing-warming cycle of cryopreservation and re-animation. Multiple mechanisms for cellular damage during this process have been identified (solute effects, intra or extracellular ice formation and dehydration)(399), many of which are mitigated by the use of an addition of organic solvents as cryoprotectants (such as DMSO) which was used in these studies. More recently research has suggested that the addition of ice re-crystallization inhibiting polymers can improve cell recovery by 50%(400). The phenomenon that we encountered however was not directly with cell recovery and appeared more related to poor delayed cellular proliferation. This problem was not investigated systematically in my studies and in the absence of a clear cause of this problem being identified, the phenomenon was broadly termed as 'cell senescence following cryopreservation', but given the mechanism is unclear, and there may not be any true relation to cellular ageing or cryopreservation process itself.

In conclusion, the establishment, growth and maintenance of feeder-layer supported *in vitro* primary close-to-patient OG cancer cell cultures is a reproducible method with an establishment rate of 70%, but it is unpredictable, temperamental and time consuming due to the variable nature of

the individual patient cancer's growth and cellular fragility following re-animation.

6.2.2 Expression of the potential OAC CSC in the different tissue and culture settings

IHC was performed to try and identify markers of cancer stem cells (CSC) in oesophageal cancer in our samples. IHC for ALDH and CD44 required careful technical optimisation for best visualisation, but proved very helpful as it clearly demonstrated a natural variation across the patient cohort which was mirrored in the flow cytometry results for these markers.

Each of the primary antibodies used for the planned characterisation (EpCam, p53, CD44, ALDH) of the close-to-patient OG cancer cell lines was carefully chosen to be specifically monoclonal and anti-human. The choices were based on a body of published literature (see Table 3) demonstrating its consistent and reliable use in human oesophagogastric cancers, which once optimised would therefore allow confidence in demonstrating that differential staining patterns were the result of tissue variance, rather than poor choice of quality antibody, reagent or methodological error.

This natural variation in expression was not limited to CSC markers but also seen in the functional analysis using TFF3 expression (see appendix images).

Evidence presented by the Schlegel group in normal (non-malignant) tissue would suggest that the keratinocyte cells that grow in the Feeder-layer system are 'conditionally reprogrammed cells', showing upregulated markers of stem cells, whilst retaining markers of original tissue type (172). However, this is not the case in studied OG tissues, where the chosen markers of CSC (ALDH & CD44) appear in the malignant tissue,

grown in the Feeder-layer system, but do not appear in any corresponding 'normal' OG tissues. This would suggest that these are demonstrating pre-existing and enduring markers of potential CSC, rather than an effect of the ROCKi & Feeder-layer 'conditionally reprogrammed' growth conditions.

Although expression of CD44 & ALDH in the primary patient tumour was reflected in the corresponding generated *in vitro* patient cells and xenografts, these markers showed graded expression across the different patient tumours displaying the inherent heterogeneity between individual patient tumours.

The flow cytometry analysis of the individual patient-derived cell cultures was useful and confirmed their nature as epithelial (Cytokeratin) and dysplastic (EpCam), matching their *in vivo* parent tissue characteristics. However, attempts to sub-select potential CSC populations were less successful. The variable levels of the potential CSC markers of ALDH and CD44 between the patient-derived cell cultures, is probably accurate as this reflects the previously discussed literature (Introduction 1.8) showing that there is no universally accepted marker for OG cancer CSC, and further emphasises the heterogeneous nature of this cancer type. Without an obvious sub-populations of CSC within each close-to-patient cell culture efforts to sub-select this population would have be futile, and therefore sub-selection of a more tumorigenic CSC population for analysis and potentially advantageous xenografting was abandoned.

It is unclear whether the original patient tissue from which the close-to-patient cell cultures was derived had a similarly homogeneous nature (whether positive or negative stain) cell population for CD44 or ALDH as was apparent at flow cytometry. However, given the good correlation between the patient tissue and close-to-patient cancer cells using FFPE, there must be a

degree of suspicion that the repeated cycles of *in vitro* feeder-layer culture has to some extent resulted in loss of the tissue heterogeneity resulting in the homogeneous CD44 and ALDH staining where this was present in the patient-derived cells.

The study of the potential OAC CSC markers CD44 and ALDH for each of the PDX cancers was similar to the graded expression profile previously discussed for the close-to-patient cells, but the disappearance and re-appearance of CD44 in just two of the cancer cell cultures was unexpected and the reason for this is not clear. This could represent the prominence or lack of importance of a certain cell sub group within that tumour growth phase, or that CD44 positive OAC cells which may have CSC properties may display situational expression according to the local growth environment. This also suggests that whilst there was maintenance of cells with a CSC-like phenotype in culture, there was an element of sub-selection of cell populations from the primary tissue to the *in vitro* cultures and their corresponding patient-derived xenografts.

CD44 and ALDH were present individually or concurrently in the majority of the patient biopsies, however, the heterogeneous presence of these previously reported OAC CSC would suggest that CD44 and ALDH do not comprehensively identify all of CSC population. It could also alternatively be concluded that ALDH and CD44 do not accurately identifying CSCs or that there may not be a population of CSC that is classically present in OAC.

The persistent interest and increasing belief in the CSC hypothesis is driven by an accumulating volume of evidence(401) and the anticipation that the CSC hypothesis provides an elegant explanation to the problem tumour cell senescence, recurrence, and chemo-resistant clonal expansion,

(331, 347, 402) however the mechanism of this hypothesis may not be so straight forward in OAC.

Firstly in the normal squamous oesophagus (unlike the crypts of the classic gut mucosa) it has been shown that symmetric cell division was random throughout the basal layer, and asymmetric cell division to produce two cells with different cellular fates did not occur in specific cell compartments. (403) This would suggest that there is not a universal and structured, stem cell driven, reproductive functional unit within the human oesophageal mucosa.

Secondly, stem-ness may not be able to be defined due to rapid and reversible cellular phenotypic changes in response to the cell's local microenvironment, and therefore to isolate and use representative cells from patient tumours in model systems is problematic and results likely imperfect. (404). This lack of evidence to support the CSC theory in OAC may also go some way to explain the paucity of reliable molecular prognostic biomarkers in OAC (405)

6.2.3 Establishment of patient-derived xenografts

Subcutaneous xenografting of the OG cancer close-to-patient cancer cells into immune-compromised mice resulted in 15-25% forming PDX. Of those that formed epithelial tumours, they displayed the same histological architecture and morphology as the original oesophageal tumour, with same phenotypic characteristics demonstrated by cytokeratin, EpCam and p53 IHC. This would suggest that where they formed, the xenografts were representative of the original patient tumour. This is a significant accomplishment, as this is the first time that the same oesophageal cancer has been able to be grown *in vitro* and *ex vivo* within the laboratory setting for individual patients, which

allows huge potential advantages over isolated cell line(406) or PDX(181) scientific study of oesophageal carcinoma.

Not all of the close-to-patient cells were engrafted in an attempt to form xenografts due to the availability of animals, slow growing cells, loss of patient samples from technical laboratory problems, and poor cellular viability following cryopreservation. Some of the close-to-patient cells only formed PDX after multiple engraftment attempts, and each of the close-to-patient cell cultures were not all afforded the same number of engraftment attempts. Different strains of immune-compromised mice were also utilised throughout the process, depending upon their availability (MF-1 / CD-1 Nude, SCID, RAG), and in common with the literature no strain of immunocompromised animal appeared to show an advantageous engraftment rate(181, 183).

A method widely reported in the literature to improve engraftment rates is to implant a CSC enriched cell population(337, 361, 373, 374). An attempt was made to analyse the primary close-to-patient OG cancer cell cultures for potential sub-populations of CSCs, that could be sorted by flow cytometry and undergo preferential xenografting. However there was no indication of the presence of a sub-population of CSC using the markers examined. This could be due to inaccuracy of the markers chosen and in future research it would be useful to re-visit this line of investigation with other alternative CSC markers in future studies.

This variability in xenograft establishment may be symptomatic of dissimilar tumorigenicity of different cancer cell clones of the individual close-to-patient cancer cell cultures, or due to a variation in the aggressiveness of the original cancers. This engraftment was not investigated systematically, and so although no conclusions can be drawn about those that did not

form PDX, there remains an unanswered question regarding the carcinogenic nature of these close-to-patient cell cultures that did not easily form PDX. Whilst a genetic test of the epithelial cells that are derived from this method would provide more certainty that representative cancer cells are being grown, the markers chosen and reported in this study have been validated at the protein level by a number of different groups and I feel are therefore reliable for the purposes of cellular and tissue characterisation, for which they are employed. Using IHC, I was able to demonstrate key and important tissue characteristics (such as the malignant phenotype) which may be missed in a global gene expression analysis in a cellularly complex tissue. For example, P53 would have appeared similar in both the malignant and normal tissue, and also, the variable levels of the ALDH enzyme from sample to sample, showing intra-patient heterogeneity, may not have been evident.

It would be ideal to investigate the differences between the individual patient cell cultures on a genetic basis. A comparison of gene expression patterns between the tissues, the cultured cells and PDX by microarray analysis would provide significant insight into the similarity between the models, clonal selection and the comparison with clinical and modelled chemo-sensitivity analyses, and forms part of our future research plans. But such analysis (comparing a varied patient tissue, comprising both cancer and a variety of stromal and other microenvironment cells, with groups of cancer cells grown in the mesenchymal feeder layer system or the 3D-TGA) would provide complex results with intrinsic variability, requiring detailed analysis, generating quantities of data beyond the scope of this current study.

6.3 3D-TGA Optimisation

6.3.1 Growth and cytotoxicity

The close-to-patient OG cancer cells had developed into early clusters by day 3, and a total 7 day period was found to be the optimum time for sustained growth. Despite the reported 3D matrigel culture formation of ROCKi established malignant mammary and prostate cell clusters by Schlegel et al, that they do not relate how much longer it took for these clusters to form (172, 173). Studies of colonic cancer using a similar ROCKi method, reported sphere/cluster formation all within 7 days (188). Although the 7 day OG 3D-TGA may only capture the early growth phase of a slow growing OG cancer, it provides a uniform assay length which also incorporates those cancers which may grow more quickly, and importantly allows a standardised cytotoxicity studies to occur whilst the all the patient cell clusters are still in their growth phases.

Despite its widespread application for evaluation of cell growth, the use of alamarBlue as a single metric to measure tumour growth and assess cytotoxicity (albeit as a screening mechanism) is a limitation(407). In future investigations, it would be ideal to use a second parallel method such as CyQUANT (408)cell proliferation assay (ThermoFisher) which measures DNA content rather than metabolic activity, and has been used widely in the assessment of chemotherapeutics(409, 410). However, although there is the advantage of being able to store multi-time course samples before delayed batch analysis, the process for analysis introduces an element of error (especially when performing complex multi-well high throughput analysis) as cells have to be removed (in a reproducible representative proportion) from the 3D matrix, media and plate, prior to freezing and lysis; before being corralled for delayed

Fluorescence analysis. When performing drug specific in-depth cytotoxicity studies in future, it may be preferable to measure cell proliferation with BrdU and apoptosis with Caspase (411) which will not only provide a corroboration of the alamarBlue result, but also provide a further mechanistic insight.

6.3.2 Matrix Stiffness

The standard BME matrix concentration previously successfully used for lung and prostate PDX cells within the 3D-TGA was 3mg/ml (180, 191, 238). But my results demonstrate that for primary close-to-patient OG tumour cells within the 3D-TGA, a BME concentration of at least a 6mg/ml is required to truly suspend the cells effectively in the 3D matrix, and 12mg/ml matrix was used for growth of the OG cancer clusters over a 7 day period.

It is well known that matrix stiffness is an important factor in the TME providing physical regulatory cues for some aspects cell growth, motility and differentiation(412). Tumour tissue has an increased stiffness in comparison to normal tissue and in *in vitro* models this has been implicated in tumour progression (413), with collagen in particular thought to be a significant contributor (414). This may explain the need for a higher concentration BME for the OG primary patient cancer cells to grow effectively, and this may be closer to the actual stiffness seen in growing cancer tissue. In breast cancer models, increased stiffening of the matrix with LOX-mediated modified collagen crosslinking and the addition of fibroblasts promoted invasion and progression with enhancing integrin signaling(415, 416). Migration of tumour cells within the matrix as well as invasion is thought to be governed by matrix stiffness(417). Stiffness has also been shown to modify gene expression of components known to impact on cell adhesion including caveolin and beta1 integrin and differentially

enhance metastatic potential (418). However, malignant progression and invasion is different from rate of cellular proliferation, and it has been shown in other cell types that although the rate of cellular proliferation is dependent upon matrix stiffness, as the matrix becomes more compliant, so there is a lag phase prior to established growth, before a longer doubling time is also seen (419). It is unclear whether this slower growth rate better reflects the clinical picture of *in vivo* tumour growth rates, or whether this is usually individual patient culture dependant.

Indeed it is also important to consider the impact of the increase in the relative concentration of the components of the BME. Increased concentrations of constituents (including but not limited to integrin family) such as laminin and collagen would therefore result in engagement of more of their receptors. These physical interactions provide key signals which promote growth, survival and prevent anoikis, in concert and sometimes overwhelming the paracrine growth factor signalling such as EGF, providing a more complex cell-to-TME interaction than matrix stiffness alone. The relative stiffness of the TME, increased concentration of the BME components and the many parameters that this affects (including growth, proliferation, and invasion) and the variation both between tumour types and individual patients underlines the need for increasingly complex 3D culture models to more accurately reflect the *in vivo* environment to allow accurate growth evaluation, unravel key pathways and assessment chemotherapeutic resistance (420).

6.3.3 ROCKi supplementation

Studies examining the conditional reprogramming of epithelial cells using ROCKi have demonstrated that the process does not select for a small sub-population of cells from the original tissue,

but the induction (which rapidly occurs within 2 days) results from the conditional reprogramming of the entire cell population(173). Despite the stem-like state of the conditionally reprogrammed cells, they do not express transcription factors characteristic of embryonic or pluripotent stem cells(172). This is encouraging, as it reduces the obvious concern that by using this method for primary OG cancer tissue, a small sub-population will have been selected and the cell phenotype will be changed and with it the all-important chemo sensitivity and drug resistance profile.

The presence of ROCKi within the cultures has a small positive effect on the establishment and growth of OG cells in the 3D-TGA. This may reflect different parts of the cellular mechanisms involved in the initial establishment and then subsequent growth of the cells within the 3D–TGA receiving its subsequent stimulation cues from the 3D TME, such as the engagement of the receptors for laminin and collagen by BME, which produces a cell protective anti-anoikis signalling cascade. This hypothesis is thought to be why the initially established conditionally reprogrammed primary cells were able to form normal structures or tumours so successfully in 3D or *in vivo*(172, 173). Indeed, other groups routinely use ROCKi (Y-27632) to avoid anoikis in the initial establishment of cells from primary tissue before then growing these in 3D cell culture models (171, 421).

To achieve 3D culture growth of Barrett's Oesophagus (and colonic carcinoma) Sato et al, used ROCKi (Y-27632) for the first 2 days to avoid initial anoikis, followed by culture in their optimised 'basal cell culture medium' in adjusted 3D culture conditions (referred to as 'human stem cell culture' – HISC). They showed that this growth was dependant on supplementation with a large number of additional growth

factors (including Wnt 3A, EGF, Noggin, Nicotinamide, TGF, SB202190 and FGF 10(171). However, despite Barrett's and OAC cancer being so closely linked biologically we have shown that this multiple supplementation is not necessary for growth of OG cancer within our system. It can be postulated that this may be because the conditions described by Sato et al were developed for the colorectal stem cell niche, and may explain why Sato et al did not have enduring success at growing oesophageal cancer which we now know has a quite separate proliferative basis, distinct from the classical crypt structure of gut mucosa(403).

In future studies it would be ideal to aim to perform both the 2D feeder layer culture and the 3D-TGA without routine supplementation with ROCKi. Clearly its role as an anti-apoptotic factor is vital in the initial culture establishment, but its enduring presence as a foreign stimulant is not ideal whilst cells are undergoing attempted representative chemo-toxicity assays. There are two alternate potential molecules that could be trialled, which have shown much promise within the field of (non-malignant) stem-cell research. These are the small molecule HA-100 which removes the need for feeder-layer culture(422), and the potentially more TME relevant human serum-derived protein 1α1(423).

6.3.4 Microenvironment dependant TFF3 expression

TFF3 was expressed universally throughout the primary patient tissue, not expressed in the *ex vivo* feeder layer environment, and then once again universally expressed in the PDX tumours, and by the cells in the 3D-TGA.

Unlike CD44, this universal demonstration of presence and absence in different environments, points towards the setting of the cellular growth being the trigger for TFF3 expression. TFF3 is a functional protein secreted from the apical membrane of

established mucosa. (384) This would suggest that whilst the cells are growing in the setting of a 3D tumour microenvironment such as a PDX, they have the correct environmental cues to promote cellular functionality as well as growth, unlike the 2D feeder-layer growth setting where there is no tumour microenvironment.

Importantly TFF3 is seen selectively expressed in the 3D-TGA when previously absent in 2D. This selective expression of TFF3 in a 3D TME with mesenchymal support (either *in vivo* or *ex vivo*) would suggest that a resumption of apical–basal polarisation, cell-cell interactions and environmental cues (which are absent in monolayer culture) are required for these close-to-patient cells to return to functional status. This reinforces the importance of representative 3D culture, as has been shown in other tissue types,(424) for the production of relevant assay results. This presumed resumption of function is encouraging as it suggests that when subsequently undergoing chemotherapeutic testing in the 3D-TGA the cancer cell clusters have resumed a functional phenotype and maybe behaving in a similar manner as one might expect in their original human tumour microenvironment.

6.4 Chemotherapeutic Evaluation

6.4.1 Mesenchymal cell co-culture increases chemo-resistance

The increased chemo-resistance in the presence of mesenchymal cells in the 3D-TGA underlines the overall importance of the stromal component of the TME, and paracrine interaction between the tumour epithelial cells and their support cells, and the importance of including them in both *in vitro* and *in vivo* assays for pre-clinical drug screening.

This study and previous work published by our group (238) shows that the role of the stromal component of the TME in influencing the chemo-resistance is both drug- and individual tumour-dependent. This variation is a more accurate reflection of the diverse clinical outcomes to chemotherapy treatment, where OAC patients individually display variable magnitudes of response to individual drugs and the SOC therapy.(57, 425, 426)

6.4.2 The 3D-TGA accurately models clinical chemo-sensitivity

The 3D assay using close-to-patient cancer cells co-cultured with mesenchymal cells provides a clinically-relevant assessment of patient sensitivity to the ECF chemotherapeutic agents, accurately predicting individual clinical chemo-therapeutic response with a sensitivity and specificity of 100%. Although numbers are small, this is a particularly exciting finding, as attempts to correlate laboratory chemo-therapeutic outcomes to individual patient clinical response and provide personalised chemotherapy have previously been unsuccessful.(204, 206) Corresponding survival data would be helpful for clinical application, but has not been reported as it is immature and remains difficult to interpret for a group of this size.

6.4.3 Efficacy of combination chemotherapy

Using standard chemotherapy agents alone, the drug triplet of ECF was the most effective regimen evaluated in the 3D-TGA, closely followed by the Cisplatin/Fluorouracil (5-FU) doublet, which reflects the apparent increased efficacy of the peri-operative ECF triplet over the pre-operative Cisplatin/5-FU doublet observed in clinical practice.(425) However, in a head-to-head clinical evaluation,(427) the marginal gain in chemotherapy–efficacy seen from addition of Epirubicin to Cisplatin/5-FU (improved TRG, progression & disease free survival, but not overall survival) is offset by both a significant increase in the toxic side-effects from receiving triplet chemotherapy, and a reduced number of patients completing chemotherapy cycles.(427) This oesophageal 3D-TGA, therefore, has a key role to play: for example, in this study the 3D-TGA results suggest that patients OBX 70 and OBX 18 may not require the addition of Epirubicin to the Cisplatin/5-FU doublet to achieve sensitivity, while patient OBX 71 may require triplet ECF chemotherapy to accomplish chemo-sensitivity (Figure 37). The oesophageal 3D-TGA not only allows identification of patients who will potentially not benefit from the SOC chemotherapy, but those that may benefit from a tailored chemotherapy regimen, with reduced exposure to unnecessary or ineffective drugs and their associated side-effects.

6.4.4 Chemo-sensitivity was unchanged pre and post neoadjuvant chemotherapy

The absence of change in chemo-sensitivity between chemo-naïve and matched chemo-exposed patient samples was initially surprising, since the neoadjuvant chemotherapy might be expected to select for chemo-resistant clones. However, the pre- and post-treatment samples tested were all from patients in which the primary tumours were graded TRG 4-5 and therefore

already chemo-resistant. The 3D-TGA result is thus reflective of the clinical observation that patients who do not respond to neoadjuvant chemotherapy (with a TRG of 4-5) do not have improved survival outcomes with further rounds of the same chemotherapy post-operatively (57, 428). Although there was no material change in chemo-sensitivity, three of the five patients who had samples obtained pre- and post-chemotherapy (including one patient with 2 biopsy samples taken) had mismatched CD44/ ALDH expression pre- and post-chemotherapy. This could be influenced by clonal selection following exposure to neoadjuvant chemotherapy, and may also be indicative of the time interval and spatial heterogeneity within the tumour tissue itself.

6.4.5 Novel Drug Assessment: Panobinostat

The 3D-TGA can also be used to assess novel drugs, alone or in combination with SOC, across a panel of individual patient cancer cells allowing evaluation of the potential clinical impact across the spectrum of that disease type, ultimately for potential translation into clinical practice.

I tested Panobinostat in the oesophageal 3D-TGA alone, and in combination with ECF because it has been shown to potentiate the action of anthracyclines (e.g. Epirubicin),(285) which are part of the current SOC therapy. The strikingly improved efficacy against oesophageal tumours in our 3D-TGA, shown by combining Panobinostat with the SOC treatment is an exciting prospect. It converted 50% of the previously chemotherapy resistant patient tumour samples into chemo-sensitive responders, suggesting that a future clinical regimen with a HDACi such as Panobinostat, may provide an avenue for more successful global treatment of this frequently chemo-resistant tumour type.

6.4.6 Evaluation of cancer stroma targeting PDE5i drugs

In oesophageal cancer, the TME and tumour stroma particularly, is suspected of playing a key role in promoting drug resistance (429, 430) I therefore sought to evaluate the effectiveness of the PDE5i drug Vardenafil, which have been reported to interfere with the function of stromal component of the TME (291).

Our results showed that that addition of PDE5i to ECF SOC chemotherapy significantly reduces the chemo-resistance seen in the 3D-TGA with hMSC co-culture, but this occurs in an individual patient cancer sample specific manner.

Whilst an overall significant decrease in chemo-resistance and the eye-catching headline that "adding PDE5i to the SOC chemotherapy regimen converts 75% of chemo-resistant OAC into chemo-sensitive tumours" is true for absolute values with respect to the proposed threshold for chemo-resistance, it is important to consider these results for individual patients and without overlap of the individual IC_{50} confidence intervals even if the IC_{50} value itself crosses the chemo-sensitivity threshold.

As well as PDE5i only significantly altering chemo sensitivity in half of the samples with co-culture induced chemo-resistance, it is important to note that chemo-resistance to ECF in the 3D-TGA was not always hMSC mediated, and addition of PDE5i to ECF chemotherapy also does not appear to have a material effect on chemo-sensitivity where the hMSC co-culture is not significantly increasing chemo-resistance.

Significant changes in the SOC ECF IC_{50} (whether driven by mesenchymal co-culture or addition of PDE5i) are not simply patient related, but cancer sample specific, which underlines the complexity of the causes of chemo-resistance in OG cancer and the likely multi-factorial nature of the various resistance

pathways. There is even some variation amongst the same patient's cancer samples, and it is unclear why this occurs. It may reflect clonal selection following exposure to neoadjuvant chemotherapy or the *ex vivo* culture conditions, or may be indicative of spatial heterogeneity within the tumour tissue itself when sampling occurred. Therefore, although the overall effect of PDE5i is statistically significant, it is not universal and should be regarded as having a patient-specific and cancer-specific action.

When co-cultured in the 3D-TGA with tumour cells, the hMSCs are hypothesised to undergo a degree of phenotypic change through physical and paracrine interactions as previously described, and become more CAF-like, and demonstrate the properties of activated cancer-associated fibroblasts, which have been shown to have a direct effect on the malignant properties of the tumour(110, 431) such as invasion (111) and importantly chemotherapy resistance (130, 132, 134, 139). PDE5i drugs are thought to prevent the development of stromal cells into activated cancer-associated fibroblasts(291), thus preventing the CAF-induced chemo-resistance.

The promising *ex vivo* action of PDE5i demands further evaluation. This could be studied in future 3D-TGA experiments by monitoring the expression of a-SMA by hMSCs indicating any conversion to an activated-CAF phenotype on co-culture(111), and how this compares with hMSC driven chemo resistance. This expression of a-SMA could be used as a baseline for comparison for a repeated the assay in the presence of PDE5i, for both cancers which are thought to respond and to be resistant to the effects of PDE5i with ECF chemotherapy, and compare this to the a-SMA levels and resultant chemo-resistance.

PDE5i administration in erectile dysfunction and pulmonary hypertension has an excellent clinical record for safe and routine use, with few side effects(432, 433). This would appear to make the drug ideal for re-purposing for use in the treatment of OAC, vastly reducing the normal costs of bringing a new pharmaceutical agent into routine practice.

Currently there is no published human toxicity data for PDE5i administration in conjunction with chemotherapy, as these drugs are not routinely prescribed together. However, in animal studies, there are reports of cardio-vascular toxicity when Vardenafil administered in conjunction with other classes of chemotherapy agents(434). I therefore chose to examine the tolerability and toxicity of PDE5i in conjunction with the SOC for OG cancer in a modelled *in vivo* environment, using patient-derived xenografts. As this following *in vivo* investigation was not part of this *ex vivo* doctoral research into the '*Ex Vivo* Modelling Of Oesophago-Gastric Cancer', the results of this *in vivo* toxicity study are not enclosed and can be provided on request.

6.4.7 Tumour Stroma

The close-to-patient OG cancer cells display increased growth and chemo-resistance within the 3D-TGA in the presence of hMSCs, which would suggest that tumour-stroma interactions are an important part of the 3D TME. This is in line with experience published throughout the literature with 3D cell culture, where it has been shown that co-culture of OG adenocarcinoma cells with stromal cells results in greater establishment and reduced apoptosis(435), and indeed many of these advanced models (with active formation of intestinal epithelial sphere like organoids) are fibroblast dependant(436, 437). Notably, at extended growth time points, viable intestinal tissue was obligatorily associated with a robust underlying

stroma (437). However, it is known from 2D tissue culture that different primary patient cells grow and develop at different rates, and similar evidence from breast cancer would suggest that 3D TME cell growth, and its establishment and enhanced by a supporting hMSC stroma, is cell line dependant(102).

Tumour stromal cells have been shown to be vitally involved in key aspects of tumour cell functionality such as tumour growth, carcinoma progression, epithelial-mesenchymal transition, angiogenesis, invasion and metastasis(104, 117). Evidence shows that hMSC selectively home to tumours, where they contribute to the formation of tumour-associated stroma (116). These migrating hMSCs, and those from adjacent stromal tissue layers, can be demonstrated to change in morphology to the CAF phenotype (115, 435) and not only exhibit the same functional properties as CAFs promoting tumour progression, but also have similar gene expression profiles as the host CAFs (120). As a result, hMSCs are frequently used as a uniform and constant source of CAFs for the modelling of tumour-stromal interactions, allowing the study of the significant role that stromal support has to play within the TME, and interplay between the cell types (117-120). Studies of the *in vitro* TME have shown the key functional role of this cellular stromal TME component in epithelial-mesenchymal transition(104) driving malignant invasion(118) and promoting metastasis(117). The crucial role played by CAFs in the promotion of carcinogenesis is mediated by a variety of growth factors known to be secreted by these cells in the tumour stroma (438). This includes the growth factor HGF and also TGF-beta (which has a predominantly stromal expression pattern when mediating OAC epithelial-mesenchymal transition) in oesophago-gastric carcinoma (439, 440). This

therefore make CAFs an ideal target for potential chemotherapeutic strategies(441).

As part of this thesis I have not investigated any potential phenotypic change displayed by hMSCs when co-cultured in 3D with the epithelial cancer cells. This could be done by using IHC pre and post culture to look for expression a-SMA which may signal an adaptation to a CAF type phenotype. However, the origin of the CAF is not thought to be solely from migratory hMSCs but also from normal resident tissue fibroblasts (NAFs) and conversion of local cells (with endothelial-mesenchymal transition and epithelial-mesenchymal transition)(442). As hMSCs in co-culture with patient tumour cells may not effectively replicate the patient CAF population, in future it may be beneficial to use the patient's own tumour derived CAFs and introduce other cellular components to produce a more complex multicellular model in an attempt to reproduce the most representative TME as possible, with the closest representation of the patient itself. The potentially more representative modelled tumour's microenvironment could then be evaluated for increased collagen fibre length which is only mediated by a sub-set of SMA-positive CAFs, and its heterogeneous expression can be compared with the patient's primary cancer and clinical outcomes, where it correlates with poor patient survival (443).

However, the use of mCherry labelled hMSCs throughout all patient 3D-TGAs has the advantage of being a constant cell type throughout all of the assays, removing inter-variability and a potential confounding factor. Their growth can also be measured objectively, thereby allowing an assessment of the individual cellular parts of the model, and specifically the growth of the patient's epithelial tumour cells in response to chemo-therapy. It is also distinct component and reproducible across all the assays

and between patients allowing variations in the 3D-TGA assay results to be objectively and systematically examined, without confusion from confounding unmeasurable growth from another cell type.

It is a fundamental requirement for basic drug development, toxicology and high throughput screening that the culture model used should correspond with a reproducible and clinically significant outcome. This was not reliably the case with traditional 2D tissue culture models. However, the frequently held belief that a 3D matrix is better for modelling a more realistic cell physiology simply because it is 3D, can result in models producing data which is 3D matrix-specific but not necessarily *in vivo* relevant, and therefore the purpose of many of the 3D cell culture methods remain in question (158). Therefore, it is vital that these new 'more realistic' multi-cellular 3D models undergo the necessary validation against *in vivo* markers and clinical outcomes, for any results from the 3D model to be considered relevant. Whilst this has been performed with respect to drug sensitivity data the OG 3D-TGA model of the TME is admittedly simplistic using a single cell type to represent the multi-cellular stromal compartment of the OG TME, which in particular includes the immune infiltrate (e.g. T-cells and macrophages) and vascular endothelial cells(444). Whilst the use of hMSCs alone is clearly an incomplete representation, it is a starting point none-the-less, and despite its conceded oversimplification has shown in this study to have a significant effect upon both 3D tumour growth and chemo-sensitivity analyses.

Further development of 3D cancer models with a representative TME would need to consider the relevant components and their contributions to chemo-resistance. These TME can be grouped

into mesenchymal cellular components, haematopoietic cellular components and non-cellular components (extracellular matrix including the basement membrane which is rich in collagen, laminin and fibronectin and the interstitial matrix which is rich in proteoglycans and glycoproteins) which is attempted to be partially represented by Cultrex BME in our 3D models(149, 401). The mesenchymal cellular component (fibroblasts, hMSCs and endothelial cells) have all been shown to help develop a tumour niche and support cancer progression(445), (and endocytes in promoting malignant neo-angiogenesis(446)). We already have a modelled representation of the mesenchymal cell component thought the inclusion of hMSCs, however it would be ideal to improve this by the integrated use of patient's own CAFs (as previously discussed). The haematopoietic cellular component (the myeloid and lymphoid cells from the bone marrow e.g. T-cells, B-cells, macrophages and neutrophils) have been shown to both promote tumour development(447, 448) and elimination(449), and are a source of much recent interest with the very exciting recent advances made with the novel immunotherapy targeting drugs(450). There is evidence that this haematopoietic component of the TME may also be an important future therapeutic target in oesophageal cancer, with markers of immune checkpoint modulation (such as programmed death-1 and programmed death ligand-1) highly expressed(444), which suggests that novel immune-modulating antibody drugs (e.g. CTLA-4 and PD-1 inhibitors) may hold promise. Future modelling of this immune cellular component of the TME in our OG 3D-TGA would therefore be an important step forward and methods could be adapted from breast cancer where 3D culture systems including T-cells and natural killer cells have already been established(451).

6.5 Limitations and Opportunities

There are a number of potential limitations to the methodology that has been used in this study, which need to be appreciated to allow a fuller understanding and interpretation of the results.

6.5.1 Evaluation of close-to-patient OG cancer cell lines

There are limitations to the accuracy of the molecular biological characterisation performed within this study of the individual patient cancer cell lines. Whilst IHC was instructive of cell type as an adenocarcinoma, flow cytometry with HLA staining demonstrating human origin, and xenograft formation indicating malignant phenotype, it would have been highly beneficial to have performed an more definitive assessment of the cell derivation with a genomic based technique such as short tandem repeat analysis proving cell lineage from the original patient tissue.

Although the individual patient cell lines prior to engraftment were HLA stained, the subsequent xenografts were not. Despite this oversight, the xenografts were characterised with mono-clonal human-specific antibodies (such as EpCam clone Ber-EP4 and CD44 clone DF1485) demonstrating that the xenograft tumours were indeed of human and not murine origin.

Whilst the IHC and HLA staining is helpful, only a minority of the patient cell lines formed xenografts. Although the 15-25% engraftment success rate is in line with the literature, this raises questions about the malignant phenotype of >75% that did not engraft easily. It would be informative to have investigated these patient derived cell lines that did not engraft further with other laboratory techniques such as invasion and migration assays. However whilst this would have been enlightening if the patient cell lines demonstrated these characteristics, this would not have provided definitive evidence of malignant phenotype as not all

cancer cell lines (e.g. MCF7s) show laboratory evidence of invasion and migration.

Of note a minority of the patients in this study were also enrolled in the OCCMAS trial where whole genome sequencing was performed on their tumour samples. Fortunately some of the matching close-to-patient *in vitro* cell lines (established in this study) also underwent the whole genome sequencing as part a parallel study and were shown to closely resemble the original patient tumour (101). The current plan (as funds allow) is to continue this whole genome sequencing work of the resection matched close-to-patient *in vitro* cell lines, and then in this limited number of cases where matched sequencing data from tissue is available, to verify and then examine the mutations which are present.

The lack of definitive genetic evidence for the origin and character of the whole cohort of individual patient *in vitro* cell lines means that the cancer cell cluster establishment methodology and chemotherapeutic effectiveness findings must be tempered with caution, and indeed any practical translation into clinical practice could not be based upon IHC evidence alone.

The ideal option for future continuation of this work would be to perform a mutational analysis of the parent tumour and then match this to the *in vitro* cell line. This would not only provide firm evidence of the character and phenotype, but also allow an in-depth examination of the clone of cells which have preferentially proliferated *in vitro*, and whether this mutational signature is subsequently persevered through both the passaging and freezing process, but also following exposure to the clinical chemotherapeutics.

6.5.2 Tumour heterogeneity

During initial tumour sampling from the patient at OGD, I only sampled a small part of the surface of the main tumour and never any lymph nodes, and therefore have potentially only developed a model of a certain sub-population of the whole disease burden. Currently in OG cancer we have no clear understanding of how the tumour clones will alter between the tumour primary, tumour lymph nodes and any distant metastases, or whether this has any effect on their relative chemo-sensitivity. But we do know from other solid organ malignancies clonal development and subsequent expansion is different in the primary malignant mass, and the metastases, and that this evolves over time in response to environmental pressures, eventually leading to multiple and genetically almost completely different tumour clones in the different locations in a given patient.(452, 453) The heterogeneity of disseminated disease could therefore potentially explain the frequently poor response seen to therapy at this advanced stage, and also could explain why tumour biomarkers from the primary tumour struggle to individually predict prognosis or chemo-therapeutic sensitivity in patients with metastatic disease(454). However, new evidence had recently suggested that the functional driving mutations and clonal selection occurs before the onset of cancer dissemination, and not in the later arising sub-clones, and that the intra-tumoural heterogeneity seen is mostly non-functional passenger mutations. (455) It is suggestive that a key mutation acquired early in a tumours natural history is plasticity, and that the phenotypic heterogeneity observed in the cancer is the ability to respond and change to different challenges (such as areas of hypoxia) without the need for genetic change. This plasticity may also extend to multi-drug chemo-resistance and manifest differently according to the effect of altered tumour

micro-environments and different growth pressures applied by the chemotherapeutic toxicity.

The current method of individual patient OG cancer cultures and 3D-TGA pharmaceutical evaluation is designed to evaluate the primary tumour mass, and was measured against the clinical response of the primary mass, however over half of the patients had lymph node metastases. It would therefore be advantageous in future to sample and grow cells from the tumour lymph nodes where present and separately examine the chemo-sensitivity of these populations. This is one of the key advantages of this methodological technique; as not only can the tumour plasticity be challenged and potential phenotypic changes occur by culturing in an *ex vivo* TME, but the tumour can be sampled and tested from various locations, at multiple chronological points, thereby enabling assessment of changes in chemotherapeutic resistance profiles so that chemotherapy regimens could be altered accordingly.

It is unclear however, whether the heterogeneity of the tumour cell clones is lost or maintained over the subsequent process of cellular establishment and expansion in *ex vivo* feeder cell culture, prior to growth in 3D as cancer cell clusters. This lack of proven heterogeneity and correlation with the host tissue is one of the criticisms of this technique, and although there will be some clonal selection pressure during the *ex vivo* establishment and passaging it is unclear how extensive this is (as it has been shown to be remarkably limited in both breast(456) and colorectal cancer(457)), or how any clonal selection affects the overall assessment of apparent chemo-resistance. The chemo-sensitivity of the dominant tumour clones which establish and grow *ex vivo* appear to correlate correctly with the clinical chemotherapeutic response in this study, and therefore the

heterogeneity of chemotherapeutic sensitivity within the primary tumour mass may not be as vital as the apparent differences seen between the metastatic populations.

6.5.3 Assessment of clinical response to chemotherapy

Histological tumour regression grade reflects the broad variation of tumour response to chemotherapy, rather than the crude TRG grouping into response/no-response used in this study. There has been recent evidence to show that OG tumours graded histopathologically as TRG 3 in response to ECF chemotherapy may have overall survival benefits that are more similar to TRG 4-5 cancers (458), rather than TRG 1-2 cancers, as originally thought (426, 459). Indeed, Mandard TRG 3 histopathological grading does not indicate as robust a degree of chemo-response as TRG 1 & 2. However, the definition of TRG 3 is 'fibrosis predominates' with chemotherapy therefore appearing to provide some benefit, and therefore in this study of chemotherapy activity and sensitivity TRG3 has been has been grouped with TRG 1-2, representing chemo-sensitivity as it is elsewhere in the literature (426, 459). Whilst this maybe a crude grouping solution, I felt it was preferred to grouping TRG 3 with the non-response group of TRG 4-5 as clearly there is chemo-sensitivity, even if the tumour is not fully chemo-sensitive to the ECF combination.

Using histopathological TRG as a routine stand-alone marker of biological response to chemotherapy is an acceptable method of judging primary tumour response. However, it does not address the response of any nodal metastases, which potentially as different tumour clones, may respond differently. Recently two studies have highlighted the importance of nodal down staging following neoadjuvant chemotherapy as an important marker of response to chemotherapy (63, 460). Indeed they show that

nodal down-staging in conjunction with TRG can be a more powerful tool and may identify patients without a definite TRG response who might still benefit from further chemotherapy. Furthermore, systemic chemotherapy also treats micro-metastases, as proven by the reduction in metastatic disease in chemotherapy responders (460), which is not evaluated by TRG.

6.5.4 Evaluation of *ex vivo* chemo-sensitivity

The judgement of whether one of the close-to-patient cell cultures within the 3D model was deemed chemo-sensitive or chemo-resistant is based upon some broad assumptions that can be questioned.

Firstly, the concentrations of chemotherapy administered to individual patients are variable according to the imprecise BSA calculations and are varied again once undergoing metabolism and excretion and again varied at intra-tumoural levels due to tissue penetration. This enormous scope for individual patient variation of peak serum concentration of chemotherapy has not been scrutinized and a single averaged mean peak serum concentration is used for all patients to compare with the 3D-TGA model concentrations. Indeed, the validity of this comparative method can be also questioned, as I am comparing individual patient modelled chemo-sensitivities with individual clinical responses to chemotherapy, but using averaged chemotherapy concentrations as the peak values, rather than the peak value the individual patient is actually exposed to.

Secondly, the CMax is a reflection of the peak serum concentration of the drug and therefore the highest concentration that could potentially be delivered to the tumour in the patient. So when translated into the static *ex vivo* assay (although the CMax is higher than what would be consistently experienced *in vivo*) this represents an accurate threshold above

which any remaining *ex vivo* live tumour cells could be confidently considered resistant, with comparison *in vivo* scenario. However, using this approach a patient's tumours could be considered sensitive to chemotherapy, when the *in vivo* reality is a consistently lower plasma concentration of chemotherapy, which results in the patient's tumour not actually responding to the chemotherapy. In attempt to partially adjust for this, a 10% error bar was placed around the deemed peak plasma concentration, but the results that fall within this zone should still be interpreted with caution and these patients could alternatively be termed a 'potential partial responder' to chemotherapy.

Thirdly, the concept of IC_{50} as an accepted level for adequate chemo-toxicity is arbitrary. This presumes that 50% cytotoxicity is a complete response to the chemotherapeutic exposure. Whilst there must be 'deemed cut-off level' for analysis of toxicity, it is unclear how this relates to clinical cytotoxicity and whether IC_{30} or IC_{10} would be more relevant value which would result in cytotoxicity and tumour shrinkage *in vivo*.

Fourthly, many of the modelled ECF chemo-resistance values lay only just either side of the IC_{50} value, and so although I employed an arbitrary 10% SD either side of the IC_{50} value this leaves a very small margin for these values being correct or incorrect evaluations of chemo-sensitivity. Indeed with the study sample size so small (n=9) there is potential that these evaluated culture chemo-sensitivity results (suggesting that the cultured cells are 'just chemo-sensitive' or 'just chemo-resistant') are an anomalous result and there is no true predictive value in this assay, especially given that the chemo-sensitivity profile was altered between sensitive and resistance, without a dramatic alteration in the IC_{50} value, by the addition of hMSCs.

6.5.5 Opportunities for future work

This system for growing individual patient cancer cells and modelling them in 3D, opens up many new exciting opportunities for future study of OG cancer and advancing clinical care.

A comparison of gene expression patterns between the tissues, close-to-patient cancer cultures and PDX models would provide an excellent insight into the similarity between the original patient cells and those present within the tumour models, and also start to shed some light on the maintenance of OG tumour heterogeneity in these models.

Improving and refining the engraftment rate of the PDX tumours is a key future goal and will open yet another avenue for scientific investigation of OG tumour biology and pharmacological evaluation. Close-to-patient cell cultures retrovirally transduced to express D-Luciferin will allow orthotopic *in vivo* PDX studies via bioluminescent imaging, and preliminary work in this area has been performed.

The 3D models themselves can be refined as previously discussed, firstly using individual patient CAFs (which I have for approx. 50% of the cancer-cell-cultures) in place of (or in combination with) the hMSCs as part of the tumour stroma.

It would be ideal to be able to obtain individual patient chemotherapy mean peak serum concentration levels to allow direct correlation with the patient's tumour model so that chemotherapy exposure was accurately matched.

However, despite the previously outlined potential flaws with direct clinical correlation, this 3D model's chemo-response already accurately reflects individual patients' clinical chemo-sensitivity. This research therefore needs evaluation across a much wider patient cohort within the setting of a clinical trial,

and if this assay then continues to be predictive, it could potentially be used to routinely guide individual patient therapy in the clinic, with the avoidance of unnecessary chemotherapy or administration of tailored chemotherapy for individual patient benefit.

6.6 Research Conclusions

I present here the first published evidence of a reliable technique to establish individual close-to-patient OAC cells and grow them in a TME-relevant assay, without having to genetically induce immortality (e.g. using a telomerase approach(461, 462)). Although requiring careful attention to detail, the method does not require specialised equipment or materials found outside of a normal tissue culture laboratory, and could be scaled to high-throughput processing,(239) to screen for novel chemotherapeutics effective against this commonly resistant carcinoma. As well as use studying chemo-resistance, there are many other promising applications for 3D culture of primary cells including the cell biology of individual cancers, their similarities, cellular interactions and the relationship to the phenotypical heterogeneity of the disease as a whole.

Other techniques such as organotypic modelling,(106, 237) xenografts, and spheroid culture(369, 463) have all been attempted to study oesophageal cancer in a more relevant setting, and in some cases using cancer cells taken directly from the patient. However, all of these above models have critical differences with the *in vivo* disease and none provides an ideal system reflecting the complex 3D structure of the clinical tumour and its components whilst enabling practical method for evaluation and study of the disease characteristic or functional mechanisms (174, 230). The popular organoid culture system has shown much promise for modelling the stem cell niche in colorectal cancer.(147) However, it requires media supplementation to re-capitulate the environment of the Lgr5 stem-cell niche and Wnt pathway, which are not present in oesophageal cancer, and also does not incorporate any component of the tumour stroma.(464) I have demonstrated the importance of including human stromal mesenchymal cells in the

context of studying drug sensitivity, and this is frequently missing in cancer models used for drug discovery (464).

I believe that the 3D-TGA model described here-in, using close-to-patient epithelial tissue, a humanised TME, biologically-active 3D matrix and mesenchymal stromal support cells, reproduces some of the key micro-environmental components of the human tumour. Other cell types (for example, cells of the immune system and vascular endothelial cells) may also provide important signals in the case of some individual tumours, so further refinement will be required to model other influences on drug sensitivity or oesophageal tumour biology. However, the correlation between the *in vitro* 3D-TGA assessment of chemo-sensitivity and the observed clinical response described here, demonstrates that in its current format, it is already a useful tool and this is a significant step forward towards the goal of delivering personalised health care and personalised oncological therapy in particular. However, to demonstrate its clinical applicability for providing tailored treatment for individual patients, our findings will require confirmation in an expanded cohort.

In its current format, this novel method of expanding individual patient oesophageal cancer cells in the laboratory and using them for drug screening, has potential for both reducing the use of animals in the early stages of drug development (due to availability of a more clinically-relevant *in vitro* assay), and potential to have a significant impact on clinical outcomes by enabling accurate identification of new treatments, in a more cost-effective manner, including those targeting the stroma.

7 References

1. Parkin DM, Bray F, Ferlay J, Pisani P. Global cancer statistics, 2002. CA: a cancer journal for clinicians. 2005;55(2):74-108.
2. Kamangar F, Dores GM, Anderson WF. Patterns of cancer incidence, mortality, and prevalence across five continents: defining priorities to reduce cancer disparities in different geographic regions of the world. Journal of clinical oncology : official journal of the American Society of Clinical Oncology. 2006;24(14):2137-50.
3. Cancer Research UK http://www.cancerresearchuk.org/health-professional/cancer-statistics. Oesophageal cancer statisticsaccessed January 2016 [
4. Cunningham D, Allum WH, Stenning SP, Thompson JN, Van de Velde CJ, Nicolson M, et al. Perioperative chemotherapy versus surgery alone for resectable gastroesophageal cancer. The New England journal of medicine. 2006;355(1):11-20.
5. Fareed KR, Ilyas M, Kaye PV, Soomro IN, Lobo DN, Parsons SL, et al. Tumour regression grade (TRG) analyses in patients with resectable gastro-oesophageal adenocarcinomas treated with platinum-based neoadjuvant chemotherapy. Histopathology. 2009;55(4):399-406.
6. Fareed KR, Kaye P, Soomro IN, Ilyas M, Martin S, Parsons SL, et al. Biomarkers of response to therapy in oesophago-gastric cancer. Gut. 2009;58(1):127-43.
7. Allum WH, Blazeby JM, Griffin SM, Cunningham D, Jankowski JA, Wong R, et al. Guidelines for the management of oesophageal and gastric cancer. Gut. 2011;60(11):1449-72.
8. Lao-Sirieix P, Caldas C, Fitzgerald RC. Genetic predisposition to gastro-oesophageal cancer. Current opinion in genetics & development. 2010;20(3):210-7.
9. Statistics OfN. Cancer registration statistics 2014 (released 2016), England Statistical bulletins. http://wwwonsgovuk/ons/rel/vsob1/cancer-statistics-registrations--england--series-mb1-/indexhtml. 2013.
10. UK CR. Oesophageal cancer incidence statistics. Cancer Research UK, website accessed January 2017. 2013.
11. Brown LM, Devesa SS, Chow WH. Incidence of adenocarcinoma of the esophagus among white Americans by sex, stage, and age. Journal of the National Cancer Institute. 2008;100(16):1184-7.
12. Blot WJ, Devesa SS, Kneller RW, Fraumeni JF, Jr. Rising incidence of adenocarcinoma of the esophagus and gastric cardia. JAMA : the journal of the American Medical Association. 1991;265(10):1287-9.
13. Pera M. Trends in incidence and prevalence of specialized intestinal metaplasia, barrett's esophagus, and adenocarcinoma

of the gastroesophageal junction. World journal of surgery. 2003;27(9):999-1008; discussion 6-8.
14. Romano M, Ricci V, Zarrilli R. Mechanisms of disease: Helicobacter pylori-related gastric carcinogenesis--implications for chemoprevention. Nature clinical practice Gastroenterology & hepatology. 2006;3(11):622-32.
15. Vaughan TL, Davis S, Kristal A, Thomas DB. Obesity, alcohol, and tobacco as risk factors for cancers of the esophagus and gastric cardia: adenocarcinoma versus squamous cell carcinoma. Cancer epidemiology, biomarkers & prevention : a publication of the American Association for Cancer Research, cosponsored by the American Society of Preventive Oncology. 1995;4(2):85-92.
16. Wild CP, Hardie LJ. Reflux, Barrett's oesophagus and adenocarcinoma: burning questions. Nature reviews Cancer. 2003;3(9):676-84.
17. Merry AH, Schouten LJ, Goldbohm RA, van den Brandt PA. Body mass index, height and risk of adenocarcinoma of the oesophagus and gastric cardia: a prospective cohort study. Gut. 2007;56(11):1503-11.
18. Corley DA, Kubo A, Levin TR, Block G, Habel L, Zhao W, et al. Abdominal obesity and body mass index as risk factors for Barrett's esophagus. Gastroenterology. 2007;133(1):34-41; quiz 311.
19. Corley DA, Kubo A, Zhao W. Abdominal obesity and the risk of esophageal and gastric cardia carcinomas. Cancer epidemiology, biomarkers & prevention : a publication of the American Association for Cancer Research, cosponsored by the American Society of Preventive Oncology. 2008;17(2):352-8.
20. Murray CJ, Richards MA, Newton JN, Fenton KA, Anderson HR, Atkinson C, et al. UK health performance: findings of the Global Burden of Disease Study 2010. Lancet. 2013;381(9871):997-1020.
21. NICE. Referral for suspected cancer (CG27). http://wwwniceorguk/CG027#tabs-nohdr-2. 2005;Clinical guidelines, CG27.
22. Hallissey MT, Allum WH, Jewkes AJ, Ellis DJ, Fielding JW. Early detection of gastric cancer. Bmj. 1990;301(6751):513-5.
23. Bytzer P, Hansen JM, Schaffalitzky de Muckadell OB, Malchow-Moller A. Predicting endoscopic diagnosis in the dyspeptic patient. The value of predictive score models. Scandinavian journal of gastroenterology. 1997;32(2):118-25.
24. Bramble MG, Suvakovic Z, Hungin AP. Detection of upper gastrointestinal cancer in patients taking antisecretory therapy prior to gastroscopy. Gut. 2000;46(4):464-7.
25. Wayman J, Hayes N, Griffin SM. The response of early gastric cancer to proton-pump inhibitors. The New England journal of medicine. 1998;338(26):1924-5.

26. Biondi A, Hyung WJ. Seventh edition of TNM classification for gastric cancer. Journal of clinical oncology : official journal of the American Society of Clinical Oncology. 2011;29(32):4338-9; author reply 40-2.
27. Talsma K, van Hagen P, Grotenhuis BA, Steyerberg EW, Tilanus HW, van Lanschot JJ, et al. Comparison of the 6th and 7th Editions of the UICC-AJCC TNM Classification for Esophageal Cancer. Annals of surgical oncology. 2012;19(7):2142-8.
28. Stahl M, Budach W, Meyer HJ, Cervantes A, Group EGW. Esophageal cancer: Clinical Practice Guidelines for diagnosis, treatment and follow-up. Annals of oncology : official journal of the European Society for Medical Oncology / ESMO. 2010;21 Suppl 5:v46-9.
29. Smalley SR, Benedetti JK, Haller DG, Hundahl SA, Estes NC, Ajani JA, et al. Updated analysis of SWOG-directed intergroup study 0116: a phase III trial of adjuvant radiochemotherapy versus observation after curative gastric cancer resection. Journal of clinical oncology : official journal of the American Society of Clinical Oncology. 2012;30(19):2327-33.
30. Walsh TN, Noonan N, Hollywood D, Kelly A, Keeling N, Hennessy TP. A comparison of multimodal therapy and surgery for esophageal adenocarcinoma. The New England journal of medicine. 1996;335(7):462-7.
31. Tepper J, Krasna MJ, Niedzwiecki D, Hollis D, Reed CE, Goldberg R, et al. Phase III trial of trimodality therapy with cisplatin, fluorouracil, radiotherapy, and surgery compared with surgery alone for esophageal cancer: CALGB 9781. Journal of clinical oncology : official journal of the American Society of Clinical Oncology. 2008;26(7):1086-92.
32. van Hagen P, Hulshof MC, van Lanschot JJ, Steyerberg EW, van Berge Henegouwen MI, Wijnhoven BP, et al. Preoperative chemoradiotherapy for esophageal or junctional cancer. The New England journal of medicine. 2012;366(22):2074-84.
33. Allum WH, Stenning SP, Bancewicz J, Clark PI, Langley RE. Long-term results of a randomized trial of surgery with or without preoperative chemotherapy in esophageal cancer. Journal of clinical oncology : official journal of the American Society of Clinical Oncology. 2009;27(30):5062-7.
34. Kelsen DP, Ginsberg R, Pajak TF, Sheahan DG, Gunderson L, Mortimer J, et al. Chemotherapy followed by surgery compared with surgery alone for localized esophageal cancer. The New England journal of medicine. 1998;339(27):1979-84.
35. Ychou M, Boige V, Pignon JP, Conroy T, Bouche O, Lebreton G, et al. Perioperative chemotherapy compared with surgery alone for resectable gastroesophageal adenocarcinoma: an FNCLCC and FFCD multicenter phase III trial. Journal of

clinical oncology : official journal of the American Society of Clinical Oncology. 2011;29(13):1715-21.
36. Stahl M, Walz MK, Stuschke M, Lehmann N, Meyer HJ, Riera-Knorrenschild J, et al. Phase III comparison of preoperative chemotherapy compared with chemoradiotherapy in patients with locally advanced adenocarcinoma of the esophagogastric junction. Journal of clinical oncology : official journal of the American Society of Clinical Oncology. 2009;27(6):851-6.
37. Choi AH, Kim J, Chao J. Perioperative chemotherapy for resectable gastric cancer: MAGIC and beyond. World journal of gastroenterology : WJG. 2015;21(24):7343-8.
38. Leong T, Smithers BM, Michael M, Gebski V, Boussioutas A, Miller D, et al. TOPGEAR: a randomised phase III trial of perioperative ECF chemotherapy versus preoperative chemoradiation plus perioperative ECF chemotherapy for resectable gastric cancer (an international, intergroup trial of the AGITG/TROG/EORTC/NCIC CTG). BMC cancer. 2015;15:532.
39. Seshacharyulu P, Ponnusamy MP, Haridas D, Jain M, Ganti AK, Batra SK. Targeting the EGFR signaling pathway in cancer therapy. Expert opinion on therapeutic targets. 2012;16(1):15-31.
40. Terashima M, Kitada K, Ochiai A, Ichikawa W, Kurahashi I, Sakuramoto S, et al. Impact of expression of human epidermal growth factor receptors EGFR and ERBB2 on survival in stage II/III gastric cancer. Clinical cancer research : an official journal of the American Association for Cancer Research. 2012;18(21):5992-6000.
41. Kim MA, Lee HS, Lee HE, Jeon YK, Yang HK, Kim WH. EGFR in gastric carcinomas: prognostic significance of protein overexpression and high gene copy number. Histopathology. 2008;52(6):738-46.
42. Gowryshankar A, Nagaraja V, Eslick GD. HER2 status in Barrett's esophagus & esophageal cancer: a meta analysis. Journal of gastrointestinal oncology. 2014;5(1):25-35.
43. Boku N. HER2-positive gastric cancer. Gastric cancer : official journal of the International Gastric Cancer Association and the Japanese Gastric Cancer Association. 2014;17(1):1-12.
44. Bang YJ, Van Cutsem E, Feyereislova A, Chung HC, Shen L, Sawaki A, et al. Trastuzumab in combination with chemotherapy versus chemotherapy alone for treatment of HER2-positive advanced gastric or gastro-oesophageal junction cancer (ToGA): a phase 3, open-label, randomised controlled trial. Lancet. 2010;376(9742):687-97.
45. Wang J, Saukel GW, Garberoglio CA, Srikureja W, Hsueh CT. Pathological complete response after neoadjuvant chemotherapy with trastuzumab-containing regimen in gastric cancer: a case report. J Hematol Oncol. 2010;3:31.

46. Safran H, Dipetrillo T, Akerman P, Ng T, Evans D, Steinhoff M, et al. Phase I/II study of trastuzumab, paclitaxel, cisplatin and radiation for locally advanced, HER2 overexpressing, esophageal adenocarcinoma. International journal of radiation oncology, biology, physics. 2007;67(2):405-9.
47. Lordick F, Kang YK, Chung HC, Salman P, Oh SC, Bodoky G, et al. Capecitabine and cisplatin with or without cetuximab for patients with previously untreated advanced gastric cancer (EXPAND): a randomised, open-label phase 3 trial. The lancet oncology. 2013;14(6):490-9.
48. Hurt CN, Nixon LS, Griffiths GO, Al-Mokhtar R, Gollins S, Staffurth JN, et al. SCOPE1: a randomised phase II/III multicentre clinical trial of definitive chemoradiation, with or without cetuximab, in carcinoma of the oesophagus. BMC cancer. 2011;11:466.
49. Shah MA, Jhawer M, Ilson DH, Lefkowitz RA, Robinson E, Capanu M, et al. Phase II study of modified docetaxel, cisplatin, and fluorouracil with bevacizumab in patients with metastatic gastroesophageal adenocarcinoma. Journal of clinical oncology : official journal of the American Society of Clinical Oncology. 2011;29(7):868-74.
50. Hong TS, Wo JY, Kwak EL. Targeted therapies with chemoradiation in esophageal cancer: development and future directions. Seminars in radiation oncology. 2013;23(1):31-7.
51. Ohtsu A, Shah MA, Van Cutsem E, Rha SY, Sawaki A, Park SR, et al. Bevacizumab in combination with chemotherapy as first-line therapy in advanced gastric cancer: a randomized, double-blind, placebo-controlled phase III study. Journal of clinical oncology : official journal of the American Society of Clinical Oncology. 2011;29(30):3968-76.
52. Cunningham D, Stenning SP, Smyth EC, Okines AF, Allum WH, Rowley S, et al. Peri-operative chemotherapy with or without bevacizumab in operable oesophagogastric adenocarcinoma (UK Medical Research Council ST03): primary analysis results of a multicentre, open-label, randomised phase 2-3 trial. The lancet oncology. 2017.
53. Young K, Smyth E, Chau I. Ramucirumab for advanced gastric cancer or gastro-oesophageal junction adenocarcinoma. Therap Adv Gastroenterol. 2015;8(6):373-83.
54. Wilke H, Muro K, Van Cutsem E, Oh SC, Bodoky G, Shimada Y, et al. Ramucirumab plus paclitaxel versus placebo plus paclitaxel in patients with previously treated advanced gastric or gastro-oesophageal junction adenocarcinoma (RAINBOW): a double-blind, randomised phase 3 trial. The lancet oncology. 2014;15(11):1224-35.
55. Fuchs CS, Tomasek J, Yong CJ, Dumitru F, Passalacqua R, Goswami C, et al. Ramucirumab monotherapy for previously treated advanced gastric or gastro-oesophageal junction

adenocarcinoma (REGARD): an international, randomised, multicentre, placebo-controlled, phase 3 trial. Lancet. 2014;383(9911):31-9.
56. Cunningham D, Starling N, Rao S, Iveson T, Nicolson M, Coxon F, et al. Capecitabine and oxaliplatin for advanced esophagogastric cancer. The New England journal of medicine. 2008;358(1):36-46.
57. Saunders JH, Bowman CR, Reece-Smith AM, Pang V, Dorrington MS, Mumtaz E, et al. The role of adjuvant platinum-based chemotherapy in esophagogastric cancer patients who received neoadjuvant chemotherapy prior to definitive surgery. Journal of surgical oncology. 2017;9999:1-9.
58. Fareed KR, Al-Attar A, Soomro IN, Kaye PV, Patel J, Lobo DN, et al. Tumour regression and ERCC1 nuclear protein expression predict clinical outcome in patients with gastro-oesophageal cancer treated with neoadjuvant chemotherapy. British journal of cancer. 2010;102(11):1600-7.
59. Mandard AM, Dalibard F, Mandard JC, Marnay J, Henry-Amar M, Petiot JF, et al. Pathologic assessment of tumor regression after preoperative chemoradiotherapy of esophageal carcinoma. Clinicopathologic correlations. Cancer. 1994;73(11):2680-6.
60. Becker K, Mueller JD, Schulmacher C, Ott K, Fink U, Busch R, et al. Histomorphology and grading of regression in gastric carcinoma treated with neoadjuvant chemotherapy. Cancer. 2003;98(7):1521-30.
61. Becker K, Fumagalli U, Mueller JD, Fink U, Siewert JR, Hofler H. Neoadjuvant chemotherapy for patients with locally advanced gastric carcinoma: effect on tumor cell microinvolvement of regional lymph nodes. Cancer. 1999;85(7):1484-9.
62. Guo K, Cai L, Zhang Y, Zhu JF, Rong TH, Lin P, et al. The predictive value of histological tumor regression grading (TRG) for therapeutic evaluation in locally advanced esophageal carcinoma treated with neoadjuvant chemotherapy. Chinese journal of cancer. 2012;31(8):399-408.
63. Noble F, Nolan L, Bateman AC, Byrne JP, Kelly JJ, Bailey IS, et al. Refining pathological evaluation of neoadjuvant therapy for adenocarcinoma of the esophagus. World journal of gastroenterology : WJG. 2013;19(48):9282-93.
64. Lordick F, Ott K, Krause BJ, Weber WA, Becker K, Stein HJ, et al. PET to assess early metabolic response and to guide treatment of adenocarcinoma of the oesophagogastric junction: the MUNICON phase II trial. The lancet oncology. 2007;8(9):797-805.
65. Downey RJ, Akhurst T, Ilson D, Ginsberg R, Bains MS, Gonen M, et al. Whole body 18FDG-PET and the response of esophageal cancer to induction therapy: results of a prospective

trial. Journal of clinical oncology : official journal of the American Society of Clinical Oncology. 2003;21(3):428-32.
66. Flamen P, Lerut A, Van Cutsem E, De Wever W, Peeters M, Stroobants S, et al. Utility of positron emission tomography for the staging of patients with potentially operable esophageal carcinoma. Journal of clinical oncology : official journal of the American Society of Clinical Oncology. 2000;18(18):3202-10.
67. Heeren PA, Jager PL, Bongaerts F, van Dullemen H, Sluiter W, Plukker JT. Detection of distant metastases in esophageal cancer with (18)F-FDG PET. Journal of nuclear medicine : official publication, Society of Nuclear Medicine. 2004;45(6):980-7.
68. Kato H, Miyazaki T, Nakajima M, Takita J, Kimura H, Faried A, et al. The incremental effect of positron emission tomography on diagnostic accuracy in the initial staging of esophageal carcinoma. Cancer. 2005;103(1):148-56.
69. Roedl JB, Blake MA, Holalkere NS, Mueller PR, Colen RR, Harisinghani MG. Lymph node staging in esophageal adenocarcinoma with PET-CT based on a visual analysis and based on metabolic parameters. Abdominal imaging. 2009;34(5):610-7.
70. Pan L, Gu P, Huang G, Xue H, Wu S. Prognostic significance of SUV on PET/CT in patients with esophageal cancer: a systematic review and meta-analysis. European journal of gastroenterology & hepatology. 2009;21(9):1008-15.
71. Omloo JM, van Heijl M, Hoekstra OS, van Berge Henegouwen MI, van Lanschot JJ, Sloof GW. FDG-PET parameters as prognostic factor in esophageal cancer patients: a review. Annals of surgical oncology. 2011;18(12):3338-52.
72. Rizk NP, Tang L, Adusumilli PS, Bains MS, Akhurst TJ, Ilson D, et al. Predictive value of initial PET-SUVmax in patients with locally advanced esophageal and gastroesophageal junction adenocarcinoma. Journal of thoracic oncology : official publication of the International Association for the Study of Lung Cancer. 2009;4(7):875-9.
73. van Heijl M, Omloo JM, van Berge Henegouwen MI, Hoekstra OS, Boellaard R, Bossuyt PM, et al. Fluorodeoxyglucose positron emission tomography for evaluating early response during neoadjuvant chemoradiotherapy in patients with potentially curable esophageal cancer. Annals of surgery. 2011;253(1):56-63.
74. van Heijl M, Phoa SS, van Berge Henegouwen MI, Omloo JM, Mearadji BM, Sloof GW, et al. Accuracy and reproducibility of 3D-CT measurements for early response assessment of chemoradiotherapy in patients with oesophageal cancer. European journal of surgical oncology : the journal of the European Society of Surgical Oncology and the British Association of Surgical Oncology. 2011;37(12):1064-71.

75. Ott K, Weber WA, Lordick F, Becker K, Busch R, Herrmann K, et al. Metabolic imaging predicts response, survival, and recurrence in adenocarcinomas of the esophagogastric junction. Journal of clinical oncology : official journal of the American Society of Clinical Oncology. 2006;24(29):4692-8.
76. Weber WA, Ott K, Becker K, Dittler HJ, Helmberger H, Avril NE, et al. Prediction of response to preoperative chemotherapy in adenocarcinomas of the esophagogastric junction by metabolic imaging. Journal of clinical oncology : official journal of the American Society of Clinical Oncology. 2001;19(12):3058-65.
77. Ilson DH, Minsky BD, Ku GY, Rusch V, Rizk N, Shah M, et al. Phase 2 trial of induction and concurrent chemoradiotherapy with weekly irinotecan and cisplatin followed by surgery for esophageal cancer. Cancer. 2012;118(11):2820-7.
78. Kauppi JT, Oksala N, Salo JA, Helin H, Karhumaki L, Kemppainen J, et al. Locally advanced esophageal adenocarcinoma: response to neoadjuvant chemotherapy and survival predicted by ([18F])FDG-PET/CT. Acta oncologica. 2012;51(5):636-44.
79. Wieder HA, Brucher BL, Zimmermann F, Becker K, Lordick F, Beer A, et al. Time course of tumor metabolic activity during chemoradiotherapy of esophageal squamous cell carcinoma and response to treatment. Journal of clinical oncology : official journal of the American Society of Clinical Oncology. 2004;22(5):900-8.
80. Gillham CM, Lucey JA, Keogan M, Duffy GJ, Malik V, Raouf AA, et al. (18)FDG uptake during induction chemoradiation for oesophageal cancer fails to predict histomorphological tumour response. British journal of cancer. 2006;95(9):1174-9.
81. Javeri H, Xiao L, Rohren E, Lee JH, Liao Z, Hofstetter W, et al. The higher the decrease in the standardized uptake value of positron emission tomography after chemoradiation, the better the survival of patients with gastroesophageal adenocarcinoma. Cancer. 2009;115(22):5184-92.
82. Vallbohmer D, Holscher AH, Dietlein M, Bollschweiler E, Baldus SE, Monig SP, et al. [18F]-Fluorodeoxyglucose-positron emission tomography for the assessment of histopathologic response and prognosis after completion of neoadjuvant chemoradiation in esophageal cancer. Annals of surgery. 2009;250(6):888-94.
83. Lorenzen S, von Gall C, Stange A, Haag GM, Weitz J, Haberkorn U, et al. Sequential FDG-PET and induction chemotherapy in locally advanced adenocarcinoma of the Oesophago-gastric junction (AEG): the Heidelberg Imaging program in Cancer of the oesophago-gastric junction during Neoadjuvant treatment: HICON trial. BMC cancer. 2011;11:266.
84. Monjazeb AM, Riedlinger G, Aklilu M, Geisinger KR, Mishra G, Isom S, et al. Outcomes of patients with esophageal cancer

staged with [(1)(8)F]fluorodeoxyglucose positron emission tomography (FDG-PET): can postchemoradiotherapy FDG-PET predict the utility of resection? Journal of clinical oncology : official journal of the American Society of Clinical Oncology. 2010;28(31):4714-21.
85. Murthy SB, Patnana SV, Xiao L, Rohren E, Hofstetter WL, Swisher SG, et al. The standardized uptake value of 18-fluorodeoxyglucose positron emission tomography after chemoradiation and clinical outcome in patients with localized gastroesophageal carcinoma. Oncology. 2010;78(5-6):316-22.
86. Wu AJ, Goodman KA. Positron emission tomography imaging for gastroesophageal junction tumors. Seminars in radiation oncology. 2013;23(1):10-5.
87. Lao-Sirieix P, Boussioutas A, Kadri SR, O'Donovan M, Debiram I, Das M, et al. Non-endoscopic screening biomarkers for Barrett's oesophagus: from microarray analysis to the clinic. Gut. 2009;58(11):1451-9.
88. Okines AF, Gonzalez de Castro D, Cunningham D, Chau I, Langley RE, Thompson LC, et al. Biomarker analysis in oesophagogastric cancer: Results from the REAL3 and TransMAGIC trials. European journal of cancer. 2013;49(9):2116-25.
89. Madhusudan S, Hickson ID. DNA repair inhibition: a selective tumour targeting strategy. Trends Mol Med. 2005;11(11):503-11.
90. Abbotts R, Thompson N, Madhusudan S. DNA repair in cancer: emerging targets for personalized therapy. Cancer Manag Res. 2014;6:77-92.
91. Abdel-Fatah T, Arora A, Gorguc I, Abbotts R, Beebeejaun S, Storr S, et al. Are DNA repair factors promising biomarkers for personalized therapy in gastric cancer? Antioxid Redox Signal. 2013;18(18):2392-8.
92. Doherty R, Madhusudan S. DNA Repair Endonucleases: Physiological Roles and Potential as Drug Targets. Journal of biomolecular screening. 2015;20(7):829-41.
93. Al-Attar A, Gossage L, Fareed KR, Shehata M, Mohammed M, Zaitoun AM, et al. Human apurinic/apyrimidinic endonuclease (APE1) is a prognostic factor in ovarian, gastro-oesophageal and pancreatico-biliary cancers. British journal of cancer. 2010;102(4):704-9.
94. Olaussen KA, Dunant A, Fouret P, Brambilla E, Andre F, Haddad V, et al. DNA repair by ERCC1 in non-small-cell lung cancer and cisplatin-based adjuvant chemotherapy. The New England journal of medicine. 2006;355(10):983-91.
95. Soria JC. ERCC1-tailored chemotherapy in lung cancer: the first prospective randomized trial. Journal of clinical oncology : official journal of the American Society of Clinical Oncology. 2007;25(19):2648-9.

96. Bradbury PA, Kulke MH, Heist RS, Zhou W, Ma C, Xu W, et al. Cisplatin pharmacogenetics, DNA repair polymorphisms, and esophageal cancer outcomes. Pharmacogenetics and genomics. 2009;19(8):613-25.
97. Kwon HC, Roh MS, Oh SY, Kim SH, Kim MC, Kim JS, et al. Prognostic value of expression of ERCC1, thymidylate synthase, and glutathione S-transferase P1 for 5-fluorouracil/oxaliplatin chemotherapy in advanced gastric cancer. Annals of oncology : official journal of the European Society for Medical Oncology / ESMO. 2007;18(3):504-9.
98. Arora A, Agarwal D, Abdel-Fatah TM, Lu H, Croteau DL, Moseley P, et al. RECQL4 helicase has oncogenic potential in sporadic breast cancers. The Journal of pathology. 2016;238(4):495-501.
99. Mo D, Fang H, Niu K, Liu J, Wu M, Li S, et al. Human Helicase RECQL4 Drives Cisplatin Resistance in Gastric Cancer by Activating an AKT-YB1-MDR1 Signaling Pathway. Cancer research. 2016;76(10):3057-66.
100. Cancer Genome Atlas Research N. Comprehensive molecular characterization of gastric adenocarcinoma. Nature. 2014;513(7517):202-9.
101. Secrier M, Li X, de Silva N, Eldridge MD, Contino G, Bornschein J, et al. Mutational signatures in esophageal adenocarcinoma define etiologically distinct subgroups with therapeutic relevance. Nature genetics. 2016;48(10):1131-41.
102. Sasser AK, Mundy BL, Smith KM, Studebaker AW, Axel AE, Haidet AM, et al. Human bone marrow stromal cells enhance breast cancer cell growth rates in a cell line-dependent manner when evaluated in 3D tumor environments. Cancer letters. 2007;254(2):255-64.
103. Katano T, Ootani A, Mizoshita T, Tanida S, Tsukamoto H, Ozeki K, et al. Gastric mesenchymal myofibroblasts maintain stem cell activity and proliferation of murine gastric epithelium in vitro. The American journal of pathology. 2015;185(3):798-807.
104. Giannoni E, Bianchini F, Masieri L, Serni S, Torre E, Calorini L, et al. Reciprocal activation of prostate cancer cells and cancer-associated fibroblasts stimulates epithelial-mesenchymal transition and cancer stemness. Cancer research. 2010;70(17):6945-56.
105. Zhang P, Lo A, Huang Y, Huang G, Liang G, Mott J, et al. Identification of genetic loci that control mammary tumor susceptibility through the host microenvironment. Scientific reports. 2015;5:8919.
106. Grugan KD, Miller CG, Yao Y, Michaylira CZ, Ohashi S, Klein-Szanto AJ, et al. Fibroblast-secreted hepatocyte growth factor plays a functional role in esophageal squamous cell carcinoma invasion. Proceedings of the National Academy of

Sciences of the United States of America. 2010;107(24):11026-31.
107. Horie M, Saito A, Mikami Y, Ohshima M, Morishita Y, Nakajima J, et al. Characterization of human lung cancer-associated fibroblasts in three-dimensional in vitro co-culture model. Biochemical and biophysical research communications. 2012;423(1):158-63.
108. Courrech Staal EF, Wouters MW, van Sandick JW, Takkenberg MM, Smit VT, Junggeburt JM, et al. The stromal part of adenocarcinomas of the oesophagus: does it conceal targets for therapy? European journal of cancer. 2010;46(4):720-8.
109. Courrech Staal EF, Smit VT, van Velthuysen ML, Spitzer-Naaykens JM, Wouters MW, Mesker WE, et al. Reproducibility and validation of tumour stroma ratio scoring on oesophageal adenocarcinoma biopsies. European journal of cancer. 2011;47(3):375-82.
110. Saadi A, Shannon NB, Lao-Sirieix P, O'Donovan M, Walker E, Clemons NJ, et al. Stromal genes discriminate preinvasive from invasive disease, predict outcome, and highlight inflammatory pathways in digestive cancers. Proceedings of the National Academy of Sciences of the United States of America. 2010;107(5):2177-82.
111. Underwood TJ, Hayden AL, Derouet M, Garcia E, Noble F, White MJ, et al. Cancer-associated fibroblasts predict poor outcome and promote periostin-dependent invasion in oesophageal adenocarcinoma. The Journal of pathology. 2015;235(3):466-77.
112. Radisky D, Hagios C, Bissell MJ. Tumors are unique organs defined by abnormal signaling and context. Seminars in cancer biology. 2001;11(2):87-95.
113. Bissell M. Q&A: Mina Bissell on tumors as organs. Cancer discovery. 2013;3(1):7.
114. Junttila MR, de Sauvage FJ. Influence of tumour micro-environment heterogeneity on therapeutic response. Nature. 2013;501(7467):346-54.
115. Spaeth EL, Dembinski JL, Sasser AK, Watson K, Klopp A, Hall B, et al. Mesenchymal stem cell transition to tumor-associated fibroblasts contributes to fibrovascular network expansion and tumor progression. PloS one. 2009;4(4):e4992.
116. Hall B, Dembinski J, Sasser AK, Studeny M, Andreeff M, Marini F. Mesenchymal stem cells in cancer: tumor-associated fibroblasts and cell-based delivery vehicles. International journal of hematology. 2007;86(1):8-16.
117. Karnoub AE, Dash AB, Vo AP, Sullivan A, Brooks MW, Bell GW, et al. Mesenchymal stem cells within tumour stroma promote breast cancer metastasis. Nature. 2007;449(7162):557-63.

118. De Wever O, Demetter P, Mareel M, Bracke M. Stromal myofibroblasts are drivers of invasive cancer growth. International journal of cancer Journal international du cancer. 2008;123(10):2229-38.
119. Mishra PJ, Mishra PJ, Glod JW, Banerjee D. Mesenchymal stem cells: flip side of the coin. Cancer research. 2009;69(4):1255-8.
120. Mishra PJ, Mishra PJ, Humeniuk R, Medina DJ, Alexe G, Mesirov JP, et al. Carcinoma-associated fibroblast-like differentiation of human mesenchymal stem cells. Cancer research. 2008;68(11):4331-9.
121. McMillin DW, Negri JM, Mitsiades CS. The role of tumour-stromal interactions in modifying drug response: challenges and opportunities. Nature reviews Drug discovery. 2013;12(3):217-28.
122. Correia AL, Bissell MJ. The tumor microenvironment is a dominant force in multidrug resistance. Drug resistance updates : reviews and commentaries in antimicrobial and anticancer chemotherapy. 2012;15(1-2):39-49.
123. Meads MB, Gatenby RA, Dalton WS. Environment-mediated drug resistance: a major contributor to minimal residual disease. Nature reviews Cancer. 2009;9(9):665-74.
124. Farmer P, Bonnefoi H, Anderle P, Cameron D, Wirapati P, Becette V, et al. A stroma-related gene signature predicts resistance to neoadjuvant chemotherapy in breast cancer. Nat Med. 2009;15(1):68-74.
125. Castells M, Thibault B, Delord JP, Couderc B. Implication of tumor microenvironment in chemoresistance: tumor-associated stromal cells protect tumor cells from cell death. International journal of molecular sciences. 2012;13(8):9545-71.
126. Xu Y, Tabe Y, Jin L, Watt J, McQueen T, Ohsaka A, et al. TGF-beta receptor kinase inhibitor LY2109761 reverses the anti-apoptotic effects of TGF-beta1 in myelo-monocytic leukaemic cells co-cultured with stromal cells. British journal of haematology. 2008;142(2):192-201.
127. Lis R, Touboul C, Mirshahi P, Ali F, Mathew S, Nolan DJ, et al. Tumor associated mesenchymal stem cells protects ovarian cancer cells from hyperthermia through CXCL12. International journal of cancer Journal international du cancer. 2011;128(3):715-25.
128. Rafii A, Mirshahi P, Poupot M, Faussat AM, Simon A, Ducros E, et al. Oncologic trogocytosis of an original stromal cells induces chemoresistance of ovarian tumours. PloS one. 2008;3(12):e3894.
129. Jin L, Tabe Y, Konoplev S, Xu Y, Leysath CE, Lu H, et al. CXCR4 up-regulation by imatinib induces chronic myelogenous leukemia (CML) cell migration to bone marrow stroma and

promotes survival of quiescent CML cells. Molecular cancer therapeutics. 2008;7(1):48-58.
130. Roodhart JM, Daenen LG, Stigter EC, Prins HJ, Gerrits J, Houthuijzen JM, et al. Mesenchymal stem cells induce resistance to chemotherapy through the release of platinum-induced fatty acids. Cancer cell. 2011;20(3):370-83.
131. Sirica AE. The role of cancer-associated myofibroblasts in intrahepatic cholangiocarcinoma. Nat Rev Gastroenterol Hepatol. 2012;9(1):44-54.
132. Castells M, Thibault B, Mery E, Golzio M, Pasquet M, Hennebelle I, et al. Ovarian ascites-derived Hospicells promote angiogenesis via activation of macrophages. Cancer letters. 2012;326(1):59-68.
133. Sun Y, Campisi J, Higano C, Beer TM, Porter P, Coleman I, et al. Treatment-induced damage to the tumor microenvironment promotes prostate cancer therapy resistance through WNT16B. Nature medicine. 2012;18(9):1359-68.
134. Ruan K, Bao S, Ouyang G. The multifaceted role of periostin in tumorigenesis. Cellular and molecular life sciences : CMLS. 2009;66(14):2219-30.
135. Pasquet M, Golzio M, Mery E, Rafii A, Benabbou N, Mirshahi P, et al. Hospicells (ascites-derived stromal cells) promote tumorigenicity and angiogenesis. International journal of cancer Journal international du cancer. 2010;126(9):2090-101.
136. Benito J, Shi Y, Szymanska B, Carol H, Boehm I, Lu H, et al. Pronounced hypoxia in models of murine and human leukemia: high efficacy of hypoxia-activated prodrug PR-104. PloS one. 2011;6(8):e23108.
137. Theunissen JW, de Sauvage FJ. Paracrine Hedgehog signaling in cancer. Cancer research. 2009;69(15):6007-10.
138. Olive KP, Jacobetz MA, Davidson CJ, Gopinathan A, McIntyre D, Honess D, et al. Inhibition of Hedgehog signaling enhances delivery of chemotherapy in a mouse model of pancreatic cancer. Science. 2009;324(5933):1457-61.
139. Fingas CD, Bronk SF, Werneburg NW, Mott JL, Guicciardi ME, Cazanave SC, et al. Myofibroblast-derived PDGF-BB promotes Hedgehog survival signaling in cholangiocarcinoma cells. Hepatology. 2011;54(6):2076-88.
140. Catenacci DV, Junttila MR, Karrison T, Bahary N, Horiba MN, Nattam SR, et al. Randomized Phase Ib/II Study of Gemcitabine Plus Placebo or Vismodegib, a Hedgehog Pathway Inhibitor, in Patients With Metastatic Pancreatic Cancer. Journal of clinical oncology : official journal of the American Society of Clinical Oncology. 2015;33(36):4284-92.
141. Kaye SB, Fehrenbacher L, Holloway R, Amit A, Karlan B, Slomovitz B, et al. A phase II, randomized, placebo-controlled study of vismodegib as maintenance therapy in patients with ovarian cancer in second or third complete remission. Clinical

cancer research : an official journal of the American Association for Cancer Research. 2012;18(23):6509-18.
142. Berlin J, Bendell JC, Hart LL, Firdaus I, Gore I, Hermann RC, et al. A randomized phase II trial of vismodegib versus placebo with FOLFOX or FOLFIRI and bevacizumab in patients with previously untreated metastatic colorectal cancer. Clinical cancer research : an official journal of the American Association for Cancer Research. 2013;19(1):258-67.
143. Reardon DA, Akabani G, Coleman RE, Friedman AH, Friedman HS, Herndon JE, 2nd, et al. Salvage radioimmunotherapy with murine iodine-131-labeled antitenascin monoclonal antibody 81C6 for patients with recurrent primary and metastatic malignant brain tumors: phase II study results. Journal of clinical oncology : official journal of the American Society of Clinical Oncology. 2006;24(1):115-22.
144. Ricchi P, Zarrilli R, Di Palma A, Acquaviva AM. Nonsteroidal anti-inflammatory drugs in colorectal cancer: from prevention to therapy. British journal of cancer. 2003;88(6):803-7.
145. Loeffler M, Kruger JA, Niethammer AG, Reisfeld RA. Targeting tumor-associated fibroblasts improves cancer chemotherapy by increasing intratumoral drug uptake. The Journal of clinical investigation. 2006;116(7):1955-62.
146. Fang J, Hu B, Li S, Zhang C, Liu Y, Wang P. A multi-antigen vaccine in combination with an immunotoxin targeting tumor-associated fibroblast for treating murine melanoma. Mol Ther Oncolytics. 2016;3:16007.
147. Gillet JP, Calcagno AM, Varma S, Marino M, Green LJ, Vora MI, et al. Redefining the relevance of established cancer cell lines to the study of mechanisms of clinical anti-cancer drug resistance. Proceedings of the National Academy of Sciences of the United States of America. 2011;108(46):18708-13.
148. Hausser HJ, Brenner RE. Phenotypic instability of Saos-2 cells in long-term culture. Biochemical and biophysical research communications. 2005;333(1):216-22.
149. Pietras K, Ostman A. Hallmarks of cancer: interactions with the tumor stroma. Experimental cell research. 2010;316(8):1324-31.
150. Joyce JA, Pollard JW. Microenvironmental regulation of metastasis. Nature reviews Cancer. 2009;9(4):239-52.
151. Rubin EH, Gilliland DG. Drug development and clinical trials--the path to an approved cancer drug. Nature reviews Clinical oncology. 2012;9(4):215-22.
152. DiMasi JA, Feldman L, Seckler A, Wilson A. Trends in risks associated with new drug development: success rates for investigational drugs. Clinical pharmacology and therapeutics. 2010;87(3):272-7.

153. Hutchinson L, Kirk R. High drug attrition rates--where are we going wrong? Nature reviews Clinical oncology. 2011;8(4):189-90.
154. Rubio-Viqueira B, Hidalgo M. Direct in vivo xenograft tumor model for predicting chemotherapeutic drug response in cancer patients. Clinical pharmacology and therapeutics. 2009;85(2):217-21.
155. Johnson JI, Decker S, Zaharevitz D, Rubinstein LV, Venditti JM, Schepartz S, et al. Relationships between drug activity in NCI preclinical in vitro and in vivo models and early clinical trials. British journal of cancer. 2001;84(10):1424-31.
156. Prentis RA, Lis Y, Walker SR. Pharmaceutical innovation by the seven UK-owned pharmaceutical companies (1964-1985). British journal of clinical pharmacology. 1988;25(3):387-96.
157. Kola I, Landis J. Can the pharmaceutical industry reduce attrition rates? Nature reviews Drug discovery. 2004;3(8):711-5.
158. Astashkina A, Mann B, Grainger DW. A critical evaluation of in vitro cell culture models for high-throughput drug screening and toxicity. Pharmacology & therapeutics. 2012;134(1):82-106.
159. Sandberg R, Ernberg I. Assessment of tumor characteristic gene expression in cell lines using a tissue similarity index (TSI). Proceedings of the National Academy of Sciences of the United States of America. 2005;102(6):2052-7.
160. Ertel A, Verghese A, Byers SW, Ochs M, Tozeren A. Pathway-specific differences between tumor cell lines and normal and tumor tissue cells. Molecular cancer. 2006;5(1):55.
161. Gazdar AF, Gao B, Minna JD. Lung cancer cell lines: Useless artifacts or invaluable tools for medical science? Lung cancer. 2010;68(3):309-18.
162. Begley CG, Ellis LM. Drug development: Raise standards for preclinical cancer research. Nature. 2012;483(7391):531-3.
163. Kirk R, Hutchinson L. Oncology trials--the elephant in the room. Nature reviews Clinical oncology. 2012;9(4):185-6.
164. Schilsky RL. Personalized medicine in oncology: the future is now. Nature reviews Drug discovery. 2010;9(5):363-6.
165. Trusheim MR, Burgess B, Hu SX, Long T, Averbuch SD, Flynn AA, et al. Quantifying factors for the success of stratified medicine. Nature reviews Drug discovery. 2011;10(11):817-33.
166. Pei XF, Noble MS, Davoli MA, Rosfjord E, Tilli MT, Furth PA, et al. Explant-cell culture of primary mammary tumors from MMTV-c-Myc transgenic mice. In vitro cellular & developmental biology Animal. 2004;40(1-2):14-21.
167. Kim JB, Stein R, O'Hare MJ. Three-dimensional in vitro tissue culture models of breast cancer-- a review. Breast cancer research and treatment. 2004;85(3):281-91.
168. Dairkee SH, Deng G, Stampfer MR, Waldman FM, Smith HS. Selective cell culture of primary breast carcinoma. Cancer research. 1995;55(12):2516-9.

169. Mitra A, Mishra L, Li S. Technologies for deriving primary tumor cells for use in personalized cancer therapy. Trends in biotechnology. 2013;31(6):347-54.
170. Weeber F, van de Wetering M, Hoogstraat M, Dijkstra KK, Krijgsman O, Kuilman T, et al. Preserved genetic diversity in organoids cultured from biopsies of human colorectal cancer metastases. Proceedings of the National Academy of Sciences of the United States of America. 2015;112(43):13308-11.
171. Sato T, Stange DE, Ferrante M, Vries RG, Van Es JH, Van den Brink S, et al. Long-term expansion of epithelial organoids from human colon, adenoma, adenocarcinoma, and Barrett's epithelium. Gastroenterology. 2011;141(5):1762-72.
172. Liu X, Ory V, Chapman S, Yuan H, Albanese C, Kallakury B, et al. ROCK inhibitor and feeder cells induce the conditional reprogramming of epithelial cells. The American journal of pathology. 2012;180(2):599-607.
173. Suprynowicz FA, Upadhyay G, Krawczyk E, Kramer SC, Hebert JD, Liu X, et al. Conditionally reprogrammed cells represent a stem-like state of adult epithelial cells. Proceedings of the National Academy of Sciences of the United States of America. 2012;109(49):20035-40.
174. Garman KS, Orlando RC, Chen X. Review: Experimental models for Barrett's esophagus and esophageal adenocarcinoma. American journal of physiology Gastrointestinal and liver physiology. 2012;302(11):G1231-43.
175. Kalabis J, Wong GS, Vega ME, Natsuizaka M, Robertson ES, Herlyn M, et al. Isolation and characterization of mouse and human esophageal epithelial cells in 3D organotypic culture. Nature protocols. 2012;7(2):235-46.
176. Smalley KS, Lioni M, Noma K, Haass NK, Herlyn M. In vitro three-dimensional tumor microenvironment models for anticancer drug discovery. Expert opinion on drug discovery. 2008;3(1):1-10.
177. Seol HS, Suh YA, Ryu YJ, Kim HJ, Chun SM, Na DC, et al. A patient-derived xenograft mouse model generated from primary cultured cells recapitulates patient tumors phenotypically and genetically. Journal of cancer research and clinical oncology. 2013;139(9):1471-80.
178. Julien S, Merino-Trigo A, Lacroix L, Pocard M, Goere D, Mariani P, et al. Characterization of a large panel of patient-derived tumor xenografts representing the clinical heterogeneity of human colorectal cancer. Clinical cancer research : an official journal of the American Association for Cancer Research. 2012;18(19):5314-28.
179. Monsma DJ, Monks NR, Cherba DM, Dylewski D, Eugster E, Jahn H, et al. Genomic characterization of explant tumorgraft models derived from fresh patient tumor tissue. Journal of translational medicine. 2012;10:125.

180. Reece-Smith A. Improving the in vitro modeling of oesophageal cancer. Research Thesis for the degree of Doctor of Medicine, University of Nottingham, Nottingham, UK. July 2014.
181. Dodbiba L, Teichman J, Fleet A, Thai H, Sun B, Panchal D, et al. Primary esophageal and gastro-esophageal junction cancer xenograft models: clinicopathological features and engraftment. Laboratory investigation; a journal of technical methods and pathology. 2013;93(4):397-407.
182. Wu X, Zhang J, Zhen R, Lv J, Zheng L, Su X, et al. Trastuzumab anti-tumor efficacy in patient-derived esophageal squamous cell carcinoma xenograft (PDECX) mouse models. Journal of translational medicine. 2012;10:180.
183. Siolas D, Hannon GJ. Patient-derived tumor xenografts: transforming clinical samples into mouse models. Cancer research. 2013;73(17):5315-9.
184. Firestone B. The challenge of selecting the 'right' in vivo oncology pharmacology model. Current opinion in pharmacology. 2010;10(4):391-6.
185. Lee GY, Kenny PA, Lee EH, Bissell MJ. Three-dimensional culture models of normal and malignant breast epithelial cells. Nat Methods. 2007;4(4):359-65.
186. S M, S C, S M, V S, P M, P T, et al. Isolation and Culture of Human Microvascular endothelium for comparison of the morphological and molecular characteristics of Microvascular endothelial cells under normal gravity against simulated micro gravity. Journal of stem cells & regenerative medicine. 2010;6(3):173-4.
187. Palechor-Ceron N, Suprynowicz FA, Upadhyay G, Dakic A, Minas T, Simic V, et al. Radiation induces diffusible feeder cell factor(s) that cooperate with ROCK inhibitor to conditionally reprogram and immortalize epithelial cells. The American journal of pathology. 2013;183(6):1862-70.
188. Ohata H, Ishiguro T, Aihara Y, Sato A, Sakai H, Sekine S, et al. Induction of the stem-like cell regulator CD44 by Rho kinase inhibition contributes to the maintenance of colon cancer-initiating cells. Cancer research. 2012;72(19):5101-10.
189. Sato T, Clevers H. Growing self-organizing mini-guts from a single intestinal stem cell: mechanism and applications. Science. 2013;340(6137):1190-4.
190. Ashley N, Jones M, Ouaret D, Wilding J, Bodmer WF. Rapidly Derived Colorectal Cancer Cultures Recapitulate Parental Cancer Characteristics and Enable Personalised Therapeutic Assays. The Journal of pathology. 2014.
191. Onion D, Argent R, Collier P, Grabowska A. Personal Communication from body of work performed at the EVPC, Division of Cancer and Stem Cells. Faculty of Medicine & Health Sciences, School of Medicine University of Nottingham, Nottingham, UK 2013.

192. Menache A. Trends in animal use and replacement in the 'Three Is' of industry. Alternatives to laboratory animals : ATLA. 2012;40(6):P20-1.
193. Jeanes AI, Maya-Mendoza A, Streuli CH. Cellular microenvironment influences the ability of mammary epithelia to undergo cell cycle. PloS one. 2011;6(3):e18144.
194. Dhiman HK, Ray AR, Panda AK. Three-dimensional chitosan scaffold-based MCF-7 cell culture for the determination of the cytotoxicity of tamoxifen. Biomaterials. 2005;26(9):979-86.
195. Froeling FE, Marshall JF, Kocher HM. Pancreatic cancer organotypic cultures. Journal of biotechnology. 2010;148(1):16-23.
196. Roskelley CD, Srebrow A, Bissell MJ. A hierarchy of ECM-mediated signalling regulates tissue-specific gene expression. Current opinion in cell biology. 1995;7(5):736-47.
197. Bissell MJ, Radisky DC, Rizki A, Weaver VM, Petersen OW. The organizing principle: microenvironmental influences in the normal and malignant breast. Differentiation; research in biological diversity. 2002;70(9-10):537-46.
198. Weaver VM, Lelievre S, Lakins JN, Chrenek MA, Jones JC, Giancotti F, et al. beta4 integrin-dependent formation of polarized three-dimensional architecture confers resistance to apoptosis in normal and malignant mammary epithelium. Cancer cell. 2002;2(3):205-16.
199. Breslin S, O'Driscoll L. Three-dimensional cell culture: the missing link in drug discovery. Drug discovery today. 2013;18(5-6):240-9.
200. Tung YC, Hsiao AY, Allen SG, Torisawa YS, Ho M, Takayama S. High-throughput 3D spheroid culture and drug testing using a 384 hanging drop array. The Analyst. 2011;136(3):473-8.
201. Markovitz-Bishitz Y, Tauber Y, Afrimzon E, Zurgil N, Sobolev M, Shafran Y, et al. A polymer microstructure array for the formation, culturing, and high throughput drug screening of breast cancer spheroids. Biomaterials. 2010;31(32):8436-44.
202. Yoshii Y, Waki A, Yoshida K, Kakezuka A, Kobayashi M, Namiki H, et al. The use of nanoimprinted scaffolds as 3D culture models to facilitate spontaneous tumor cell migration and well-regulated spheroid formation. Biomaterials. 2011;32(26):6052-8.
203. Hirschhaeuser F, Menne H, Dittfeld C, West J, Mueller-Klieser W, Kunz-Schughart LA. Multicellular tumor spheroids: an underestimated tool is catching up again. Journal of biotechnology. 2010;148(1):3-15.
204. Horman SR, To J, Orth AP. An HTS-compatible 3D colony formation assay to identify tumor-specific chemotherapeutics. Journal of biomolecular screening. 2013;18(10):1298-308.

205. Fiebig HH, Maier A, Burger AM. Clonogenic assay with established human tumour xenografts: correlation of in vitro to in vivo activity as a basis for anticancer drug discovery. European journal of cancer. 2004;40(6):802-20.
206. Brouquet A, Taleb P, Lot AS, Beauchet A, Julie C, Prevost G, et al. A model of primary culture of colorectal cancer and liver metastasis to predict chemosensitivity. The Journal of surgical research. 2011;166(2):247-54.
207. Xiang X, Phung Y, Feng M, Nagashima K, Zhang J, Broaddus VC, et al. The development and characterization of a human mesothelioma in vitro 3D model to investigate immunotoxin therapy. PloS one. 2011;6(1):e14640.
208. Byun YS, Tibrewal S, Kim E, Yco L, Sarkar J, Ivanir Y, et al. Keratocytes derived from spheroid culture of corneal stromal cells resemble tissue resident keratocytes. PloS one. 2014;9(11):e112781.
209. Liu J, Ma L, Xu J, Liu C, Zhang J, Liu J, et al. Spheroid body-forming cells in the human gastric cancer cell line MKN-45 possess cancer stem cell properties. International journal of oncology. 2013;42(2):453-9.
210. Singh SK, Clarke ID, Terasaki M, Bonn VE, Hawkins C, Squire J, et al. Identification of a cancer stem cell in human brain tumors. Cancer research. 2003;63(18):5821-8.
211. Foty R. A simple hanging drop cell culture protocol for generation of 3D spheroids. J Vis Exp. 2011(51).
212. Fischbach C, Chen R, Matsumoto T, Schmelzle T, Brugge JS, Polverini PJ, et al. Engineering tumors with 3D scaffolds. Nat Methods. 2007;4(10):855-60.
213. Caicedo-Carvajal CE, Liu Q, Remache Y, Goy A, Suh KS. Cancer Tissue Engineering: A Novel 3D Polystyrene Scaffold for In Vitro Isolation and Amplification of Lymphoma Cancer Cells from Heterogeneous Cell Mixtures. J Tissue Eng. 2011;2011:362326.
214. Shimony N, Avrahami I, Gorodetsky R, Elkin G, Tzukert K, Zangi L, et al. A 3D rotary renal and mesenchymal stem cell culture model unveils cell death mechanisms induced by matrix deficiency and low shear stress. Nephrol Dial Transplant. 2008;23(6):2071-80.
215. Unsworth BR, Lelkes PI. Growing tissues in microgravity. Nature medicine. 1998;4(8):901-7.
216. Rhee HW, Zhau HE, Pathak S, Multani AS, Pennanen S, Visakorpi T, et al. Permanent phenotypic and genotypic changes of prostate cancer cells cultured in a three-dimensional rotating-wall vessel. In vitro cellular & developmental biology Animal. 2001;37(3):127-40.
217. Lewis ML, Moriarity DM, Campbell PS. Use of microgravity bioreactors for development of an in vitro rat salivary gland cell

culture model. Journal of cellular biochemistry. 1993;51(3):265-73.
218. Rimann M, Graf-Hausner U. Synthetic 3D multicellular systems for drug development. Current opinion in biotechnology. 2012;23(5):803-9.
219. Kimlin LC, Casagrande G, Virador VM. In vitro three-dimensional (3D) models in cancer research: an update. Molecular carcinogenesis. 2013;52(3):167-82.
220. Loessner D, Stok KS, Lutolf MP, Hutmacher DW, Clements JA, Rizzi SC. Bioengineered 3D platform to explore cell-ECM interactions and drug resistance of epithelial ovarian cancer cells. Biomaterials. 2010;31(32):8494-506.
221. Nugraha B, Hong X, Mo X, Tan L, Zhang W, Chan PM, et al. Galactosylated cellulosic sponge for multi-well drug safety testing. Biomaterials. 2011;32(29):6982-94.
222. Xu F, Wu J, Wang S, Durmus NG, Gurkan UA, Demirci U. Microengineering methods for cell-based microarrays and high-throughput drug-screening applications. Biofabrication. 2011;3(3):034101.
223. Huang G, Wang S, He X, Zhang X, Lu TJ, Xu F. Helical spring template fabrication of cell-laden microfluidic hydrogels for tissue engineering. Biotechnology and bioengineering. 2013;110(3):980-9.
224. Kleinman HK, Martin GR. Matrigel: basement membrane matrix with biological activity. Seminars in cancer biology. 2005;15(5):378-86.
225. Geiger B. Cell biology. Encounters in space. Science. 2001;294(5547):1661-3.
226. Amatangelo MD, Bassi DE, Klein-Szanto AJ, Cukierman E. Stroma-derived three-dimensional matrices are necessary and sufficient to promote desmoplastic differentiation of normal fibroblasts. The American journal of pathology. 2005;167(2):475-88.
227. Harma V, Virtanen J, Makela R, Happonen A, Mpindi JP, Knuuttila M, et al. A comprehensive panel of three-dimensional models for studies of prostate cancer growth, invasion and drug responses. PloS one. 2010;5(5):e10431.
228. Huh D, Kim HJ, Fraser JP, Shea DE, Khan M, Bahinski A, et al. Microfabrication of human organs-on-chips. Nature protocols. 2013;8(11):2135-57.
229. Benam KH, Dauth S, Hassell B, Herland A, Jain A, Jang KJ, et al. Engineered in vitro disease models. Annual review of pathology. 2015;10:195-262.
230. LaBarbera DV, Reid BG, Yoo BH. The multicellular tumor spheroid model for high-throughput cancer drug discovery. Expert opinion on drug discovery. 2012;7(9):819-30.

231. Contino G, Eldridge MD, Secrier M, Bower L, Fels Elliott R, Weaver J, et al. Whole-genome sequencing of nine esophageal adenocarcinoma cell lines. F1000Res. 2016;5:1336.
232. Vinci M, Gowan S, Boxall F, Patterson L, Zimmermann M, Court W, et al. Advances in establishment and analysis of three-dimensional tumor spheroid-based functional assays for target validation and drug evaluation. BMC biology. 2012;10:29.
233. Hickman JA, Graeser R, de Hoogt R, Vidic S, Brito C, Gutekunst M, et al. Three-dimensional models of cancer for pharmacology and cancer cell biology: capturing tumor complexity in vitro/ex vivo. Biotechnology journal. 2014;9(9):1115-28.
234. Underwood TJ, Derouet MF, White MJ, Noble F, Moutasim KA, Smith E, et al. A comparison of primary oesophageal squamous epithelial cells with HET-1A in organotypic culture. Biology of the cell / under the auspices of the European Cell Biology Organization. 2010;102(12):635-44.
235. Green N, Huang Q, Khan L, Battaglia G, Corfe B, MacNeil S, et al. The development and characterization of an organotypic tissue-engineered human esophageal mucosal model. Tissue engineering Part A. 2010;16(3):1053-64.
236. Okawa T, Michaylira CZ, Kalabis J, Stairs DB, Nakagawa H, Andl CD, et al. The functional interplay between EGFR overexpression, hTERT activation, and p53 mutation in esophageal epithelial cells with activation of stromal fibroblasts induces tumor development, invasion, and differentiation. Genes & development. 2007;21(21):2788-803.
237. Andl CD, McCowan KM, Allison GL, Rustgi AK. Cathepsin B is the driving force of esophageal cell invasion in a fibroblast-dependent manner. Neoplasia. 2010;12(6):485-98.
238. Onion D, Argent RH, Reece-Smith AM, Craze ML, Pineda RG, Clarke PA, et al. 3-Dimensional Patient-Derived Lung Cancer Assays Reveal Resistance to Standards-of-Care Promoted by Stromal cells but Sensitivity to Histone Deacetylase Inhibitors. Molecular cancer therapeutics. 2016.
239. Krausz E, de Hoogt R, Gustin E, Cornelissen F, Grand-Perret T, Janssen L, et al. Translation of a tumor microenvironment mimicking 3D tumor growth co-culture assay platform to high-content screening. Journal of biomolecular screening. 2013;18(1):54-66.
240. Koukourakis GV, Kouloulias V, Koukourakis MJ, Zacharias GA, Zabatis H, Kouvaris J. Efficacy of the oral fluorouracil pro-drug capecitabine in cancer treatment: a review. Molecules. 2008;13(8):1897-922.
241. EF DBDDB. A formula to estimate the approximate surface area if height and weight be known. Archives Internal Medicine. 1916;5(5):303–11.

242. Felici A, Verweij J, Sparreboom A. Dosing strategies for anticancer drugs: the good, the bad and body-surface area. European journal of cancer. 2002;38(13):1677-84.
243. Baker SD, Verweij J, Rowinsky EK, Donehower RC, Schellens JH, Grochow LB, et al. Role of body surface area in dosing of investigational anticancer agents in adults, 1991-2001. Journal of the National Cancer Institute. 2002;94(24):1883-8.
244. Kaestner SA, Sewell GJ. Chemotherapy dosing part I: scientific basis for current practice and use of body surface area. Clinical oncology. 2007;19(1):23-37.
245. Gurney H. How to calculate the dose of chemotherapy. British journal of cancer. 2002;86(8):1297-302.
246. Beumer JH, Chu E, Salamone SJ. Body-surface area-based chemotherapy dosing: appropriate in the 21st century? Journal of clinical oncology : official journal of the American Society of Clinical Oncology. 2012;30(31):3896-7.
247. Gamelin E, Delva R, Jacob J, Merrouche Y, Raoul JL, Pezet D, et al. Individual fluorouracil dose adjustment based on pharmacokinetic follow-up compared with conventional dosage: results of a multicenter randomized trial of patients with metastatic colorectal cancer. Journal of clinical oncology : official journal of the American Society of Clinical Oncology. 2008;26(13):2099-105.
248. Corrie P. Cytotoxic chemotherapy: clinical aspects. Medicine. 2008;36(1):24-8.
249. Plosker GL, Faulds D. Epirubicin. A review of its pharmacodynamic and pharmacokinetic properties, and therapeutic use in cancer chemotherapy. Drugs. 1993;45(5):788-856.
250. Nielsen D, Maare C, Skovsgaard T. Cellular resistance to anthracyclines. Gen Pharmacol. 1996;27(2):251-5.
251. Hortobagyi GN. Anthracyclines in the treatment of cancer. An overview. Drugs. 1997;54 Suppl 4:1-7.
252. Woolston CM, Madhusudan S, Soomro IN, Lobo DN, Reece-Smith AM, Parsons SL, et al. Thioredoxin interacting protein and its association with clinical outcome in gastro-oesophageal adenocarcinoma. Redox Biol. 2013;1:285-91.
253. Dobbs NA, Twelves CJ. What is the effect of adjusting epirubicin doses for body surface area? British journal of cancer. 1998;78(5):662-6.
254. Eksborg S, Hardell L, Bengtsson NO, Sjodin M, Elfsson B. Epirubicin as a single agent therapy for the treatment of breast cancer--a pharmacokinetic and clinical study. Medical oncology and tumor pharmacotherapy. 1992;9(2):75-80.
255. Coukell AJ, Faulds D. Epirubicin. An updated review of its pharmacodynamic and pharmacokinetic properties and therapeutic efficacy in the management of breast cancer. Drugs. 1997;53(3):453-82.

256. Robert J. Clinical pharmacokinetics of epirubicin. Clinical pharmacokinetics. 1994;26(6):428-38.
257. Danesi R, Innocenti F, Fogli S, Gennari A, Baldini E, Di Paolo A, et al. Pharmacokinetics and pharmacodynamics of combination chemotherapy with paclitaxel and epirubicin in breast cancer patients. British journal of clinical pharmacology. 2002;53(5):508-18.
258. Mayne Pharma Ltd. Epirubicin Hydrochloride for Injection. UK Medicines and Healthcare products Regulatory Agency http://wwwmhragovuk/home/groups/par/documents/websiteresources/con2025068pdf. 2006.
259. Lunardi G, Venturini M, Vannozzi MO, Tolino G, Del ML, Bighin C, et al. Influence of alternate sequences of epirubicin and docetaxel on the pharmacokinetic behaviour of both drugs in advanced breast cancer. Annals of oncology : official journal of the European Society for Medical Oncology / ESMO. 2002;13(2):280-5.
260. Stordal B, Davey M. Understanding cisplatin resistance using cellular models. IUBMB Life. 2007;59(11):696-9.
261. Pfizer. Cisplatin Product Information Sheet. Feb 2010:10.
262. Tegeder I, Brautigam L, Seegel M, Al-Dam A, Turowski B, Geisslinger G, et al. Cisplatin tumor concentrations after intra-arterial cisplatin infusion or embolization in patients with oral cancer. Clinical pharmacology and therapeutics. 2003;73(5):417-26.
263. Rademaker-Lakhai JM, Crul M, Zuur L, Baas P, Beijnen JH, Simis YJ, et al. Relationship between cisplatin administration and the development of ototoxicity. Journal of clinical oncology : official journal of the American Society of Clinical Oncology. 2006;24(6):918-24.
264. Minami H, Ohe Y, Niho S, Goto K, Ohmatsu H, Kubota K, et al. Comparison of pharmacokinetics and pharmacodynamics of docetaxel and Cisplatin in elderly and non-elderly patients: why is toxicity increased in elderly patients? Journal of clinical oncology : official journal of the American Society of Clinical Oncology. 2004;22(14):2901-8.
265. Gouyette A, Apchin A, Foka M, Richard JM. Pharmacokinetics of intra-arterial and intravenous cisplatin in head and neck cancer patients. European journal of cancer & clinical oncology. 1986;22(3):257-63.
266. Kanamori Y, Kigawa J, Minagawa Y, Irie T, Itamochi H, Cheng X, et al. Clinical responses and platinum concentrations in tumors after intra-arterial and intravenous administration of cisplatin in the same patients with cervical cancer. Gynecologic and obstetric investigation. 1997;44(1):57-60.
267. Longley DB, Harkin DP, Johnston PG. 5-fluorouracil: mechanisms of action and clinical strategies. Nature reviews Cancer. 2003;3(5):330-8.

268. MacMillan WE, Wolberg WH, Welling PG. Pharmacokinetics of fluorouracil in humans. Cancer research. 1978;38(10):3479-82.
269. Meta-analysis Group In C, Piedbois P, Rougier P, Buyse M, Pignon J, Ryan L, et al. Efficacy of intravenous continuous infusion of fluorouracil compared with bolus administration in advanced colorectal cancer. Journal of clinical oncology : official journal of the American Society of Clinical Oncology. 1998;16(1):301-8.
270. Gamelin E, Boisdron-Celle M. Dose monitoring of 5-fluorouracil in patients with colorectal or head and neck cancer--status of the art. Critical reviews in oncology/hematology. 1999;30(1):71-9.
271. Saam J, Critchfield GC, Hamilton SA, Roa BB, Wenstrup RJ, Kaldate RR. Body surface area-based dosing of 5-fluoruracil results in extensive interindividual variability in 5-fluorouracil exposure in colorectal cancer patients on FOLFOX regimens. Clinical colorectal cancer. 2011;10(3):203-6.
272. Saif MW, Choma A, Salamone SJ, Chu E. Pharmacokinetically guided dose adjustment of 5-fluorouracil: a rational approach to improving therapeutic outcomes. Journal of the National Cancer Institute. 2009;101(22):1543-52.
273. Walko CM, Lindley C. Capecitabine: a review. Clinical therapeutics. 2005;27(1):23-44.
274. European Medicines Agency. Xeloda Scientific Product Information. http://www.ema.europa.eu/docs/en_GB/document_library/EPAR_-_Scientific_Discussion/human/000316/WC500058145.pdf. 2005.
275. Reigner B, Blesch K, Weidekamm E. Clinical pharmacokinetics of capecitabine. Clinical pharmacokinetics. 2001;40(2):85-104.
276. Ceccacci E, Minucci S. Inhibition of histone deacetylases in cancer therapy: lessons from leukaemia. British journal of cancer. 2016;114(6):605-11.
277. Insinga A, Monestiroli S, Ronzoni S, Carbone R, Pearson M, Pruneri G, et al. Impairment of p53 acetylation, stability and function by an oncogenic transcription factor. The EMBO journal. 2004;23(5):1144-54.
278. Anne M, Sammartino D, Barginear MF, Budman D. Profile of panobinostat and its potential for treatment in solid tumors: an update. Onco Targets Ther. 2013;6:1613-24.
279. Dawson MA, Kouzarides T. Cancer epigenetics: from mechanism to therapy. Cell. 2012;150(1):12-27.
280. Bose P, Dai Y, Grant S. Histone deacetylase inhibitor (HDACI) mechanisms of action: Emerging insights. Pharmacology & therapeutics. 2014;143(3):323-36.

281. Atadja P. Development of the pan-DAC inhibitor panobinostat (LBH589): successes and challenges. Cancer letters. 2009;280(2):233-41.
282. San-Miguel JF, Hungria VT, Yoon SS, Beksac M, Dimopoulos MA, Elghandour A, et al. Panobinostat plus bortezomib and dexamethasone versus placebo plus bortezomib and dexamethasone in patients with relapsed or relapsed and refractory multiple myeloma: a multicentre, randomised, double-blind phase 3 trial. The lancet oncology. 2014;15(11):1195-206.
283. Morita S, Oizumi S, Minami H, Kitagawa K, Komatsu Y, Fujiwara Y, et al. Phase I dose-escalating study of panobinostat (LBH589) administered intravenously to Japanese patients with advanced solid tumors. Investigational new drugs. 2012;30(5):1950-7.
284. Kubo M, Kanaya N, Petrossian K, Ye J, Warden C, Liu Z, et al. Inhibition of the proliferation of acquired aromatase inhibitor-resistant breast cancer cells by histone deacetylase inhibitor LBH589 (panobinostat). Breast cancer research and treatment. 2013;137(1):93-107.
285. Regel I, Merkl L, Friedrich T, Burgermeister E, Zimmermann W, Einwachter H, et al. Pan-histone deacetylase inhibitor panobinostat sensitizes gastric cancer cells to anthracyclines via induction of CITED2. Gastroenterology. 2012;143(1):99-109 e10.
286. Bayer. Levitra (Vardenafil hydrochloride). Product scientific and clinical information. European Medicines Agency. 2014.
287. Corbin J. PDE5 inhibition and fibrosis. Int J Impot Res. 2005;17(6):546.
288. Huaux F, Noel S, Dhooghe B, Panin N, Lo Re S, Lison D, et al. Dysregulated proinflammatory and fibrogenic phenotype of fibroblasts in cystic fibrosis. PloS one. 2013;8(5):e64341.
289. Agarwal V RM, Agrawal V, Singh H, Chaturvedi S. Phosphodiesterase-5 Inhibitors Attenuate Fibrotic Phenotype and Restore Anti-Fibrotic Resopnses of Cutaneous Fibroblasts in Patients with Scleroderma. Arthritis Rheumatol 2016;68 (suppl 10). .
290. Ammirante M, Shalapour S, Kang Y, Jamieson CA, Karin M. Tissue injury and hypoxia promote malignant progression of prostate cancer by inducing CXCL13 expression in tumor myofibroblasts. Proceedings of the National Academy of Sciences of the United States of America. 2014;111(41):14776-81.
291. A Hayden AC, E Garcia, S Thirdborough, G Thomas, T Underwood. Stromal targeting with phosphodiesterase type 5 inhibitors in oesophageal adenocarcinoma. Gut. 2015;64(Suppl 1):A1–A584.
292. Graziano F, Arduini F, Ruzzo A, Bearzi I, Humar B, More H, et al. Prognostic analysis of E-cadherin gene promoter hypermethylation in patients with surgically resected, node-

positive, diffuse gastric cancer. Clinical cancer research : an official journal of the American Association for Cancer Research. 2004;10(8):2784-9.
293. Ohno T, Aihara R, Kamiyama Y, Mochiki E, Asao T, Kuwano H. Prognostic significance of combined expression of MUC1 and adhesion molecules in advanced gastric cancer. European journal of cancer. 2006;42(2):256-63.
294. Takeno S, Noguchi T, Fumoto S, Kimura Y, Shibata T, Kawahara K. E-cadherin expression in patients with esophageal squamous cell carcinoma: promoter hypermethylation, Snail overexpression, and clinicopathologic implications. American journal of clinical pathology. 2004;122(1):78-84.
295. Zhao XJ, Li H, Chen H, Liu YX, Zhang LH, Liu SX, et al. Expression of e-cadherin and beta-catenin in human esophageal squamous cell carcinoma: relationships with prognosis. World journal of gastroenterology : WJG. 2003;9(2):225-32.
296. Xu XL, Ling ZQ, Chen SZ, Li B, Ji WH, Mao WM. The impact of E-cadherin expression on the prognosis of esophageal cancer: a meta-analysis. Diseases of the esophagus : official journal of the International Society for Diseases of the Esophagus / ISDE. 2014;27(1):79-86.
297. DiMaio MA, Kwok S, Montgomery KD, Lowe AW, Pai RK. Immunohistochemical panel for distinguishing esophageal adenocarcinoma from squamous cell carcinoma: a combination of p63, cytokeratin 5/6, MUC5AC, and anterior gradient homolog 2 allows optimal subtyping. Human pathology. 2012;43(11):1799-807.
298. Taniere P, Borghi-Scoazec G, Saurin JC, Lombard-Bohas C, Boulez J, Berger F, et al. Cytokeratin expression in adenocarcinomas of the esophagogastric junction: a comparative study of adenocarcinomas of the distal esophagus and of the proximal stomach. The American journal of surgical pathology. 2002;26(9):1213-21.
299. Doki Y, Shiozaki H, Tahara H, Kobayashi K, Miyata M, Oka H, et al. Prognostic value of DNA ploidy in squamous cell carcinoma of esophagus. Analyzed with improved flow cytometric measurement. Cancer. 1993;72(6):1813-8.
300. Kaketani K, Saito T, Kobayashi M. Flow cytometric analysis of nuclear DNA content in esophageal cancer. Aneuploidy as an index for highly malignant potential. Cancer. 1989;64(4):887-91.
301. Lee KH, Lee JS, Lee JH, Kim SW, Suh C, Kim WK, et al. Prognostic value of DNA flow cytometry in stomach cancer: a 5-year prospective study. British journal of cancer. 1999;79(11-12):1727-35.
302. D'Agnano I, D'Angelo C, Savarese A, Carlini M, Garofalo A, Bottari L, et al. DNA ploidy, proliferative index, and epidermal growth factor receptor: expression and prognosis in patients with

gastric cancers. Laboratory investigation; a journal of technical methods and pathology. 1995;72(4):432-8.
303. Patriarca C, Macchi RM, Marschner AK, Mellstedt H. Epithelial cell adhesion molecule expression (CD326) in cancer: a short review. Cancer treatment reviews. 2012;38(1):68-75.
304. Kimura H, Kato H, Faried A, Sohda M, Nakajima M, Fukai Y, et al. Prognostic significance of EpCAM expression in human esophageal cancer. International journal of oncology. 2007;30(1):171-9.
305. Mitas M, Almeida JS, Mikhitarian K, Gillanders WE, Lewin DN, Spyropoulos DD, et al. Accurate discrimination of Barrett's esophagus and esophageal adenocarcinoma using a quantitative three-tiered algorithm and multimarker real-time reverse transcription-PCR. Clinical cancer research : an official journal of the American Association for Cancer Research. 2005;11(6):2205-14.
306. Balzar M, Winter MJ, de Boer CJ, Litvinov SV. The biology of the 17-1A antigen (Ep-CAM). Journal of molecular medicine. 1999;77(10):699-712.
307. Went PT, Lugli A, Meier S, Bundi M, Mirlacher M, Sauter G, et al. Frequent EpCam protein expression in human carcinomas. Human pathology. 2004;35(1):122-8.
308. Stoecklein NH, Siegmund A, Scheunemann P, Luebke AM, Erbersdobler A, Verde PE, et al. Ep-CAM expression in squamous cell carcinoma of the esophagus: a potential therapeutic target and prognostic marker. BMC cancer. 2006;6:165.
309. Driemel C, Kremling H, Schumacher S, Will D, Wolters J, Lindenlauf N, et al. Context-dependent adaption of EpCAM expression in early systemic esophageal cancer. Oncogene. 2013.
310. Goldstein I, Marcel V, Olivier M, Oren M, Rotter V, Hainaut P. Understanding wild-type and mutant p53 activities in human cancer: new landmarks on the way to targeted therapies. Cancer Gene Ther. 2011;18(1):2-11.
311. Levine AJ. p53, the cellular gatekeeper for growth and division. Cell. 1997;88(3):323-31.
312. Vousden KH, Lu X. Live or let die: the cell's response to p53. Nature reviews Cancer. 2002;2(8):594-604.
313. Moll UM, Petrenko O. The MDM2-p53 interaction. Molecular cancer research : MCR. 2003;1(14):1001-8.
314. Ong CA, Lao-Sirieix P, Fitzgerald RC. Biomarkers in Barrett's esophagus and esophageal adenocarcinoma: predictors of progression and prognosis. World journal of gastroenterology : WJG. 2010;16(45):5669-81.
315. Olivier M, Hollstein M, Hainaut P. TP53 mutations in human cancers: origins, consequences, and clinical use. Cold Spring Harb Perspect Biol. 2010;2(1):a001008.

316. Bullock AN, Henckel J, DeDecker BS, Johnson CM, Nikolova PV, Proctor MR, et al. Thermodynamic stability of wild-type and mutant p53 core domain. Proceedings of the National Academy of Sciences of the United States of America. 1997;94(26):14338-42.
317. Finlay CA, Hinds PW, Tan TH, Eliyahu D, Oren M, Levine AJ. Activating mutations for transformation by p53 produce a gene product that forms an hsc70-p53 complex with an altered half-life. Mol Cell Biol. 1988;8(2):531-9.
318. Hall PA, Lane DP. p53 in tumour pathology: can we trust immunohistochemistry?--Revisited! The Journal of pathology. 1994;172(1):1-4.
319. Hinds PW, Finlay CA, Quartin RS, Baker SJ, Fearon ER, Vogelstein B, et al. Mutant p53 DNA clones from human colon carcinomas cooperate with ras in transforming primary rat cells: a comparison of the "hot spot" mutant phenotypes. Cell Growth Differ. 1990;1(12):571-80.
320. Novotna K, Trkova M, Pazdro A, Smejkal M, Soukupova A, Kodetova D, et al. TP53 gene mutations are rare in nondysplastic Barrett's esophagus. Digestive diseases and sciences. 2006;51(1):110-3.
321. Bian YS, Osterheld MC, Bosman FT, Benhattar J, Fontolliet C. p53 gene mutation and protein accumulation during neoplastic progression in Barrett's esophagus. Modern pathology : an official journal of the United States and Canadian Academy of Pathology, Inc. 2001;14(5):397-403.
322. Reid BJ, Prevo LJ, Galipeau PC, Sanchez CA, Longton G, Levine DS, et al. Predictors of progression in Barrett's esophagus II: baseline 17p (p53) loss of heterozygosity identifies a patient subset at increased risk for neoplastic progression. The American journal of gastroenterology. 2001;96(10):2839-48.
323. Weaver JM, Ross-Innes CS, Shannon N, Lynch AG, Forshew T, Barbera M, et al. Ordering of mutations in preinvasive disease stages of esophageal carcinogenesis. Nature genetics. 2014;46(8):837-43.
324. Elizabeth Catherine Smyth SHW, Matthew Guy Nankivell, David Gonzalez de Castro, Andrew Wotherspoon, Alicia Frances Clare Okines, Ruth E Langley, Sally Patricia Stenning, David Cunningham. Effect of TP53 mutation status on survival in the MAGIC trial. Journal of clinical oncology : official journal of the American Society of Clinical Oncology. 2015 33((suppl 3; abstr 71)).
325. Ge H, Gardner J, Wu X, Rulifson I, Wang J, Xiong Y, et al. Trefoil Factor 3 (TFF3) Is Regulated by Food Intake, Improves Glucose Tolerance and Induces Mucinous Metaplasia. PloS one. 2015;10(6):e0126924.

326. di Pietro M, Fitzgerald RC. Research advances in esophageal diseases: bench to bedside. F1000prime reports. 2013;5:44.
327. Ross-Innes CS, Debiram-Beecham I, O'Donovan M, Walker E, Varghese S, Lao-Sirieix P, et al. Evaluation of a minimally invasive cell sampling device coupled with assessment of trefoil factor 3 expression for diagnosing Barrett's esophagus: a multi-center case-control study. PLoS medicine. 2015;12(1):e1001780.
328. Reya T, Morrison SJ, Clarke MF, Weissman IL. Stem cells, cancer, and cancer stem cells. Nature. 2001;414(6859):105-11.
329. Dean M, Fojo T, Bates S. Tumour stem cells and drug resistance. Nature reviews Cancer. 2005;5(4):275-84.
330. Suva ML, Riggi N, Stehle JC, Baumer K, Tercier S, Joseph JM, et al. Identification of cancer stem cells in Ewing's sarcoma. Cancer research. 2009;69(5):1776-81.
331. Rosen JM, Jordan CT. The increasing complexity of the cancer stem cell paradigm. Science. 2009;324(5935):1670-3.
332. O'Brien CA, Kreso A, Jamieson CH. Cancer stem cells and self-renewal. Clinical cancer research : an official journal of the American Association for Cancer Research. 2010;16(12):3113-20.
333. Ouyang G, Wang Z, Fang X, Liu J, Yang CJ. Molecular signaling of the epithelial to mesenchymal transition in generating and maintaining cancer stem cells. Cellular and molecular life sciences : CMLS. 2010;67(15):2605-18.
334. Albers AE, Chen C, Koberle B, Qian X, Klussmann JP, Wollenberg B, et al. Stem cells in squamous head and neck cancer. Critical reviews in oncology/hematology. 2012;81(3):224-40.
335. Awad O, Yustein JT, Shah P, Gul N, Katuri V, O'Neill A, et al. High ALDH activity identifies chemotherapy-resistant Ewing's sarcoma stem cells that retain sensitivity to EWS-FLI1 inhibition. PloS one. 2010;5(11):e13943.
336. Douville J, Beaulieu R, Balicki D. ALDH1 as a functional marker of cancer stem and progenitor cells. Stem cells and development. 2009;18(1):17-25.
337. Quintana E, Shackleton M, Sabel MS, Fullen DR, Johnson TM, Morrison SJ. Efficient tumour formation by single human melanoma cells. Nature. 2008;456(7222):593-8.
338. Clevers H. Stem cells, asymmetric division and cancer. Nature genetics. 2005;37(10):1027-8.
339. Szilvassy SJ, Humphries RK, Lansdorp PM, Eaves AC, Eaves CJ. Quantitative assay for totipotent reconstituting hematopoietic stem cells by a competitive repopulation strategy. Proceedings of the National Academy of Sciences of the United States of America. 1990;87(22):8736-40.

340. Scheel C, Weinberg RA. Phenotypic plasticity and epithelial-mesenchymal transitions in cancer and normal stem cells? International journal of cancer Journal international du cancer. 2011;129(10):2310-4.
341. Floor S, van Staveren WC, Larsimont D, Dumont JE, Maenhaut C. Cancer cells in epithelial-to-mesenchymal transition and tumor-propagating-cancer stem cells: distinct, overlapping or same populations. Oncogene. 2011;30(46):4609-21.
342. Maheswaran S, Haber DA. Circulating tumor cells: a window into cancer biology and metastasis. Current opinion in genetics & development. 2010;20(1):96-9.
343. Graham SM, Jorgensen HG, Allan E, Pearson C, Alcorn MJ, Richmond L, et al. Primitive, quiescent, Philadelphia-positive stem cells from patients with chronic myeloid leukemia are insensitive to STI571 in vitro. Blood. 2002;99(1):319-25.
344. Mohrin M, Bourke E, Alexander D, Warr MR, Barry-Holson K, Le Beau MM, et al. Hematopoietic stem cell quiescence promotes error-prone DNA repair and mutagenesis. Cell stem cell. 2010;7(2):174-85.
345. Viale A, De Franco F, Orleth A, Cambiaghi V, Giuliani V, Bossi D, et al. Cell-cycle restriction limits DNA damage and maintains self-renewal of leukaemia stem cells. Nature. 2009;457(7225):51-6.
346. Hirschmann-Jax C, Foster AE, Wulf GG, Nuchtern JG, Jax TW, Gobel U, et al. A distinct "side population" of cells with high drug efflux capacity in human tumor cells. Proceedings of the National Academy of Sciences of the United States of America. 2004;101(39):14228-33.
347. Shekhani MT, Jayanthy AS, Maddodi N, Setaluri V. Cancer stem cells and tumor transdifferentiation: implications for novel therapeutic strategies. American journal of stem cells. 2013;2(1):52-61.
348. Collins AT, Berry PA, Hyde C, Stower MJ, Maitland NJ. Prospective identification of tumorigenic prostate cancer stem cells. Cancer research. 2005;65(23):10946-51.
349. Eramo A, Lotti F, Sette G, Pilozzi E, Biffoni M, Di Virgilio A, et al. Identification and expansion of the tumorigenic lung cancer stem cell population. Cell death and differentiation. 2008;15(3):504-14.
350. Takaishi S, Okumura T, Tu S, Wang SS, Shibata W, Vigneshwaran R, et al. Identification of gastric cancer stem cells using the cell surface marker CD44. Stem cells. 2009;27(5):1006-20.
351. Tirino V, Desiderio V, d'Aquino R, De Francesco F, Pirozzi G, Graziano A, et al. Detection and characterization of CD133+ cancer stem cells in human solid tumours. PloS one. 2008;3(10):e3469.

352. Tirino V, Desiderio V, Paino F, De Rosa A, Papaccio F, Fazioli F, et al. Human primary bone sarcomas contain CD133+ cancer stem cells displaying high tumorigenicity in vivo. FASEB journal : official publication of the Federation of American Societies for Experimental Biology. 2011;25(6):2022-30.
353. Grotenhuis BA, Dinjens WN, Wijnhoven BP, Sonneveld P, Sacchetti A, Franken PF, et al. Barrett's oesophageal adenocarcinoma encompasses tumour-initiating cells that do not express common cancer stem cell markers. The Journal of pathology. 2010;221(4):379-89.
354. Ahmad J, Arthur K, Maxwell P, Kennedy A, Johnston BT, Murray L, et al. Re: Grotenhuis et al. Barrett's oesophageal adenocarcinoma encompasses tumour-initiating cells that do not express common cancer stem cell markers. J Pathol 2010; 221: 379-389. The Journal of pathology. 2011;224(1):143-5.
355. Becker L, Huang Q, Mashimo H. Immunostaining of Lgr5, an intestinal stem cell marker, in normal and premalignant human gastrointestinal tissue. TheScientificWorldJournal. 2008;8:1168-76.
356. Becker L, Huang Q, Mashimo H. Lgr5, an intestinal stem cell marker, is abnormally expressed in Barrett's esophagus and esophageal adenocarcinoma. Diseases of the esophagus : official journal of the International Society for Diseases of the Esophagus / ISDE. 2010;23(2):168-74.
357. Souza RF, Schwartz RE, Mashimo H. Esophageal stem cells and 3D-cell culture models. Annals of the New York Academy of Sciences. 2011;1232:316-22.
358. von Rahden BH, Kircher S, Lazariotou M, Reiber C, Stuermer L, Otto C, et al. LgR5 expression and cancer stem cell hypothesis: clue to define the true origin of esophageal adenocarcinomas with and without Barrett's esophagus? Journal of experimental & clinical cancer research : CR. 2011;30:23.
359. Januchowski R, Wojtowicz K, Zabel M. The role of aldehyde dehydrogenase (ALDH) in cancer drug resistance. Biomedicine & pharmacotherapy = Biomedecine & pharmacotherapie. 2013;67(7):669-80.
360. Deng S, Yang X, Lassus H, Liang S, Kaur S, Ye Q, et al. Distinct expression levels and patterns of stem cell marker, aldehyde dehydrogenase isoform 1 (ALDH1), in human epithelial cancers. PloS one. 2010;5(4):e10277.
361. Ginestier C, Hur MH, Charafe-Jauffret E, Monville F, Dutcher J, Brown M, et al. ALDH1 is a marker of normal and malignant human mammary stem cells and a predictor of poor clinical outcome. Cell stem cell. 2007;1(5):555-67.
362. Su Y, Qiu Q, Zhang X, Jiang Z, Leng Q, Liu Z, et al. Aldehyde dehydrogenase 1 A1-positive cell population is enriched in tumor-initiating cells and associated with progression of bladder cancer. Cancer epidemiology, biomarkers &

prevention : a publication of the American Association for Cancer Research, cosponsored by the American Society of Preventive Oncology. 2010;19(2):327-37.
363. Li T, Su Y, Mei Y, Leng Q, Leng B, Liu Z, et al. ALDH1A1 is a marker for malignant prostate stem cells and predictor of prostate cancer patients' outcome. Laboratory investigation; a journal of technical methods and pathology. 2010;90(2):234-44.
364. Tanei T, Morimoto K, Shimazu K, Kim SJ, Tanji Y, Taguchi T, et al. Association of breast cancer stem cells identified by aldehyde dehydrogenase 1 expression with resistance to sequential Paclitaxel and epirubicin-based chemotherapy for breast cancers. Clinical cancer research : an official journal of the American Association for Cancer Research. 2009;15(12):4234-41.
365. Almanaa TN, Geusz ME, Jamasbi RJ. A new method for identifying stem-like cells in esophageal cancer cell lines. Journal of Cancer. 2013;4(7):536-48.
366. Zhang G, Ma L, Xie YK, Miao XB, Jin C. Esophageal cancer tumorspheres involve cancer stem-like populations with elevated aldehyde dehydrogenase enzymatic activity. Molecular medicine reports. 2012;6(3):519-24.
367. Yang L, Ren Y, Yu X, Qian F, Bian BS, Xiao HL, et al. ALDH1A1 defines invasive cancer stem-like cells and predicts poor prognosis in patients with esophageal squamous cell carcinoma. Modern pathology : an official journal of the United States and Canadian Academy of Pathology, Inc. 2013.
368. Ajani JA, Wang X, Song S, Suzuki A, Taketa T, Sudo K, et al. ALDH-1 expression levels predict response or resistance to preoperative chemoradiation in resectable esophageal cancer patients. Molecular oncology. 2014;8(1):142-9.
369. Smit JK, Faber H, Niemantsverdriet M, Baanstra M, Bussink J, Hollema H, et al. Prediction of response to radiotherapy in the treatment of esophageal cancer using stem cell markers. Radiotherapy and oncology : journal of the European Society for Therapeutic Radiology and Oncology. 2013;107(3):434-41.
370. Ponta H, Sherman L, Herrlich PA. CD44: from adhesion molecules to signalling regulators. Nat Rev Mol Cell Biol. 2003;4(1):33-45.
371. Sneath RJ, Mangham DC. The normal structure and function of CD44 and its role in neoplasia. Mol Pathol. 1998;51(4):191-200.
372. Zhao JS, Li WJ, Ge D, Zhang PJ, Li JJ, Lu CL, et al. Tumor initiating cells in esophageal squamous cell carcinomas express high levels of CD44. PloS one. 2011;6(6):e21419.
373. Zhang C, Li C, He F, Cai Y, Yang H. Identification of CD44+CD24+ gastric cancer stem cells. Journal of cancer research and clinical oncology. 2011;137(11):1679-86.

374. Chen W, Zhang X, Chu C, Cheung WL, Ng L, Lam S, et al. Identification of CD44+ cancer stem cells in human gastric cancer. Hepato-gastroenterology. 2013;60(124):949-54.
375. Fujiwara D, Kato K, Nohara S, Iwanuma Y, Kajiyama Y. The usefulness of three-dimensional cell culture in induction of cancer stem cells from esophageal squamous cell carcinoma cell lines. Biochemical and biophysical research communications. 2013;434(4):773-8.
376. Naor D, Nedvetzki S, Golan I, Melnik L, Faitelson Y. CD44 in cancer. Crit Rev Clin Lab Sci. 2002;39(6):527-79.
377. Basakran NS. CD44 as a potential diagnostic tumor marker. Saudi Med J. 2015;36(3):273-9.
378. Suprynowicz FA, Kamonjoh CM, Krawczyk E, Agarwal S, Wellstein A, Agboke FA, et al. Conditional cell reprogramming involves non-canonical beta-catenin activation and mTOR-mediated inactivation of Akt. PloS one. 2017;12(7):e0180897.
379. Driemel C, Kremling H, Schumacher S, Will D, Wolters J, Lindenlauf N, et al. Context-dependent adaption of EpCAM expression in early systemic esophageal cancer. Oncogene. 2014;33(41):4904-15.
380. Wong HH, Chu P. Immunohistochemical features of the gastrointestinal tract tumors. Journal of gastrointestinal oncology. 2012;3(3):262-84.
381. Zhang SS, Huang QY, Yang H, Xie X, Luo KJ, Wen J, et al. Correlation of p53 status with the response to chemotherapy-based treatment in esophageal cancer: a meta-analysis. Annals of surgical oncology. 2013;20(7):2419-27.
382. Kastelein F, Biermann K, Steyerberg EW, Verheij J, Kalisvaart M, Looijenga LH, et al. Aberrant p53 protein expression is associated with an increased risk of neoplastic progression in patients with Barrett's oesophagus. Gut. 2013;62(12):1676-83.
383. Skacel M, Petras RE, Rybicki LA, Gramlich TL, Richter JE, Falk GW, et al. p53 expression in low grade dysplasia in Barrett's esophagus: correlation with interobserver agreement and disease progression. The American journal of gastroenterology. 2002;97(10):2508-13.
384. Dunn LJ, Jankowski JA, Griffin SM. Trefoil Factor Expression in a Human Model of the Early Stages of Barrett's Esophagus. Digestive diseases and sciences. 2015;60(5):1187-94.
385. Chou TC. Drug combination studies and their synergy quantification using the Chou-Talalay method. Cancer research. 2010;70(2):440-6.
386. Sohnle PG, Hahn BL, Erdmann MD. Effect of fluconazole on viability of Candida albicans over extended periods of time. Antimicrobial agents and chemotherapy. 1996;40(11):2622-5.

387. Garcia I, Pascual A, Conejo C, Salvador J, Perea EJ. Effect of antimicrobial and antineoplastic drugs on the uptake of fluconazole by human neutrophils and tissue culture cells. European journal of clinical microbiology & infectious diseases : official publication of the European Society of Clinical Microbiology. 1993;12(12):944-7.
388. Baas IO, Mulder JW, Offerhaus GJ, Vogelstein B, Hamilton SR. An evaluation of six antibodies for immunohistochemistry of mutant p53 gene product in archival colorectal neoplasms. The Journal of pathology. 1994;172(1):5-12.
389. Rogel A, Popliker M, Webb CG, Oren M. p53 cellular tumor antigen: analysis of mRNA levels in normal adult tissues, embryos, and tumors. Mol Cell Biol. 1985;5(10):2851-5.
390. Barnes DM, Hanby AM, Gillett CE, Mohammed S, Hodgson S, Bobrow LG, et al. Abnormal expression of wild type p53 protein in normal cells of a cancer family patient. Lancet. 1992;340(8814):259-63.
391. Bennett WP, Hollstein MC, Hsu IC, Sidransky D, Lane DP, Vogelstein B, et al. Mutational spectra and immunohistochemical analyses of p53 in human cancers. Chest. 1992;101(3 Suppl):19S-20S.
392. Zhao R, Quaroni L, Casson AG. Identification and characterization of stemlike cells in human esophageal adenocarcinoma and normal epithelial cell lines. The Journal of thoracic and cardiovascular surgery. 2012;144(5):1192-9.
393. Sampah ME, Shen L, Jilek BL, Siliciano RF. Dose-response curve slope is a missing dimension in the analysis of HIV-1 drug resistance. Proceedings of the National Academy of Sciences of the United States of America. 2011;108(18):7613-8.
394. Biotec M. MACS® Tissue Storage Solution Data Sheet. http://wwwmiltenyibioteccom/. 2013.
395. Cunningham RE. Tissue disaggregation. Methods in molecular biology. 2010;588:327-30.
396. Plantamura E, Huyghe G, Panterne B, Delesalle N, Thepot A, Reverdy ME, et al. Validation of the BacT/ALERT(R)3D automated culture system for the detection of microbial contamination of epithelial cell culture medium. Cell Tissue Bank. 2012;13(3):453-9.
397. Choi JH, Lee CG, Lim YJ, Kang HW, Lim CY, Choi JS. Prevalence and risk factors of esophageal candidiasis in healthy individuals: a single center experience in Korea. Yonsei Med J. 2013;54(1):160-5.
398. Schelenz S, Abdallah S, Gray G, Stubbings H, Gow I, Baker P, et al. Epidemiology of oral yeast colonization and infection in patients with hematological malignancies, head neck and solid tumors. J Oral Pathol Med. 2011;40(1):83-9.
399. Mazur P. Freezing of living cells: mechanisms and implications. Am J Physiol. 1984;247(3 Pt 1):C125-42.

400. Deller RC, Pessin JE, Vatish M, Mitchell DA, Gibson MI. Enhanced non-vitreous cryopreservation of immortalized and primary cells by ice-growth inhibiting polymers. Biomater Sci. 2016;4(7):1079-84.
401. Pattabiraman DR, Weinberg RA. Tackling the cancer stem cells - what challenges do they pose? Nature reviews Drug discovery. 2014;13(7):497-512.
402. Clevers H. The cancer stem cell: premises, promises and challenges. Nature medicine. 2011;17(3):313-9.
403. Barbera M, di Pietro M, Walker E, Brierley C, MacRae S, Simons BD, et al. The human squamous oesophagus has widespread capacity for clonal expansion from cells at diverse stages of differentiation. Gut. 2015;64(1):11-9.
404. Mather JP. In vitro models. Stem cells. 2012;30(2):95-9.
405. McCormick Matthews LH, Noble F, Tod J, Jaynes E, Harris S, Primrose JN, et al. Systematic review and meta-analysis of immunohistochemical prognostic biomarkers in resected oesophageal adenocarcinoma. British journal of cancer. 2015;113(1):107-18.
406. Garcia E, Hayden A, Birts C, Britton E, Cowie A, Pickard K, et al. Authentication and characterisation of a new oesophageal adenocarcinoma cell line: MFD-1. Scientific reports. 2016;6:32417.
407. Quent VM, Loessner D, Friis T, Reichert JC, Hutmacher DW. Discrepancies between metabolic activity and DNA content as tool to assess cell proliferation in cancer research. Journal of cellular and molecular medicine. 2010;14(4):1003-13.
408. Jones LJ, Gray M, Yue ST, Haugland RP, Singer VL. Sensitive determination of cell number using the CyQUANT cell proliferation assay. Journal of immunological methods. 2001;254(1-2):85-98.
409. Bittman R, Li Z, Samadder P, Arthur G. Anticancer activity of a ceramide analog containing a disulfide linkage. Cancer letters. 2007;251(1):53-8.
410. Okawa Y, Hideshima T, Steed P, Vallet S, Hall S, Huang K, et al. SNX-2112, a selective Hsp90 inhibitor, potently inhibits tumor cell growth, angiogenesis, and osteoclastogenesis in multiple myeloma and other hematologic tumors by abrogating signaling via Akt and ERK. Blood. 2009;113(4):846-55.
411. Lehmann J, Retz M, Sidhu SS, Suttmann H, Sell M, Paulsen F, et al. Antitumor activity of the antimicrobial peptide magainin II against bladder cancer cell lines. Eur Urol. 2006;50(1):141-7.
412. Engler AJ, Sen S, Sweeney HL, Discher DE. Matrix elasticity directs stem cell lineage specification. Cell. 2006;126(4):677-89.
413. Paszek MJ, Zahir N, Johnson KR, Lakins JN, Rozenberg GI, Gefen A, et al. Tensional homeostasis and the malignant phenotype. Cancer cell. 2005;8(3):241-54.

414. Provenzano PP, Eliceiri KW, Campbell JM, Inman DR, White JG, Keely PJ. Collagen reorganization at the tumor-stromal interface facilitates local invasion. BMC medicine. 2006;4(1):38.
415. Levental KR, Yu H, Kass L, Lakins JN, Egeblad M, Erler JT, et al. Matrix crosslinking forces tumor progression by enhancing integrin signaling. Cell. 2009;139(5):891-906.
416. Ng MR, Brugge JS. A stiff blow from the stroma: collagen crosslinking drives tumor progression. Cancer cell. 2009;16(6):455-7.
417. Zaman MH, Trapani LM, Sieminski AL, Mackellar D, Gong H, Kamm RD, et al. Migration of tumor cells in 3D matrices is governed by matrix stiffness along with cell-matrix adhesion and proteolysis. Proceedings of the National Academy of Sciences of the United States of America. 2006;103(29):10889-94.
418. Demou ZN. Gene expression profiles in 3D tumor analogs indicate compressive strain differentially enhances metastatic potential. Ann Biomed Eng. 2010;38(11):3509-20.
419. Hadjipanayi E, Mudera V, Brown RA. Close dependence of fibroblast proliferation on collagen scaffold matrix stiffness. Journal of tissue engineering and regenerative medicine. 2009;3(2):77-84.
420. Weigelt B, Ghajar CM, Bissell MJ. The need for complex 3D culture models to unravel novel pathways and identify accurate biomarkers in breast cancer. Adv Drug Deliv Rev. 2014;69-70:42-51.
421. Sato T, Vries RG, Snippert HJ, van de Wetering M, Barker N, Stange DE, et al. Single Lgr5 stem cells build crypt-villus structures in vitro without a mesenchymal niche. Nature. 2009;459(7244):262-5.
422. Yu J, Chau KF, Vodyanik MA, Jiang J, Jiang Y. Efficient feeder-free episomal reprogramming with small molecules. PloS one. 2011;6(3):e17557.
423. Pijuan-Galito S, Tamm C, Schuster J, Sobol M, Forsberg L, Merry CL, et al. Human serum-derived protein removes the need for coating in defined human pluripotent stem cell culture. Nat Commun. 2016;7:12170.
424. Inman JL, Bissell MJ. Apical polarity in three-dimensional culture systems: where to now? J Biol. 2010;9(1):2.
425. Bowman C, Saunders J, Pang V, Catton J, Welch N, Duffy J, et al. Survival benefit of perioperative MAGIC and OE02 chemotherapy regimens in those with and without chemotherapy responsive oesophago-gastric cancer. Short paper abstracts from the International Surgical Congress of the ASGBI, 1-2 May 2014. The British journal of surgery. 2015;102(Suppl 1):1-301.
426. Reece-Smith AM, Saha S, Cunnell ML, Hameed K, Bessell EM, Duffy JP, et al. MAGIC in practice: experience of peri-operative ECF/X chemotherapy in gastro-esophageal

adenocarcinomas. Journal of surgical oncology. 2012;106(6):748-52.
427. Derek Alderson REL, Matthew Guy Nankivell, Jane M. Blazeby, Michael Griffin, Adrian Crellin, Heike I. Grabsch, Alicia Frances Clare Okines, Cindy Goldstein, Stephen Falk, Joyce Thompson, Richard Krysztopik, Fareeda Y. Coxon, Susan Pritchard, Rupert Langer, Sally Patricia Stenning, David Cunningham. Neoadjuvant chemotherapy for resectable oesophageal and junctional adenocarcinoma: results from the UK Medical Research Council randomised OEO5 trial Journal of clinical oncology : official journal of the American Society of Clinical Oncology. 2015;33((suppl; abstr 4002)).
428. Mirza A, Pritchard S, Welch I. The postoperative component of MAGIC chemotherapy is associated with improved prognosis following surgical resection in gastric and gastrooesophageal junction adenocarcinomas. International journal of surgical oncology. 2013;2013:781742.
429. Pennathur A, Gibson MK, Jobe BA, Luketich JD. Oesophageal carcinoma. Lancet. 2013;381(9864):400-12.
430. Lin EW, Karakasheva TA, Hicks PD, Bass AJ, Rustgi AK. The tumor microenvironment in esophageal cancer. Oncogene. 2016.
431. Han Y, Zhang Y, Jia T, Sun Y. Molecular mechanism underlying the tumor-promoting functions of carcinoma-associated fibroblasts. Tumour biology : the journal of the International Society for Oncodevelopmental Biology and Medicine. 2015;36(3):1385-94.
432. Ventimiglia E, Capogrosso P, Montorsi F, Salonia A. The safety of phosphodiesterase type 5 inhibitors for erectile dysfunction. Expert Opin Drug Saf. 2016;15(2):141-52.
433. Cui Y, Liu X, Shi L, Gao Z. Efficacy and safety of phosphodiesterase type 5 (PDE5) inhibitors in treating erectile dysfunction after bilateral nerve-sparing radical prostatectomy. Andrologia. 2016;48(1):20-8.
434. Coyle B. Personal Communication from Beth Coyle, Associate Professor, Faculty of Medicine & Health Sciences, School of Medicine. University of Nottingham, Nottingham, UK. 2015.
435. Nomoto-Kojima N, Aoki S, Uchihashi K, Matsunobu A, Koike E, Ootani A, et al. Interaction between adipose tissue stromal cells and gastric cancer cells in vitro. Cell and tissue research. 2011;344(2):287-98.
436. Katano T, Ootani A, Mizoshita T, Tanida S, Tsukamoto H, Ozeki K, et al. Establishment of a long-term three-dimensional primary culture of mouse glandular stomach epithelial cells within the stem cell niche. Biochemical and biophysical research communications. 2013;432(4):558-63.

437. Ootani A, Li X, Sangiorgi E, Ho QT, Ueno H, Toda S, et al. Sustained in vitro intestinal epithelial culture within a Wnt-dependent stem cell niche. Nature medicine. 2009;15(6):701-6.
438. Bhowmick NA, Neilson EG, Moses HL. Stromal fibroblasts in cancer initiation and progression. Nature. 2004;432(7015):332-7.
439. Anderson MR, Harrison R, Atherfold PA, Campbell MJ, Darnton SJ, Obszynska J, et al. Met receptor signaling: a key effector in esophageal adenocarcinoma. Clin Cancer Res. 2006;12(20 Pt 1):5936-43.
440. Rees JR, Onwuegbusi BA, Save VE, Alderson D, Fitzgerald RC. In vivo and in vitro evidence for transforming growth factor-beta1-mediated epithelial to mesenchymal transition in esophageal adenocarcinoma. Cancer Res. 2006;66(19):9583-90.
441. Bhome R, Al Saihati HA, Goh RW, Bullock MD, Primrose JN, Thomas GJ, et al. Translational aspects in targeting the stromal tumour microenvironment: from bench to bedside. New Horiz Transl Med. 2016;3(1):9-21.
442. Xing F, Saidou J, Watabe K. Cancer associated fibroblasts (CAFs) in tumor microenvironment. Front Biosci (Landmark Ed). 2010;15:166-79.
443. Hanley CJ, Noble F, Ward M, Bullock M, Drifka C, Mellone M, et al. A subset of myofibroblastic cancer-associated fibroblasts regulate collagen fiber elongation, which is prognostic in multiple cancers. Oncotarget. 2016;7(5):6159-74.
444. Lin EW, Karakasheva TA, Hicks PD, Bass AJ, Rustgi AK. The tumor microenvironment in esophageal cancer. Oncogene. 2016;35(41):5337-49.
445. Quante M, Tu SP, Tomita H, Gonda T, Wang SS, Takashi S, et al. Bone marrow-derived myofibroblasts contribute to the mesenchymal stem cell niche and promote tumor growth. Cancer cell. 2011;19(2):257-72.
446. Butler JM, Kobayashi H, Rafii S. Instructive role of the vascular niche in promoting tumour growth and tissue repair by angiocrine factors. Nature reviews Cancer. 2010;10(2):138-46.
447. Zou W. Regulatory T cells, tumour immunity and immunotherapy. Nat Rev Immunol. 2006;6(4):295-307.
448. Pollard JW. Tumour-educated macrophages promote tumour progression and metastasis. Nature reviews Cancer. 2004;4(1):71-8.
449. Restifo NP, Dudley ME, Rosenberg SA. Adoptive immunotherapy for cancer: harnessing the T cell response. Nat Rev Immunol. 2012;12(4):269-81.
450. Hodi FS, O'Day SJ, McDermott DF, Weber RW, Sosman JA, Haanen JB, et al. Improved survival with ipilimumab in patients with metastatic melanoma. The New England journal of medicine. 2010;363(8):711-23.

451. Augustine TN, Dix-Peek T, Duarte R, Candy GP. Establishment of a heterotypic 3D culture system to evaluate the interaction of TREG lymphocytes and NK cells with breast cancer. Journal of immunological methods. 2015;426:1-13.
452. Kuukasjarvi T, Karhu R, Tanner M, Kahkonen M, Schaffer A, Nupponen N, et al. Genetic heterogeneity and clonal evolution underlying development of asynchronous metastasis in human breast cancer. Cancer research. 1997;57(8):1597-604.
453. Sveen A, Loes IM, Alagaratnam S, Nilsen G, Holand M, Lingjaerde OC, et al. Intra-patient Inter-metastatic Genetic Heterogeneity in Colorectal Cancer as a Key Determinant of Survival after Curative Liver Resection. PLoS genetics. 2016;12(7):e1006225.
454. Greaves M, Maley CC. Clonal evolution in cancer. Nature. 2012;481(7381):306-13.
455. Williams MJ, Werner B, Barnes CP, Graham TA, Sottoriva A. Identification of neutral tumor evolution across cancer types. Nature genetics. 2016;48(3):238-44.
456. Bruna A, Rueda OM, Greenwood W, Batra AS, Callari M, Batra RN, et al. A Biobank of Breast Cancer Explants with Preserved Intra-tumor Heterogeneity to Screen Anticancer Compounds. Cell. 2016;167(1):260-74 e22.
457. Francies HE, Barthorpe A, McLaren-Douglas A, Barendt WJ, Garnett MJ. Drug Sensitivity Assays of Human Cancer Organoid Cultures. Methods in molecular biology. 2016.
458. Fergus Noble ML, Rob Walker, Richard Turkington,Damian McManus, Matt Bedford,EwenGrifths, John Whiting,Nicola Grehan, J Robert O'Neil, Richard JE Skipworth, Vicki Save, Rupesh Sutaria, Stuart Mercer, John H Saunders, Irshad N Soomro, Simon L Parsons, Rebecca C Fitzgerald, Timothy J Underwood. A multicentre cohort study to redefine and validate pathologicalassessment of response to neoadjuvant therapy in treated oesopha-gogastric adenocarcinoma. British Journal Of Surgery 2016;103 ((S7):5–6).
459. Davies AR, Pillai A, Sinha P, Sandhu H, Adeniran A, Mattsson F, et al. Factors associated with early recurrence and death after esophagectomy for cancer. Journal of surgical oncology. 2014;109(5):459-64.
460. Davies AR, Gossage JA, Zylstra J, Mattsson F, Lagergren J, Maisey N, et al. Tumor stage after neoadjuvant chemotherapy determines survival after surgery for adenocarcinoma of the esophagus and esophagogastric junction. Journal of clinical oncology : official journal of the American Society of Clinical Oncology. 2014;32(27):2983-90.
461. Kiyozuka Y, Asai A, Yamamoto D, Senzaki H, Yoshioka S, Takahashi H, et al. Establishment of novel human esophageal cancer cell line in relation to telomere dynamics and telomerase activity. Digestive diseases and sciences. 2000;45(5):870-9.

462. Shen ZY, Xu LY, Li EM, Shen J, Zheng RM, Cai WJ, et al. Immortal phenotype of the esophageal epithelial cells in the process of immortalization. Int J Mol Med. 2002;10(5):641-6.
463. Peng D, Hu T, Soutto M, Belkhiri A, Zaika A, El-Rifai W. Glutathione peroxidase 7 has potential tumour suppressor functions that are silenced by location-specific methylation in oesophageal adenocarcinoma. Gut. 2014;63(4):540-51.
464. Sachs N, Clevers H. Organoid cultures for the analysis of cancer phenotypes. Current opinion in genetics & development. 2014;24:68-73.

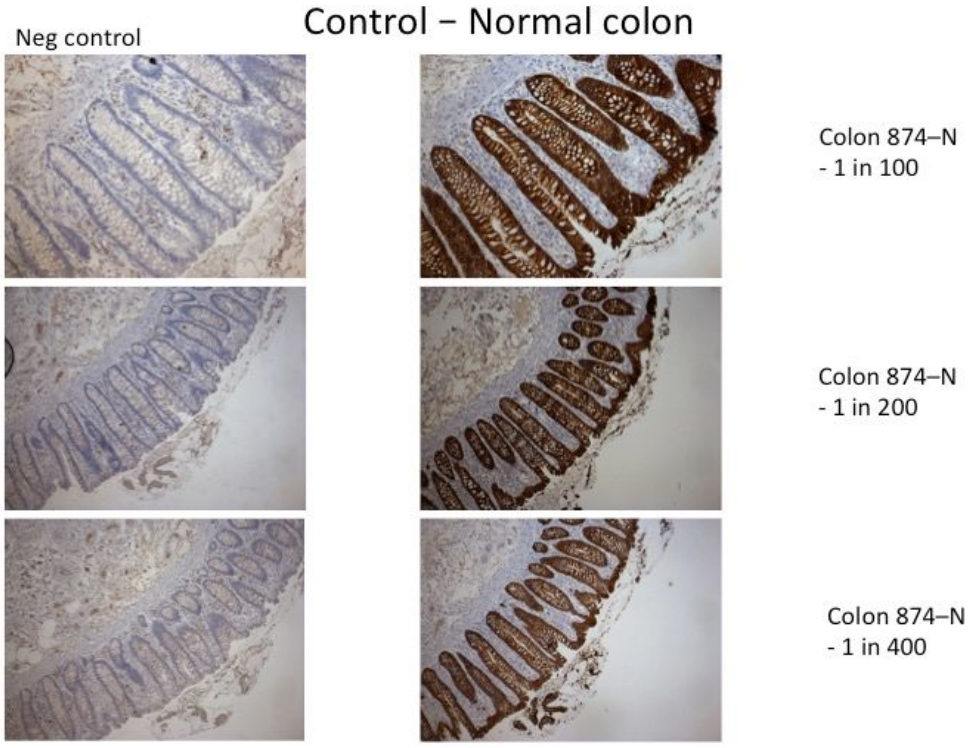
8 Appendices

8.1 Epcam optimisation

Epcam Optimisation

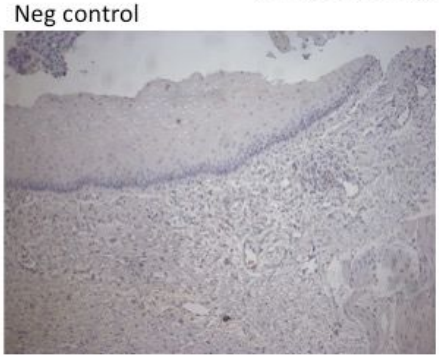
- Control - colonic tissue: epithelium stains
- No staining of normal squamous oesophagus
- Staining of oesophageal adenocarcinoma
- Normal columnar gastric epithelium stains

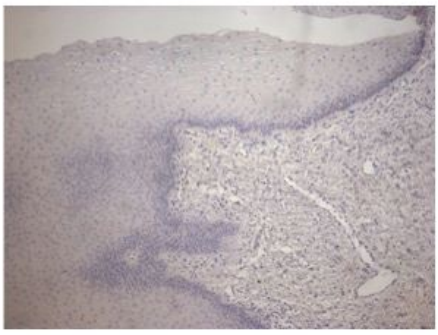
Optimum dilution 1 in 100 (clone Ber EP4)



Normal Squamous Oesophagus

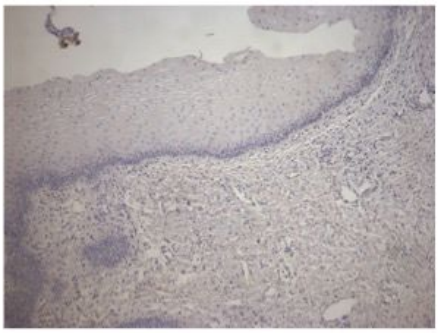
Neg control





OES150-N
1 in 100

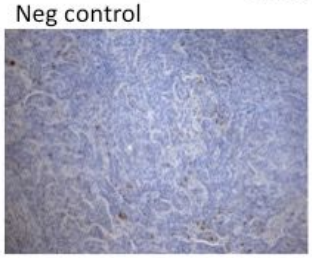
Epcam does not stain normal squamous epithelium

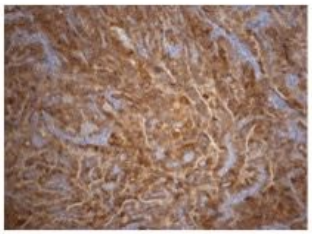


OES150-N
1 in 200

Oesophageal Adenocarcinoma

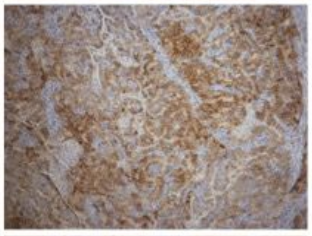
Neg control





OES 154-T
- 1 in 100

Epcam stains malignant oesophageal carcinoma.



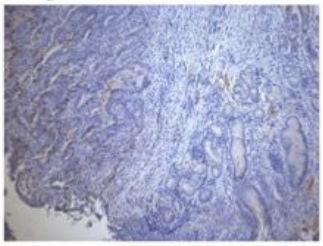
OES 154-T
- 1 in 200



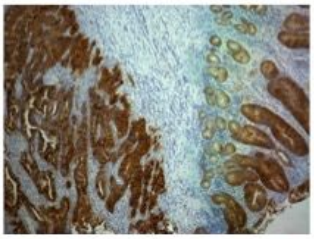
OES 154-T
- 1 in 400

Adenocarcinoma and gastric epithelium

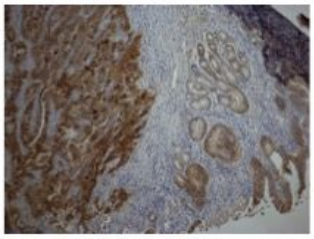
Neg control



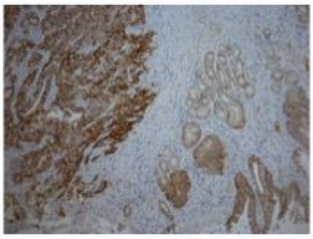
GOJ carcinoma abutting the gastric columnar epithelium



OES 154-T - 1 in 100

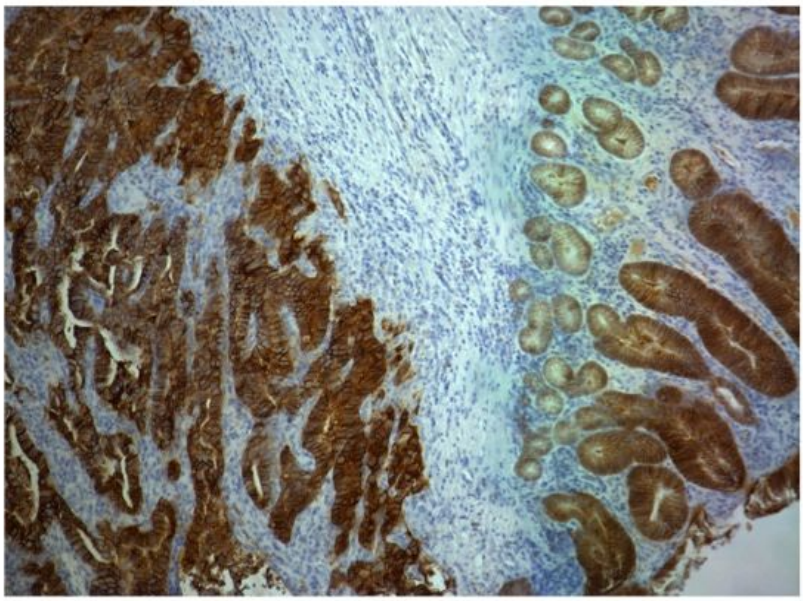


OES 154-T - 1 in 200



OES 154-T - 1 in 400

Oesophageal adenocarcinoma & normal columnar mucosa



Example of the optimum 1 in 100 dilution

8.2 CD44 optimisation

CD44 optimisation

- Control - normal oesophageal squamous epithelium, basal epithelium stains.
- Staining of oesophageal adenocarcinoma successful

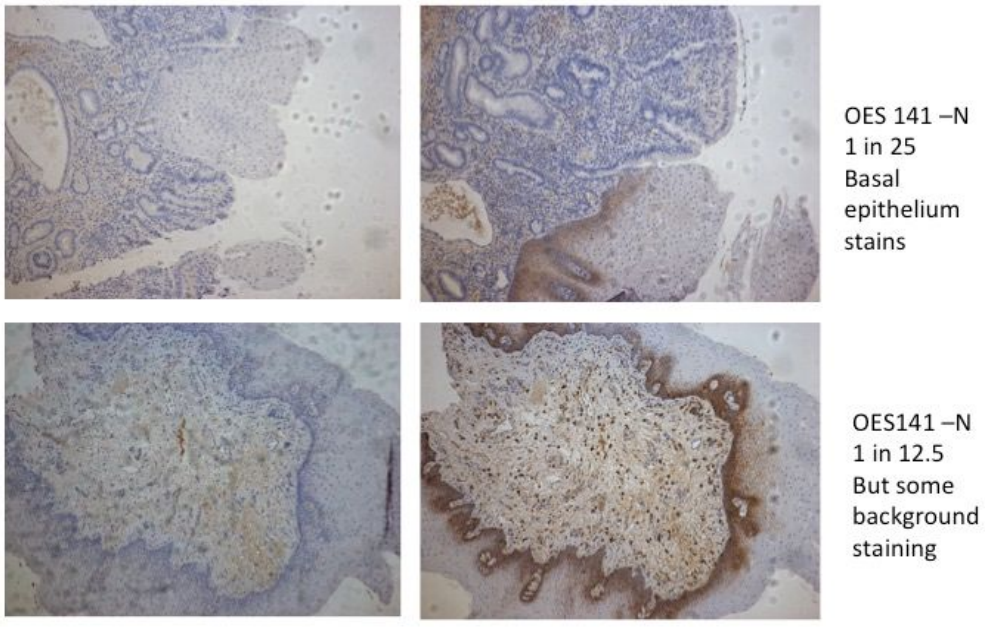
Optimum primary antibody dilution of 1 in 25

- Optimisation of secondary and visualisation to improve brightness of primary stain without background stromal staining from higher concentration of primary antibody

HRP better than Biotinylation

Normal oesophageal tissue

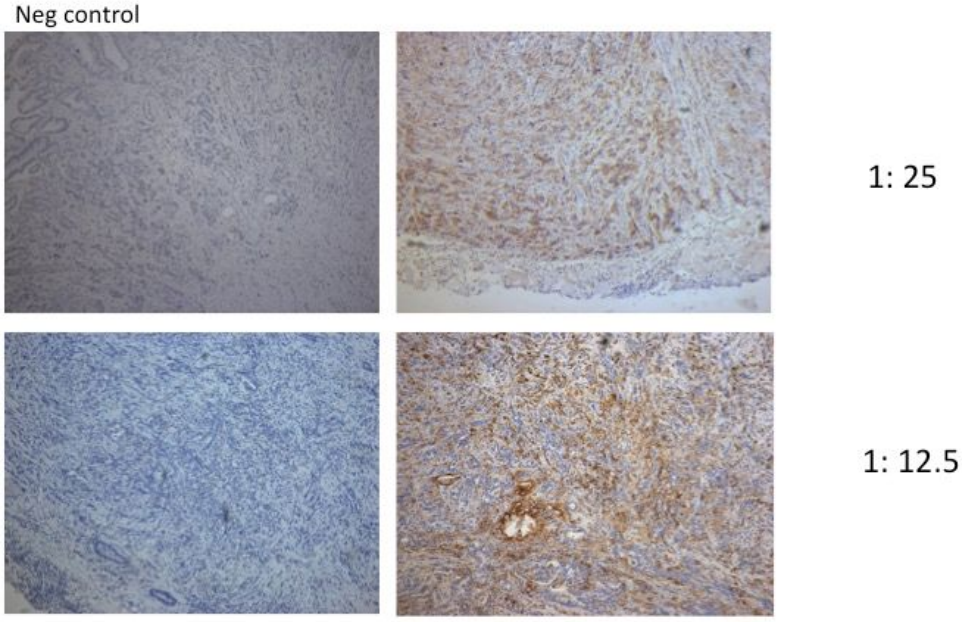
Neg control



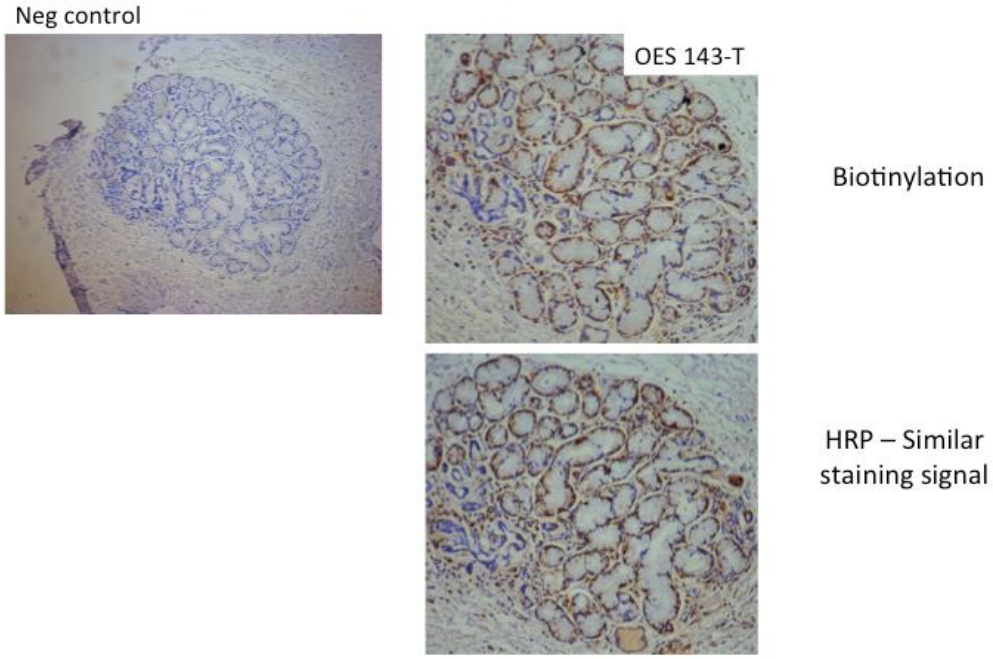
OES 141 –N
1 in 25
Basal epithelium stains

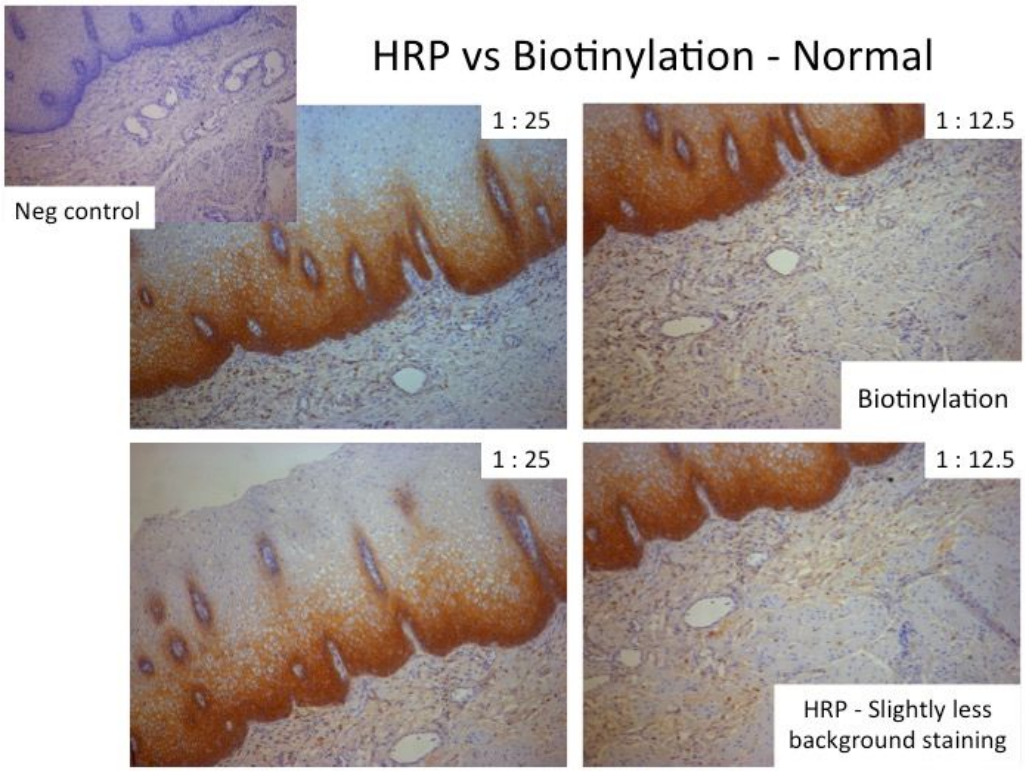
OES141 –N
1 in 12.5
But some background staining

Oesophageal Adenocarcinoma

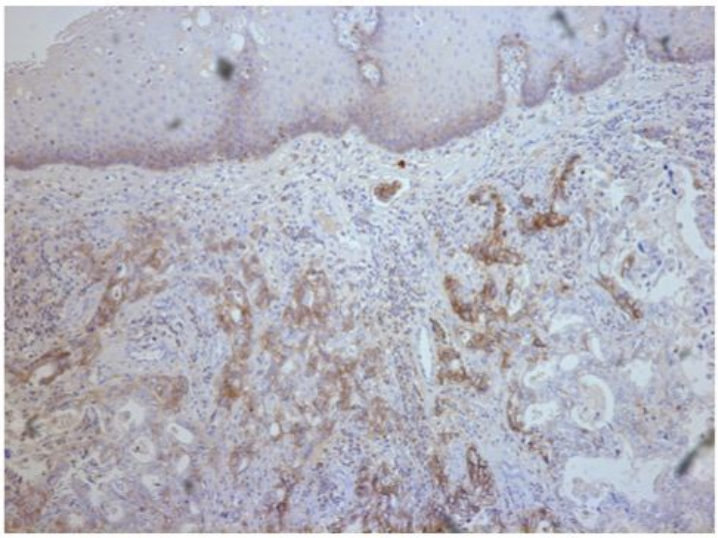


HRP vs Biotinylation - Tumour





Oesophageal adenocarcinoma undermining normal squamous mucosa



OES 145

Example of the optimum 1 in 25 dilution with HRP

8.3 p53 optimisation

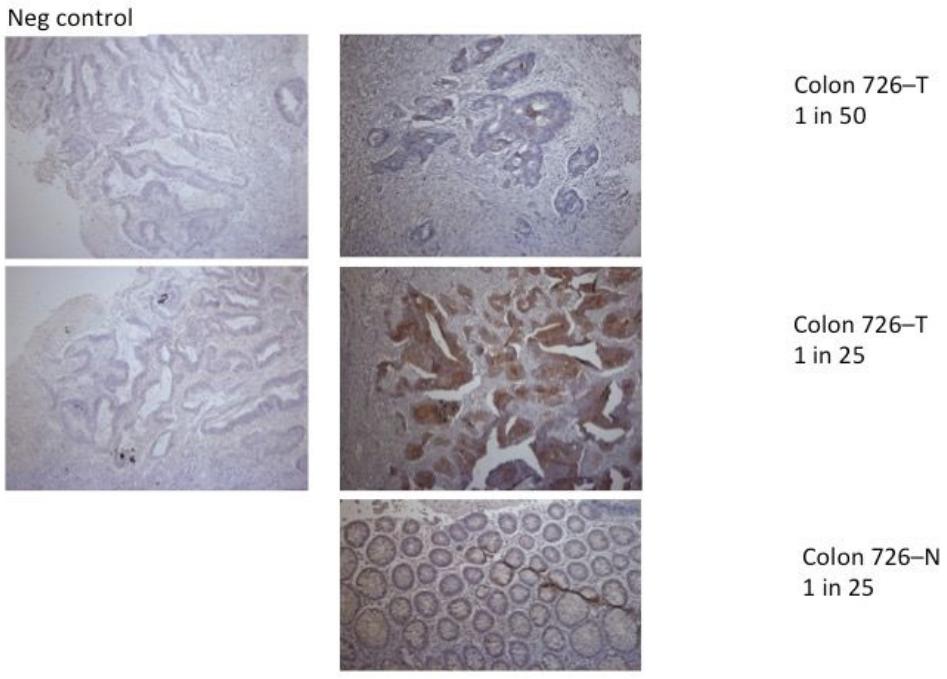
p53 Optimisation

- Control - colonic tissue: tumour not normal
- No staining of normal squamous oesophagus
- Staining of oesophageal adenocarcinoma, but less clearly than colon at same dilution (stains but difficult reliably visualising at 1 in 50)

Optimum dilution for Oesophageal tissue 1 in 25

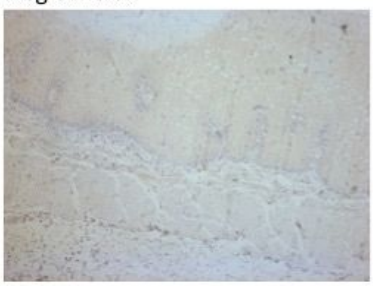
Compromise between clearly highlighting p53 in OAC cell nucleus and mild stromal background stain

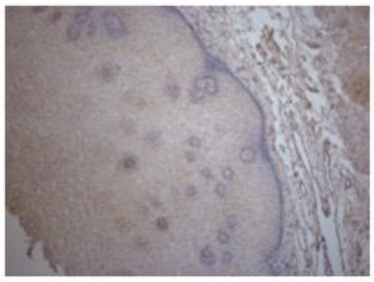
Control – Colonic adenocarcinoma



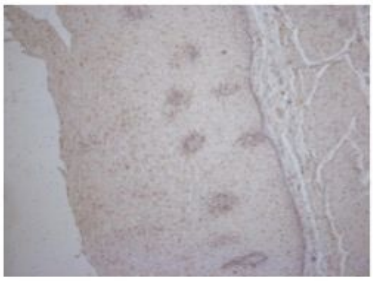
Normal Squamous Oesophagus

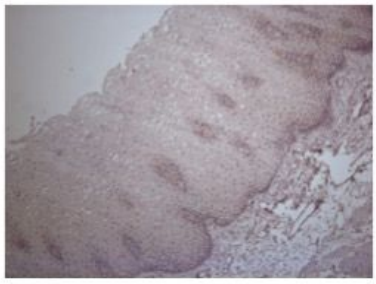
Neg control





OES153-n
1 in 50



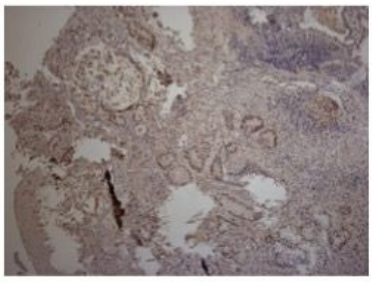


OES 153-n
1 in 25

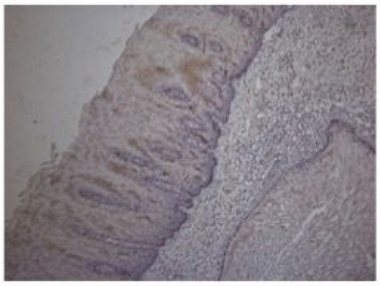
Oesophageal Adenocarcinoma

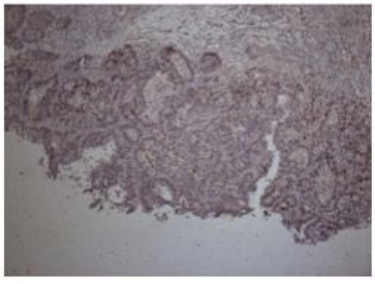
Neg control





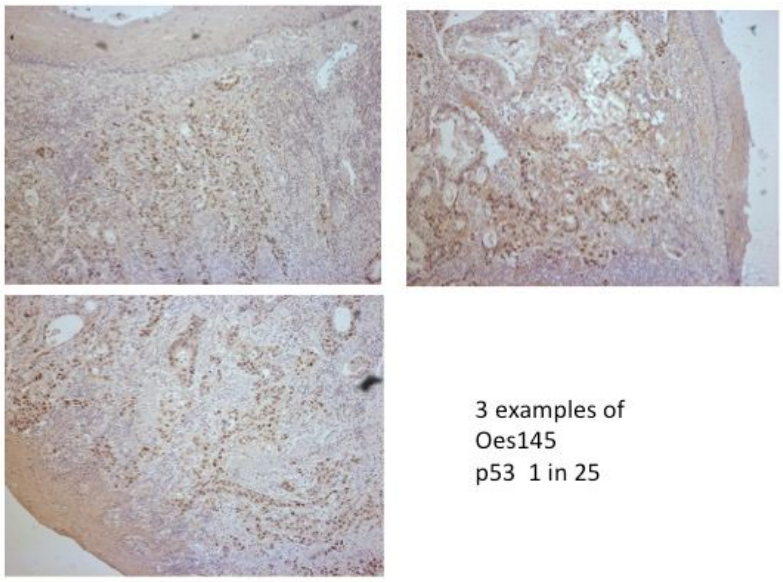
Oes151 tumour
and normal pair
1 in 25





Oes125 tumour
and normal pair
1 in 25

Compromise between clearly highlighting p53 in OAC cell nucleus and mild stromal background staining



3 examples of
Oes145
p53 1 in 25

8.4 ALDH optimisation

ALDH Optimisation

- Control tissue – liver
- Different retrieval methods suggested in literature

Citric Acid optimum retrieval method

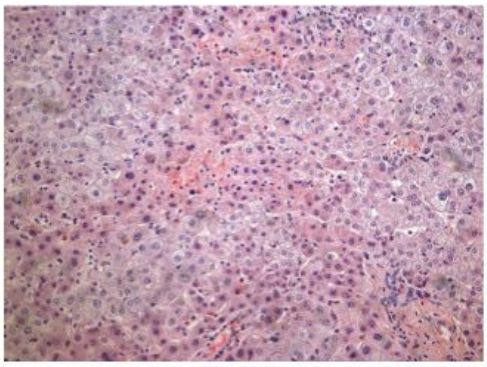
- No staining of normal squamous oesophagus
- Staining of oesophageal adenocarcinoma

Optimum primary antibody dilution of 1 in 100

- Optimisation of visualisation

Biotinylation better than HRP

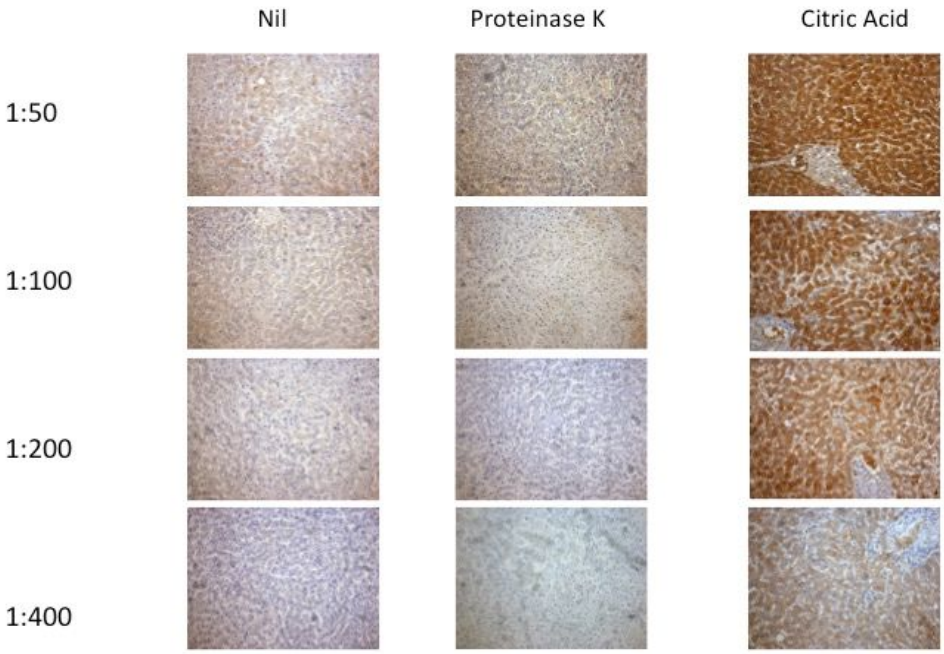
Normal Liver



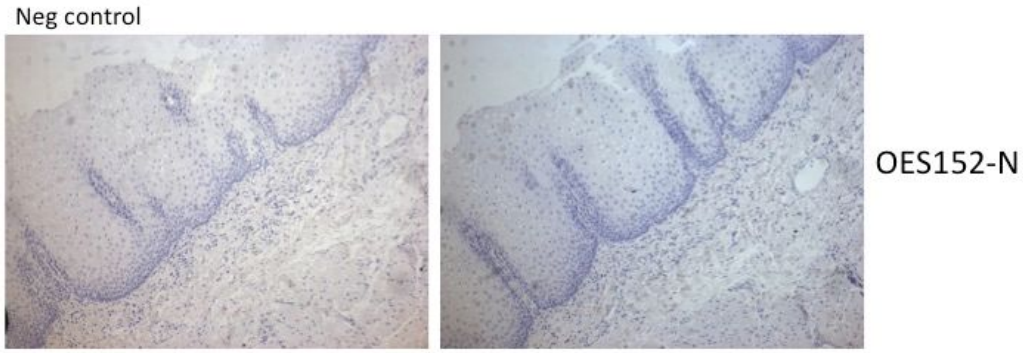
Liver 209 – 14 N

HE: Normal liver architecture

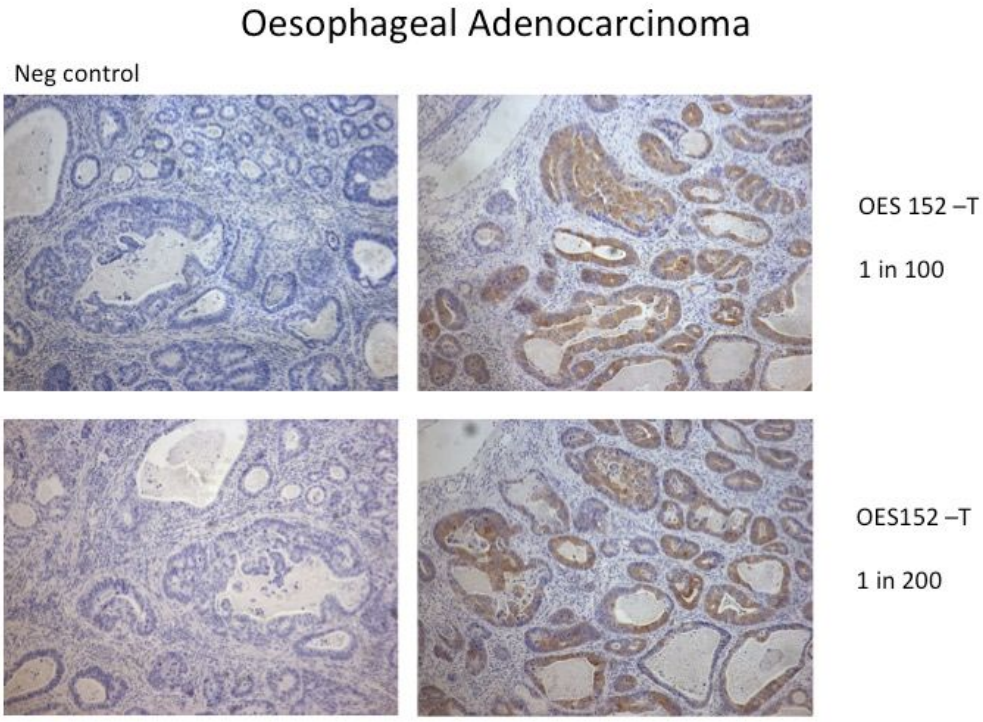
Optimisation of Retrieval methodology

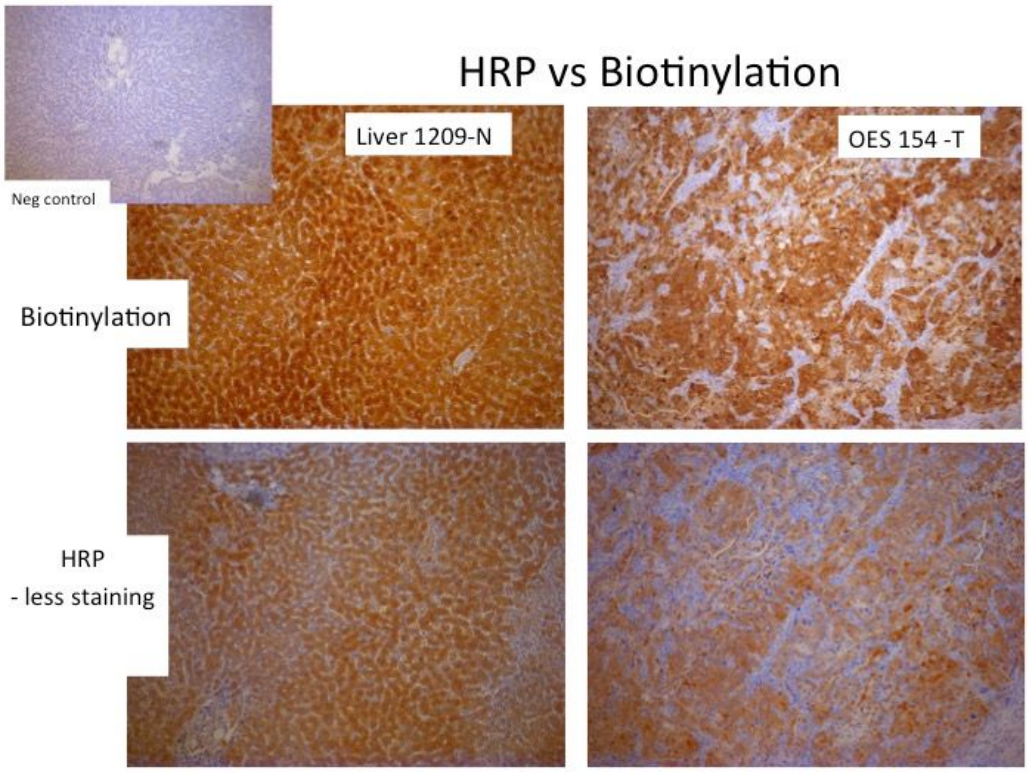


Normal oesophageal squamous tissue

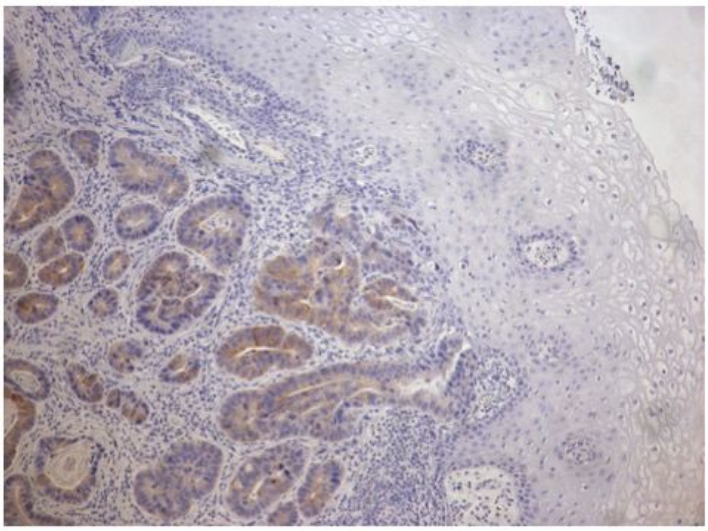


Normal oesophageal squamous epithelium doesn't't stain for ALDH


Oesophageal Adenocarcinoma
Neg control
OES 152 –T
1 in 100
OES152 –T
1 in 200


HRP vs Biotinylation
Neg control
Liver 1209-N
OES 154 -T
Biotinylation
HRP
- less staining

Malignant adenocarcinoma tissue undermining the adjacent normal squamous epithelium



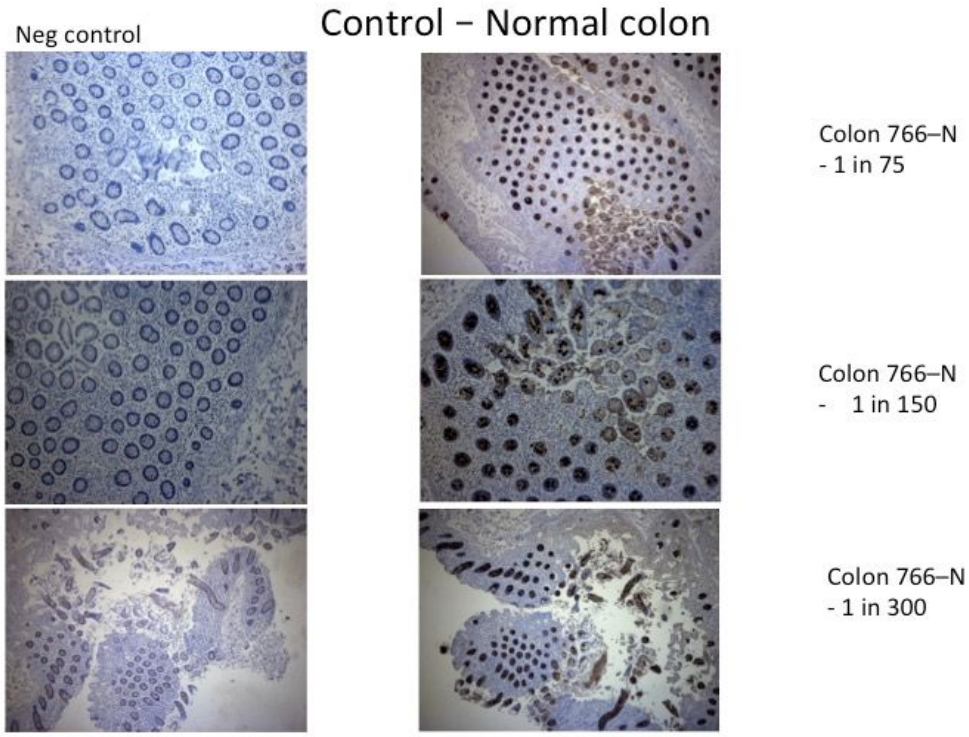
Optimised ALDH staining 1:100 with minimal background

8.5 TFF3 optimisation

TFF3 Optimisation

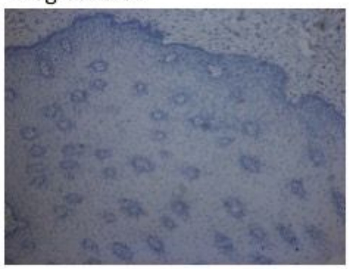
- Control – Normal colon
- No staining of normal squamous oesophagus, but 1 in 300 starts to stain the stroma.
- Staining of oesophageal adenocarcinoma, more precise at 1 in 150 than 1 in 300

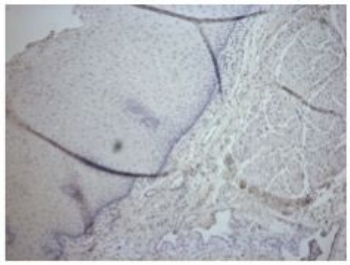
Optimum dilution 1 in 150 (3ug/ml)



Normal tissue control

Neg control

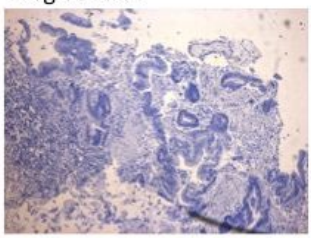


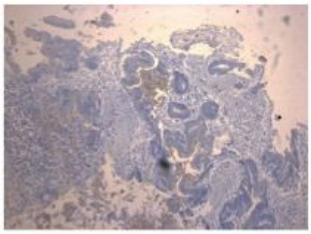


OES153 - N

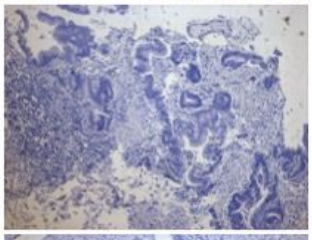
Oesophageal Adenocarcinoma

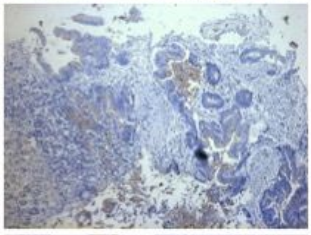
Neg control



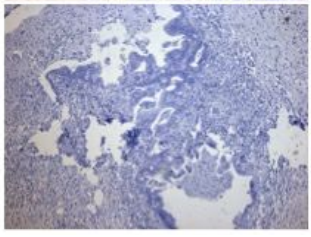


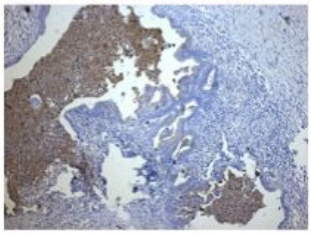
OES 136-T
- 1 in 75





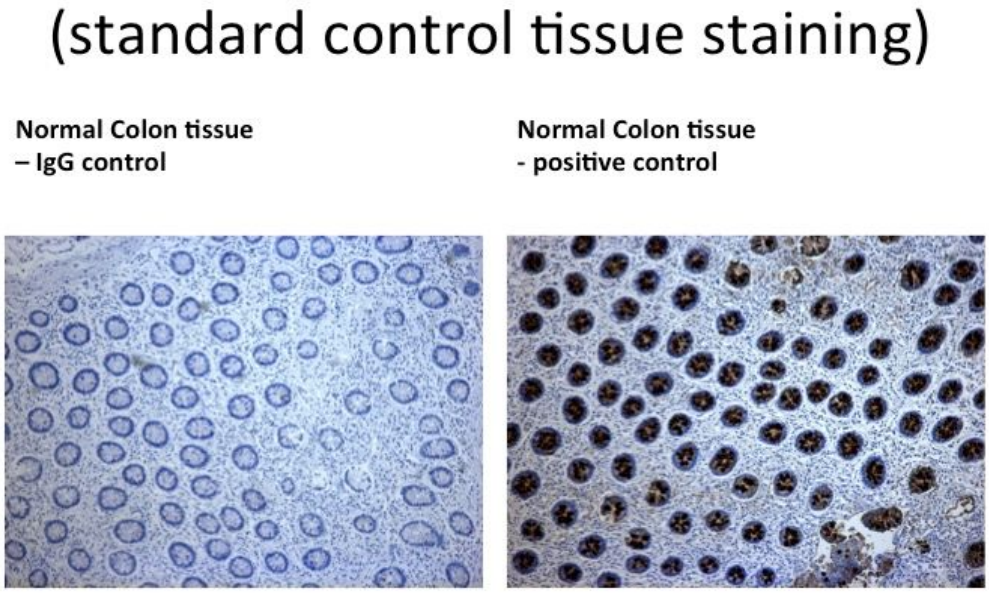
OES 136-T
- 1 in 150
(3ug/ml)

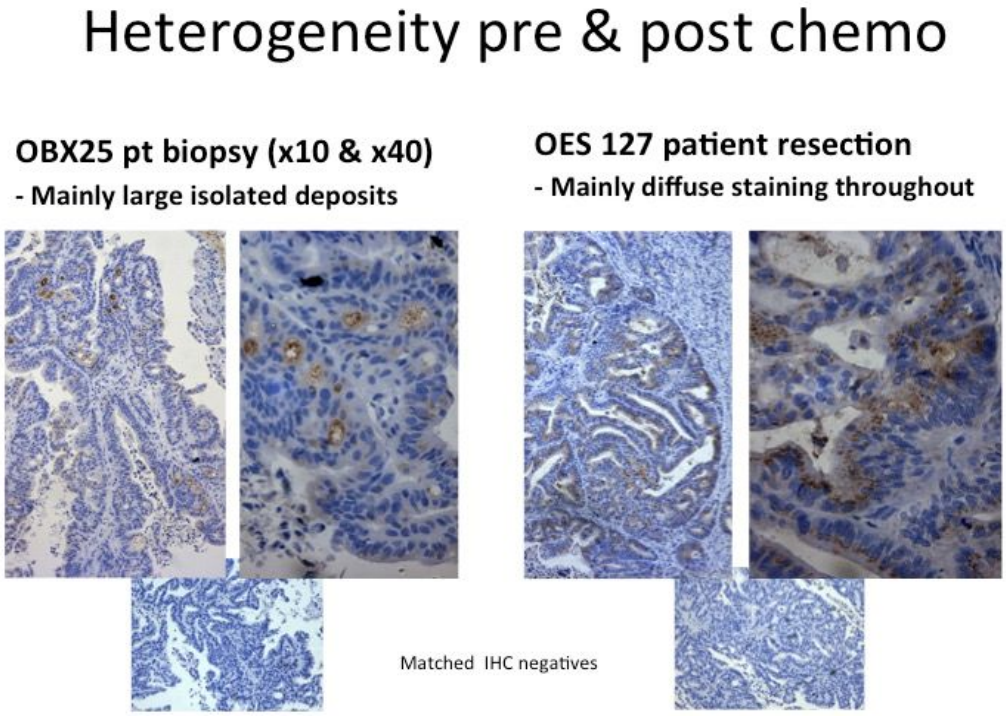




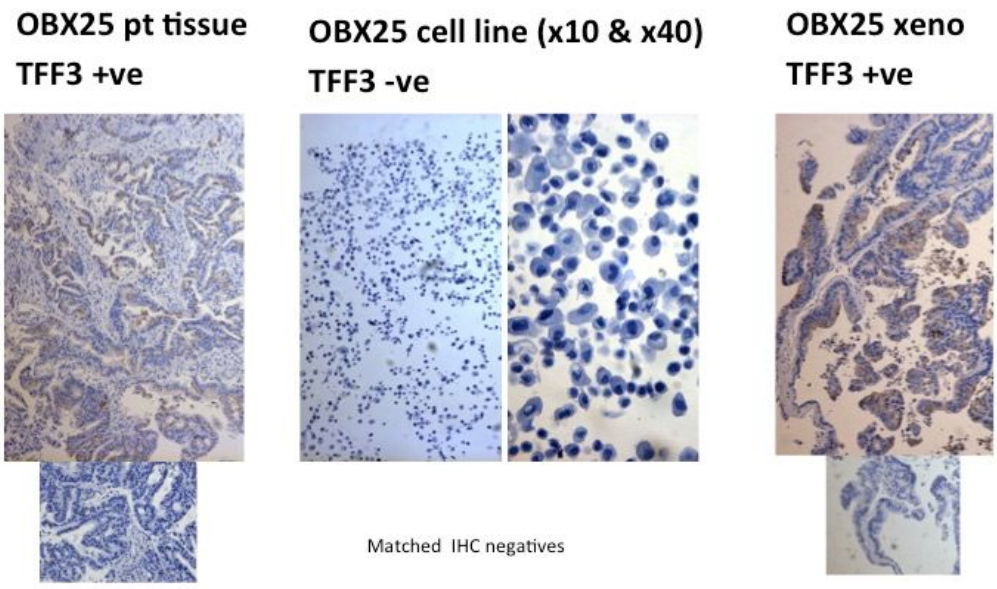
OES-136-T
- 1 in 300

8.6 TFF3 Heterogeneity within Oesophageal Adenocarcinoma tissue

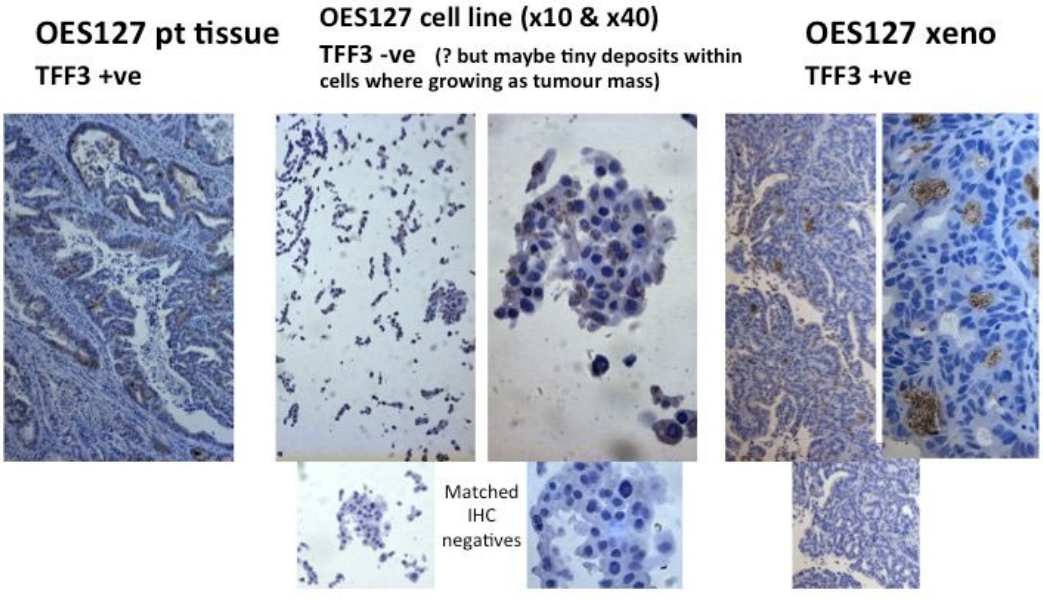




Heterogeneity between OBX formats



Heterogeneity between OES formats

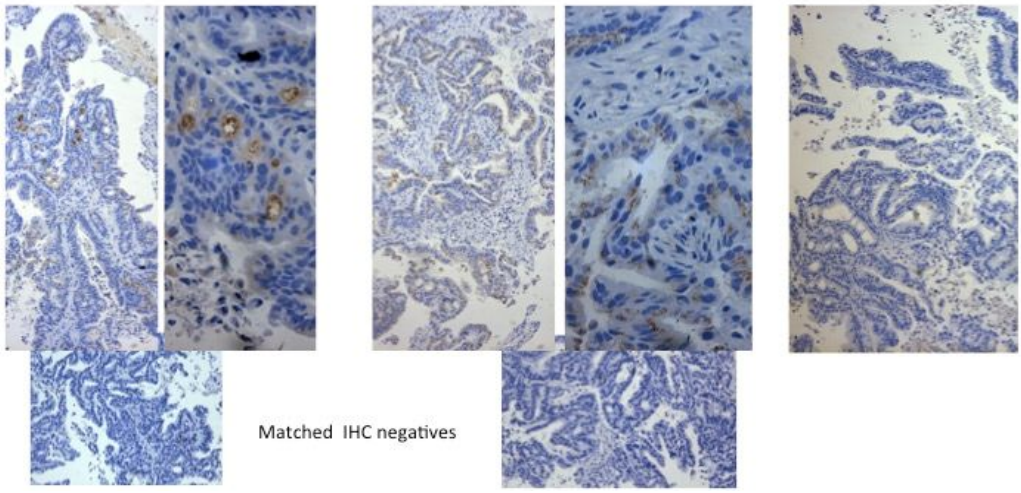


Heterogeneity within tumour samples

(approx 2-3mm distant from each other on the same slide & section)

OBX25 (x10 & x40)

- discrete staining **- diffuse staining** **- reduced staining**



8.7 TFF3 Immunofluorescence

TFF3 immunofluorescence optimisation imaging

Trefoil factor 3 (TFF3), which 'is highly specific for cells with an intestinal phenotype' is used in conjunction with the cytosponge for diagnosis of Barrett's oesophagus [1]. However, other papers [2] suggest that TFF3 is not universally present, and a marker of a more established columnar epithelium [3].

Presence of TFF3 in my cell lines confirm that these are not normal squamous epithelia (like the use of Epcam). But it will not confirm that they are cancer – the cells expressing TFF3 could be metaplastic or dysplastic.

1. Research advances in esophageal diseases: bench to bedside. Massimiliano di Pietro, Rebecca C Fitzgerald. F1000Prime Rep. 2013
2. Barrett's esophagus is characterized by expression of gastric-type mucins (MUC5AC, MUC6) and TFF peptides (TFF1 and TFF2). Warson C, et al. Hum Pathol. 2002
3. Trefoil Factor Expression in a Human Model of the Early Stages of Barrett's Esophagus. Dunn LJ et al. Dig Dis Sci. 2015

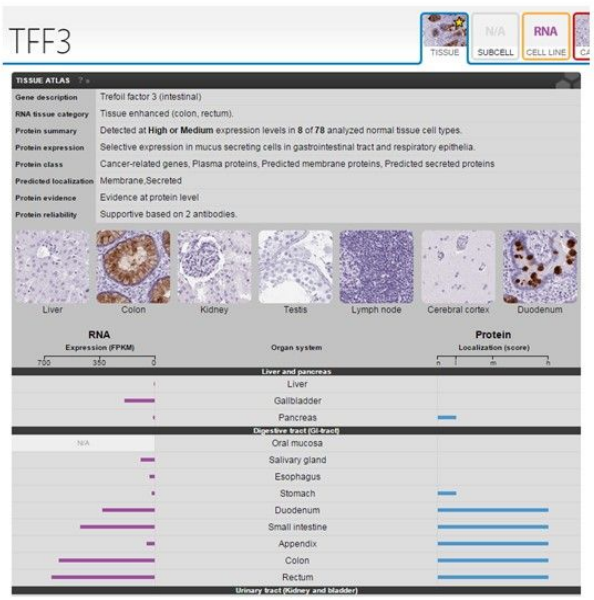
TFF3 in oesophageal cancer

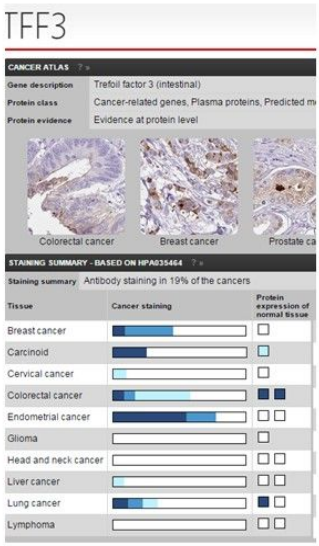
TFF3 is secretory proteins expressed in the goblet cells of the gastrointestinal mucosa and (although their function is not defined) is thought to be involved in conjunction with mucous in the protection, maintenance and repair of the intestinal mucosa.

From the cohort wide analysis, the appearance, disappearance and reappearance of TFF3 from patient, to 2D, and back in xenografts appears to be genuine rather than a technical error. And as a functional molecule, this is a surrogate marker of resumption of tissue architecture, and thus allowing expression of original patient cellular phenotype.

It would therefore be ideal to investigate the presence of TFF3 in the 3D-TGA grown cell clusters to understand if the 3D-TGA is proving a functional microenvironment. I plan to use immunofluorescence to stain for TFF3 on my 3D TGA cancer clusters that I have frozen to see if the patient cellular phenotype is re-established in 3D.

TFF3 not present in normal oesophageal squamous epithelium and likely present, but not reported, in Oesophageal Cancer



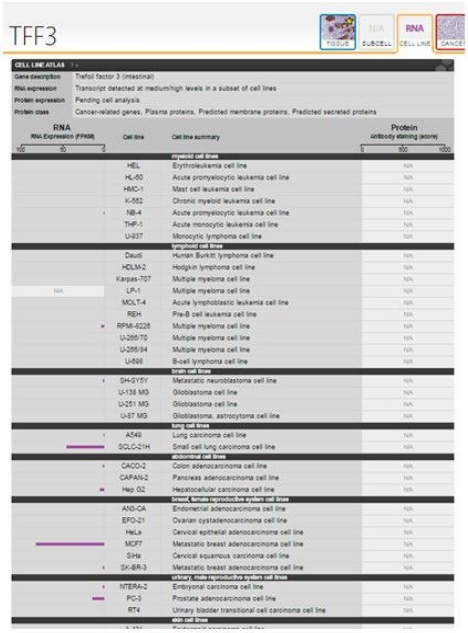


http://www.proteinatlas.org/ENSG00000160180-TFF3/cancer

Efficacy of antibody chosen

- The TFF3 Ab used for IHC not recommended for IF. However would be good to keep consistency.
- If we are to test the IF and the Ab, then we need a tissue which we know expresses TFF3.
- I looked on the protein atlas and MCF7 cells appeared to be one of the few cell lines that did so (albeit at RNA expression level).

Cell Lines expressing TFF3



- TFF3 infrequently expressed across cell lines
- MCF7s appear best (unexpected from a breast rather than intestinal cancer.)
- However, readily available within lab
- MCF7 IF slides made up

Potential pitfalls

- Do MCF7s actually express/ secrete TFF3 or just found as an incidental RNA expression finding?
- Does our TFF3 IHC antibody work for IF also?
- Will the IF assay work on frozen coverslips / cells adequately?
- Will there be any TFF3 to see in the MCF7 and oesophageal samples given its low staining levels if excreted & then washed off?

Slides stained

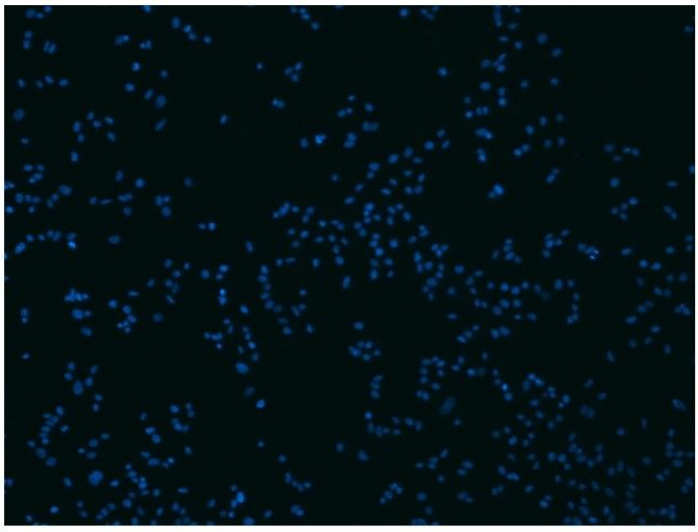
1. IgG control (confirm specificity of Ab primary)
2. E-Cadherin control (check Ab secondary)
3. TFF3 on Fresh MCF7s (check primary Ab)
4. TFF3 on Frozen slide (check frozen method)

Other issues when staining the 3D cultures:

- Potential background staining of murine BME
- Penetration of gel matrix with the Ab & secondary etc
- Destruction/ survival of clusters following extraction from BME and the fixing / freezing process

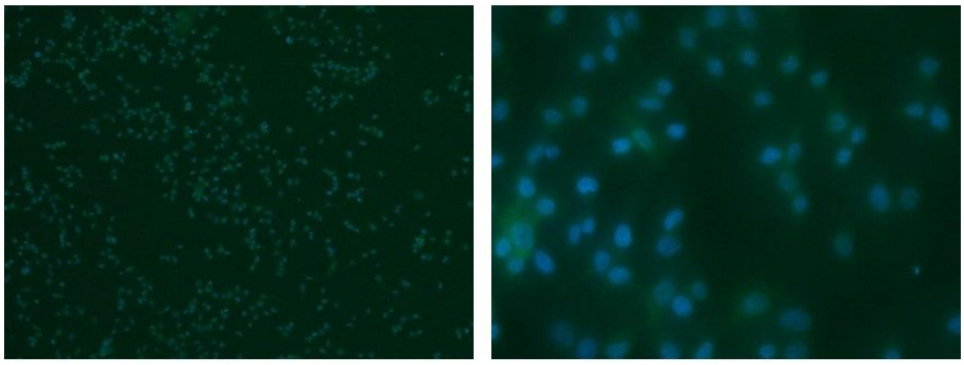
IgG x10

Blue = DAPI
Green = TFF3



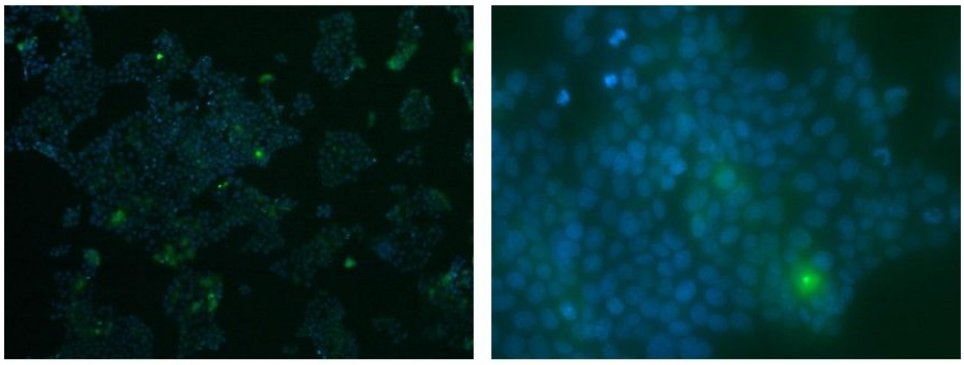
E-Cadherin

x10 x40



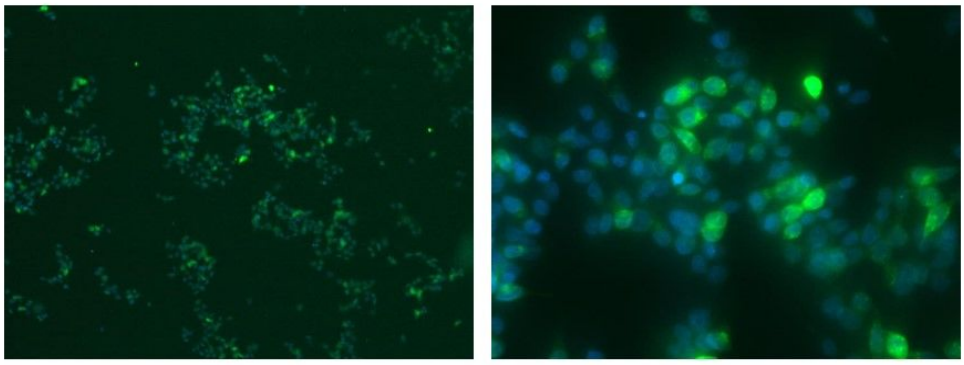
TFF3 on fresh MCF7s

x10 x40



TFF3 on frozen MCF7s

x10 **x40**



Conclusions

1. Primary Ab & secondary Ab work specifically
2. TFF3 IHC Ab works for IF
3. TFF3 is expressed by MCF7 cells
4. Frozen method works
5. Excreted TFF3 is not washed off during the staining process and is retained intra-cellularly by the MCF7s

Conclusion:

Frozen MCF7 cells are a reasonable control to use when IF TFF3 staining the 3D-TGA cancer clusters